Determination of rate constants of low volatile, particle-bound, long-lived, persistent pollutants by OH-radicals

by

Viviane Tchendjou
From Yaounde (Cameroon)

Inaugural-Dissertation to obtain the academic degree Doctor rerum naturalium (Dr. rer. Nat.) submitted to the Departement of Biology, Chemistry and Pharmacy of Freie Universität Berlin

Berlin 2016

Erstgutachter/in: Prof. Dr. rer. nat. Eckart Rühl

Zweitgutachter/in: Prof. Dr. rer. nat. Janina Maultzsch

Tag der Disputation: 02.12.2016

To my Son

Acknowledgments

Writing scientific projets is an important and difficult challenge for every young researcher. After submitting and successfully defending my dissertation thesis, it's now the time to publish it. I would like to take this opportunity to reflect all people who have encouraged, supported and helped me during this long period.

First of all, I am very thankful to my research supervisor Professor Eckart Rühl, who has given me an opportunity to work not only under his guidance for this dissertation project, but also as scientific employee at the Institute for Chemistry and Biochemistry of the Free University Berlin.

I would also like to express my gratitude to Professor Janina Maultzsch for her endless support, valuable suggestions and unfailing assistance. It would not be intellectually honest if I do not extend my thanks to the Cameroonian scholars in Germany, namely Prof. David Pouhè, Dr. habil. Chicgoua Noubactep, and especially Dr. Patrice Ndonfack, without which, I would never have completed some experimental analyses.

In addition, I would like to thank my laboratory colleagues at the University of Yaoundé and at the Free University Berlin for their collaboration.

I would also thank my brother Brice Tchendjou for his kind words of encouragement.

I am also greatly indebted to the DAAD for having provided me a fellowship for the first years of my research in Germany.

Finally, I also express my special and sincere thanks to Professor Jacob Emmanuel Mabe for his intellectual and untiring moral assistance in the last three years of my research project. This doctoral thesis could have not been finished without his stylistic and systematic modifications.

Thank you very much, everyone!

Berlin, 12 December 2016

Abstract

Understanding the behavior of persistent organic pollutants (POPs) under environmental conditions is fundamental in shaping environmental engineering and science. POPs are organic compounds not only of substantial atmospheric life time and low vapor pressure, but also with certain chemical and physical properties which are harmful to the environment and the health. To date, research on the significance of POPs is impaired by the lack of kinetic data for assessing their environmental relevance. The present study examines the degradation by indirect photolysis of selected semi-volatile Biocides, as terbuthylazine (TBA), lindane, and simazine.

The laboratory experiments were performed with OH-radicals under normal atmospheric conditions. The experiments were carried out in a reaction chamber, where layers (mono and multi) of investigated substances deposited on nano-sized silica (Aerosil) were exposed to OH-radicals. H_2O_2 was used as the best available OH-radical source for the experimental setup. The progress of the photolysis was monitored using mainly Raman spectroscopy. IR spectroscopy data, NMR and mass spectroscopy were used as complementary methods uniquely to characterize the reaction products.

The obtained results could be rationalized by a Retro-Diels-Alder ring cleavage as an important and complementary step of herbicide degradation. The spectrum calculation was performed after structure optimization and frequency calculation with the help of the Quantum Chemistry code Turbomole or Gaussian.

Achieved results can be summarized as follows:

- In order to estimate the concentration of OH-radials formed in the reaction chamber, the reaction of terbuthylazine (TBA) with OH-radicals was considered as a reference for the indirect photolysis reaction. The OH rate constant has been calculated from the fitted rate constant at 1255 cm^{-1} as follows:

$k_{OH}(CH_2) = \lambda / C_{OH} =$ **$(3.9 \pm 0.59) \times 10^{-3} / (163 \pm 31) \times 10^{6}$** $= (2.73163 \pm 0.645) \times 10^{-11}\ cm^3 \cdot s^{-1}$

The corresponding OH-radical concentration value is the following (taking into account the lower value): **$C_{[OH]} = (163 \pm 31) \times 10^{6}$ molecules.cm^{-3} $= (2.7 \pm 0.5) \times 10^{-13}$ Mol.L^{-1}**

Using TBA for quantifying OH-radicals, we succeeded in estimating the rate constant of indirect photolysis of TBA. the results of laboratory experiments investigating the process of OH-radical formation via photolysis of aqueous hydrogen peroxide (H_2O_2), which occurs in an open storage within a reaction chamber. Other precursors for the formation of OH-radicals included nitrate (NO_3^-), ozone (O_3) and water (H_2O). However, O_3 could not be used as OH-radical source in the experimental setup used in our work because of the possibility of ozonolysis to occur. Also, the obtained levels of OH-radicals from H_2O photolysis are high in humid air.

-We showed that the Raman spectra of TBA do not practically change with time when the irradiation lamp in the reaction chamber is turned off.
-Using the Igor Pro software, we found the important physical parameter λ from the time-dependence of the intensities or areas of the observed Raman bands. It followed from the detailed analysis of the Raman bands that the overall rate constant could be realistically determined by the time-dependent behavior of the Raman band at 524 cm^{-1}.

The confidence range for the overall rate constant was defined by using the following formula: $\mathbf{0.0018 \pm 0.0003 \leq \lambda\ (524) \leq 0.0020 \pm 0.0001\ s^{-1}}$.
The corresponding range for the OH-radical concentration by considering TBA as a reference substance was determined as follows:
$(163 \pm 31) \times 10^6 \leq C_{[OH]}$ in $cm^{-3} \leq (184 \pm 9) \times 10^6$.

The rate constant of the reaction in the case of simazine was obtained from the fitted rate constant at the band 1255 cm^{-1}:
$k_{OH}(CH_2) = \lambda / C_{OH} = \mathbf{(3.9 \pm 0.59) \times 10^{-3} / (163 \pm 31) \times 10^6} = (2.73163 \pm 0.645) \times 10^{-11}\ cm^3 \cdot s^{-1}$

The rate constant of lindane for the 2992.8 cm^{-1} area was estimated as following:
$k_{OH} = \lambda / C_{OH} = (2.555 \pm 0.0376) \times 10^{-3} / \mathbf{(163 \pm 31) \cdot 10^6} = (156.442 \pm 12.129) \cdot 10^{-13}\ cm^3 \cdot s^{-1}$.

The present results allow us, not only to better understand the Raman spectroscopic method for the monitoring of TBA photolysis, but also to extend the method to the case of other pesticides under study.

Zusammenfassung

Das Verständnis des Verhaltens von den persistenten organischen Schadstoffen (englisch: POPs) unter Umweltbedingungen spielt eine Schlüsselrolle bei der Gestaltung der Umwelttechnik und Wissenschaft. POPs sind organische Verbindungen nicht nur von substantieller atmosphärischer Lebensdauer und geringem Dampfdruck, sondern auch mit bestimmten chemischen und physikalischen Eigenschaften, die schädlich für die Umwelt und die Gesundheit sind. Bis heute wird die Forschung über POPs durch das Fehlen von kinetischen Daten zur Bewertung ihrer Umweltrelevanz beeinträchtigt. Die vorliegende Studie untersucht die Degradation durch indirekte Photolyse von ausgewählten halbflüchtigen Pestiziden, wie Terbutylazine (TBA), Lindane und Simazine.

Die Laborexperimente mit OH-Radikalen wurden unter normalen atmosphärischen Bedingungen durchgeführt. Die Versuche erfolgten in einer Reaktionskammer, in der Monoschichten und Multischichten der abgeschiedenen Substanz (z.B. Lindan) von Silicat-Nanopartikel (Aerosil) zu OH-Radikalen ausgesetzt wurden. H_2O_2 wurde als die beste verfügbare OH-Radikal-Quelle für den Versuchsaufbau verwendet. Das Fortschreiten der Photolyse wurde hauptsächlich unter Verwendung der Raman-Spektroskopie überwacht. IR-spektroskopische Daten, NMR und Massenspektroskopie wurden als ergänzende Methoden zur eindeutigen Charakterisierung der Reaktionsprodukte verwendet. Die erreichten Ergebnisse konnten durch eine Retro-Diels-Alder-Ringspaltung als wichtiger und komplementärer Prozess des Herbizids Abbau rationalisiert werden. Die Spektrumkalkulation wurde nach Strukturoptimierung und Frequenzberechnung mit Hilfe des Quantenchemie-Pakets Turbomole oder Gaussian durchgeführt.

Die erzielten Ergebnisse können folgendermaßen zusammengefasst werden:

- Um die Konzentration von in der Reaktionskammer gebildeten OH-Radialen abzuschätzen, wurde die Reaktion von Terbuthylazin (TBA) mit OH-Radikalen als Referenz für die indirekte Photolyse Reaktion berücksichtigt. Die OH- Geschwindigkeitskonstante wurde von der Einbauskonstante bei 1255 cm^{-1} wie folgt berechnet:

k_{OH} $(CH_2) = \lambda / C_{OH} =$ **$(3.9 \pm 0.59) \times 10^{-3} / (163 \pm 31)\times10^{6} = (2.73163 \pm 0.645)\cdot10^{-11}$ $cm^3 \cdot s^{-1}$**

Der entsprechende OH-Radikal-Konzentrationswert ist der folgende (unter Berücksichtigung des niedrigeren Wertes): **$C_{[OH]} = (163\pm 31)\times10^{6}$ molecules.$cm^{-3} = (2.7 \pm 0.5) \times10^{-13}$ Mol.L^{-1}**

- Die Laborexperimente untersuchten den Prozess der OH-Radikalbildung via Photolyse von wässrigem Wasserstoffperoxid (H_2O_2), die in einer Reaktionskammer in einer offenen Lagerung auftrat. Andere Vorstufen für die Bildung von OH-Radikalen enthielten Nitrat (NO_3^-), Ozon (O_3) und Wasser (H_2O). Dennoch O_3 konnte in unserer Arbeit nicht als OH-Radikalquelle in dem Versuchsaufbau verwendet werden, da die Möglichkeit der Ozonolyse erfolgte. Auch die erhaltenen Mengen an OH-Radikalen aus H_2O Photolyse waren hoch in feuchter Luft.
- Wir zeigten, dass die Raman-Spektren vom TBA praktisch nicht mit der Zeit ändern, wenn die Bestrahlungslampe in der Reaktionskammer ausgeschaltet ist. Bei Verwendung der Software Igor Pro fanden wir den Reaktionsparameter λ aus der Zeitabhängigkeit der Intensitäten oder Bereiche der beobachteten Raman-Banden. Aus der detaillierten Analyse der Raman-Banden folgte, dass die Gesamtgeschwindigkeitskonstante durch das zeitabhängige Verhalten der Raman-Bande bei 524 cm^{-1} bestimmt werden konnte.

Das Konfidenzintervall für die Gesamtgeschwindigkeitskonstante wurde unter Verwendung der folgenden Formel definiert: $\mathbf{0.0018 \pm 0.0003 \leq \lambda\ (524) \leq 0.0020 \pm 0.0001\ s^{-1}.}$

Der entsprechende Bereich für die Berechnung der OH-Konzentration unter Berücksichtigung des TBA wurde folgendermaßen bestimmt:
$\mathbf{(163 \pm 31)\ x\ 10^6 \leq C\ [OH]\ molecules \cdot cm^{-3} \leq (184 \pm 9)\ x\ 10^6.}$

Die Geschwindigkeitskonstante der Reaktion im Falle von Simazine wurde aus der Einbaugeschwindigkeitskonstante bei 1255 cm^{-1} erhalten:
$k_{OH}\ (CH_2) = \lambda / C_{OH} = \mathbf{(3.9 \pm 0.59)\ x\ 10^{-3}} / \mathbf{(163 \pm 31) x 10^6} = (2.73163 \pm 0.645)\ x10^{-11}\ cm^3 \cdot s^{-1}$

Die Geschwindigkeitskonstante von Lindan für die 2992,8 cm^{-1} Gebiete wurde wie folgt geschätzt:
$k_{OH} = \lambda / C_{OH} = (2.555 \pm 0.0376)\ x\ 10^{-3} / \mathbf{(163 \pm 31) \cdot 10^6} = (156.442 \pm 12.129) \cdot 10^{-13}\ cm^3 \cdot s^{-1}$.

Die vorliegenden Ergebnisse erlauben uns, nicht nur das Raman-Spektroskopie-Verfahren für die Überwachung der TBA Photolyse besser zu verstehen, sondern auch die Methode auf andere untersuchte Pestiziden zu erweitern.

Table of contents

1. Introduction

1.1 Scientific Background

Since the first half of the twentieth century, chlorinated insecticides (Table A0.1) and polychlorinated biphenyls have been produced in high quantities in order to improve standard of living via increased agricultural yields. These chemicals belong to the group of persistent organic pollutants (POPs). Later on, POPs and related species, including chlorinated dioxins, chlorinated furans and dibenzofurans, were identified as a serious public health and environmental problem, even at low levels [1].

POPs and their reaction products also accumulate in organisms and concentrate along food chains [2]. Climate change, understood as global warming would increase the hazardous effects of POPs as increased temperatures would increase the concentration of volatiles and accelerate their atmospheric transport [3, 4, 5]. The use of POPs is still only restricted in western countries. In the developing world, POPs are still intensely used for various reasons in a wide range of application [6].

Thus, there is a universal need to mitigate contamination and pollution by POPs. The perceived environmental and social risk posed by POPs has initiated the establishment of international agreements of which the Stockholm Convention (SC) is the most important. These agreements intent (i) to protect the population and the natural resources from negative effects of POPs and (ii) to remediate or mitigate the contamination. The ambition of the SC is to promote international coordinated action to decrease the presence of POPs in the environment [2]. This effort includes the remediation of already polluted sites. The SC was signed in 1997, adopted in 2001, implemented in 2004 and currently has 178 parties [7].

Efforts to realize the objective of the Stockholm Convention go through innovative technologies aiming at minimizing the environmental impacts of POPs [8]. However, the design and the optimization of relevant technologies require profound scientific knowledge on their properties [9]. Multidisciplinary research (e.g. agriculture, biomedicine, chemical and

physical sciences) has focused on the quest for efficient methods to control the emissions of POPs [10]. Results indicate large diversities and variability in the chemical and physical properties of POPs. Chemical properties include chemical stability, redox reactivity, solubility in water, whereas physical properties include molecular size and ebullition temperature [11, 12]. Results also indicate large diversities in the used experimental procedures. It is therefore difficult (or even impossible) to reliably give a general (quantitative) overview on the environmental behavior of POPs.

Admittedly, a systematic holistic work would potentially solve this problem as the basic processes governing environmental remediation are known for decades [13]. Available remediation approaches are based on (i) adsorption, (ii) co-precipitation and flocculation, (iii) biological and chemical degradation, (iv) filtration, (v) volatilization and (vi) combinations of processes [14]. As an example, the efficiency of plants (phytoremediation) as detoxifiers, filters or traps has been proven in cleaning up soils polluted with crude oil, explosives, landfill leachates, metals, pesticides, pharmaceuticals, radionuclide, and solvents [15].

Research must also identify the physical and chemical properties that are relevant for the migration and the toxicity of POPs into organisms. Clearly, the central question from the physicochemical point of view must be answered, why POPs are persistent, immobile or mobile in the environment. These are the key factors determining the danger for the environment and human life. Relevant intrinsic properties of POPs need to be examined that influence their mobility in the geosphere**.**

Different research projects are currently defining the principles for observation, simulation, prevention, mitigation, adaptation, remediation and restoration of the natural and man-made environmental damages, including contamination [16]. Among the scientific methodologies, there are suitable techniques for surface treatment to obtain monolayer adsorbents, allowing the chemical characterization of environmental adsorption and reactive processes under controlled conditions in the laboratory. Physical chemistry can also help together with the possibility offered by the monolayer technologies to obtain more precise data on the total amount of POPs entering the environment, since the preliminary information in the available databases is highly uncertain and often insufficient [17, 18].

Despite ongoing research focusing on the biodegradation rate constants of POPs, there are still many open questions about their effects on the ecosystem and health [19]. It is clear that much more research remains to be done in developing and refining our understanding and quantification of the sources and sinks of POPs [17, 20]. One alternative is the use of short-lived pesticides. Another way is to store POPs or put them into closed systems [21]. This latter solution is unfortunately not only associated with enormous costs for user countries, but requires a collective action, that must be globally better coordinated. Research must also continue in order to optimize the scientific methods of understanding the mechanisms of degradation processes of POPs and to minimize their negative effects.

1.2 The aim of the work

The aim of the present work is to investigate the reactive degradation not of all persistent organic pollutants (POPs), but of the biocides and pesticides in the laboratory under realistic conditions, which resemble the conditions in the atmospheric environment and allow us to determine reactive processes leading to the indirect oxidation of the substances under study. In this work, it is aimed to identify the products that are formed upon these reactive processes. From a methodological point of view the suitability of mass spectroscopy, NMR and Raman spectroscopy is explored. POPs are documented to be (i) resistant to biotic and abiotic degradation (i.e. they are persistent) especially by photolysis via the actinic flux of solar radiation as well as reactions of most atmospheric trace gases, (ii) soluble in lipids (stored in fats) and slowly metabolized.

With the help of Raman spectroscopy, the degradation pathways and mechanisms can be further clarified, and with a better understanding of the degradation processes, a proper evaluation of the extent of contamination by POPs can be expected. The obtained data will enable the investigation of key factors that are relevant for the understanding of the involved chemical transformations. Moreover, advanced and adequate experimental tools to determine the rate constants of POPs (e.g. low volatile, particle-bound) will be developed.

A specific objective of the study is to validate the expected experimental approach by oxidizing the surface of the monolayer samples adsorbed on nanoparticles, which have a high surface-to-bulk ratio using Raman spectroscopy and Raman microscopy. Due to low vapor pressure under environmental conditions, it is expected that only monolayers of the samples can be formed due to the limited source strength [22]. Therefore, this work is focused on

monolayers of low volatile or semi-volatile compounds. Rate constants are determined and degradation reaction mechanisms induced by atmospheric trace gases, such as OH-radicals and ozone, are proposed.

A profound analysis of the behavior of biocides will be deepened in the following chapters of this Thesis. It should be emphasized at this point only that the measure for the elimination of biocides, which are characterized by their environmental degradation rate constant.

1.3 Methodology

The methodology employed in this research work consisted of the establishment of a reliable method for the monitoring of the OH-concentration for the indirect photo-oxidation processes of terbuthylazine by OH-radicals. This information allowed us not only to determine the rate constants of other pesticides which are currently not reliably known [23], but also to consider the chemical and physical parameters affecting the environmental life-time and the travel distance of long-living pesticides.

It is well known that OH-radicals are highly reactive species, oxidizing even inert species, such as pesticides in the atmosphere [24]. Therefore, we focused in this work on reactions of chloro-triazine derivatives with OH-radicals. This includes terbuthylazine, lindane and simazine. Note however that experimental data on the OH-induced degradation of pesticides were hardly available in the literature [25, 26, 27]

The rate constants of different classes of pesticides with OH-radicals have been estimated, especially those obtained from structure reactivity relations (QSAR), but their reliability remains uncertain [28]. This is because the rate constants of pesticides are affected by many factors, which are not always properly described by simple structure reactivity relations. In addition, environmental variability of trace gas concentrations and diurnal variations of physical parameters may also add to the complexity found in the atmospheric environment.

The specific investigations carried in this study were needed to understand in detail the mechanisms of the reaction of OH-radicals with semi-volatile compounds, such as lindane (γ – hexachloro cyclohexane; $C_6H_6Cl_6$) [29, 30] and simazine (6-chloro-N, N'-diethyl-1,3,5-triazine-2,4-diamine; $C_7H_{12}ClN_5$) [31], which are related to the atmospheric environment. To

achieve our objectives, we calculated the relative intensities of specific Raman bands in the spectrum of the investigated pesticide before, during and after the indirect photo-degradation reaction. The results obtained from the present study prove to be useful to determine the corresponding OH-rate constant in the environment.

1.4 Outline of this Thesis

This thesis consists of four chapters. It begins with an Introduction into the scientific background, followed by background information on the methods used in this work, the experimental and theoretical approach, the obtained results, and ends with a Summary and Conclusion. Furthermore supplementary information is compiled in an Appendix. The literature cited in the thesis are listed separately at the end of this Thesis

Chapter 1 is the introductory chapter, which describes the scientific background of the research leading to the need of this Thesis. It highlights the environmental role of persistent organic pollutants (POPs). A thorough characterization regarding their environmental behavior is needed for understanding how the environmental impact of POPs by indirect photo-oxidation can be described.

Chapter 2 describes the background of Raman spectroscopy, reaction kinetics of chemical processes, and theoretical models employed in this work. Furthermore, details on the development of the experimental approach regarding implementation and optimization of Raman spectroscopy, as well as methods for characterizing molecules by vibrational spectroscopy are presented. On the other hand, emphasis is put on kinetic models that can be used to describe the reaction mechanisms based on indirect photo-oxidation of pesticides by OH-radicals.

Chapter 3 is concerned with the description of the experimental setup and sample preparation. The experimental reaction chamber is described which was constructed in order to simulate atmospheric conditions in the laboratory. It also describes the method of OH-radical production in the reaction chamber by using three sources of production, namely ozone, water and hydrogen peroxide. Since the samples were inert nanoparticle substrates, it is detailed in Chapter 4 how the sample preparation made use of aerosil-R-972, an inert, hydrophobic, fumed silica. The calibration of the experiment is presented, as well as the

approach on determining the concentration of OH-radicals. Note that the latter quantity directly leads to the determination of the rate constants of the biocides studied.

Chapter 4 presents in the first part the results obtained in the framework of the research together with the discussion of these results. Firstly, the choice of the most suitable OH-radical source is discussed. Subsequently, the analysis of Raman data on reaction kinetics is used to determine the OH-concentration. In order to better understand the mechanisms of indirect photo-oxidation of pesticides by OH-radicals, two other methods for product characterization besides Raman spectroscopy are also us discussed, i.e. nuclear magnetic resonance (NMR) and mass spectroscopy. These methods also help to analyze the obtained reaction products and offer additional possibilities to explain the reaction pathway. The experimental results are compared to simulations using state-of-the-art quantum chemical calculations.

This chapter focuses in the second part on the theoretical calculations of the molecular geometries and vibrational (Raman) spectra, which are compared with experimental spectra in order to define realistic pathways for the indirect photo-degradation processes of the investigated semi-volatile organic compounds. Here, model simulations are performed to describe the vibrational modes of the molecules, including terbuthylazine (TBA), simazine and lindane, as well as their oxidation products.

Last but not least, a summary of the environmental effects of the biocides is presented.

Chapter 5 compiles the conclusions from this work. Here the Thesis's main results and contributions are summarized. Alternative strategies for environmental improvement and future prospects are briefly discussed.

2. Background and methods

2.1 Pesticides in the environment and degradation processes

2.1.1 Transport and degradation processes

To understand the mechanisms of transportation of pesticides, it is necessary to characterize the primary processes that determine their decomposition in soils and surface waters. All analytical models used to measure the reactivity of biocides or to describe their dispersal process showed that their degradation in the environment is low (10%) [32]. Apart from their biodegradation, biocides and their reaction products are formed during atmospheric combustion process or interactions with OH radicals or ozone. They also result from various common processes like (i) the incineration of hospital, household and industrial wastes, (ii) the production of electrical and thermal energy, (iii) the use of coal and wood to heat buildings and (iv) forest fires. Moreover, POPs are mostly characterized by (i) their high stability in the environment (persistency), (ii) their acute toxicity to humans and other organisms, (iii) their potency for bioaccumulation, and (iv) their semi-volatility [33]. These four (4) characteristics make POPs a source of environmental and human health hazards in all regions of the world as they can travel very long distances, mainly in the atmosphere (see Figure 2.1) [34, 35, 21, 36, 37].

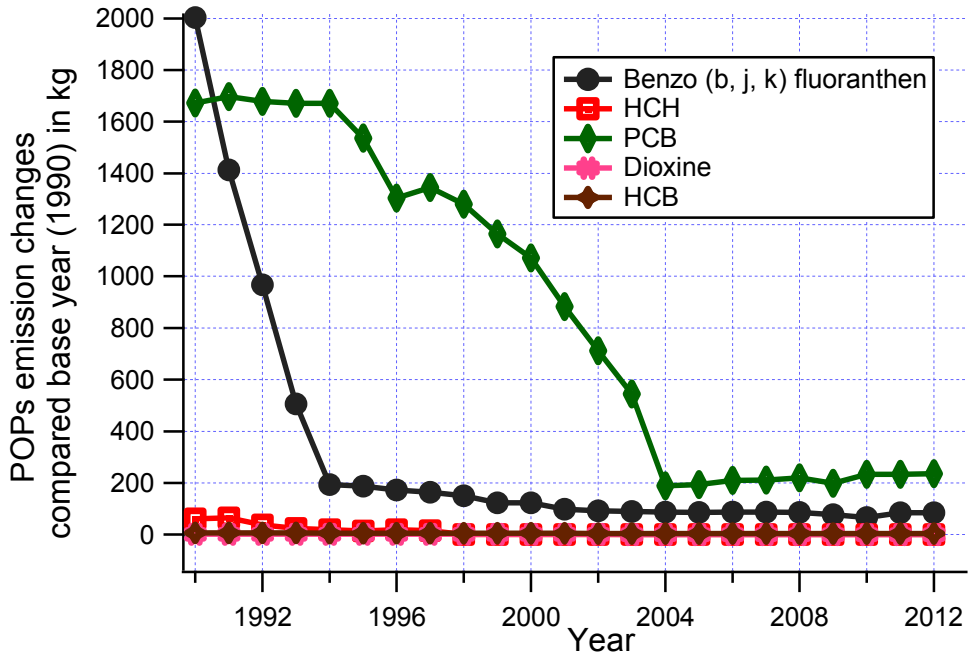

Figure 2.1: Emissions of selected persistent organic pollutants (POPs) during 1990–2012. The selected POPs are representative for Benzo (b, j, k) fluoranthen, HCH (Lindane), PCB (polychlorinated biphenyls), Dioxine and HCB (hexachloro benzene). Plotted data are from ref. [38]. The lines connect points to facilitate visualization.

2.2 Spectroscopic methods for the detection of pesticides

Raman spectroscopy is an approach that can be used to investigate the molecular structure by inelastically scattered radiation [39]. This technique is complementary to infrared (IR) spectroscopy [40] and is mainly used to analyze molecular vibrations. It is named after the physicist Chandra Sekhara Venkata Raman (1888–1970) who experimentally demonstrated the effect of the inelastically scattering of light in 1928. Strictly speaking however, Raman presented the experimental validation of an effect theoretically predicted by Adolf Gustav Stephan Smekal (1895–1959) five years earlier (1923) [41] and was awarded the Nobel Prize in physics in 1930 [42]. Fundamentally, Raman spectroscopy and IR spectroscopy provide information about the vibrations of molecular bonds where the observed Raman or IR bands correspond to the allowed transitions between different vibrational energy levels [43].

Raman spectroscopy has gained increasing interest as a powerful characterization tool in chemistry, physics, and related disciplines. Due to its versatility, it is used for the analysis of the composition of liquids, gases, and solids [44]. Raman spectroscopy is based on the Raman effect, which is the inelastic scattering of photons of a monochromatic source by the sample. The Raman effect is termed inelastic because during the scattering process, partial energy

exchange takes place between the incident photon and the scattering molecules, such that the amount of energy exchanged corresponds to a transition between specific energy levels which are less energetic than the incident light energy (e.g. vibrational levels or rotational levels in the case of an incident photon in the near UV, visible, and near IR).

Specifically, in Raman scattering, either the scattered photon is less energetic (red-shifted) than the incident photon and the corresponding process is termed Stokes Raman scattering or it is more energetic (blue-shifted) than the incident photon and the corresponding process is termed anti-Stokes Raman scattering. The anti-Stokes process is only possible if the molecule was already in a thermally excited state before the interaction with light so that the scattered photon can gain energy from the molecule. As a result, at room temperature the anti-Stokes process may be rather weak in intensity, so that often the Stokes process is commonly used in practice for spectroscopic studies.

The development of Raman spectroscopy was initially closely related to that of detection systems for the measurement of light intensity. The first photoelectric-based Raman detector was mentioned in 1942 by Rank and Wiegand [45]. It was followed by the development of photomultipliers and then the introduction of charge coupled device (CCD) detectors (with the introduction of the Cary Model 81 Raman spectrometer) [46]. Subsequently and most importantly, research was focused on the development of improved excitation sources, from lamps of various elements (He, Hg, etc.) [43, 44] to laser sources (Ar^+; Kr^+; Nd:YAG lasers) for the implementation of Raman spectroscopy [44, 47]. In the 1960s, important developments in the Raman instrumentation took place, which led to higher quality of measurements. Despite the development of lasers, Raman spectroscopy remained confined in scientific laboratories for many years. Moreover, Raman spectroscopy was heavily limited by fluorescence which is a relatively much stronger light emission from the sample and can interfere with the weak Raman signal.

While prism setups were used for the dispersion of scattered light in early Raman systems, holographic gratings first appeared in 1968 [46], what led to the expansion of commercial Raman scattering instruments. In the 1970s, array detectors were introduced to replace photomultiplier tubes that were used with scanning spectrometers [44]. The 2-dimensional charge coupled device (CCD) detectors helped to reduce the measurement time from hours to minutes. In the 1980s, the introduction of fiber optic probes followed [44, 47] for the first

process measurements [45]. At the same time, interferometer-based Raman systems that employed 1064 nm lasers were also introduced [46].

Progress in the development of Raman spectroscopy continued through 1986 with the introduction of a commercial interferometer based on Fourier transform Raman (FT-Raman) analysis, which was combined with a near infrared excitation source for the measurement of Raman spectra [48]. The application of this technique showed that the near infrared laser excitation not only could reduce the sample fluorescence thereby making the measurement of fluorescing samples possible, but also allowed for the use of more powerful lasers without the risk for photo-decomposition of the sample.

Many FT-Raman measurements therefore expanded considerably [39, 46, 49, 50, 51, 52]. The database of spectroscopic information obtained with the help of Raman spectroscopy was comparable and/or complementary with the information available or obtained from infrared absorption spectroscopy. As mentioned above, the Raman spectroscopy technique is based on inelastic scattering. In the scattering process, the emission of the inelastically scatted light (i.e. the Raman signal) by a substance is accompanied by strong Rayleigh scattering (named after Lord Rayleigh who first discovered elastic light scattering), which is based on the elastic scattering of photons. In practice, Rayleigh scattering can be separated from the weak Raman scattering [53, 54] by using a Notch filter.

From 1990, there were two new optical elements that simplified the optical designs of Raman spectrometers, which consisted of the analysis of the scattered light collected using a lens [55]. Today, except for medical, biochemical or industrial applications, Raman microscopy has become the second favorite technique (after IR) for the analysis of geomaterials or biomaterials in the archeology, history, arts etc [56].

It helps to identify the natural origin and artificial gems of materials via the identification of micro-inclusions.

A typical Raman experimental setup is composed of:

- A laser source and eventually a laser line filter;
- A sample holder;
- Optical elements for directing the incident exciting light to the sample, for collecting the scattered light and for the coupling of the light with the spectral analysis device;
- An optical filter to remove Rayleigh scattering before spectral analysis;

- A spectrometer (single, double or triple monochromator) as the spectral analysis device;
- A sensitive light detector;
- A user interface for the acquisition and the treatment of spectral data.

It was readily found that the use of a triple monochromator Raman spectrometer is more efficient in rejecting stray light than a double monochromator, which in turn was more efficient than a single monochromator spectrometer [57]. It is also possible to use a triple Raman spectrometer without the need for a Notch filter. This is because a triple spectrometer is made of three spectral analysis stages or elements and the two first stages can be arranged in subtractive manner in order to reject Rayleigh scattering before analysis by the final stage.
Laser line filters serve to transmit the laser line while supressing other ambient light [58]. Hence, line filters are used to reduce the spectral noise of the laser source and to pass only the desired laser wavelength through a steep transition. The use of laser line filters and notch filters facilitates the simultaneous measurement of the Stokes and anti-Stokes Raman scattering [59]. If the energy shift, $w_1 - w_2$, of the scattered light waves from the incident one it is called Stokes shift, then scattered light waves with positive Stokes shifts are called Raman Stokes lines, and those with negative Stokes shifts are called Raman anti-Stokes lines [60]. The Stokes and anti-Stokes components contain the same frequency information.

The most Raman experiments look at the Stokes-shifted scatter.The Raman effect has a very rich history and offers various applications in chemistry, physics, biology, medicine, pharmacy, archaeology etc. [61]. Raman spectroscopy constitutes today a very versatile technique. On the one hand many different variations of the technique are possible, such as e.g., linear or spontaneous Raman, nonlinear Raman, FT Raman, optical activity Raman, etc. [62, 63]. On the other hand, many other aspects including the following are worth mentioning:

- Characterization of the molecular composition of a material in different states of matter (solid, liquid, gas) and in a wide range of temperature.
- Little to no sample preparation is needed.
- Non-destructive analysis is possible.
- The study of aqueous solutions is possible in contrast to IR absorption and the measurement through glass window is possible, allowing remote detection.
- A spatial resolution in microscopy (1 to 5 µm depending on the laser used).

In some modern Raman spectroscopy instruments such as triple Raman spectrometers, Raman shifts from the laser line down to 10 cm^{-1} or lower can be measured. This allows the visualization of low energy motions in crystalline compounds.

2.2.1 Classical Raman effect

The Raman effect is based on the inelastic scattering of a photon by a molecule [63, 64, 65]. When light hits matter, it may be scattered in different ways. When a diatomic molecule is irradiated by light, an electric dipole moment μ is induced, which is dependent on the polarizability α of the molecule and on the electric field E created by the incident radiation at the location of the molecule [66], as follows:

$$\mu = \alpha E \tag{1}$$

Equation (1) sets the basis for both the classical and the quantum mechanical treatment of Raman scattering [67]. Let consider the incident optical electric field to be a plane wave expressed by Equation (2):

$$E = E_0 \cos 2\pi \nu_0 t \tag{2}$$

Here, ν_0 is the frequency of the incident light and E_0 is the amplitude of the electric field. Equation (3) will become,

$$\mu = \alpha \ E_0 \cos 2\pi \nu_0 t \tag{3}$$

In the harmonic oscillator approximation about the equilibrium configuration of the atoms vibrating in a molecule with a frequency ν_m, the nuclear displacement q is expressed as follows in Equation (4):

$$q = q_0 \cos 2\pi \nu_m t \tag{4}$$

Here, q_0 is the vibrational amplitude. Since the polarizability α depends on the molecular coordinates, for small displacements "q", α can be expanded in a Taylor series about the equilibrium configuration ("*O*") of the molecule as follows [68]:

$$\alpha = \alpha_O + \left(\frac{\partial \alpha}{\partial q}\right)_O q \ + \left(\frac{\partial^2 \alpha}{\partial^2 q}\right)_O q^2 + \ldots. \tag{5}$$

Where α_0 is the polarizability of the molecule at the equilibrium configuration and $(\partial\alpha/\partial q)_O$ is the rate of change of α with respect to q, evaluated at the equilibrium configuration. By substituting the above relations equation (2), (4) and (5) into equation (1), we can rewrite and organize equation (1) as follows:

$$\begin{aligned}
&\mu = \alpha E \\
&= \alpha E_0 \cos 2\pi \nu_0 t \\
&= \left[\alpha_O + \left(\frac{\partial \alpha}{\partial q}\right)_O q_0 \cos 2\pi \nu_m t\right] E_0 \cos 2\pi \nu_0 t + \left[\left(\frac{\partial^2 \alpha}{\partial^2 q}\right)_0 q_0^2 . \cos^2 (2\pi \nu_m t)\right] E_0 \cos 2\pi \nu_0 t + \ldots \\
&= \alpha_O E_0 \cos 2\pi \nu_0 t + \frac{1}{2} E_0 q_0 \left(\frac{\partial \alpha}{\partial q}\right)_O \left[\cos 2\pi (\nu_0 + \nu_m) t + \cos 2\pi (\nu_0 - \nu_m) t\right] \\
&+ \frac{1}{2} E_0 q_0^2 \left(\frac{\partial^2 \alpha}{\partial^2 q}\right)_0 \cos(2\pi \nu_m t) \left[\cos 2\pi (\nu_0 + \nu_m) t + \cos 2\pi (\nu_0 - \nu_m) t\right] + \ldots \\
&= \alpha_O E_0 \cos 2\pi \nu_0 t + \frac{1}{2} E_0 q_0 \left(\frac{\partial \alpha}{\partial q}\right)_O \left[\cos 2\pi (\nu_0 + \nu_m) t + \cos 2\pi (\nu_0 - \nu_m) t\right] + \frac{1}{2} E_0 q_0^2 \left(\frac{\partial^2 \alpha}{\partial^2 q}\right) \\
&\left[2 \cos 2\pi \nu_0 t + \cos 2\pi (\nu_0 + 2\nu_m) t + \cos 2\pi (\nu_0 - 2\nu_m) t\right] + ..
\end{aligned} \tag{6}$$

Here, the first term in equation (6) represents an oscillating dipole that radiates light of the same frequency ν_0 as the incident radiation; this corresponds to Rayleigh scattering. The second term depends of the molecular vibrational frequency ν_m and represents anti-Stokes scattering $\cos[2\pi(\nu_0 + \nu_m) \cdot t]$, Stokes scattering $\cos[2\pi(\nu_0 - \nu_m) \cdot t]$. Rotational Raman scattering may occur only when the polarizability of the molecule is anisotropic [69]

but for vibrational Raman spectroscopy there is a need for a change in polarizability upon vibrational excitation. In fact, if $(\partial\alpha/\partial q)_0$ is zero, the vibration is not Raman-active. Also if the fields are weak, then the linear effect of polarizability tensor is limited to:

$$\mu = \alpha E$$

But in the case of strong fields, for example in lasers, the equation is rewritten:

$$\mu = \alpha E + \beta E^2 + \gamma E^3 + ...$$

The effects of non-linear optics (NLO) are considered and the term β is called hyperpolarizability. Thus, for a given vibrational mode "q" to be Raman-active, the rate of change of the polarizability (α) with respect to the vibration must be non-zero: this represents the selection rule for Raman scattering. The above classical treatment correctly describes the frequency dependence of the scattered light. However, concerning the scattered light intensity, there are discrepancies between the classical theory, which predicts the same intensity for both Stokes and anti-Stokes Raman scattering and the experiment, which shows that the anti-Stokes bands are much weaker. In reality the Raman scattering intensity is proportional to the number of scattering molecules, and the population of molecules in the vibrational ground state (at $\nu = 0$) is much larger than that in the excited vibrational states at $\nu = 1$, 2, and so on (Maxwell-Boltzmann distribution law holds). The population at different energy levels is described by the Boltzmann distribution given by equation (7):

$$\frac{N_n}{N_m} = \frac{g_n}{g_m} \exp\left[\frac{-(E_n - E_m)}{kT}\right] \qquad (7)$$

Where N_n is the number of molecules in the excited vibrational energy level (n), N_m is the number of molecule in the lower vibrational energy level (m), E_n and E_m are energies of the vibrational levels (n) and (m), respectively, k is the Boltzmann constant (1.3807 x $10^{-23}\ J \cdot K^{-1}$), and g is the degeneracy of the levels n and m. For most states, g equals 1, but for degenerate vibrations, it is greater than 1. As the consequence of the Boltzmann distribution, the Stokes lines are much stronger than the anti-Stokes lines under normal conditions [70]. As a matter of fact, it is customary to measure only the Stokes side of the Raman spectrum at room temperature.

In comparison with infrared spectroscopy (IR), Raman scattering provides the same vibrational information. However, while the selection rule for Raman scattering is defined by

a non-zero change of the polarizability with respect to the molecular motion, IR activity (i.e., IR selection rule) is given by a non-zero change in the dipole moment during the molecular motion, and therefore, not all vibrational modes of a molecule are Raman or IR active [71, 72]. For this reason, Raman scattering and IR absorption are complementary [73, 74]. The signal intensity for different modes can differ dramatically between IR absorption and Raman scattering. In molecules with a center of inversion, which leads to mutual prohibition, vibrations are either symmetrical and Raman active or asymmetric and IR active [75].

2.2.1.1 Resonance Raman Spectroscopy

The most dominant scattering method is undoubtedly the elastic scattering (Rayleigh scattering), which is due to the electron cloud relaxation without any nuclear movement [76]. The interaction of light with electrons which leads at the same time to the movement of nuclei involves Raman scattering or inelastic scattering. Therefore the inelastically scattered light may have a longer (Stokes shift) or shorter (anti-Stokes shift) wavelengths than the incident light [77]. These shifts provide information about the characteristic excitation energies of rotations and vibrations in the investigated substance.

The theory of Raman scattering is based on the principle that electromagnetic (EM) radiation consists of an oscillating electric field that can interact with the molecule such that energy is either gained or lost by the incident photon. The polarizability of the molecules plays the decisive role for Raman scattering; when light propagates and passes over a molecule, the radiation releases the electromagnetic energy which can interfere and deform the electronic cloud around the nuclei. Since Raman spectroscopy relies on inelastic scattering, molecules undergo vibration due to transfer of energy between the light quanta and the material [78, 79]. For Raman spectroscopy, the incident light should be monochromatic and can be obtained from laser sources with wavelengths in the visible and near infrared range (light between 400 and 700 nm) [80, 81].

A photon incident to a molecule can be scattered elastically (Rayleigh scattering) or inelastically (Raman scattering) as depicted in Figure 2.1. The scattering of an incident photon of frequency E_0 by a molecule may be considered to simultaneously involve the transition of the molecule from an initial state of energy E_i to a vitual state (i.e without excited state formation) and then to a finial state of energy E_f with the emission of a photon

(the scattered photon). In general the final state of the molecule after interaction with the photon is the same as the initial state and the scattered photon has the same energy as the incident photon, and the corresponding process is known as elastic scattering (i.e. with energy exchange) and called Rayleigh scattering. When the finial state of the molecule after scattering is different from the initial state, the corresponding process is said to be inelastic (i.e. with energy exchange between the photon and the molecule) and called Stokes Raman scattering or anti-Stokes Raman if the final state is a higher or lower energy state, respectively. Therefore, the inelastically scattered photon is weaker (Stokes Raman scattering) or higher (anti-Stokes Raman scattering) in energy than the incident photon.

The corresponding photon energy difference equals the change in the molecule's internal energy by a small amount that for instance corresponds to the change in the vibrational energy of the molecule, and the overall process simple correspond to a vibrational transition with a change of +1 or -1 in the vibrational quantum number. In normal conditions, the initial state of the molecule is usually the electronic ground state and the Stokes Raman process is the most likely process as opposed to the anti-Stokes process which requires the molecule to already be in an excited state (i.e e.g. excited vibrational state) before a scatting interaction with light. For this reason the anti-Stokes process becomes probable only at high temperatures [82, 83, 84].

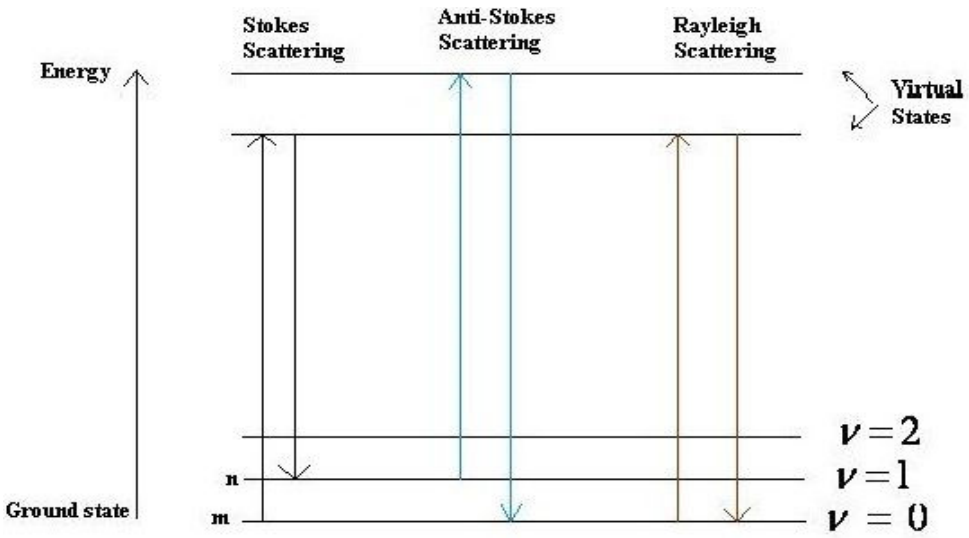

Figure 2.2: Energy level diagram of molecular light-scattering processes.

2.2.1.2 Raman microscopy

Recent advances in laser physics have given rise to a Raman technique combined with optical microscopes which can offer a spatial resolution. Today, the Raman microscope is a laser-based apparatus for implementing Raman spectroscopy for chemical imaging. By measuring Raman spectra at numerous locations, Raman spectroscopy profiles of the sample surface is obtained, which can be used to construct multidimensional hyperspectral imaging of the mapped sample plane. Moreover, confocal Raman microscopy offers the possibility to create "Raman cubes" in order to achieve a 3-dimensional (3D) profiling for transparent samples. In this variant of Raman microscopy, the confocality is realized by tightly focusing the scattered light through a small pinhole (this confocal pinhole can be adjustable in most today's commercial Raman devices) before re-collimating it, what helps to reject out-of-focus light. A similar confocal arrangement can also be inserted in the path of the incident laser beam to further improve resolution in 3D [85, 86].

Also, the 3D resolution is essential for imaging tissues or cellular structures. With Raman microscopy, one can easily identify polymorphic structures of a material and also get some information on the thermodynamic conditions of their formation [87]. The optical microscopic method allows the identification of the physical structures of the material analyzed and chemical composition. Therefore, it is possible to make *in situ* analyses using transportable optical probes [88]. In Raman microscopy, a customized microscope setup is coupled to a high grade Raman spectrometer, thus providing a sophisticated platform capable of producing conventional images in addition to generating Raman spectra from sample areas approaching the diffraction limit (≈ 1 micron) [89]. This combination enables high spatial resolution and sensitivity. The important characteristics of Raman microscopy are directly related to both the focusing of the incident laser radiation onto the sample and the collection of the scattered light through high numerical aperture microscope objectives.

Next to Raman spectroscopy, a Raman micro-spectrometer is best suited for the analysis of the first molecular layers of the surface of particles. Depending on how the Raman signal is detected, there are two types of Raman spectrometers: conventional and Fourier Transform Raman spectrometers, both of which can be fitted with a microscope. In association with chemometrics, Raman microscopy is able to resolve the heterogeneity within the samples even on the micron scale. It allows a better understanding of the processes of formation and

aging of atmospheric particles [90]. In this connection, the essential characteristics of Raman microscopy is based on its ability to identify and to study the impact of environmental contaminants (dyes, heavy metals, emerging substances, pesticides) [91, 92]. Note however that chemical imaging based on spontaneous Raman scattering (i.e. linear Raman) is relatively slow due to the weak Raman effect. Hence, in order to obtain fast chemical imaging, nonlinear Raman processes, such as stimulated Raman scattering (SRS) and coherent anti-Stokes Raman scattering (CARS) can be used [93].

Raman microscopy retains the studied sample throughout the experiment, since it is not destructive and ideal for optical characterization, but as already stated above, it has some limitations [94, 95], such as the rather long data acquisition time. Some minerals and particularly compounds of complex structure may require long data acquisition times. This is often due to the strong absorption of the laser light by opaque samples.

Despite all efforts for the development of Raman microscopy since 1990, this technique has remained a second choice in industrial laboratories behind IR spectroscopy, especially because of the problem caused by the sample fluorescence, although the use of laser excitation in the near-infrared (e.g. at 1,064 nm) makes it possible to eliminate this problem.
In Raman microscopy, fluorescence has an extraordinary sensitivity which can mask the low Raman scattering [96]. This is common when organic materials and minerals are in the same medium under investigation.

2.2.2 Mass spectrometry

The low concentrations of pesticides and their products in the medium can be determined by using mass spectrometric methods. This method is based on series of operations, such as extraction and purification of pesticides from air, sediment, living things and more other. The pesticide residues are separated and purified from co-extracted and clean-up. Then the sample concentration and its pesticide residues are identified by mass spectrometry. The separation or purification of target species can be done either by extraction into organic phase other by extraction of unwanted substance into organic phase.

The extraction involves the distribution of solute between two phases. The extraction efficiency of the method is constant ratio of the concentration of the solute in each solvent at equilibrium (K) (see Equation (8)):

$$K = [solute]_{org} / [solute]_{aq} = [W_{org} / V_{org}] / [W_{aq} / V_{aq}] \quad (8)$$

Where org and aq refer to organic and aqueous layers, W/V are mass/volume and K is independent of the amount of the two solvents mixed. In this work, it is used Agilent 6210 ESI-TOF (time- of-flight) method because it described the direct determination of pesticides and facilitates the detection of pesticides with more accuracy [97].

2.2.3 Nuclear magnetic resonance (NMR)

Proton NMR is a research method to identify and characterize pesticide compounds. Since most of the pesticides studied contain chlorine atom(s), proton NMR is able to identify all chlorinated products [98]. NMR is an inherently high sensitivity method. Hence the NMR experiment has to be conducted in lower pesticides concentration. The NMR technique can help to confirm and determine the percentage of isomers present in a sample. In principle, NMR helps to detect and quantify the number of magnetically distinct atoms of the type being studied. In this work, NMR spectra were recorded using the Bruker Avance III, 700 MHz SB US magnet spectrometer. They are four information which can be obtained from NMR spectra that are chemical shift, integrated intensity, relaxation time, and coupling constant. The chemical shift is investigated to determine the type of protons present in sample and its specific types like methyl or methylene. The NMR (particularly ^{1}H-NMR) characterizes spin-spin coupling [99].

2.3 Lasers

Lasers provide the appropriate radiation source for Raman spectroscopy, since the light which illuminates the sample has to be monochromatic and intense. Their wavelength choice affects the experimental capabilities regarding the sensitivity of the detection system to the laser wavelength, the spatial resolution and the sample behavior to the color of the laser line.

Laser light is generated by stimulated emission based on the creation of a population inversion [100]. As far as the lasers used in Raman spectroscopy are concerned, the important considerations are that shorter wavelength (close to molecular absorption resonances) and high intensity laser radiations are mostly preferred, since this helps to compensate the inherently weak signal intensity of spontaneous inelastic scattering [101, 102]. Regarding Raman spectrometers, the systems which commonly disperse the Raman and/or the FT-Raman signal are those with laser wavelengths less than 900 nm and the nondispersive systems are those with lasers wavelength of 1064 nm. Practically all integrated FT-Raman systems use a 1064 nm laser. To insure the precision of the Raman shift and to avoid line broadening, it is important to choose the frequency stability below 1 cm^{-1}. Therefore, the laser frequency must remain stable. In output line width, lasers can vary between 100 cm^{-1} and less than 1 cm^{-1}; but such lasers with output line width less than 10^{-4} cm^{-1} are unnecessary for analytical Raman applications.

Note however that the suitable choice of the laser wavelength can be limited by an overwhelming strong fluorescence from absorbing samples at shorter excitation wavelengths. In such cases, excitation in the deep UV or in the near IR is preferred. Nevertheless, several technical variations such as surface enhanced Raman scattering (SERS) help to overcome the low scattering cross section of the spontaneous Raman scattering and sometimes to quench fluorescence.

The beam divergence of a laser beam is the measure of the expansion of the beam far from the location where the beam radius has a minimum. When this angular spread as the beam leaves the laser head is equal to zero, then at this time, we can speak about perfectly collimated beam, but it is impossible to have these cases because the spreading of the laser beam is usually in conformity with the predictions of the diffraction theory. For example, consider a beam focused by a lens with focal length f_1, the beam radius w_0 at the focal point is given by,

$$2\, w_0 = f_1 \cdot \theta \qquad (9)$$

where θ is the divergence in radian. The divergence of the beam depends on the type of the laser. Therefore, for an Ar^+ laser, the angle divergence is less than 10^{-3} rad and for diode laser, the angle is more than 0.5 rad.

Concerning the Nd:YAG laser used in this work, it should be noted that it is a four-level gain medium. The width of this frequency range is small but this allows high efficiency and therefore low threshold pump power (see Figure 2.3).

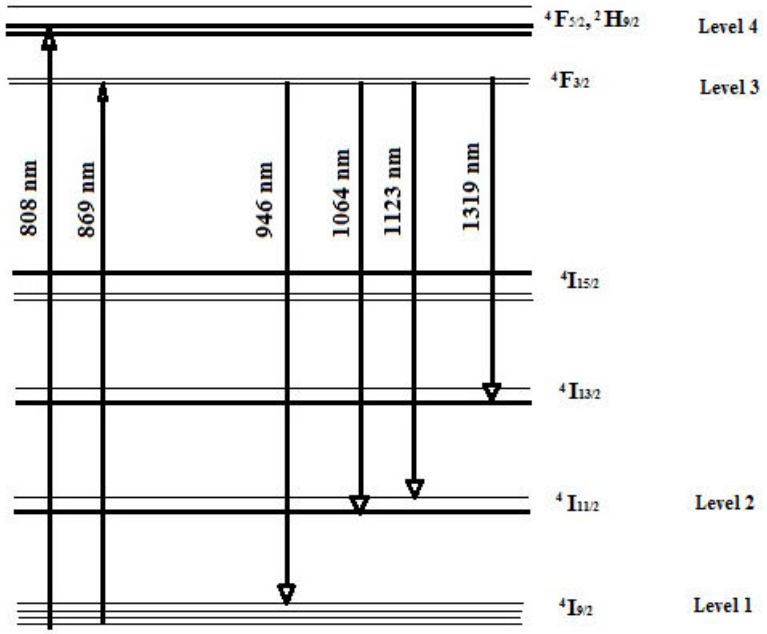

Figure 2.3: A four-level laser energy diagram use instead the level diagram of a Nd:YAG-laser. Source: Authors' own compilation and research

As depicted in Figure 2.3, in order to achieve a population inversion, for Nd:YAG-laser several excited states is needed. In such a laser, the solid-state lasers in the ground state are excited into a higher level 4 (pump band) by the pumping transition. From level 4, the atoms can decay, non-radiative process into the lower lying level 3. Since the lifetime of the lasing level (level 3) is long compared to that of the higher level 4, the population accumulates in level 3, which may relax by lasing stimulated emission into level 2. From this level, a fast, non-radiative decay into the ground state should occur and the cycle resumes.

The Nd:YAG is a Neodymium-doped yttrium aluminum garnet ($Y_3Al_5O_{12}$). Both the Nd:YAG laser fundamental line (at 1064 nm) and frequency doubled line (532 nm) are widely used for FT- and dispersive Raman spectroscopy. In a compact laser head high performance pumping of the diodes generates several Watts of 532 nm output.

2.4 Reaction kinetics

2.4.1 Fundamentals of kinetics

2.4.1.1 Reaction monitoring

In this Section, we describe the fundamental aspects related to reaction kinetics, the aim of which is to define the rate of chemical processes broken into a sequence of one or more single processes known either as elementary processes, elementary steps, or elementary reactions [103]. A kinetic analysis is used to determine the reaction rates and the factors that affect them as far as the algebraic relationship between time and the concentration of either reactants or reaction products is expressed. There are several methods for monitoring a chemical reaction and determining the concentration versus time, namely spectroscopic methods (UV-Vis, IR, Raman spectroscopy), polarimetry, electrochemistry, chromatography, etc.

With vibration spectroscopy techniques, one can well determine empirical kinetics. In the framework of this work, Raman spectroscopy is the favorite and preferred vibrational spectroscopic technique (IR absorption is limited by water). Raman spectroscopy allows non-destructive analysis with little or no preparation or extraction, remote detection and/or on-line and real-time detection. Moreover, because Raman spectroscopy also allows for the description of physicochemical chemical changes in the gas, liquid and solid phase, and can access small amounts of sample, it is a specific and well suited tool for monitoring reaction kinetics [104]. Despite the above advantages, one should recall that Raman spectroscopy can suffer from some limitations, such as low sensitivity, interfering fluorescence background that limits the study of colored substances [105].

2.4.1.2 Reaction rate

The rate of reaction is defined with respect to reagents (rate of disappearance) or products (rate of appearance) and it shows how slowly or quickly the chemical processes take place. Mathematically, the reaction rate “r” is defined as the rate of decomposition per unit volume (Equation 10).

$$r = -\frac{1}{V}\frac{dn}{dt} \tag{10}$$

Where r is expressed in mol per unit time unit volume and n is the number of moles. Since the rate of formation will have the opposite sign, the negative sign is by definition required for the rate of decomposition to be a positive number. The kinetics of a reaction determines the rate law for the given reaction, including the value for the rate constant.

2.4.1.3 Elementary reactions

Many reactions go through a series of steps via the collisions of the molecules and do not proceed in a single step. Each of these steps is called an elementary reaction. Thus an elementary reaction is a chemical reaction in which one or more of the chemical species react directly to form products in a single reaction step and with a single transition [106]. The number of reacting entities in an elementary reaction is the molecularity. Elementary reactions are either unimolecular, bimolecular, or termolecular.

A unimolecular elementary reaction involves a single molecule:

$$A \rightarrow products$$

At a constant temperature, the rate of such a reaction is proportional to the concentration of the reactant A :

$$\frac{d[A]}{dt} = -k[A]. \tag{11}$$

A bimolecular elementary reaction involves two molecules as follows:

$$A + B \rightarrow products$$

At constant temperature, the rate of a bimolecular reaction is proportional to the product of the concentration of the reacting species A and B :

$$\frac{d[A]}{dt} + \frac{d[B]}{dt} = -k[A][B] \tag{12}$$

A termolecular reaction involves the collision of three molecules at the same place and time:

$$\frac{d[A]}{dt} + \frac{d[B]}{dt} + \frac{d[C]}{dt} = -k[A][B][C] \tag{13}$$

Among all these reactions, the termolecular reaction is rare due to the fact that the probability is low to have three-reactants in simultaneous collisions (e.g. in the gas phase). Hence,

termolecular reactions can usually be broken down into a more fundamental set of bimolecular reactions [107]. However, it is not easy to derive the overall reaction scheme in this case, but solutions based on equations describing the reaction rate are possible in terms of steady-state reactions. As has been assumed above but in the following discussion, the different reaction kinetics discussed describe processes which run only in one direction, without considering an eventual reversibility of the reactions. In many systems, there are often equilibrium reactions.

2.4.1.4 Order of reaction

It is necessary to know the order of the reaction because it enables the concentration of the products to be accurately determined at any time if the rate constant is known. In general, let's consider the reaction of components A and B with the rate constant k (see Equation (14)):

$$x\ A\ +\ y\ B \xrightarrow{k} products \tag{14}$$

Where A and B are the reactants, k is the rate constant, and x, y are stoichiometry coefficient.

The differential rate law can be expressed for any one of the reactant as follows (see Equation (15)):

$$-\frac{d[A]}{dt} = k[A]^x[B]^y \tag{15}$$

where [A] and [B] are the concentrations of the reactants A and B, respectively.

The order of reaction is defined as the index or exponent that relates the rate of a chemical reaction to the concentration of the reacting substances [108]. The sum of all the exponents of the terms expressing concentrations of the molecules or atoms is the order of reaction (see Equation (16)):

$$\begin{aligned} Rate &= k[A]^x \cdot [B]^y \\ order\ of\ reaction &= x + y \end{aligned} \tag{16}$$

x and y are the partial orders of the reaction with respect to the reactants A and B, respectively. The unit of the rate constant k is depends on the order of reaction. For example,

given some values of the order of the reaction, the units of the corresponding rate constant are compiled in the following in Table 2.1:

Table 2.1: Unit of the rate constant k for a given order of the corresponding reaction

Order of reaction	**Unit of k**
0	$mol \cdot L^{-1} \cdot s^{-1}$
1	s^{-1}
2	$L \cdot mol^{-1} \cdot s^{-1}$
N	$mol^{1-n} \cdot L^{n-1} \cdot s^{-1}$

2.4.1.5 Zero-order reactions

Zero-order reactions are reactions in which the rate does not depend on the concentration of the reactants [109]. This means that the rate of the reaction is equal to the rate constant (k) of that reaction. In such reactions, the surface is generally saturated by the reactants. The form of the rate law is follows:

$$r = -\frac{d[A]}{dt} = k[A]^0 = k = cons\tan t \qquad (17)$$

where r is the reaction rate, and k is the reaction rate constant, which has unity of mol/L·s. The half-life of a reaction is the time needed for half of the reaction to completed. Zero-order reactions are characterized by their half-life given by Equation (18):

$$t_{\frac{1}{2}} = \frac{[A]_0}{2k} \qquad (18)$$

Hence, in a zero-order reaction, the half-life depends on the initial concentration of reactant and on the rate constant. Zero-order reactions occur when the rate of reaction is limited by physical factors and not by the concentrations of the reactants.

2.4.1.6 First-order reactions

A first-order reaction is a reaction which depends only on the concentration of one reactant (meaning unimolecular). Other reactants may be present, but do not contribute to the overall rate. The form of the rate law for this kind of elementary reactions is Equation (19):

$$r = -\frac{d[A]}{dt} = k[A]^1 = k[A] \tag{19}$$

where k is the first-order rate constant in units of 1/s.

The integrated rate equation for the first order reaction is given by:

$$[A] = [A]_0 \exp(-kt) \tag{20}$$

It is an exponential decay of concentration with time. The plot ln[A] against the time is a straight line for which the rate constant is the negative slope. The half-life of a first-order reaction is the time required to reduce the reactant to half of its original amount; it is constant and independent of the initial concentration. The relationship between the rate constant and the half-life of a first order reaction is as follows [110]:

$$t_{\frac{1}{2}} = \frac{\ln(2)}{k} \tag{21}$$

2.4.1.7 Second-order reactions

A second-order reaction is a reaction between two identical or different reactants which are combined in a single elementary step. One example of second order reaction is expressed by:

$$A + B \rightarrow C + (...)$$

The sum of the exponents in the rate law is equal to two.

If the two reactants are the same, the rate law is:

$$r = -\frac{d[A]}{dt} = k[A][A] = k[A]^2 \quad (22)$$

where k is the second-order reaction rate constant with units of $L \cdot mol^{-1} \cdot s^{-1}$. If the two reactants are different, the rate equation is given by:

$$r = -\frac{d[A]}{dt} = k[A][B] \quad (23)$$

where the reaction order with respect to each reactant is 1.

The integrated rate equation yields the following solution when the two reactants are the same:

$$\frac{1}{[A]} = \frac{1}{[A]_0} + kt - - - - \quad (24)$$

The half-life is given as follows [111]:

$$t_{\frac{1}{2}} = \frac{1}{k[A]_0} \quad (25)$$

When the two reactants in a second order reaction are different, the integrated rate law bears the following form (equation 26):

$$1/([B]_0 - [A]_0)\ln([B][A]_0 / [A][B]_0) = kt \quad (26)$$

In this case, the equation for the half life cannot be defined unless the half-life span of one of the reactants is known. To measure the second-order reaction rate of two different reactants, it is easier to measure the reaction rate for one of the reactants and then calculate that of the other as a difference.

Another common solution to a second order reaction law is to consider one concentration as being constant as the reaction proceeds. This special case corresponds to a pseudo-first-order reaction, meaning that the reaction depends on the concentration of only one reactant, as shown in equation 27 [63]:

$$r = k[A][B] = k'[A] \tag{27}$$

where $k' = k[B]$ in an excess of reactant B. Thus the quantity k' is referred to as pseudo-first-order rate constant.

The above expression is identical to the first-order reaction law. To obtain a pseudo-first-order reaction, it is therefore required to use an excessively large amount of one of the reactants. During the reaction, an amount of the excess reactant can react, but this amount is sometimes insignificant. Thus the concentration will be considered as constant [112].

2.4.2 Kinetics of surface-bound species

In this work the pesticides immobilized on areosil particles are reacted with ambiant oxidants, such as OH-radicals within a reaction chamber. These interactions can be described as bimolecular reactions between surface-adsorbed pesticides and gas-phase OH radicals [113]. In this context, the role of the aerosil substrate in the preparation of pesticides has to be neutral. The differential rate law describing the disappearance of a reacting pesticide, such as e.g. terbuthylazine (TBA), can be expressed as shown in Equation 28:

$dC_{[TBA]}/dt = -k_{[OH]} \bullet C_{[OH]} \bullet C_{[TBA]} - k \bullet C_{[TBA]}$, or equivalently,

$$dC_{[TBA]}/C_{[TBA]} = -k_{[OH]} \bullet C_{[OH]} \bullet dt - k \bullet dt \tag{28}$$

where $C_{[TBA]}$ is the instantaneous TBA concentration, $C_{[OH]}$ is the concentration of OH-radicals, $k_{[OH]}$ is the rate constant of the TBA reaction with OH-radicals, and k encompasses losses of TBA via all other possible routes not initiated by OH-radicals. Integrating both sides of Equation (28) between the time “0” and any time point “t” into the degradation reaction yields the following expression for the time-dependent TBA concentration.

$$\mathrm{Log}\left(C_{[TBA]}(t)/C_{0[TBA]}\right) = -k_{[OH]}\int_0^t C_{[OH]} \bullet dt - k\int_0^t dt \qquad (29)$$

where $C_{0[TBA]}$ is the initial TBA concentration before the indirect photolysis reaction. Equation (29) can be simplified by several considerations:

In the event of experimental evidence that there is practically no change in TBA in the absence of OH-radicals inside the reaction chamber, then one can reasonably neglect any loss path of TBA other than via its reaction with OH-radicals. In this case the term "k" can be neglected and the second integral term in Equation (29) can be ignored. In a typical photo oxidation kinetics study, unless vapor phase analysis is performed to directly determined the concentration of OH-radicals, first a reference compound with known OH-radial rate constant is studied in order to estimate the concentration of OH-radicals. In Equation (29), if the rate constants for many reference compounds are known as in the work by Palm et al. [31], then the only unknown, which is the integral OH-radical concentration at time t (in the first term of the right hand side of Equation (29)), can be determined. This is given by the slope of the plot of the measured concentration (in logarithmic scale) of the reference compounds versus the known rate constants. Then the OH concentration can be calculated from the slope of the plot of the integral OH concentration versus time.

However, in contrast to the study in reference [114, 115], in the present work just one reference compound (i.e. TBA) was used and one has to determine the OH concentration straight forwardly. For this purpose, in order to further simplify Equation (27), one can assume that the concentration of the overwhelming OH-radical vapor inside the reaction chamber is indeed in excess as compared to the concentration of the surfaced-bound pesticide molecules. This simplifies the kinetics analysis to a pseudo-first order reaction case, in which the OH-radicals concentration is considered constant during the reaction. Therefore, the complete integration of Equation (29) yields a mono-exponential decay function for the time-dependent TBA concentration as follows [116, 117]:

$$C_{[TBA]}(t) = C_{0[TBA]}\exp(-k_{[OH]} \bullet C_{[OH]} \bullet t) \qquad (30)$$

In this work monitoring of the decrease in the amount of the reference compound TBA as a function of time and the fitting of the experimental data with Equation (30) served to determine the ambient OH-radical concentration. With this knowledge the measurement data

for other herbicides of interest were also fitted with Equation (30) in order to determine their respective OH-radical rate constants. Since Raman spectroscopy is a linear technique, the integral intensity of Raman is proportional to the concentration of the corresponding species, therefore the fitting of Equation (30) is equivalent to fitting the areas of the observed Raman bands with exponential decay functions.

3. Experimental setup and sample preparation

3.1. Sample Preparation

3.1.1. Introduction

Nanoscopic silica substrates are utilized for coating with semi-volatile pesticides under study, which are exposed to atmospheric trace gases in order to simulate reactive processes in the laboratory. Raman spectroscopy and Raman microscopy were the techniques used to characterize pesticides after indirect photolysis. Infrared spectroscopy as well as mass spectroscopy (MS) and nuclear magnetic resonance (NMR) were employed as complementary techniques not only to describe the products, but also to determine the structure of organic compounds. As Raman spectroscopy is not only stable and easy to utilize technique for process understanding, but also requires no special preparation, it was also employed to facilitate the measurement of the samples.

3.1.2 Review on laboratory approaches on reactive degradation of pesticides

Before beginning the preparation preliminary tests were necessary to ensure that the microscopy is capable of mapping the surface structures of samples. Acetone and chloroform were used as solvents for sample preparation. Before starting the measurement of Raman spectroscopy, we first ensured that the samples are the same at all points. Furthermore, hydrophilic Aerosil particles were used to study the reaction of OH-radicals with terbuthylazine and to investigate the effect of this reaction on the atmospheric lifetime of TBA. Hydrophilic Aerosil particles were used to study the reaction of OH-radicals with TBA on SiO_2 particles with a surface area of 380 m^2/g. In the second step, hydrophobic Aerosil particles Aerosil R 972 have been used to ameliorate the adhesion of the herbicides on the glass and also for the caotings of the sample.

The above mentioned pesticide samples were used without further purification. They are deposited on nanoscopic substrates using hydrophobic Aerosil particles (Aerosil R 972, Evonic Industries, Germany). Solutions of the pesticides were prepared by dissolving the samples in acetone (99.8%) and chloroform (99.0%) from Sigma-Aldrich (Germany) as

indicated in Table 3.1. Subsequently, Aerosil R 972 was added in quantities, as indicated in Table 3.1. Moreover, Aerosil R972 is fumed silica based on hydrophilically fumed silica with a specific surface area of 130 m^2/g after being treated with DDS (Dimethyldichlorosilane) [118, 119]. Other properties of Aerosil R972 are listed in Table 3.2.

The mixing ratio of nanoparticles to pesticides was adjusted in order to form only a monolayer of the adsorbate. This is of central importance for simulating realistically the indirect photo-oxidation of pesticides in a laboratory experiment, since it is known that multilayer adsorption leads to results, which do not resemble the degradation in the atmospheric environment [120]. Furthermore, the nanoparticles have a large surface area, which facilitates interactions with oxidizing species and maximizes the pesticide concentration. The solutions were stored after preparation in a refrigerator, where they were kept until they were used.

Table 3.1: Compositions of the sample solutions

Substance	**Mass of the substance [mg]**	**Mass of aerosil R 972 [mg]**	**Acetone [mL]**	**Chloroform [mL]**
Terbuthylazine	24.4	38.5	3.1	1.0
Atrazine	25.1	39.4	3.0	1.1
Simazine	7.5	83.0	1.4	3.1
Propazine	24.4	39.4	2.5	1.1
Lindane	21.2	33.1	2.5	1.5

Table 3.2: Characteristics of Aerosil R 972 [121, 122].

Properties	**Typical value**	**Unit**
Specific surface area (BET)	110 ± 20	m^2 / g
SiO_2-content	≥ 99.8	wt.%
Average primary particle size	16	nm
Carbon content	0.6-1.2	wt.%
pH	3.6-4.4	
Appearance	Fine white powder	

Each prepared solution was treated for 30 minutes in an ultrasonic bath, in order to be well mixed and to dissolve remaining crystals. Subsequently, the liquid samples were deposited on glass slides (production from Menzel Germany, size: 1.8 mm x 1.8 mm) [123]. A 4 µL droplet was deposited on a glass slide, which was heated to 60°C, so that it dries quickly and homogenously on the glass surface. This temperature turned out to be best-suited for sample preparation, as was studied systematically by varying the drying temperature between room temperature and 70°C. Coated Aerosil R972 particles form loosely bound agglomerates and were exposed to reactive OH-radical for indirect photo-oxidation.

The homogeneity of the sample is essential for investigating the atmospheric degradation in laboratory studies. The occurrence of large crystals from the organic pesticide component, corresponding to phase segregation, was monitored by a CCD-camera attached to an optical microscope (Olympus BX41, 500 x magnification). Figure 3.1 shows a typical result of sample control, which was checked before starting each experiment. As a result, only those samples showing no phase separation have been used for further experiments.

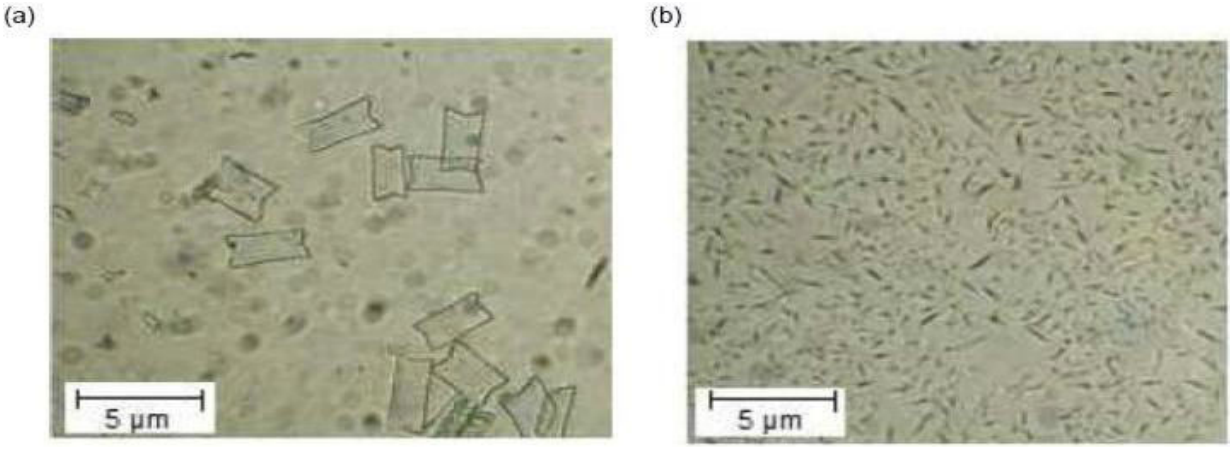

Figure 3.1: Optical microscopy image of (a) a heterogeneous sample containing simazine and Aerosil-R-972, glass carrier warmed to 40 °C; (b) homogenous sample containing the same substances but the glass carrier was warmed to 60°C.

In order to reproduce the exact location of the sample for subsequent kinetics or spectroscopic studies, the coordinates of this location were determined as follows: The x-coordinate was arbitrarily set to zero in the middle of the glass slide (see Figure 3.2). From this location the measuring point of the sample was determined. Thus, it is possible to find the same location

in sequential studies in which the sample was brought into the reaction chamber for exposure to oxidizing agents, such as OH-radicals.

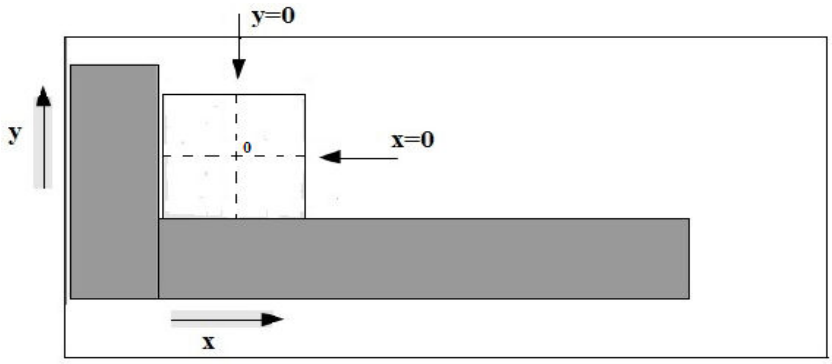

Figure 3.2: Schematic view of sample holder and sample carrier

The sample holder is a glass slide 76 x 26 mm from Menzel. The sample carrier consists of a squared glass slide carrier 1.8 x 1.8 mm purchased from Menzel. There are also alignment guides (glass) for bringing the sample carrier reproducibly into the same position (grey area in Figure 3.2). This allows for taking Raman spectra at well defined positions of the sample. The following procedure was developed in order to determine time dependent changes in concentration of the reactants and products: 9 different locations were selected within an area of 250 x 250 µm using a regular 3 x 3 array, while keeping the laser power at 20 mW and using the 50 x objective.

The method used for sample preparation has proved to be particularly suitable because we could dissolve the pesticides and desposit them on nanoparticles, which are deposited on a glass slide. These pesticide samples were exposed in the reaction chamber to OH radicals.

3.2 Materials

We had the following devices:

- Raman spectrometer: Dilor XY 800 from Horiba Jobin Yvon with Nd:YAG laser (Spectra Physics, Millennia, power: 5 W), frequency doubled Nd: YAG laser, λ = 532 nm, the emission of monochromatic green wavelength light)
- The Raman microscopy HORIBA, optical microscope (Olympus BX-41) (2)
- Bruker (Infrared) IFS 66 FT-IR spectrometer

- Bruker Avance III, 700 MHz SB US magnet 18
- Mass spectroscopy: ESI-TOF (Electrospray ionization time of flight mass-spectromer

Pesticides

The following pesticides are of commercial quality and were purchased from Sigma-Aldrich (Germany):

Terbuthylazine:	98.8% ($C_9H_{16}ClN_5$, 229.71 g/mol)
Atrazine:	98.8% ($C_8H_{14}ClN_5$, 215.68 g/mol)
Simazine:	99.9% ($C_7H_{12}ClN_5$, 201.657 g/mol)
Lindane:	99.8% ($C_6H_6Cl_6$, 290.83 g/mol)

Calculation of the surface coverage by terbuthylazine on SiO_2 particles

The coverage ratio of TBA was calculated to determine the average geometry of the structure (operational cross section). If the length C-Cl is considered as a part of longest radius, the maximum radius of TBA molecule is that of the maximum plane circle area below and it can be calculated as [124]:

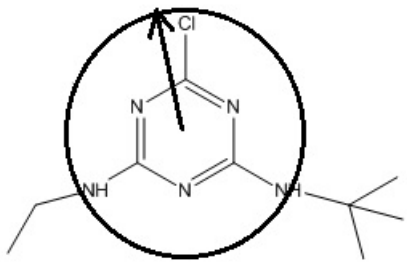

Scheme 3.1: The structure of terbuthylazine and the calculation of the maximum radius of the plane area within terbuthylazine

$R_{TBA}=(d_1 + d_2)$, where d_1 = 1.476 Å distance of –C=N-C (conjugated)
d_2 = 1.843 Å distance of X_3-C-Cl (X=C, H, N, O)

Then the radius is R_{TBA}= 0.3319 nm. The maximum plane circle area of TBA molecule is obtained:

$S_{TBA} = \pi \cdot R_{TBA}^2 = 0.346 \cdot nm^2$

The minimum number of TBA molecule ($N_{TBA\text{-}monolayer}$) are:

Case of Aerosil R 380 :

$$N_{TBA\text{-}monolayer}(R380) = \frac{380 \times m_{SiO_2}}{S_{TBA}} = \frac{380\ m^2/g \times 38.5 \times 10^{-3} g}{0.346\ \cdot (10^{-9})^2 m^2 \times 10^{-18} m^2} = 42.3 \text{ x } 10^{18} \text{ molecules} \cdot m^{-2}$$

Case of Aerosil R 972 : units incomplete (and wrong numbers)

$$N_{TBA\text{-}monolayer}(R972) = \frac{170 \times m_{SiO_2}}{S_{TBA}} = \frac{170 \times 38.5 \times 10^{-3} g}{0.346 \times 10^{-18} m^2} = 19 \text{ x } 10^{18} \text{ molecules}$$

in the Table 3.2 was used instead of 170 g/m^2

The total number of TBA molecule in 24.4 mg, where 24.4 mg is the mass taken for the experiment (see Table 3.1), can be expessed as follows:

$$N_{TBA}(R972) = \frac{m_{TBA}}{S_{TBA}} \times 6.02 \times 10^{23} molecules/mol$$

$$= \frac{24 \times 10^{-3} g}{229.71 g/mol} \times 6.02 \times 10^{23} molecules/mol$$

$$= 62.8 \text{ x } 10^{18} \text{ molecules}$$

In this calculation we state that N_{TBA}(R972) is slightly bigger than $N_{TBA\text{-}monolayer}$(R972), which is also bigger than $N_{TBA\text{-}monolayer}$(R380). In the case of Aerosil 380, the pesticides were soluble in water. Only the solubility of the herbicide terbuthylazine in water was lower [125] and the samples were not usable. As the coating with these nanoparticles turned out to be inefficient, we had to change the type of Aerosil and worked therefore with Aerosil R 972 that permitted a binding of TBA molecules on SiO_2 surface. The hydrogen bonds which can be formed by interaction of the amino groups of TBA with hydrophilic aerosil surface.

3.3 Production of OH-radicals

OH-radicals are reactive with most of chemical compounds (carbon monoxide, methane, ozone, hydrogen gas (H_2), hydroperoxy radicals (HO_2)) present in the atmosphere and can be generated by two different methods, which are described in the following.

3.3.1 Photolysis of O_3 in the presence of water vapor

Oxidation of the samples by OH-radicals was examined in a separate reaction chamber, in which the sample is placed on a suitable carrier (glass slide), where it is exposed to OH-radicals at a defined pressure, temperature, and humidity. OH-radicals were produced by the reaction of atomic singlet oxygen ($O(^1D)$) with water vapor, according to the following reactions [126, 127], where a HBO, mercury short-arc lamps without reflector 50 to 200 W (Osram, Germany) was used for photolyzing ozone the between 210 nm and 300 nm:

$$O_3 + h\nu \rightarrow O(^1D) + O_2(^1\Delta) \quad (31)$$

$$O(^1D) + H_2O \rightarrow 2OH \quad (32)$$

The photolysis light from the Hg lamp is reflected by dichroic mirrors into the reaction chamber, where *in situ* OH-radicals were produced (see Figure 3.3). The reactants, ozone and water vapor, are supplied to the reaction chamber by Teflon inlet tubes and argon is used as a carrier gas. Ozone is produced in a commercial laboratory ozonizer (Sander, Germany), yielding approximately 3% of ozone, if ambient air is used as an oxygen source. The flow rate of the gas is typically set to 150 sccm/min. The OH-concentration of such sources is known from the literature, yielding typically 10^6 radicals/cm^3 [128]. The OH-concentration, generated in this work is estimated to be 10^6 radicals/cm^3 [129] (see Figure 3.3).

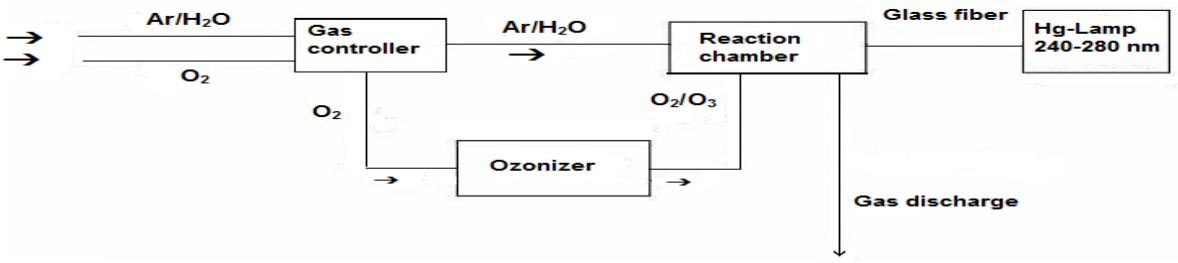

Figure 3.3: Schematic view of the reaction chamber in which OH-radicals are produced by photolysis of O_3.

3.3.2 Photolysis of hydrogen peroxide

The second way of producing OH-radicals involves the photolysis of hydrogen peroxide [130]. This source of hydroxyl radicals consists of a low-pressure mercury UV-lamp (Dinies Technologies, Germany) for photolysis, which emits short wavelength radiation (λ=185 nm). The UV-lamp is built into a cylindrical glass tube of 30 cm length and 3.5 cm width, in which the 4 W UV-lamp of 1.5 cm width and 7.5 cm length is mounted (Figure 3.4). The glass tube is coated by halocarbon wax, in order to reduce the loss of radicals produced in the source by wall reactions. The tube is sealed on both sides by rubber stopcocks which allow for adding the gaseous reactants via Teflon tubes. Aqueous hydrogen peroxide (30%, Carl Roth, Germany) or neat water vapor was flushed into the reactor by bubbling the non-reactive carrier gas argon through hydrogen peroxide solution. Throughout the tube axis, an OH-concentration is produced to react with the sample. At the upstream part of the lamp, it is observed a higher constant production of OH-concentration.

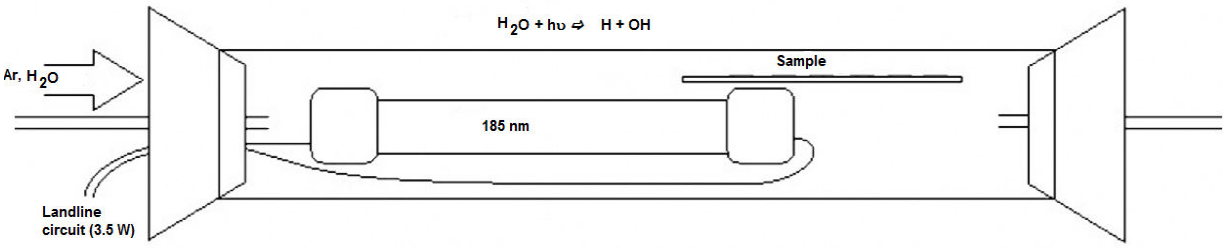

Figure 3.4: Schematic diagram of the OH-source produced by photolysis of 30% of aqueous hydrogen peroxide.

In addition to vacuum UV-radiation (λ<200 nm), there is also an effect from the thermal emission of the photolysis lamp. This leads to heating of the samples, so that the temperature in the chamber is increasing to the range of 305 K to 323 K, depending on an operating time of the light source. Hydroxyl radicals are formed from hydrogen peroxide by the following processes:

$$H_2O_2 + h\nu \rightarrow \quad OH + OH \qquad (33)$$

$$HO + H_2O_2 \rightarrow HO_2 + H_2O \qquad (34)$$

$$HO_2 + H_2O_2 \rightarrow OH + H_2O + O_2 \qquad (35)$$

$$HO_2 \text{ (or HO)} + HO_2 \rightarrow H_2O_2\ (H_2O) + O_2 \qquad (36)$$

In addition, there can also be photolysis of water [131, 132, 133]:

$$H_2O + h\nu \rightarrow \quad OH + H \tag{37}$$

This is followed by recombination reactions:

$$OH + H \rightarrow H_2O \tag{38}$$

$$OH + OH \rightarrow \quad H_2O_2 \tag{39}$$

$$H + H \rightarrow \quad H_2 \tag{40}$$

There is also a loss of OH-radicals due to reactions at the walls:

$HO + Wall \rightarrow product$

If the chamber is opened for the introduction of the sample, air enters the reaction chamber and produces additional radicals in the gas phase, such as [134]:

$$O_2 + h\nu \rightarrow \quad O + O \tag{41}$$

$$O + H_2O \rightarrow \quad OH + OH \tag{42}$$

$$O_2 + H \rightarrow \quad HO_2 \tag{43}$$

$$HO_2 + HO_2 \rightarrow H_2O_2 + O_2 \tag{44}$$

Hydrogen peroxide is degrading in aqueous solution upon storage [135]. Therefore, the concentration of H_2O_2 was determined before each experiment by titration. According to Schumb et al. [136], permanganate titration is one of the most reliable methods for determining the concentration of H_2O_2 [137]. The reaction stoichiometry is:

$$2\ MnO_4^- + 5\ H_2O_2 + 6\ H^+ \rightarrow 2\ Mn^{2+} + 8\ H_2O + O_2 \tag{45}$$

The permanganate end point is indicated by a change from violet color to brown. As soon as the concentration of hydrogen peroxide is known, the experiments can be started. The OH-concentration in the reaction chamber is determined by using degradation of terbutylazine (TBA). This compound is a suitable reference compound, since its rate constant is well-known from the literature [134, 138].

3.4 Raman Spectroscopy and Microscopy

3.4.1 Calibration procedures

Raman scattering makes use of irradiating the sample with an exciting laser beam, where the photon energy may correspond to that of an electronic transition of a particular chromophore. This corresponds to Raman scattering, where the intensity of the Raman signal increases significantly compared to non-resonant conditions. In the laboratory, it is most practicable to use a laser source that has a given excitation energy. This might be an electronic transition of the target. In Raman scattering, the energy of the impinging photons is scattering by the target molecule.

The aim of this Section is to describe Raman spectroscopy and the setup used to perform measurements, and to obtain information about the degradation of various environmental pollutants by OH-radicals. Raman spectroscopy is used to characterize OH-induced chemical decomposition processes in the particle-bound semivolatile samples. Changes in the Raman spectra relate to two observations: a weakening of spectral features coming from the reactants; and the occurrence of additional features arising from the products of reactions either with OH-radicals or other reactive species that are contained in the gas phase. The kinetics is derived from the temporal profiles which are recorded while the sample is exposed to OH-radicals.

The Raman system used in the experiments (see Figure 3.5) consists of a continuous wave Spectra Physics Nd:YAG laser (Spectra Physics, Millennia, power: 5 W). The scattered radiation is dispersed by a triple Raman spectrometer (Dilor-XY-800 mm). The Neodymium-doped Yttrium-Aluminium Garnet ($Y_3Al_5O_{12}$) laser runs by frequency doubling (λ = 532 nm) at a typical power of 200 mW. An optical microscope is attached to the Raman spectrometer. The microscope makes use of fiber optics, which guides the collimated excitation laser radiation using two mirrors into the optical microscope (Olympus BX41). This permits the use of a considerably lower laser power than in previous experiments on macroscopic samples, so that laser powers as low as 10-30 mW are sufficient for taking Raman spectra. The laser beam is focused to a spot size of 100 μm diameter in the sample under study. This intensity of the Raman bands is regarded as a reasonable compromise between the intensity of Raman signals and the thermal evaporation rates of the substance.

Evaporation rates, however, must not be taken into account in order to get reliable results for reactive processes. The spectrometer is operated in the subtractive mode in order to suppress stray light and elastically scattered light (Rayleigh and Mie scattering).

Raman signals are recorded using a liquid nitrogen cooled CCD camera system and the signals are transferred to a PC for further data reduction. The other major advantage of Raman microscopy is the use of Raman mapping, in which the spatial distribution of the sample can be probed. Kinetic analyses were also carried out using the microscope. The exposure of the samples to OH-radicals was performed using an existing exposure chamber. In the present work, we have used a reaction chamber, which can be fully integrated into the Raman spectrometer (see Figure 3.5).

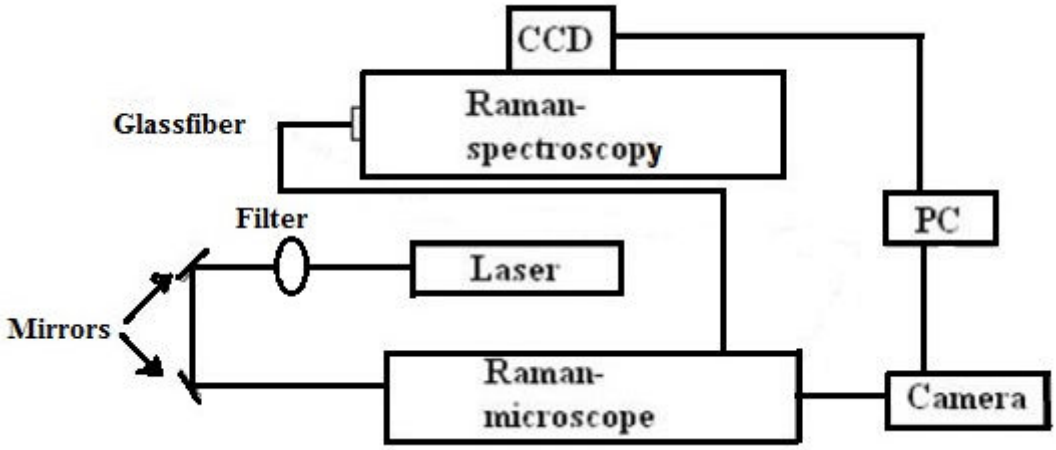

Figure 3.5: Experimental set-up of a micro-Raman spectrometer.

The experimental approach requires proper calibration of the OH concentration. We have developed a protocol, with which an *in situ* calibration of the OH-radicals concentration was successfully implemented. This is accomplished by using TBA on Aerosil-R-972 (see Table 3.2). TBA has a well-known rate constant for the reaction with OH-radicals: $k = 1.1 \times 10^{-11}$ $cm^3 \cdot s^{-1}$ [139]. This provides the unknown OH-concentration. The OH-induced decay of samples was monitored by Raman microscopy, where contour maps were taken, as shown in Figure 3.6. A simazine sample is shown in Figure 3.6 where spectral regime studied was the C-H stretching vibration which occurs between 2750 cm^{-1} and 3150 cm^{-1}. The results shown in Figure 3.6 cover an area of 50 µm x 50 µm, which was divided into 25 sections for analysis.

We can recognize in Figure 3.6 that the distribution of simazine is not entirely homogeneous. The color codes represent variation of concentration of the simazine sample; blue corresponds to low simazine concentration, and red to a high concentration. This map of Raman intensities allows us to take reproducibly spectra at different simazine concentrations, which we can then use to distinguish the reaction properties of monolayers as well as multilayers of low volatile samples adsorbed on Aerosil-R-972.

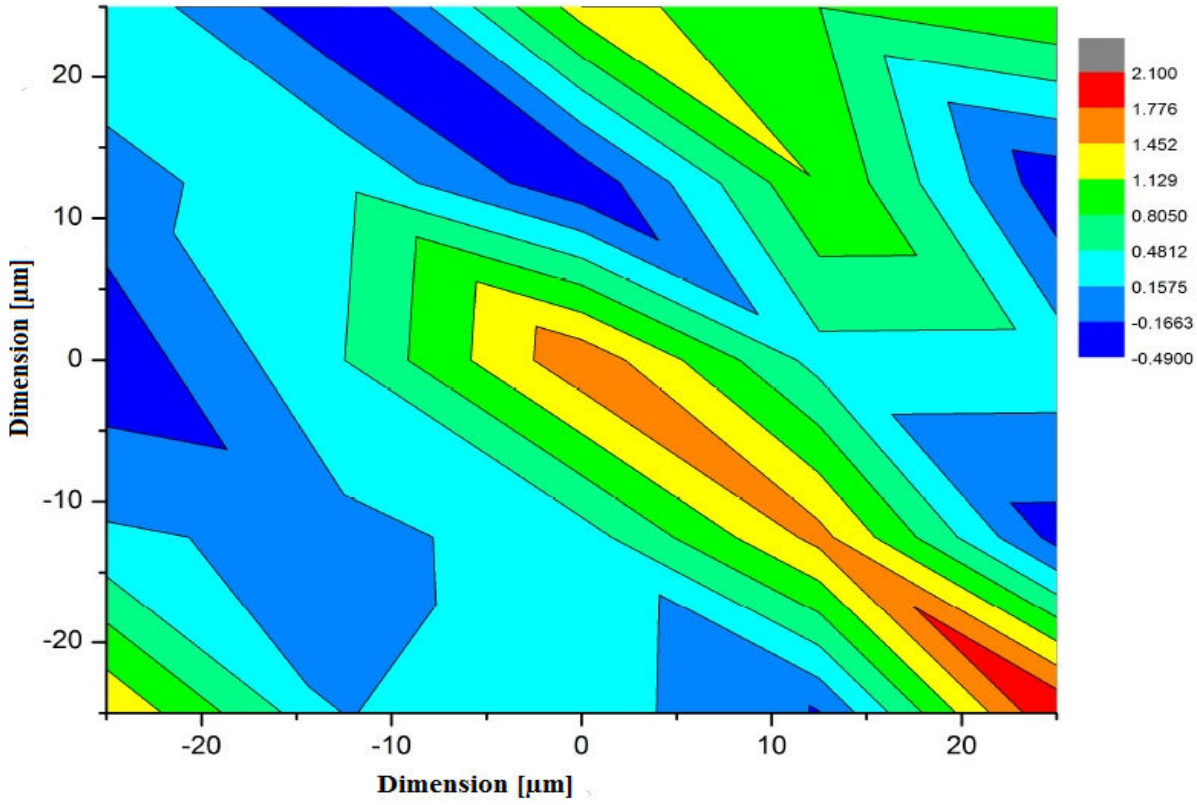

Figure 3.6: Contour diagram from Raman microscopy of simazine coated by Aerosil-R-972**.**

The Raman spectra taken during the degradation of TBA by OH-radicals are shown in Figure 3.7. This illustrates changes in intensities of vibrational modes of TBA before and after the reaction time of 30 minutes with OH-radicals, where most signal intensities drop with time. This can be an indication of thermal load and subsequent evaporation of the sample.

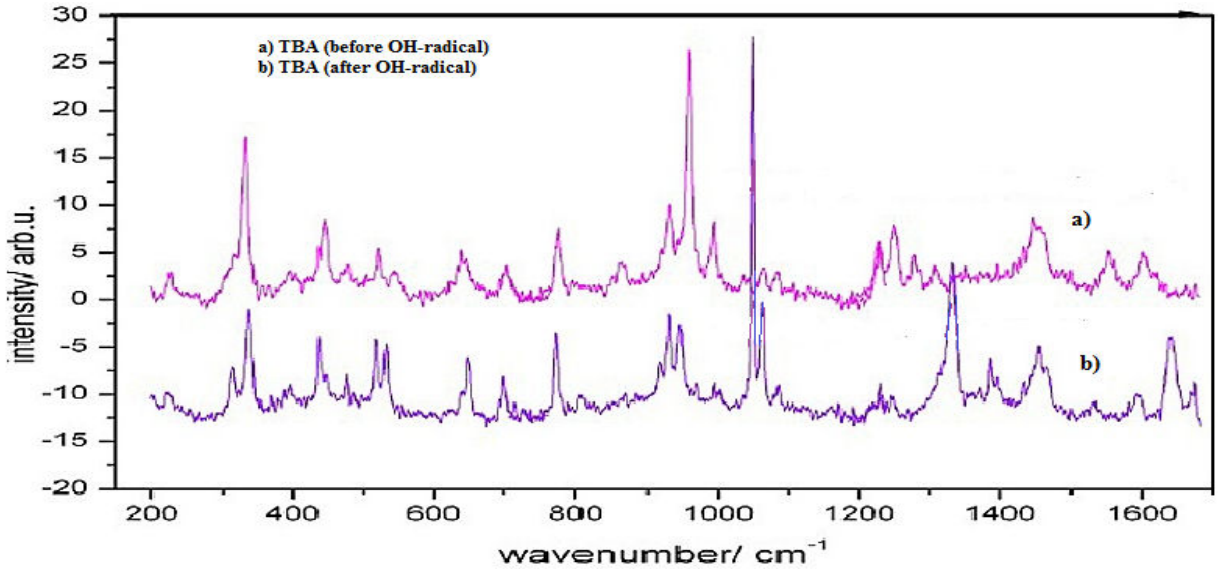

Figure 3.7: a) Raman spectra of TBA before (t = 0) and b) after the OH-radicals reaction (t = 1800 s). The TBA sample was prepared from 24.4 mg TBA and 38.5 mg Aerosil R972 in 3.1 mL acetone and 1.0 mL chloroform. The gas stream containing OH-radicals contained 100 sccm (Ar, O_2, O_3-H_2O); laser power: 200 mW; acquisition time per wavenumber increment: 2 s; number of accumulations: 25.

The reaction of OH-radicals with TBA is determined by changes in Raman mode intensities of TBA between the region 1000 cm^{-1} and 1600 cm^{-1}. In this region, we also observe the appearance of Raman signals of the oxidation product [140]. Specifically, the C-C-stretch vibration of the heterocyclic ring can be assigned to the wavenumbers 950 - 1055 cm^{-1}. Other vibrations are 770-785 cm^{-1} (rocking) and 435-570 cm^{-1}. The C-Cl-stretching vibration occurs in the 505-760 cm^{-1} regime, and the C-Cl deformation vibration is found between 250 cm^{-1} and 450 cm^{-1}. Considering the example below, the Raman intensities are taken in the region 1000 cm^{-1} and 1600 cm^{-1}.

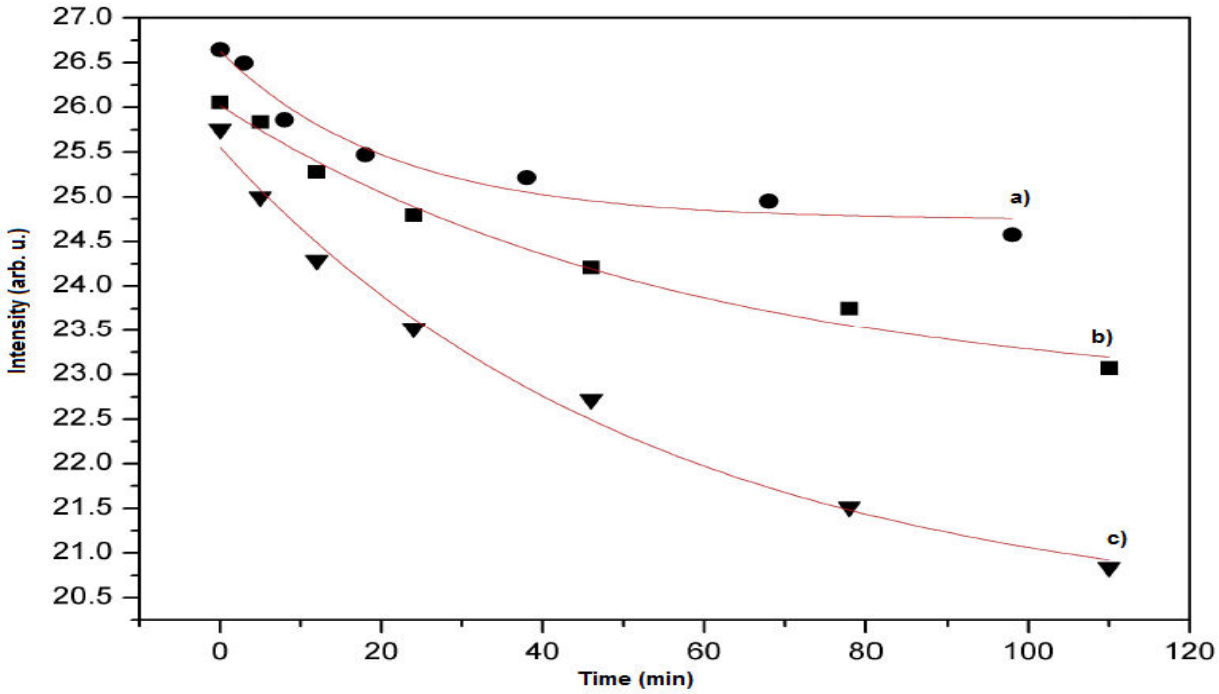

Figure 3.8: Kinetics of the degradation of TBA a) evaporation; b) reaction with ozone; and c) reaction with OH-radicals), before (t=0) and after the OH-radicals reaction (t=110 min or 6600 s). The TBA sample was prepared from 24.4 mg TBA and 38.5 mg Aerosil R972 in 3.1 mL acetone and 1.0 mL chloroform. The gas stream containing OH-radicals contained 100 sccm (Ar, O_2, 2 O_3/H_2O), laser power: 200 mW; acquisition time per wavenumber increment: 2 s; number of accumulations: 25.

Table 3.3: Equation used to fit date in Figure 3.8

equation	$Y = A_1(e^{-kt})+A_0$
a)	$1.886 \pm (0.184)(e^{-0.047t})+24.741 \pm (0.154)$
b)	$3.315 \pm (0.346)(e^{-0.017t})+ 22.706 \pm (0.379)$
c)	$5.309 \pm (0.423)(e^{-0.0187t})+20.243 \pm (0.463)$

The results from the kinetics experiment on terbuthylazine (TBA) initiated by OH-radicals are shown in Figure 3.8. The experimental results clearly indicate that evaporation is the slowest process (circles in Figure 3.8), leading to a smaller loss of Raman signal than chemical degradation. The reaction with ozone is also included in Figure 3.8 (squares). This leads to a more substantial loss of TBA. The fastest process is, as expected from the highest rate constant, the reaction with OH-radicals (triangles in Figure 3.8), even though their concentration is the lowest of all possible reactants. All curves shown in Figure 3.8 can be modeled by exponentials, specifically indicating that the reaction with OH-radicals is described by a pseudo-first order process [141].

The major problem was to show that OH-radicals can be successfully produced by different sources, which were ozone, water, and hydrogen peroxide. The first source of OH-radicals, ozone, was aimed at producing OH-radicals for the indirect photolysis, but there is also evidence for ozonolysis. This is because the mixing ratio of ozone was sufficiently high, despite its low reaction rate constant with TBA [142]. The next source used was water, but the percentage of OH-radicals obtained from water photolysis was not sufficient to follow the degradation of the low volatile samples studied.

The last source of OH-radicals used hydrogen peroxide of 30% where the photolysis wavelength was 248 nm [143], the power ranged between 100 and 200 mW [144], and the OH-concentration reached up to $2x10^{11} molecules/cm^3$ [145], which successfully led to the formation of OH-radicals. After reaction in the chamber with OH-radicals, the results were collected by Raman spectroscopy and Raman microscopy, which is explained in the following.

3.4.2 Estimation of error limits

The analysis and plotting of the data was done with an offset for clarity, as was done by Palm et al. in their work [138], for calculating the OH-rate constant of TBA on Aerosil. Indeed, they also suggested that the offset was due to the part of the substance that was not accessible to OH-radicals. Using GC/MS, they considered the offset to make their calculations. They then obtained an OH concentrations around $5-10x10^5 cm^{-3}$ and the OH rate constant of TBA on the aerosil was $K_{OH}^{TBA} = (1.1 \pm 0.2)x10^{-11} cm^3 s^{-1}$ [138]. These values were used as reference to calculate the rate constant of others pesticides. In order to monitor the effect of the UV-lamp and estimation of the offset value and origin, the reactions of TBA was monitored with the UV-lamp switched either on or off.

The experiments with the UV-lamp off were made under the same conditions as the one with UV-lamp on. The results obtained from the UV lamp on and off, respectively, are shown in Figures 3.9a and 3.9b. The error limits have also been calculated. In Figure 3.9b, one observes that the Raman intensity, due to photochemical processes in the flow reactor decreased with time. This process is only observed when the lamp is turned on, as can see below in Figure 3.9b. The offset observed in Figure 3.9 can be due to the fact that a residual part of TBA,

during the photolysis with OH-radicals did not completly react. It has to be considered in the calculation of OH-concentration.

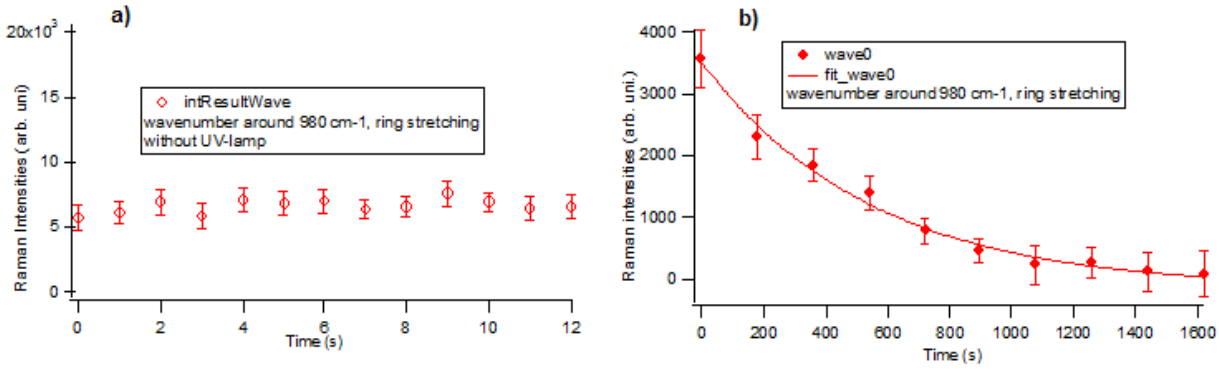

Figure 3.9: TBA Raman intensity versus time (a) when the UV-lamp is off and (b) when the UV-lamp is on for vibrational modes around 980 cm^{-1} (triazine ring).

Figure 3.9b shows that the Raman intensities decrease exponentially with the time during the photo-degradation. This is in agreement with the kinetics results discussed in Chapter 5 and the findings of Klöpfer and Wagner [146].

Furthermore, it is noticeable that in Figure 3.9a, the signals do not drop to $y_0 = 0$, that means, there is an offset present in a non photo-degradation graph. It is supposed that no photolysis reaction take place. Therefore, the offset can be due to the fact that the intensity of TBA at the beginning of the kinetic which do not reacted and do not change until the end of the process (see Figure 3.9a).

4. Results and Discussion

In the present work, we investigated the indirect photolysis reaction of semi-volatile compounds with OH-radicals [147]. The investigated substances were herbicides including the s-triazine terbutylazine, simazine and lindane. The ultimate goal of the work was to show that Raman spectroscopy can be applied as a fast and versatile method for the monitoring and the understanding of indirect photo-degradation of herbicides. Raman spectroscopic results constitute the main focus of the experimental data analysis. IR spectroscopy data are only briefly discussed in order to also account for the possibility of vibrational modes belonging to ketone functions, which are stronger in IR absorption than in Raman scattering.

A detailed data analysis procedure of the Raman data was performed to estimate the reaction parameters. The concentration of OH-radicals in the reaction chamber is first and foremost the important experimental parameter, which characterizes the laboratory conditions applied for mimicking the atmospheric degradation of the studied herbicides. The correct assignment of the experimentally observed vibrational modes in the Raman spectra was proven to be very decisive in the determination of the degradation mechanism and was achieved by a comparison of the experimental spectra with theory results from *ab initio* calculations. From the experimental and theoretical results, the OH-radical concentration could then be accurately determined and plausible reaction mechanisms describing realistic photo-degradation pathways were derived.

4.1 Degradation of terbuthylazine by indirect photooxidation

4.1.1 Monitoring of the OH-radical concentration

OH-radicals are reactive species known to oxidize pesticides in the atmosphere [148]. These reactants are formed via direct photolysis by sunlight at ambient conditions (see Chapter 3, Section 3.2). In the framework of the indirect photolysis studies in this thesis, a good knowledge of the availability of OH-radicals in the experimental reaction chamber is essential for the investigation of the kinetics of the photolysis processes. Properly quantifying the OH-

concentration enables the determination of the indirect photolysis rate constants of the considered pesticides.

The following summarizes the results of laboratory experiments investigating the process of OH-radical formation via photolysis of aqueous hydrogen peroxide (H_2O_2), which occurs in an open storage within a reaction chamber [149, 150]. Other precursors for the formation of OH-radicals include nitrate (NO_3^-), ozone (O_3) and water (H_2O) [151]. However, O_3 could not be used as OH-radical source in the experimental setup used in our work because of the possibility of ozonolysis to occur. Also, the obtained levels of OH-radicals from H_2O photolysis are high in humid air [138]. Hence, altogether, H_2O_2 was the best available OH-radical source for the experimental setup used in this work.

In order to estimate the concentration of OH-radials formed in the reaction chamber, the reaction of terbuthylazine (TBA) with OH-radicals is considered as a reference for the indirect photolysis reaction (i.e. we make use of its OH-radical reaction rate constant known from literature which is about 1.1×10^{-11} $cm^3 . s^{-1}$) [31].

An example of TBA full Raman spectrum taken before the photolysis reaction is presented in Figure 4.1, showing intense vibrational bands that can be assigned to specific bonds in TBA.

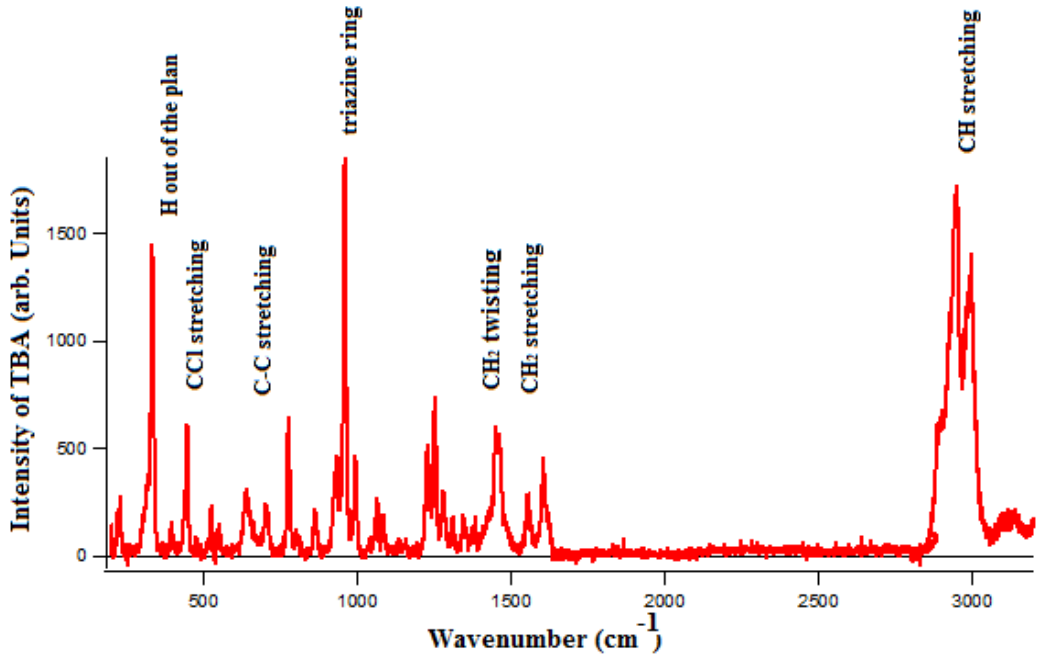

Figure 4.1: Raman spectrum of terbuthylazine before the indirect photolysis reaction.

The OH-concentration present in the medium during the photochemical reaction is calculated by doing a kinetic study of the full Raman spectra of TBA taken at regular time intervals during indirect photo-oxidation. The rate constant corresponds to the inverse of time constant for a given vibrational mode in the measured time dependent Raman spectra. Since we selected the most suitable source of OH-radical formation that should lead to a steady production of OH-radicals (TBA as reference substance) and therefore we make the following criterion regarding the temporal behavior of the measured Raman spectra: Given different Raman modes belonging to the reactive sites of the molecule, if the rate constants derived from these modes are the same or vary very little, then the obtained value can be considered to represent the overall rate constant and be used for determining the concentration of OH-radicals. Hence, upon the analysis of the full Raman spectra, the focus is then put on the spectral regions or features, which are relevant for the indirect photochemical reaction.

Depending on the observed spectral changes, more criteria may have to be defined in order to decide which mode(s) among those changing systematically with the indirect photolysis time can be used to calculate the rate constant. In fact certain modes may not or less be influenced by the overall reaction or may even describe intermediate reaction steps, such that the rate constants for such modes differ greatly and their meaning is not straightforward. Therefore, the results related to the OH-concentration calculation also point to the significant vibrational fingerprints for the indirect photolysis under study.

4.1.2 Evaluation of the Raman spectra of TBA

In the framework of the indirect photolysis studies on pesticides in this thesis, the goal is to first demonstrate the feasibility of indirect photolysis for our experimental conditions and to characterize the experimental reaction chamber via the determination of the concentration of OH-radicals produced in the chamber. Hence, in this Section, we can exploit Raman spectroscopy as a method for evaluating and validating the occurrence of TBA indirect photolysis. We briefly present the corresponding Raman spectra, which were later analyzed in order to extract the respective reaction kinetics parameters which help to determine the OH-radical concentration in the reaction chamber. Overall, the analysis of the Raman spectra consisted of (i) spectral preprocessing and correction (noise filtering and baseline subtraction) followed by the fitting of most of the observed Raman bands/peaks, (ii) calculation of the

integrated intensity (area) of the fitted Raman bands, and (iii) modeling the evolution of areas as a function of photolysis time.

A control Raman experiment was first performed in order to verify that the sample would not undergo any other changes apart from the indirect photolysis caused by OH-radicals, when it was placed inside the photolysis reaction chamber. For this purpose, the TBA sample was exposed at different time intervals in the photolysis reaction chamber when the UV-Vis irradiation lamp for the production of OH-radicals in the chamber was switched off. The corresponding Raman spectra are depicted in Figure 4.2, which shows that the Raman spectra of TBA do not practically change with time when the irradiation lamp in the reaction chamber in this case is turned off. This is consistent with the fact that the formation of OH-radicals via indirect photolysis of H_2O_2 is indeed impossible in the absence of UV-Vis irradiation. As shown in the following, the Raman spectra recorded from TBA that was exposed for photolysis in the presence of UV-Vis irradiation change drastically with the exposure time.

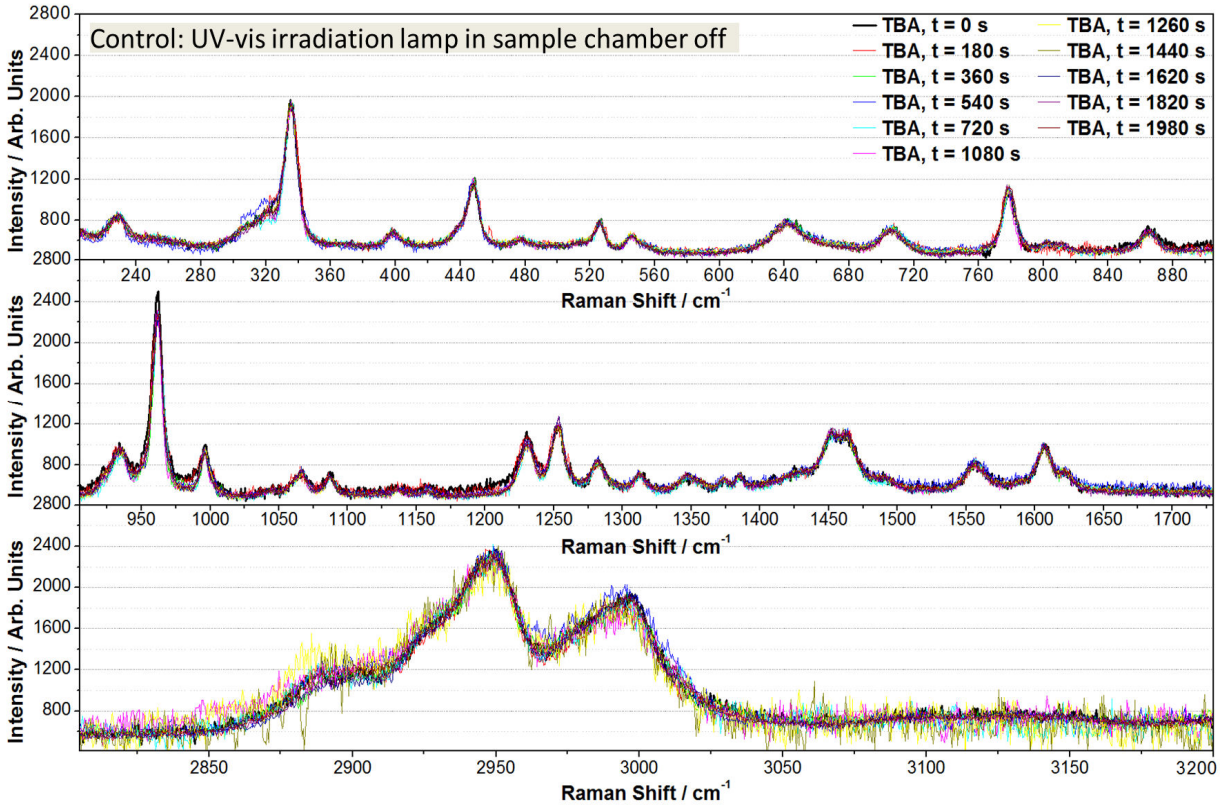

4.2: *Raman spectra of TBA that was exposed at different time intervals in the photolysis reaction chamber when the UV-Vis irradiation lamp for the production of OH-radicals in the chamber was switched off.*

The Raman spectra taken from TBA that was exposed at regular time intervals during indirect photolysis when the irradiation lamp for the production of OH-radicals in the reaction chamber was switched on are depicted in Figure 4.3, which shows the raw spectra in panel (a) and the corrected spectra either displayed vertically in panel (b) or overlaid together with zooming into different spectral windows in panel (c). Table 1 summarizes the assignment of the main Raman bands observed during TBA indirect photolysis. Some of these bands are marked in Figure 4.3 (c). The band at 227 cm^{-1} represents C—N bending. Around 524 cm^{-1}, there is an interesting deformation of the molecule with respect to a practically fixed C—Cl bond in space. The band at approx. 780 cm^{-1} is assigned to C—C stretching. The band at 1450 cm^{-1} is due to CH_2 twisting and the band appearing at 961 cm^{-1} is assigned to the characteristic breathing mode of the triazine ring. Detailed band assignment was only possible with the help of a theoretical calculation of the present work and with the help of available literature data [152].

The analysis of the Raman spectra consisted of (i) spectral preprocessing and correction (baseline subtraction) followed by the fitting of most of the observed Raman bands/peaks, (ii) calculation of the integrated intensity (area) of the fitted Raman bands, and (iii) modeling the evolution of areas as a function of photolysis time. As can be seen in Figure 4.3 (a), the raw Raman spectra taken during TBA photolysis are overlaid by a fluorescence background varying with the reaction time.

The measured Raman spectra were first preprocessed as follows: they were noise-filtered by processing them 5 times through a 2-degree/9-size Savitsky Golay smoothing algorithm (this process was mainly meant for removing spike noise, rather than for completely filtering out noise from a general viewpoint), and the baseline was approximated by a linear spline with many fitting knots and then subtracted from the experimental spectra in order to get rid of the overlaying fluorescence background and to yield the spectra displayed in Figure 4.3 (b) and (c). Important information provided by Raman spectroscopy about the photolysis reaction of TBA with OH-radical can already be emphasized here.

In fact, the noticeable changes in the Raman spectra recorded when the irradiation lamp was turned on (i.e. in the presence of OH-radicals formed in the reaction chamber via direct photolysis of H_2O_2) prove that TBA indirect photolysis by OH-radicals did indeed occur within the reaction chamber.

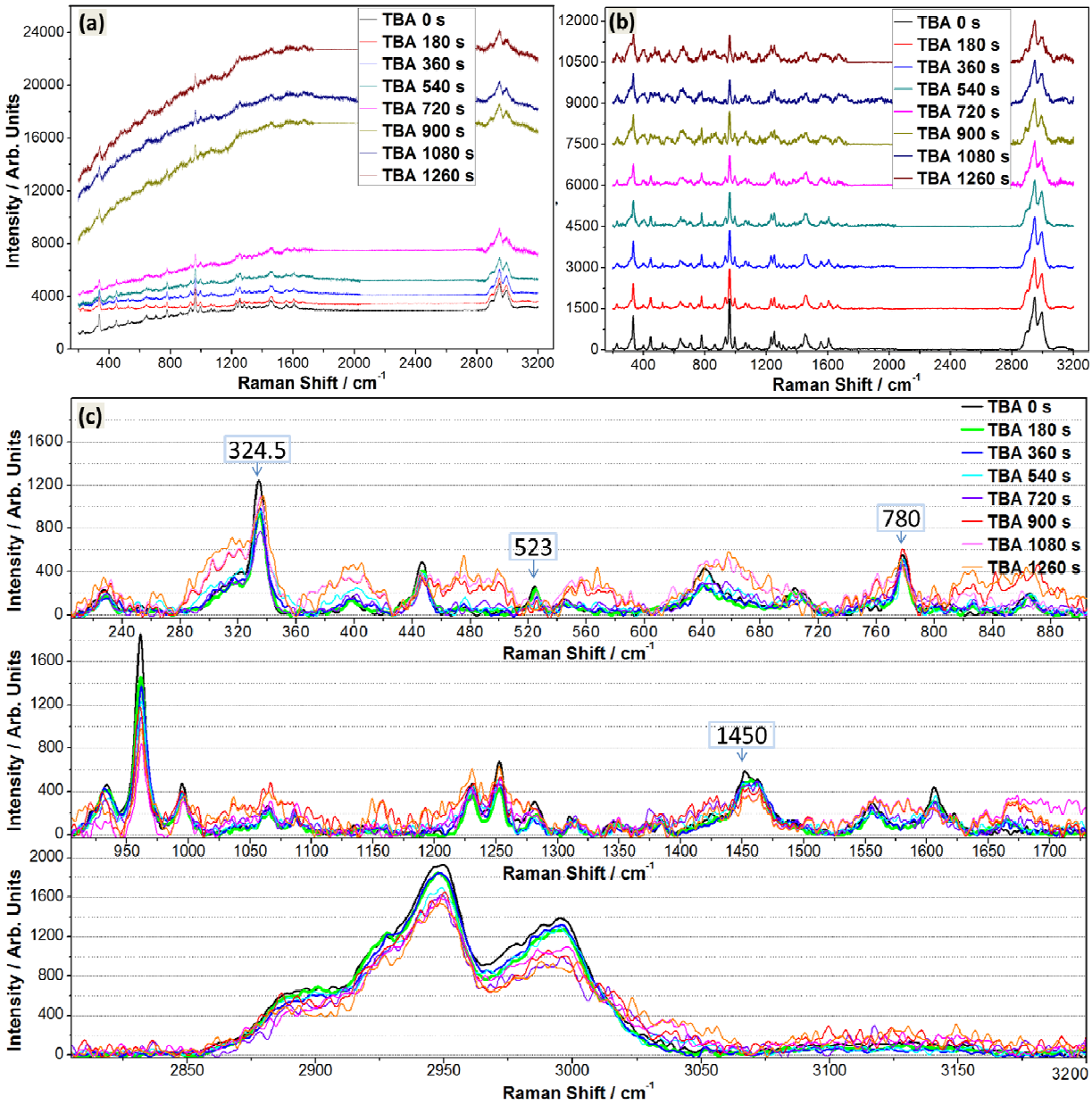

Figure 4.3: *Raman spectra at regular time intervals of TBA indirect photolysis reaction when the UV-Vis irradiation lamp for the production of OH-radicals in the reaction chamber was turned on: (a) raw spectra, (b) background-corrected spectra, and (c) zoomed view of the corrected spectra overlaid together in different spectral windows.*

Figure 4.3(c) demonstrates that TBA degrades with the reaction time, since nearly all main Raman bands of TBA exhibit a continuous decrease in intensity with time, while at the same time a few new bands appear in the spectra and increase in intensity with time [153, 154]. Presented below are the subsequent detailed analyses of the corrected Raman spectra for the calculation of the concentration of OH-radicals produced in the reaction chamber.

Table 4.1: Assignment of important Raman bands observed during TBA indirect photolysis [155, 156, 157]

Bands (cm^{-1})	227.3	334.5	523.9	778.3	864.6	933.3	961
Assignment	CH_3 Twi.	CC + CN bend	In plane Triazine ring + CC + CN bend	CH Wag.	C-N Str.	C-H Twi.	Triazine ring breath.
Bands (cm^{-1})	994.9	1064.3	1230.8	1281	1458.7	1606	2948/2995
Assignment	CC CN + ring CN CCl	+COC str.Asym. C=N ring +str. CC str. str.	H-CN Wag.	C=C aliph. CH_2 Wag.	CH_2 Twi.	C=N Str.	C-H/ Str.

4.1.3 Kinetics analysis of the Raman spectra of TBA

A detailed kinetic analysis of the TBA Raman spectra was performed. For this purpose, the observed Raman band shapes were fitted by using the Igor Pro software. This band fitting was aimed at accurately determining the positions of the bands/peaks and calculating the corresponding areas in order to precisely follow the photolysis process. The band fitting procedure is illustrated in Figure 4.4 (a), (b), and (c). This was done by first setting the approximate peak positions. It was possible to found the widths of the different bands or sub-bands, enabling a close reproduction of the experimental contours. For complex band structures, instead of individual sub-bands, the total sum area of all contributing sub-bands was used for data evaluation. The rationale for this is that the width of individual sub-bands is difficult to assess.

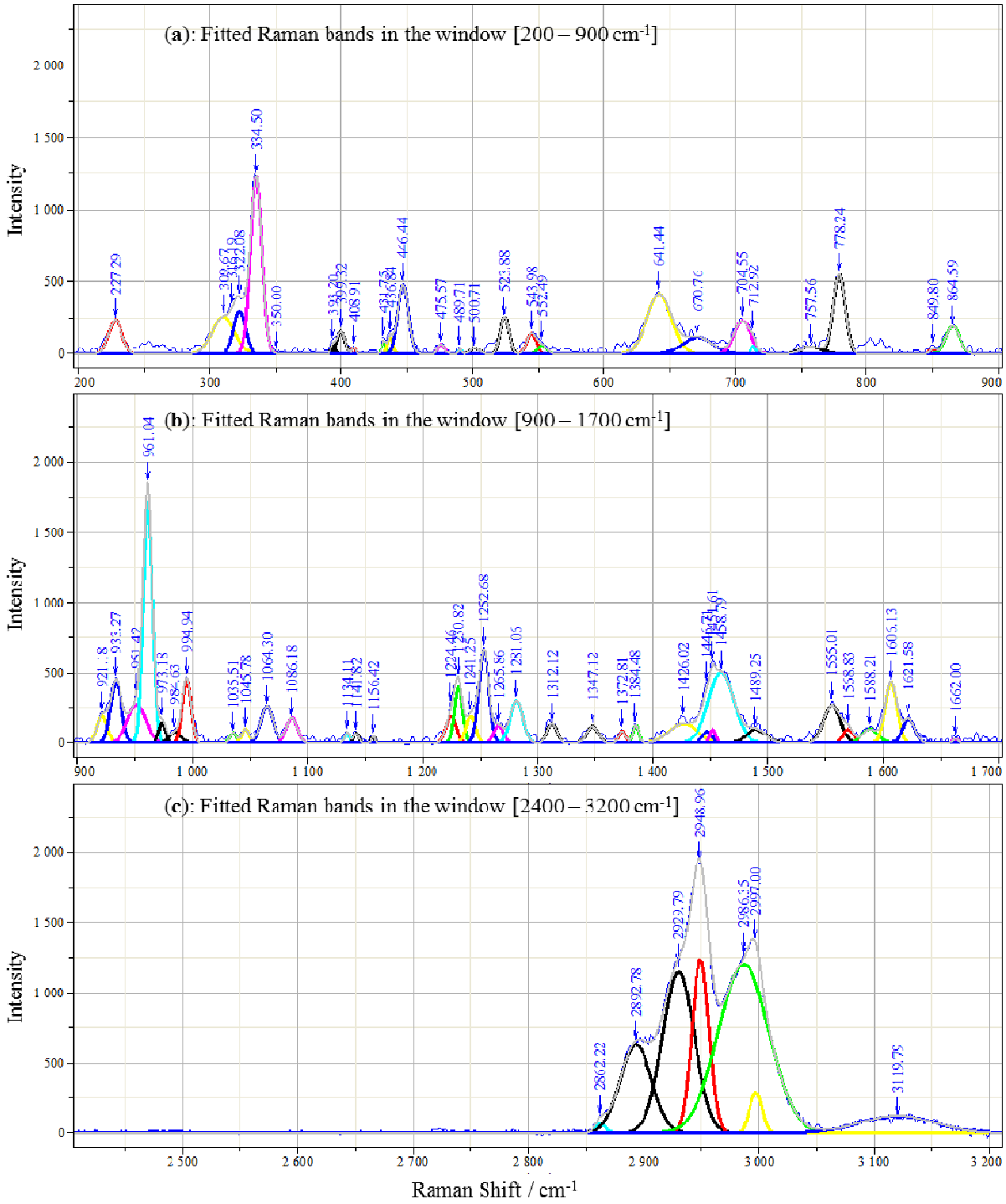

Figure 4.4: Band fitting of the Raman spectrum of TBA at the beginning of its indirect photolysis with OH radicals. The spectra at different photolysis times were fitted similarly (i.e. the peak positions are approximately marked, then the fitting program automatically adjust the bandwidths and fits the bands).

Since Raman scattering is a linear process, the integral intensity of a Raman band is proportional to the sample concentration [115]. Therefore, Equation (30) in Chapter 2 can be

rewritten to model the calculated area by mono-exponential decay functions given by Equation (46) and Equation (47).

$$f(t) = A_0 \exp(-\lambda \bullet t) \quad ; \tag{46}$$

$$\lambda = k_{[OH]} . C_{[OH]} \tag{47}$$

Here, f(t) is a Raman area, λ and A_0 are the fitting parameters. The aim of the band analysis is to find the parameter λ from the time-dependence of the intensities or areas of the observed Raman bands in order to calculate the OH-radical concentration. Note that we do not measure the TBA concentration directly but rather the Raman intensity from the sample; and as a consequence, Equation (47) will correctly describe the disappearance of TBA in the course of the photolysis, if and only if at any time (t > 0), the Raman area considered is exclusively due to the remaining TBA only and not to the reaction products. In order words, we have applied Equation (46) only to the observed Raman bands, which clearly decay with time.

It should be also informative to rearrange Equation (46) into Equation (47) in order to monitor the formation of products by investigating new bands appearing in the Raman spectra with increasing reaction time. Since the stoichiometric ratio between TBA decomposition and product formation is not known [117], the formation of products can be described by the commonly used negative mono-exponential growth function in Equation (48) [138]. However, in our case, since the reaction mechanism is not known in advance and the contribution of the formed products is minor in the measured Raman spectra, the determination of the rate constant by exploiting equation (48) was only possible for the first order process.

$$f(t) = A_0 (1 - \exp(-\lambda \bullet t)) \tag{48}$$

Kinetics analysis based on band areas (integral band intensities)

The results of the mono-exponential fitting of the calculated areas of selected Raman bands plotted as a function of the photolysis time are recapitulated by the graphs in the different Figures in the next Section. In Figure 4.5 for example, we show the case where the areas were calculated from the band fitting described above and we also show the modeling of the temporal behavior of the plotted areas with a mono-exponential decay function (Equation (48) for bands clearly decaying with time). Note that in the graphs in Figure 4.4, the parameter "λ"

was denoted by the letter “L” during fitting. A quick look at the results in Figure 4.5 reveals that the calculated Raman areas, which clearly decrease with time, are well modeled by mono-exponential decay functions. In the following we discuss the values for the rate constant obtained from the fitting of the Raman band areas.

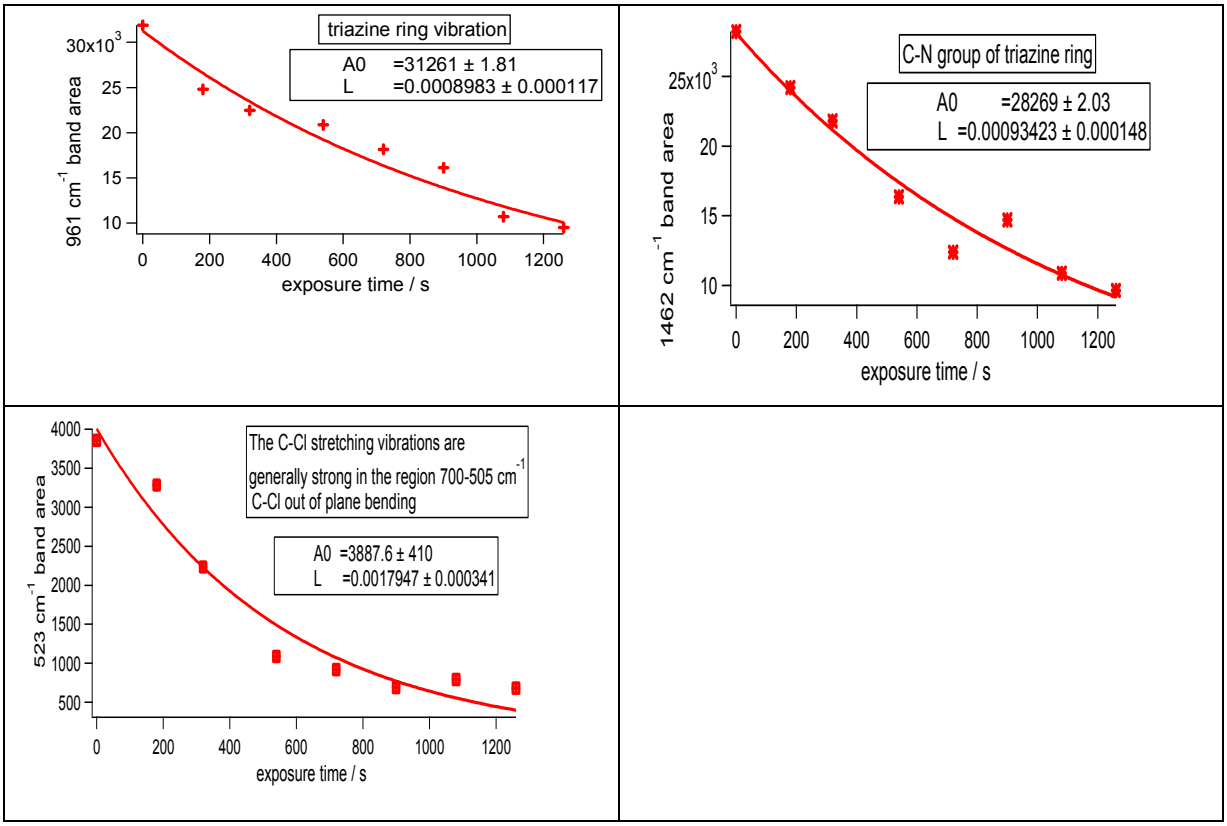

Figure 4.5: Plots of selected Raman areas as a function of photolysis time for absolute areas calculated via band fitting: The symbols represent experimental data, while the solid curves represent the fitting models for the corresponding temporal behavior (the parameter "λ" in equation (48) is denoted by the letter “L”).

Using Equation (48) the rate constant value estimated with a meaningful error is as follows:

$0.0009 \pm 0.0001 \leq \lambda \leq 0.0018 \pm 0.0003\ s^{-1}$: $\mathbf{\lambda(524\ cm^{-1}) = 0.0018 \pm 0.0003}\ s^{-1}$.

In accordance with the hypothesis made while deriving Equation (47) (i.e. constant OH-radical concentration), we need to obtain at best almost the same value of λ for each fitted area. If we first consider only the areas which clearly show an overall decay over time, then the fitting with an exponential decay function (Equation (48)) yields values of λ close to one another.

The above kinetic analysis was repeated for relative band areas calculated with respect to the area one of a given band considered as a reference band. Different bands were tested to find out whether any of them could be used as reference band. The necessary requirement in this case is for a reference band to be insensitive or very less sensitive to the photolysis changes in the studied molecule. It appeared that the band at about 780 cm^{-1} was the closest possible in this regard, and therefore, the determined values of λ are worth mentioning in this case: The fitted rate constant for relative band areas with respect to the 780 cm^{-1} band was found in the following interval:

$0.00039 \pm 0.00008 \leq \lambda \leq 0.0009 \pm 0.0002\ s^{-1}$: $\mathbf{\lambda(524\ cm^{-1}) = 0.0009 \pm 0.0002}\ s^{-1}$.

Here, $\lambda(524\ cm^{-1}) \sim 0{,}001$ is the upper bound of the interval value for the fitted in λ.

Kinetics analysis based on the peak and relative peak intensities of Raman bands

Absolute as well as relative peak intensities of the observed Raman bands have also been evaluated to describe the indirect photolysis of TBA with OH-radicals. The band or peak heights have been obtained directly by reading them from the average Raman spectrum at each reaction time. Relative peak intensities were calculated by taken as reference the intensities of the same band considered in the case of relative band area calculation. As for band areas, Equation (48) was used to fit the plots of the peak intensities as a function of reaction time, especially for bands clearly showing decreasing peak intensities with reaction time.

The rate constant derived from absolute peak intensities was found in the following interval:

$0.0002 \pm 0.0001 \leq \lambda \leq 0.0016 \pm 0.0001\ s^{-1}$: $\mathbf{\lambda(524) = 0.0016 \pm 0.0004}\ s^{-1}$.

The upper bound of the obtained interval of the λ values corresponds to the value of λ for the 524 cm^{-1} band, which being the highest, agrees very well with the value of λ obtained from the analysis of absolute band areas and relative band areas. The rate constant derived from the analysis of relative peak intensities with respect to the 780 cm^{-1} band was found in the following interval:

$0.0004 \pm 0.0001 \leq \lambda \leq 0.0020 \pm 0.0001$ s^{-1} : **$\lambda(524) = 0.0020 \pm 0.0001$** s^{-1}

The largest λ value in this case is again found to be for the 524 cm^{-1} band, which is in agreement with the upper bounds of the λ values determined so far.

4.1.3.1 Recapitulation: Confidence range of rate constant and for the OH concentration

As illustrated in the above specific cases, the rate constant was calculated from the fitting of the time dependence of either the integral intensities (areas) or peak intensities of the observed Raman bands. Table 4.2 recapitulates all the results of the kinetic analyses that were based on either the absolute band areas obtained from band fitting, relative fitted band areas with respect to any of several bands tested as reference, band peak intensities, or on relative band peak intensities (with respect to the same bands testes as reference for relative band area calculation).

Table 4.2: Ranges of λ values obtained from the kinetic analysis based on Raman band areas or intensities.

Ranges of $\lambda(s^{-1})$ values obtained from area analysis	Upper bound / remarks
Absolute band areas (obtained from band fitting) $0.0009 \pm 0.0001 \leq \lambda \leq 0.0018 \pm 0.0003$	**$\lambda(524) = 0.0018 \pm 0.0003$**
Absolute band areas (manual selection of wavenumber intervals) $0.00045 \pm 0.00005 \leq \lambda \leq 0.001 \pm 0.0002$	**$\lambda(524) = 0.0010 \pm 0.0002$**
Relative band areas (reference: 995 band) $0.0004 \pm 0.0001 \leq \lambda \leq 0.001 \pm 0.0002$	**$\lambda(524) = 0.0010 \pm 0.0002$**
Relative band areas (reference: 2950 band) $0.0003 \pm 0.00003 \leq \lambda \leq 0.0008 \pm 0.0002$	
Relative band areas (reference: entire CH region) $0.00031 \pm 0.00003 \leq \lambda \leq 0.0008 \pm 0.0001$	
Relative band areas (reference: 780 band) $0.00039 \pm 0.00008 \leq \lambda \leq 0.0009 \pm 0.0002$	**$\lambda(524) = 0.0010 \pm 0.0002$**
Ranges of λ values obtained from peak intensity analysis	
Absolute peak intensities $0.0002 \pm 0.00001 \leq \lambda \leq 0.0016 \pm 0.0004$	**$\lambda(524) = 0.0016 \pm 0.0004$**

Relative peak intensities (reference peak: 995 cm^{-1}) $0.00018 \pm 0.00005 \leq \lambda \leq 0.00034 \pm 0.00020$	**$\lambda(524) = 0.0034 \pm 0.0002$**
Relative peak intensities (reference peak: 780 cm^{-1}) $0.0004 \pm 0.0001 \leq \lambda\ (s^{1}) \leq 0.0020 \pm 0.0001$	**$\lambda(524) = 0.0020 \pm 0.0001$**
Conclusion	
Rate constant for relative peak intensities $0.0004 \pm 0.0001 \leq \lambda \leq 0.0020 \pm 0.0001$	**Rate constant for band areas** $0.0009 \pm 0.0001 \leq \lambda \leq 0.0018 \pm 0.0003$

Taking all the Raman band characteristics of TBA analyzed above, it appears that the 524 cm^{-1} band is very relevant for indirect photolysis of TBA through reaction with OH-radicals. For this reason, the Raman spectra of TBA were zoomed out around this band and are displayed in Figure 4.6 in order to clearly show the time-dependent spectral changes induced by indirect photolysis of TBA.

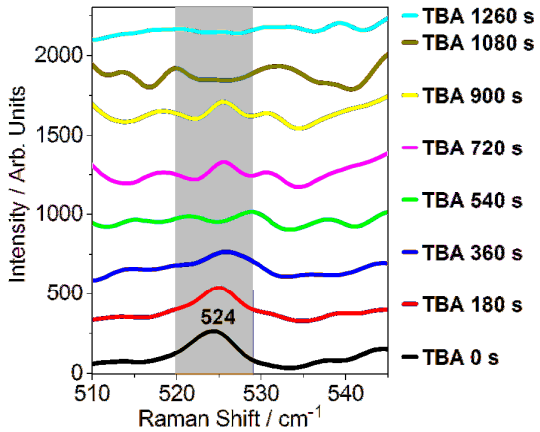

Figure 4.6: Raman spectra of TBA around the 524 cm^{-1} mode

The fitting of the 524 cm^{-1} area yields a more accurate value of λ ($0.0018 \pm 0.0003\ s^{-1}$), becaue the error on the fitted value of λ for the other decaying bands is almost of the same order of magnitude as the obtained value itself. The 524 cm^{-1} band is due to the interesting extended deformation of the TBA molecule with respect to a practically fixed C—Cl bond in space (see section 4.5). The greater rate constant accuracy obtained from the fitting of the 524 cm^{-1} area is therefore very important, since it suggests not only that the cleavage of the C-Cl bond during indirect photolysis as supported in many earlier works [158, 159] directly affects the 524 cm^{-1} band, but also that this band practically accounts for the overall change in the TBA amount due to indirect photolysis. In this case, the products formed during the reaction most likely do not contribute to the intensity of this band and consequently the fitting of its temporal evolution with a mono-exponential decay function is indeed realistic. The other

decaying bands may have small intensity contributions from the formed reaction products, and as a matter of fact, their temporal behaviors may not be entirely described by mono-exponential decay functions. Nevertheless, it is very realistic to state that all the obtained values of λ for three of the fitted bands (i.e. the ones clearly decaying with reaction time) are close to one another.

It follows from the detailed analysis of the Raman bands that the overall rate constant can be realistically determined by the time-dependent behavior of the Raman band at 524 cm^{-1}. The confidence range of the overall rate constant is given below by taking the upmost bounds of the ranges of the λ values determined from band analysis. The corresponding range for the OH-radical concentration is then determined.

The confidence range for the overall rate constant is defined as follows:

$$\mathbf{0.0018 \pm 0.0003 \leq \lambda(524) \leq 0.0020 \pm 0.0001\ s^{-1}} \qquad (49)$$

Hence, for absolute area;
$C_{[OH]} = \lambda / k_{[OH]} = (163 \pm 31)\ x10^6$ molecules $\cdot\ cm^{-3}$.
And for relative peak intensities with respect to the 780 cm^{-1} band, we have;
$C_{[OH]} = \lambda / k_{[OH]} = (184.59 \pm 9.23\ x\ 10^6$ molecules $\cdot\ cm^{-3}$
Therefore, the corresponding range for the OH-radical concentration is as follows:

$$\mathbf{(163 \pm 31)\ x10^6 \leq C_{[OH]} \leq (184 \pm 9)\ x\ 10^6\ molecules.cm^{-3}} \qquad (50)$$

The above results give the range of the OH-radical concentration in our experimental chamber as determined from the Raman band analysis. This OH-concentration depends on the setup used and can change according to the parameters influencing the ambient experimental conditions.

To sum up, because the Raman band integral intensity (band area) better reflects the amount of the measured substance in a situation where both the band width and peak height might due to a chemical reaction, we consider that the value of λ obtained for the 524 cm^{-1} band area most likely represents the overall rate constant and can therefore be used to calculate the OH-radical concentration. The corresponding OH-radical concentration value is the following:

$$\mathbf{C_{[OH]} = (163 \pm 31) x10^{6}\ molecules.cm^{-3} = (2.7 \pm 0.5)\ x10^{-13}\ Mol.L^{-1}} \quad (51)$$

The present results allow us, not only to better understand the Raman spectroscopic method for the monitoring of TBA photolysis, but also to extend the method to the case of other pesticides under study [160]. The first important insight gained from the analysis of the photo-degradation data is the exponential form of the decay curve of the intensity of specific Raman bands of TBA and the second insight is associated with the measured value of the OH-radical concentration.

As mentioned above, the value of λ obtained from the fitting of the 524 cm^{-1} band appears to be best representative of the overall rate constant. We have strived to verify this result by determining λ from Raman band parameters (band areas or intensities) evaluated differently.

4.1.3.2 Discussion of the time-dependent behavior of important Raman bands evaluated for the description of TBA indirect photolysis kinetics

Following the above detailed evaluation of Raman bands (areas and peak intensities) for the determination of the value rate constant λ, it appears that many bands (421, 523, 780, 961, 995, 1450, 1606, and 2950 cm^{-1}) are worth a particular attention. Especially the direct visualization of the Raman has shown that the 523, 1606, 1450 and 961 cm^{-1} bands in this order can be preferred for determining the rate constant.

The band at 446 cm^{-1} in the Raman spectra is the only band which contains a clear contribution from the C—Cl stretching vibration . The cleavage of the Cl atom is reported in many studies as the initial step of the degradation processes of many herbicides [161]. If the overall TBA degradation pathway was starting uniquely with the cleavage of the Cl atom and if a vibrational mode due to a pure (uncoupled) motion of the C—Cl bond could be observed in the Raman spectrum of TBA, then the evaluation of such a mode would be a direct measure of intact TBA concentration at any given reaction time and facilitated the determinationof OH-concentration. The Raman results show that the area of the 446 cm^{-1} band is constant for some time and then increase towards the end of the reaction, while its peak intensity does not globally change considerably with the reaction time. This observation is justified by

theoretical calculations (see details in the discussion in the later section) and can be understood from the fact that the 446 cm^{-1} band is not mainly due to the C-Cl motion(s).

The band at 1450 cm^{-1} is due to the deformation vibration of CH_3 and CH_2 groups. Also, the bands around 2950 cm^{-1} are due to the stretching vibrations of CH bonds. The 961 cm^{-1} band is the characteristic breathing vibration of the triazine ring. Since during the indirect photolysis of TBA, there is no breaking of the triazine ring and since the triazine ring as well as the overwhelming CH_3/CH_2 groups and CH bonds are expected to be equally present at the beginning and at the end of the reaction, we would not expect any change in the 961, 1450, and 2950 cm^{-1} bands over time and could in principle consider these bands as internal standards. However, the results above show that the intensities of these bands change with the reaction time, so that they do not behave as an internal standard. Since the observed change for each of these bands yields a rather low value of the fitted rate constant λ, such a change does not represent the complete measure of the total change in the amount of TBA either, so that the overall rate constant could not be measured via the evaluation of the intensity of each of these bands. Theoretical results which illustrate the actual motion of these bands will help to provide a definitive explication of the present situation.

Surprisingly, the bands at 995 and 780 cm^{-1} are observed in the Raman experiments to be globally constant in intensity (absolute peak or integral intensity) throughout the indirect photolysis reaction and appear in the mentioned order as the best suitable internal standards regarding the degradation changes in the TBA molecule. In fact, the values of the overall rate constant determined from the evaluation of the relative values of band areas or peak intensities with respect to either the 995 or the 780 cm^{-1} band as reference are closely matching those obtained from the evaluation of the absolute values of band areas or peak intensities. The observation of the motion described by these modes has helped to further clarify this point, as detailed in later sections.

Interestingly, the 524 and 1606 cm^{-1} bands are the only bands, which help to obtain the highest values of the rate constant λ in all cases. The evaluation of the 524 cm^{-1} band yields the highest values of λ for both absolute and relative band parameters (area or peak intensity) and which are nicely matching with one another, especially when the 995 or 780 cm^{-1} band is taken as a reference for calculation relative areas/peak-intensities (as already mentioned above these bands were the better internal standards). The 524 cm^{-1} therefore seems to be a measure

of the total change in the TBA molecule, irrespective of the degradation pathway. To further clarify why this is the case, more details will be provided later about the complex motion this band involves. The 1606 cm^{-1} band appears as the next best candidate for the determination of the overall rate constant λ, since its evaluation yields the second largest values of λ. It may as well describe the degradation of TBA, but only partly. Theoretical details about the actual motion of this band will bring further insights.

Finally, the ongoing discussion gives an already very comprehensive understanding of the obtained results for explaining the indirect photo-degradation of TBA in the experimental reaction conditions. It follows that multiple simultaneous degradation pathways are more plausible. Yet, one Raman fingerprint appears as the signature as the overall degradation process [162].

As will be described in the next sections, we have used two other alternative methods to characterize the degradation of pesticide in the presence of OH-radicals and the occurring reaction products. Namely, nuclear magnetic resonance (NMR) and mass spectroscopy (MS) were applied in order to further understand the Raman results and then to clarify the TBA indirect photo-degradation pathways. Ultimately, the Raman theory-experiment comparison helps to strengthen the final conclusion.

4.1.4 Infrared Spectra

To access other normal modes of vibration present in TBA that might less intense or inactive in Raman scattering, besides Raman spectroscopic studies, we have also studied the IR spectrum of TBA. The IR spectra of TBA were taken with the help of a IFS/66S Bruker Fourier Transform IR spectrometer in the range of 400-4000 cm^{-1}. We note the existence of bands at 3400 cm^{-1} suggesting a shift of N-H due to the nature of the environment surrounding the NH group. In addition, the C=N conjugated cyclic system band also is identified at 1622 cm^{-1}, the NH_2 twisting at 555 cm^{-1} and the stretching of secondary amine N-H at around 3267 cm^{-1}. A broad vibrational band is observed at a position around 2900 cm^{-1}, which is assigned to CH stretching. The theoretical IR spectrum of TBA in Figure 4.7 (a) matches the experimental spectrum very well, despite some band broadening seen in the experiment. It is necessary to also mention that there is a band between 1310 and 1590 cm^{-1}

that may be tentatively assigned to the combination mode involving C-C stretching and in-plane C-H in-plane-binding in the aromatic ring [163].

After photo-degradation, the results of the experimental spectra of TBA reaction products were collected as illustrated in Figure 4.7 (b). The experimental spectra in Figure 4.7 (b) show a vibrational mode at 1650 cm^{-1} corresponding to C=O stretching. This C=O stretching is also present in the theoretical spectra calculated for the reaction products revealed by NMR and MS. Thus it should be noted that each product forms OH-radicals can turn into ketone according to the mechanism of the Retro-Diels-Alder Reaction [164] . We have realized a relative decrease in the intensity of the -C-H vibration–within 2900-3300 cm^{-1} [165] (see Figure 4.7 (b)), which can witness the reduction of CH content during the indirect photolysis reaction as a result of the of alkyl chain breaking or oxidation. All these observations point to the formation of reaction products different from the initial TBA.

Note that the recorded IR spectra also confirmed the results obtained from Raman spectroscopy.

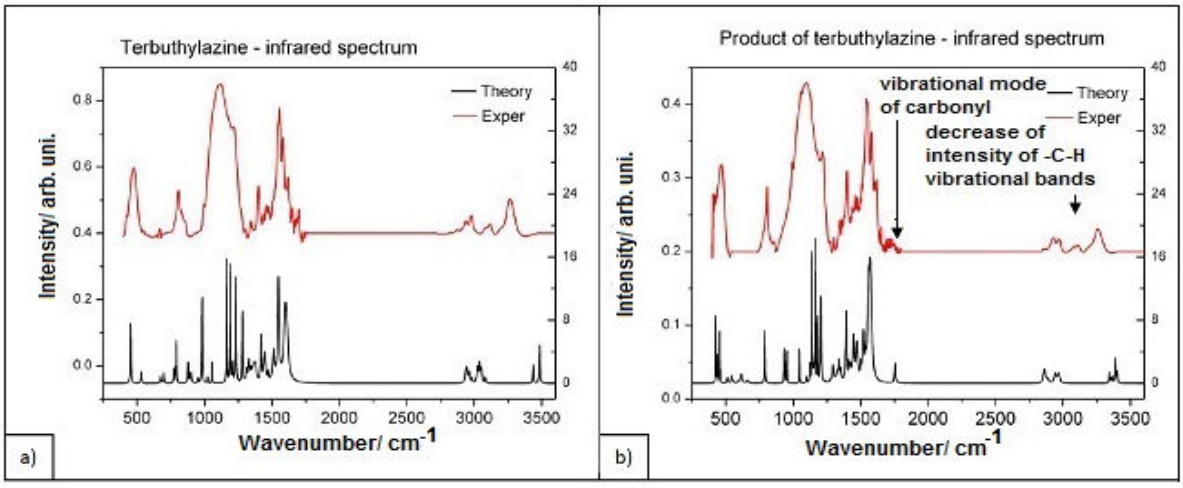

Figure 4.7: Comparison of Fourier Transform IR spectra in the range of 400-4000 cm^{-1} for a) pure TBA and b) TBA reaction products.

On the other hand, experimental/theoretical results and MS analysis show that the terbuthyl group in TBA is broken during the reaction

4.1.5 Characterization of the reaction products by NMR and mass spectrometry

Next to Raman- and IR-studies, the products of indirect photolysis of TBA were investigated by mass spectroscopy analysis (MS) [166] and nuclear magnetic resonance (NMR) [167]. MS analysis provides useful information about the mass of available fragments/products in a measured sample (see more details in Appendix A2 for terbuthylazine). However, detailed insights into their structure are needed for the full characterization of the reactants and the products. This complementary information is delivered by NMR analysis. In fact, NMR helps to gain a deeper insight into the structure of fragments identified by MS. The NMR technique uncovers the existing correlation between the different substances and the purity of the sample, by estimating the quantity of different chemical groups present within the products obtained after the indirect photolysis reaction in the investigated pesticide (e.g. TBA). In the following Section, NMR and MS results describing the indirect photolysis reaction products of the investigated pesticide samples are presented. The Retro-Diels-Alder reaction is considered in selected cases for stabling the sample degradation pathways.

4.1.5.1 Nuclear magnetic resonance

The NMR measurements in the framework of the present work were conducted by using the Bruker Avance III, 700 MHz SB US magnet spectrometer [168, 169]. The ^{1}H NMR spectra recorded at 700 MHz from the samples dissolved in $CDCl_3$ before and after the indirect photolysis of TBA are shown in Figure 4.8. The chemical shifts are reported in parts per million (ppm) from the internal standard TMS (0.0 ppm).

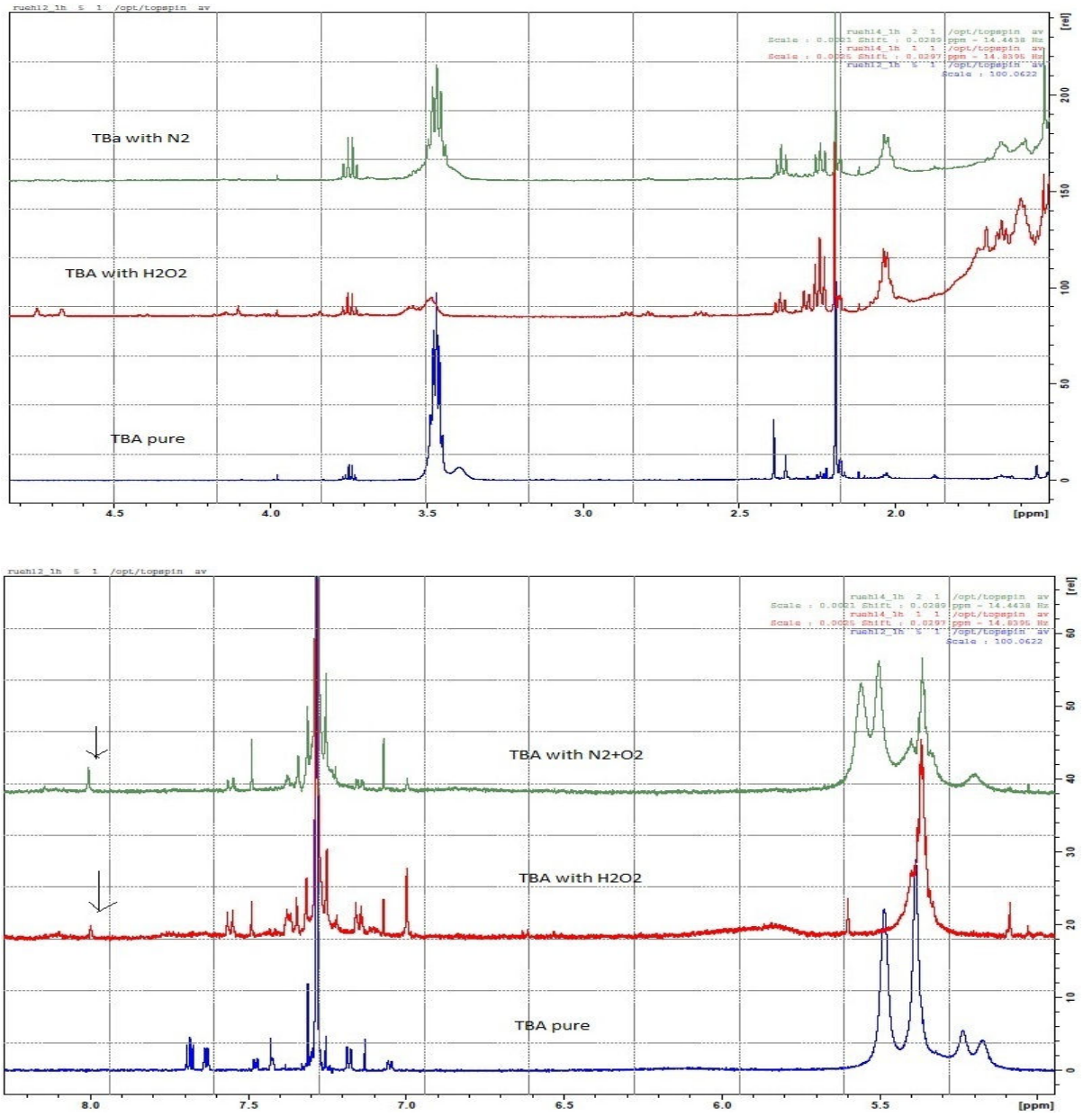

Figure 4.8: ^{1}H NMR spectrum of neat terbuthylazine and degraded terbuthylazine after indirect photolysis by OH-radicals (taking as source of OH-radicals either H_2O_2 or NO_2 formed by the reaction of the ($N_2 + O_2$) mixture with water vapor).

In Figure 4.8, the NMR signals of CH_3 protons for ethyl are observed at 1.19 ppm [170] and as evidenced, the characteristic NMR signal of the CH_3 protons of the tertbutyl methyl groups at 2.38 ppm is confirmed [171]. The signal at 3.46 ppm is due to the CH_2 protons of the ethylamino group [170, 171]. In addition, the chemical shifts of NH protons show up between 5.0 and 5.6 ppm as can be observed in Figure 4.8 and also in the Appendix A2.3.1 [172]. Normally, one should expect only two signals for the 2 protons of NH present in the ethylamino (e) and the terbutylamino (t) groups of the TBA molecule. However, we have observed many separated signals. This observation proves the presence of different TBA

isomers and we can state that they are distinct TBA isomers. As known for other triazine molecules [170] the different isomers arise from restricted rotations of the alkyamino side chains caused by the delocalization of the nitrogen lone-pair electrons into the triazine ring of TBA such that the side chain CN bond acquires a double bond character. This situation, which is due to the electronic charge distribution in the TBA molecule, can be represented by a resonance structure [173] as depicted in Figure 4.8. The above observation for many different NH proton resonances in the NMR spectrum of pure TBA therefore is in agreement with the work of Welhouse et al. [173, 175], who studied the NMR spectra of atrazine and TBA.

After indirect photolysis of TBA with OH-radicals, the NH proton resonance of the side chains gives NMR signals in the region between δ 4.5 and 5.0 ppm, as it can be observed in Figure 4.8 (see also Figure A2.4.1.1 in Appendix). Regarding the different TBA isomers, we note that several multiplets that were present in the spectrum of pure TBA have disappeared, shifted or changed in band shape and intensity after TBA indirect photolysis. Only one strong band is observed at 5.4 ppm as opposed to four bands around this position in the NMR spectrum of pure TBA. The change and the reduced number of multiplets for the signals of the NH protons mean that some TBA isomers are no longer present; suggesting that these ones were more affected than others TBA isomers during the photolysis reaction, which proves the selective formation of products (presented in Figure 4.11, page 82).

Actually, after the indirect photolysis of TBA with OH-radicals, we can see in the Figure 4.8 the presence of OH-proton detected at δ 8.0 ppm. Moreover, a doublet bands at δ 7.4 - 7.60 ppm representing NH protons neighboring a carbonyl substituent in the triazine ring was also detected in the NMR spectrum [176]. This observation suggests the formation of a product containing a carbonyl group in the triazine and corresponding to the displacement of both the double bond and the H atom on the triazine ring according to the Retro-Diels-Alder reaction mechanism [164].

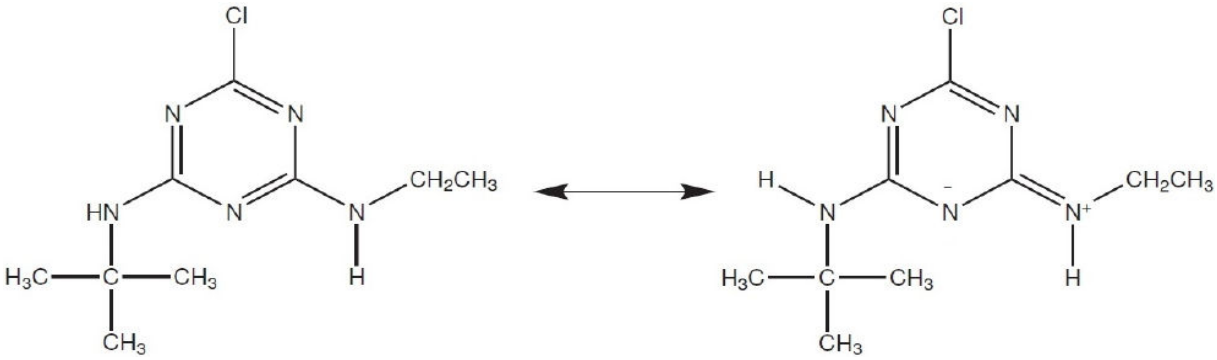

Figure 4.9: Electron-withdrawing effect of the triazine ring. They confirm electronic exchange in Figure 4.8 by a chemical shift between δ 5.5 (Fig. 4.7) and 4.5 ppm.

It follows from the above NMR results that there is an equilibrium decomposition reaction taking place during TBA indirect photolysis, leading to the modification of the TBA molecule and the presence of both OH- and carbonyl groups in the products, but leaving the aromatic ring intact. The exploration of these results in greater detail, we have also performed the MS characterization of TBA before and after its indirect photolysis by OH-radicals.

4.1.5.2 Mass Spectroscopy (MS)

Mass spectroscopy (MS) was used to identify the reaction products during TBA degradation. The sample was mixed with an Agilent 6210 ESI-TOF. A drying gas flow was set at 15 psi (1 bar). The EI-MS experiments were performed with flow rate at 4 μL/min [177]. All other parameters are optimized for a maximum of the respective abundance [M + H]. Based on the intensities ions obtained, it was possible to identify the products resulting from the indirect photolysis reaction. Candidate products of degradation are given for each compound studied after a indirect photo-degradation reaction has taken place. The examination of intermediates and end-photolysis products has provided valuable information on the feasibility of the photo-degradation process of TBA. During indirect photo-degradation of TBA by OH-radicals, we have obtained some products with OH-radicals (see Figure 4.10). Making use of the Retro-Diels-Alder mechanism with cyclo addition of the π bond, we get another opportunity of products containing the ketone. We will see later with the characterization methods if compound with ketone can be considered in this study as a product of indirect photolysis, as stated in the literature [178].

Furthermore, we have suggested intermediate degradation products of TBA and their further transformation into final products. As the end product of TBA indirect photolysis, we have proposed in this present work cyanuric acid (see section 4.5). This has also been described in the literature [179, 180]. The reaction of Retro-Diels-Alder is presented subsequently to better understand the mechanism of degradation.

Following the exposure of TBA to OH-radicals, which was done at a very low concentration, several indirect photolysis products of TBA with 230.12 m/z were detected by MS analysis. The displayed region of the spectrum contains ions of the homologous series with m/z of 230, 212, 196.16, 174.06, and 140.09, among others. The MS patterns depicted in Figure 4.10 shows the products obtained due TBA degradation by OH-radicals.

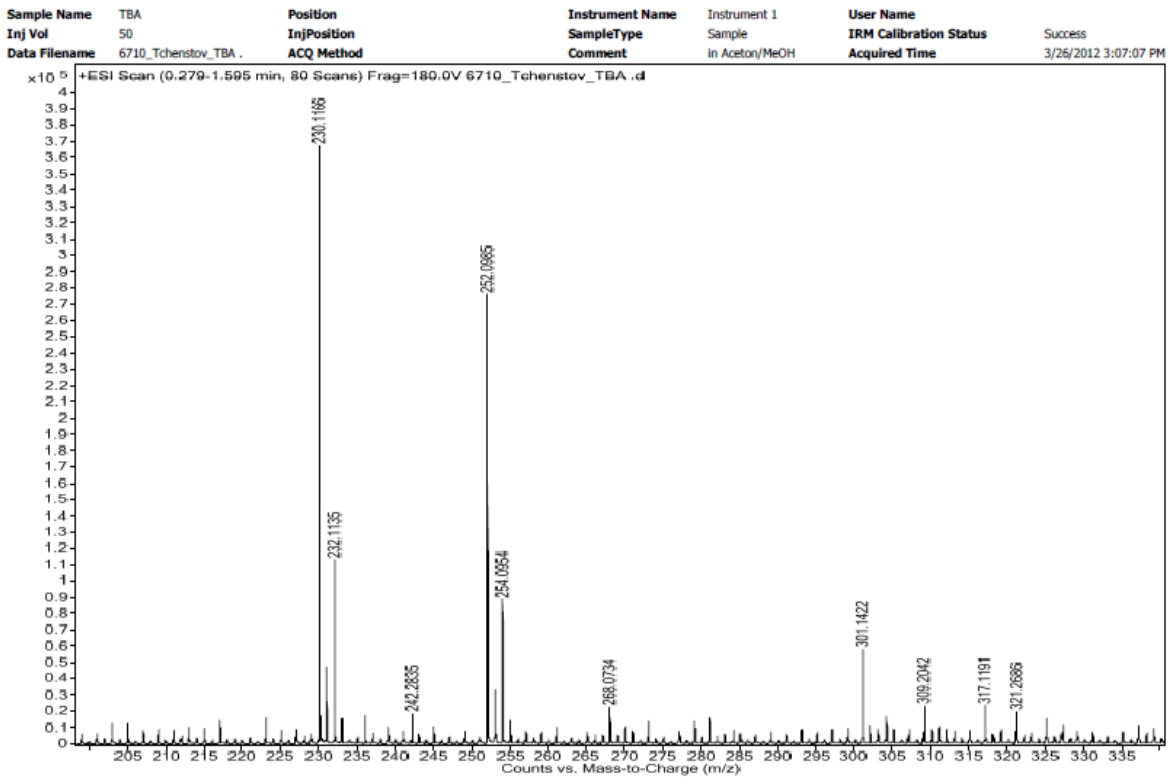

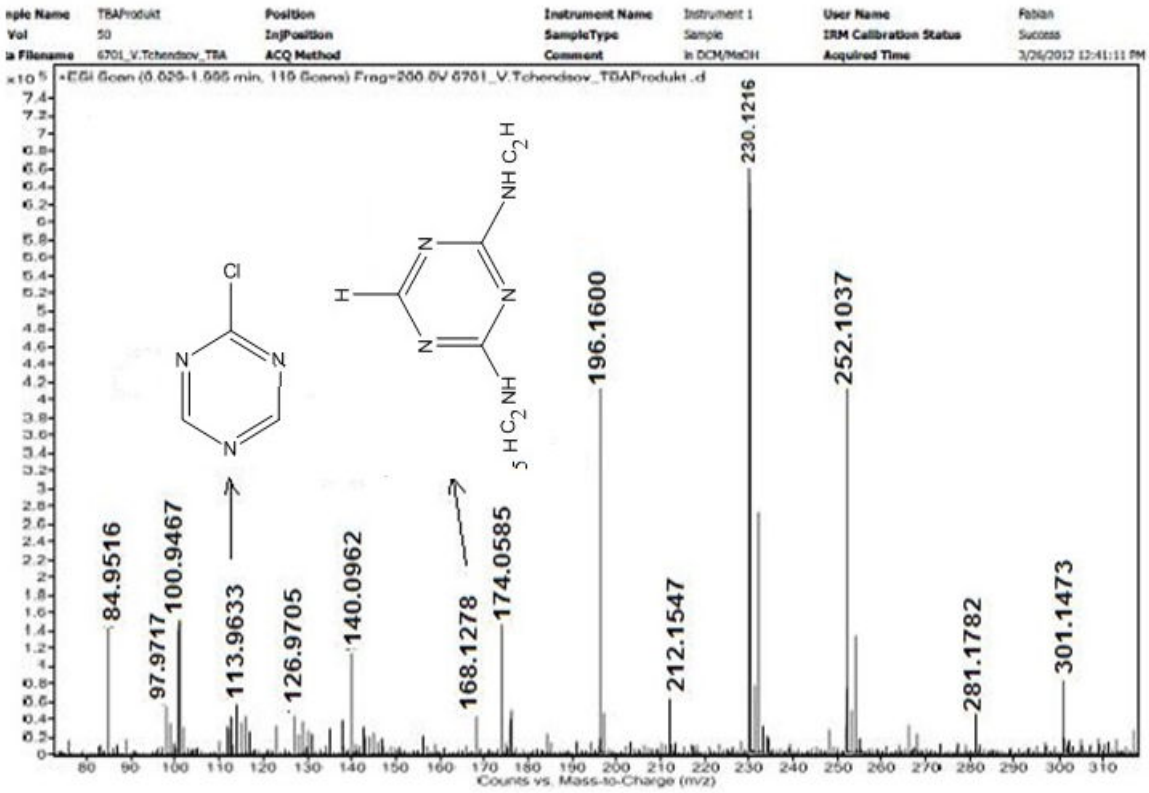

Figure 4.10: MS patterns of the photolysis degradation products of terbuthylazine recorded using an ESI source.

As reported in the literature on herbicide (containing s-triazines) degradation, the main reactions that clearly take place are dealkylation (of the lateral chains) and dechlorination [181]. This means loss of Cl with a mass number of 36 and acquisition of OH-radicals with a mass number of 17. Subsequently followed by dealkylation, a fragmentation corresponding to the loss of the terbuthyl group without dechlorination at the beginning of the reaction can take place during indirect photolysis by OH-radicals [182]. It should be mentioned that fragmentation under the impact of collision in the MS chamber depends mainly on the structure of the side-chains at positions 4 and 6, which in the present case are represented mostly by N-alkyl groups [183].

Many molecules were observed which include hydroxyl-terbuthylazine with molecular weight 212.15 and 6-ethylamino-2-tert-butylamino-1,3,5-triazine with 168.13 m/z, as depicted in the MS spectrum displayed in Figure 4.10. We have also observed the formation of ammeline with 129.7 m/z among other intermediate products leading to cyanuric acid as the end product of the reaction [184, 185]. The proposed photo-degradation pathway of TBA in the presence of OH-radicals (i.e. in the presence of OH-radicals formed by direct photolysis of hydrogen peroxide) is depicted in Figure 4.11.

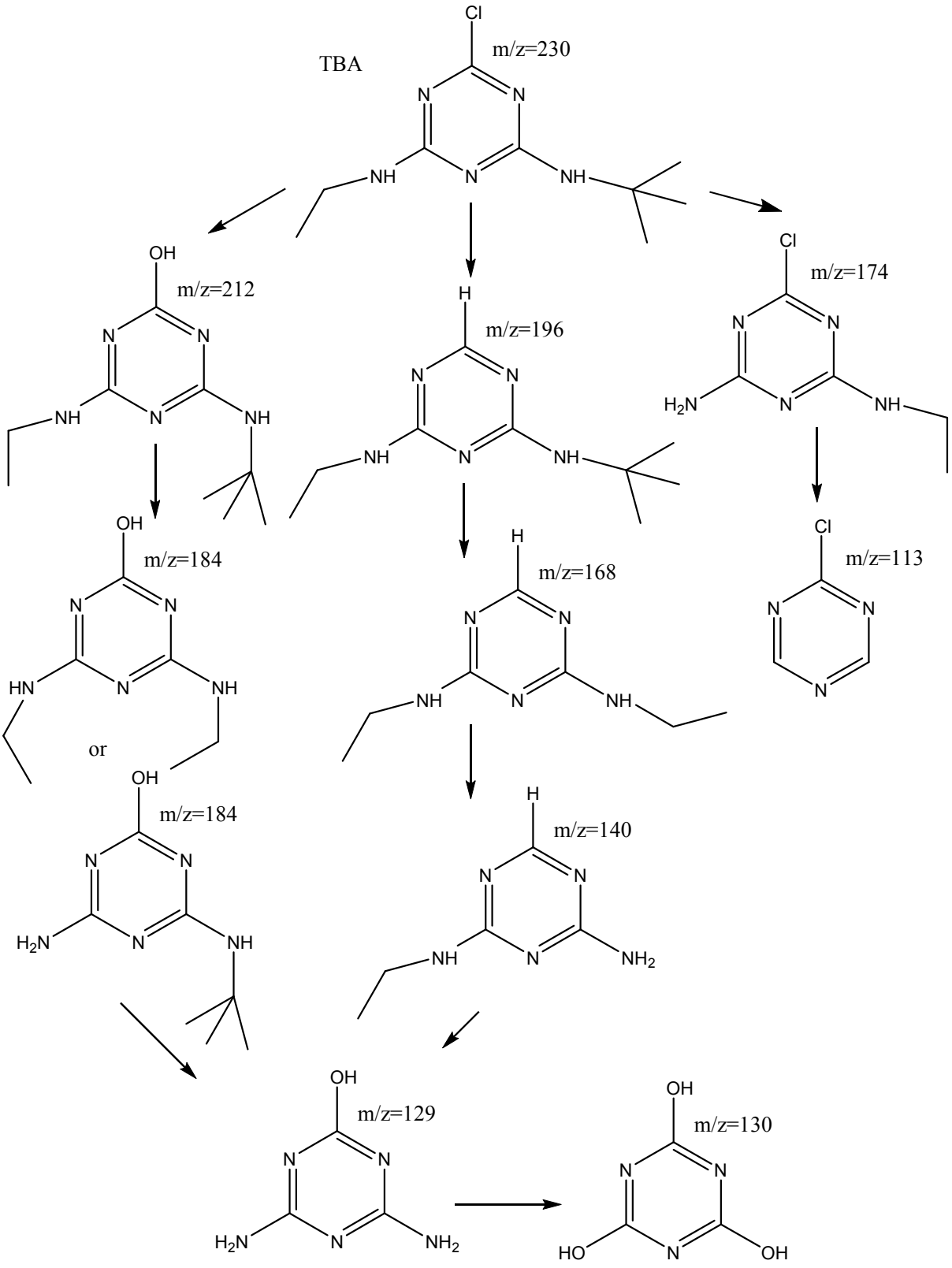

Figure 4.11: The indirect photo-degradation pathway of TBA in the presence of OH-radicals (observed in combination with NMR and MS).

The Retro-Diels-Alder mechanism can be used in the case where m/z are 212, 184, 129 (see Figure 4.9) to obtain ketone.

4.2 Degradation of simazine by indirect photo-oxidation

The results obtained from the study of the photolysis of terbuthylazine in the presence of OH-radicals are exploited in the following in order to determine the rate constant of the photo-oxidation reaction of simazine due to OH-radicals. The investigation of the reactivity of terbuthylazine with OH-radicals under atmospheric conditions has allowed us to estimate the ambient concentration of OH-radicals in the experimental setup. This knowledge was necessary for studying the photo-degradation of Simatine and other herbicides investigated in the framework of this thesis. Raman spectroscopy was used to monitor the reaction of simazine with OH-radicals, followed by a kinetic analysis of the Raman data.

Our experimental observations show that the degradation process is not the same for the different pesticides under investigation. In other words, the degradation in the case of simazine for example is found to be different from that of terbuthylazine and lindane.

4.2.1 Evaluation of Raman spectra

Raman spectroscopy was used to monitor the indirect photo-degradation of simazine in the monolayer. To this end, the Raman spectra measured from the simazine sample exposed for regular times (from 0 to 1260 s) to photo-degradation are displayed in Figure 4.12.

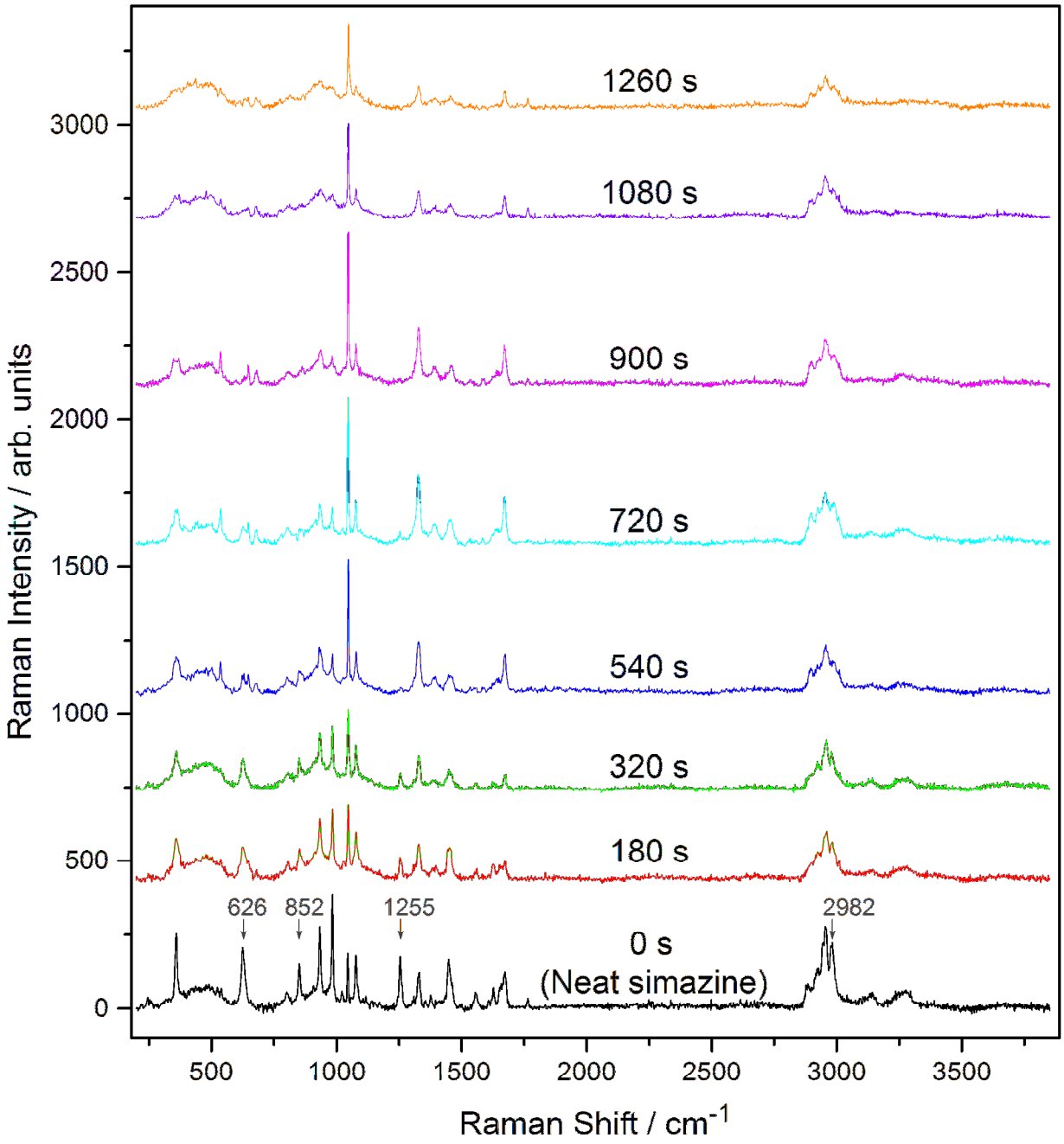

Figure 4.12: Raman spectra of simazine exposed to photo-oxidation by OH radicals for different reaction times

The Raman spectra shown in Figure 4.12 have been baseline-subtracted. It can be seen that the Raman bands of simazine decrease in intensity with reaction time. This is observed clearly for the most intense bands, including the bands in the CH stretching region around 2898 cm^{-1}, in the C-C stretching region (1150-1000) cm^{-1}, etc. Interestingly it is apparent that overall, many Raman bands of simazine quickly decrease in intensity until a photo-oxidation exposure time of about 320 s and for an exposure from 540 s some of the bands shortly regain intensity, but being in most cases quite different from the original bands in terms of band shape and

position. In particular the bands marked by the arrows in Figure 4.12 simply vanish by 320 s. This clearly suggests that the photo-oxidation reaction is such that at the very early stage, simazine quickly decomposes into one or a few intermediate products, which then also degrade later in the process. In this case, because only certain but not all Raman bands of simazine are concerned, a quick disappearance of simazine due to e.g. evaporation can be ruled out. Therefore, the correct assignment of Raman bands that are characteristic for the ongoing process and the kinetic analysis are needed to clarify the degradation mechanism further. Table 4.3 gives the assignment for some of the important bands of simazine which gradually change in intensity. The band assignment was supported by theoretical calculations and literature data; the complete band assignment can be found in the section 4.5 (theoretical calculation).

Table 4.3: Assignment of Raman bands observed during indirect photolysis of simazine

Bands (cm^{-1})	Assignment	Bands (cm^{-1})	Assignment
253	CH_3 twist.	983	Triazine ring trigonal str.
362.5	CCl str.	1072	C-OH str., C=N ring str., NH rock.
652.9	In-plane triazine ring def. + NH rock	1250.8	H-C-H Wag.
850	ring str.	1304	CH_2 twist.
864.6	C-N str.	1624	Ring def.
933.3	CCl str. + C-N str. + ring C=N str.	2948/2995	C-H str.
		3241	N-H sym. str.

4.2.2 Kinetics Analysis

The Raman spectra recorded at regular time intervals from simazine exposed to indirect photolysis were analyzed as a function of reaction time in order to extract kinetic parameters for the indirect photo-degradation. To obtain the different rate constants, the mono-exponential function $f(t) = A_0 \exp(-\lambda \bullet t)$ given in equation (46) has been used to model the time-dependent change in the Raman bands of simazine, since the integral intensity in the

Raman spectrum is directly proportional to the concentration of the corresponding species, as explained in Section 4.1.

λ is the fitting rate constant that is determined from the kinetic analysis of the experimental Raman spectra of simazine. Knowing the ambient OH-radical concentration from the analysis of the reference molecule (TBA), the OH reaction rate constant of simazine $k_{OH} = k_{OH}$ (simazine) was derived from the fitted rate constant as follows (equation 52):

$$\lambda = k_{OH} . C_{OH} \rightarrow k_{OH} = \lambda / C_{[OH]} \quad (52)$$

- **Rate constants derived from the analysis of areas**

We have used the Igor Pro software in order to perform a detailed multipeak band fitting procedure for all the vibrational bands observed in all Raman spectral recorded from the simazine sample subjected to indirect photo-oxidation at different reaction times. The areas are determined and then carefully inspected as a function of the reaction time; it appears that some Raman bands behave quite differently from others during the indirect photo-degradation reaction. The Raman bands showing gradual changes in intensity with respect to the reaction time have been summarized in Table 4.4, which gives the areas for each band at different reaction times.

Table 4.4: Areas of the Raman bands observed during simazine degradation by OH-radicals at different reaction times.

Time (s)	Band areas																
	359	**540**	**626**	**802**	**852**	**934**	**984**	**1045**	**1078**	**1255**	**1329**	**1450**	**1673**	**2884**	**2921**	**2956**	**2982**	**3129**
0	3827.31	637.507	4841.11	1061.46	2043.49	2467.65	3632.6	1290.54	2586.03	2467.26	2214.61	4248.86	2322.44	1518.2	4650.79	4388.66	6920.9	3320.32
180	5043.59	819.391	3067.39	1127.11	1948.52	1521.73	2461.02	2311.33	3020.84	1070.52	3182.69	3363.41	855.564	938.145	2640.6	5717.11	3770.65	2515.24
320	4195.82	1399.46	2543.06	1300.77	1203	1302	1679.85	2707.08	1403.87	627.631	2275.49	2183.75	814.065	918.16	2200.54	5511.02	1633.17	1486.73
540	5537.68	1399.46	969.918	941.803	1462.33	1074.64	1259.37	3189.33	1215.34	0.38	4567.02	2143.77	2354.24		2067.34	5855.8		2181.42
720	5074.64	1493.2	489.773	1314.97		1116	1493.2	3919.46	1376.43		6029.82	2701.29	2995.66		2051.79	6689.48		1440.97
900	2457.02	991.354	521.384	1214.52		791.87	991.354	3796.26	1054.1		5131.8	2008.1	2592.54		1650.4	6107.28		810.731
1080	2351.63	420.069		1471.67		390.29	420.069	2373.17	571.612		2361.17	1811.57	1372.09		1621.84	5290.11		
1260	5250.79	217.241				274.06	217.241	2391.62	5036.66		1901.25	2046.39	1081.27		1400.32	2462.9		

The areas in Table 4.4 have been plotted as a function of reaction time and the different time constants of the respective fitted mono-exponential traces were extracted as shown in Figure 4.13.

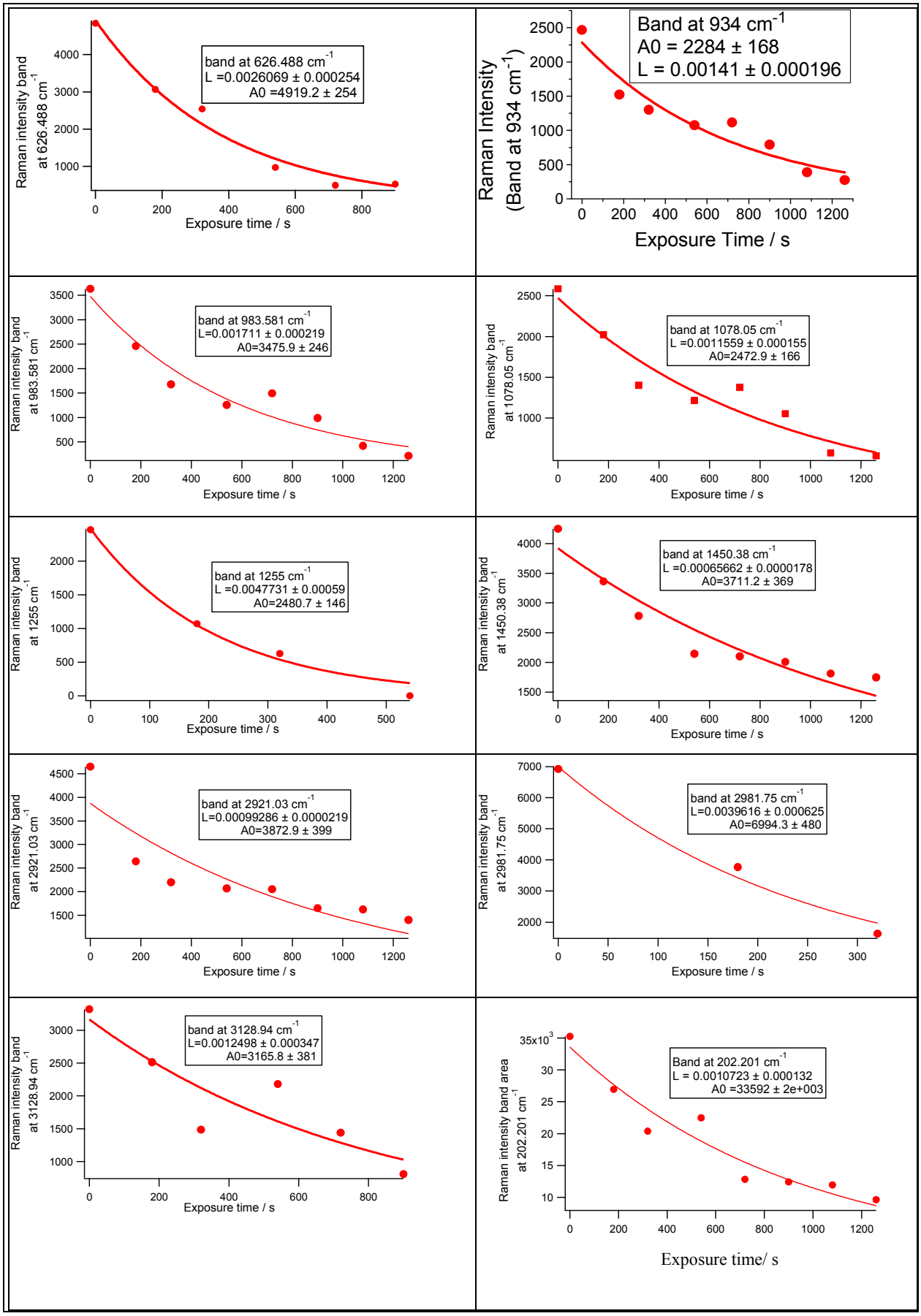
band at 626.488 cm-1
L =0.0026069 ± 0.000254
A0 =4919.2 ± 254
Raman intensity band at 626.488 cm-1
Exposure time / s
Band at 934 cm-1
A0 = 2284 ± 168
L = 0.00141 ± 0.000196
Raman Intensity (Band at 934 cm-1)
Exposure Time / s
band at 983.581 cm-1
L=0.001711 ± 0.000219
A0=3475.9 ± 246
Raman intensity band at 983.581 cm-1
Exposure time / s
band at 1078.05 cm-1
L =0.0011559 ± 0.000155
A0=2472.9 ± 166
Raman intensity band at 1078.05 cm-1
Exposure time / s
band at 1255 cm-1
L =0.0047731 ± 0.00059
A0=2480.7 ± 146
Raman intensity band at 1255 cm-1
Exposure time / s
band at 1450.38 cm-1
L =0.00065662 ± 0.0000178
A0=3711.2 ± 369
Raman intensity band at 1450.38 cm-1
Exposure time / s
band at 2921.03 cm-1
L=0.00099286 ± 0.0000219
A0=3872.9 ± 399
Raman intensity band at 2921.03 cm-1
Exposure time / s
band at 2981.75 cm-1
L=0.0039616 ± 0.000625
A0=6994.3 ± 480
Raman intensity band at 2981.75 cm-1
Exposure time / s
band at 3128.94 cm-1
L=0.0012498 ± 0.000347
A0=3165.8 ± 381
Raman intensity band at 3128.94 cm-1
Exposure time / s
Band at 202.201 cm-1
L = 0.0010723 ± 0.000132
A0 =33592 ± 2e+003
35x10-3
Raman intensity band area at 202.201 cm-1
Exposure time/ s

Figure 4.13: Plots of Raman areas as a function of time during simazine photolysis (symbols) and corresponding mono-exponential fits.

Figure 4.13 shows that the fitted rate constants describing the temporal evolution of the areas of the Raman bands of simazine range from (6.566 ± 0.178) x 10^{-4} to (4.77 ± 0.590) x 10^{-3} s^{-1}; i.e. with up to one order of magnitude spread indicating that the behavior of different bands describes different reaction mechanisms.

OH rate constant for simazine photo-degradation

In order to establish which value(s) of the fitted rate constants describes the overall simazine reaction, we have made several necessary considerations from using the theoretical as well as experimental results. The above analysis of the temporal evolution of the of the Raman areas of simazine shows that the Raman bands of simazine can be subdivided into three groups corresponding to fitted rate constants from lowest values (< 0.001) s^{-1} for just a few bands, intermediate values (~ 0.002) s^{-1} for some bands (epically those belonging to vibrations involving the triazine ring), to highest values (~ 0.004) s^{-1} for some bands involving specifically C-H and CH_2 vibrations. This analysis can be understood as follows: As far as the spectral features specifically reflecting the disappearance of simazine are concerned, the highest rate constant (4.77 ± 0.590) x 10^{-3} s^{-1} obtained has to be considered; this value corresponds to the band observed at about 1255 cm^{-1} in the Raman spectra. Hence, the OH rate constant has been calculated from the fitted rate constant at 1255 cm^{-1} as follows:

$k_{OH}(CH_2) = \lambda / C_{OH} =$ **$(3.9 \pm 0.59) \times 10^{-3} / (163 \pm 31) \times 10^{6}$** $= (2.73163 \pm 0.645) \times 10^{-11}$ $cm^3 \cdot s^{-1}$.

Based on the theoretical normal mode calculation for simazine (see Section 4.5), the vibrational mode at 1255 cm^{-1} is corresponding to the CH_2 deformation modes (twisting and bending) [184, 186]. A big impact such as the breakage of CH_2 groups (or of moieties carrying these groups) would cause the 1255 cm^{-1} mode to disappear, as clearly indicated by the fastest vanishing of this band from the Raman spectra recorded from the simazine sample after different exposure times to photo-oxidation (see Figure 4.12). Moreover, the 1255 cm^{-1} mode will be sensitive to change affecting the ethyl groups of the simazine molecule. In fact the theoretical results prove that the aforementioned vibrations described by this mode belong entirely to the ethyl groups of simazine. This is further supported by the fact the band at 2981.75 cm^{-1}, which involves CH stretching vibrations of the ethyl sites of simazine also

quickly decrease and vanish within a photo-oxidation exposure time of 320 s and yields a very similar fitted rate constant as the 1255 cm^{-1} band.

Moreover, as will be demonstrated in the following section, mass spectroscopy results have shown that there is breakage of ethyl groups from the simazine molecule. In this case, some cleaved ethyl groups, which are volatile because of the short chain length, will become invisible in the Raman spectra recorded from the solid simazine sample, what is agreement with the Raman results. The scissoring mode of the CH bonds belonging to the s-triazine ring is clearly different from that belonging to the ethyl groups, since the former appears at ~ 3150 cm^{-1}. This band does not show any significant change in intensity with the reaction time, what is in agreement with the mass spectroscopic data suggesting that the indirect photolysis of simazine should lead to an end product containing an intact s-triazine ring (with ring C-H bonds).

4.2.3 Characterization of simazine degradation products by NMR and mass spectrometry

NMR and MS data can help to elucidate the different paths of the degradation reaction under study via the identification of the reaction products and to validate the calculation of the rate constant performed above using Raman data. In the case of NMR data, the acquisition of ^{1}H NMR spectra with $CDCl_3$ as a solvent was done using a Bruker spectrometer operating at 700 MHz. Decoupling was performed at 0.80 ppm to elucidate the CH_3 group. Figure 4.14 shows the ^{1}H NMR spectra of the simazine subjected to indirect photo-oxidation.

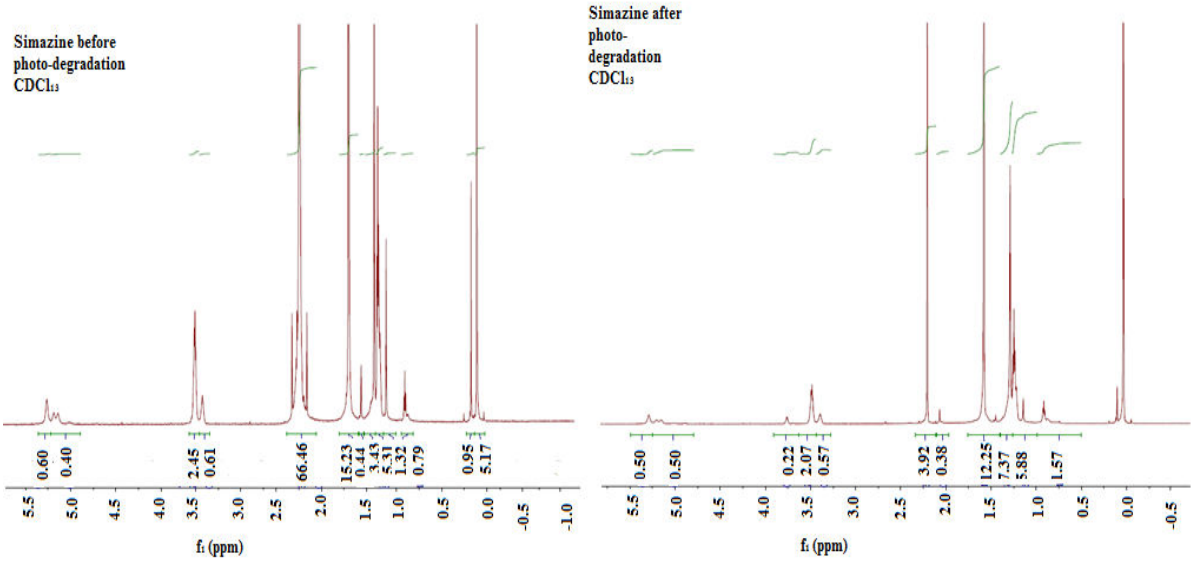

Figure 4.14: ^{1}H NMR spectrum of simazine after indirect photolysis by OH-radicals (The simazine sample was prepared from 7.5 mg and 83.0 mg Aerosil R972 in 1.4 mL acetone and 3.1 mL chloroform.)**.**

In Figure 4.14, besides the signal at 23 ppm indicates the presence of NH protons. Interestingly, the presence of OH group is indicated at 3.5 ppm in the NMR spectrum of the photo-oxidized simazine sample. Moreover, the CH_2CH_3 (ethyl) group is not present in the spectrum, which allows us to better understand the results of Raman spectroscopy.

Besides NMR investigations, the MS method was also used investigate the photo-degradation of simazine. The mass spectrum recorded from the simazine sample after photolysis is shown in Figure 4.15, where the ion fragments with the m/z values of 203, 139, 113, 101, and 81 which were observed correspond to the original simazine molecule and the main degradation products.

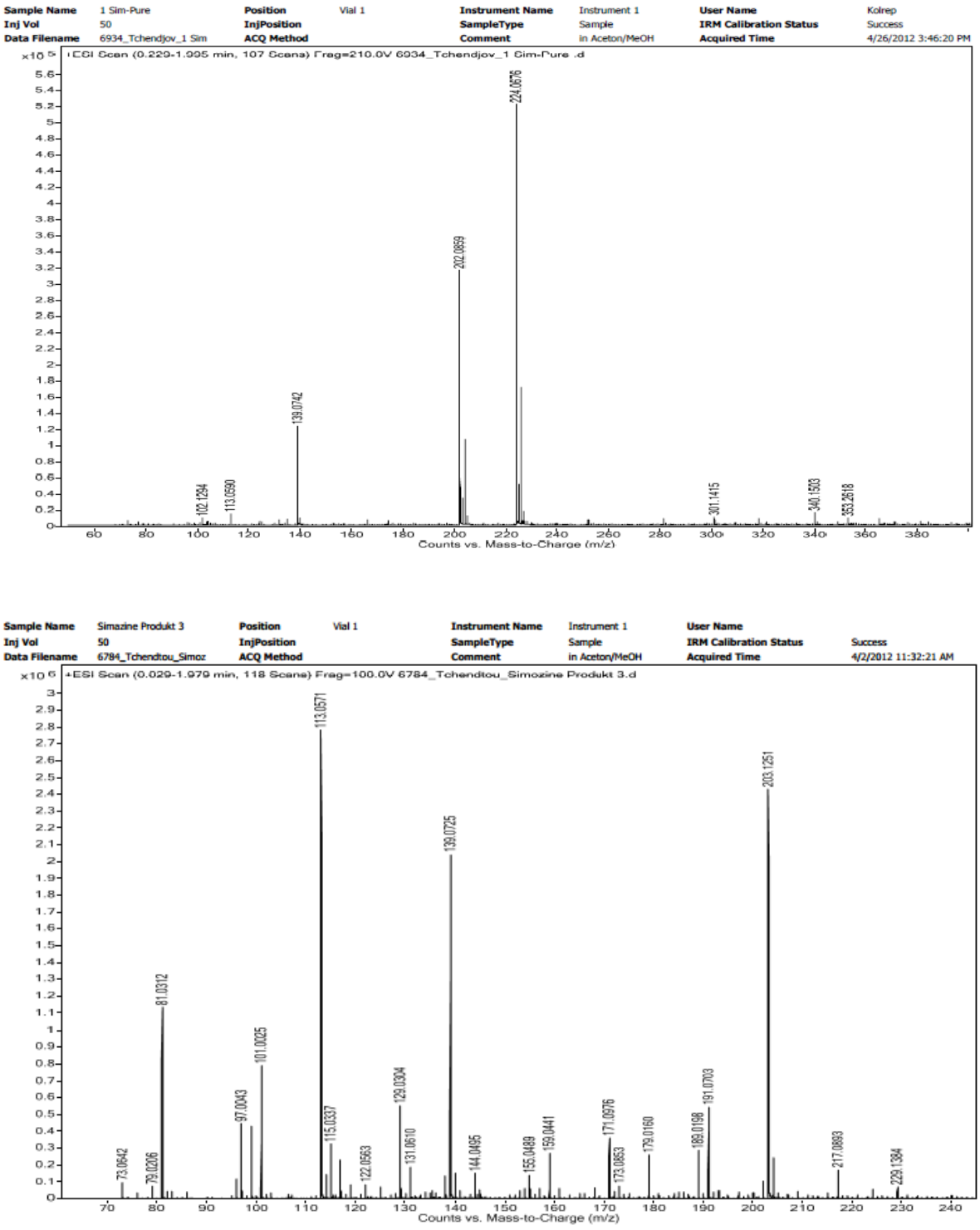

Figure 4.15: MS patterns after photolysis degradation of simazine recorded using an ESI source. MS was used to monitor the parent compound of simazine and its decomposition products**.**

Especially, the formed ion fragment signal at m/z equal to 81 can be assigned to s-triazine. The indication for the formation of hydroxyl-s-triazine is given by the signal at m/z 101. It can be also observed that the formation of 2,6-hydroxy-4-amino-1,3,5-triazine with an ion at m/z 129 is possible. The different ion fragments in the MS spectrum provide the insights

about the intermediate and final products obtained during the photolysis of simazine. Regarding the possible products formed, since the NMR data also suggest the presence of s-triazine and hydroxyl-s-triazine and the absence ethyl groups, both the NMR and MS results complete the understanding and interpretation of the Raman spectroscopy results.

4.3 Degradation of lindane (γ-hexachlorocyclohexan) by indirect photooxidation

Knowing the ambient OH-concentration in the experimental environment calculated using terbuthylazine as a reference molecule; we can determine the rate constant of the photo-oxidation reaction of γ-hexachlorocyclohexan (lindane) with OH-radicals. To this end, we proceed similarly as in the case of simazine above by evaluating the Raman spectra recorded as a function of the reaction time and by performing a kinetic analysis of the Raman data.

4.3.1 Evaluation of Raman spectra

The Raman spectra recorded form the lindane sample at different reaction times and are displayed in Figure 4.16 The shown Raman spectra have been baseline subtracted. It appears clearly in Figure 4.16 that many of the Raman bands decrease continuously in intensity with the reaction time. The areas of the numerous Raman bands of lindane displaying significant temporal variation in intensity have been considered for kinetic analysis.

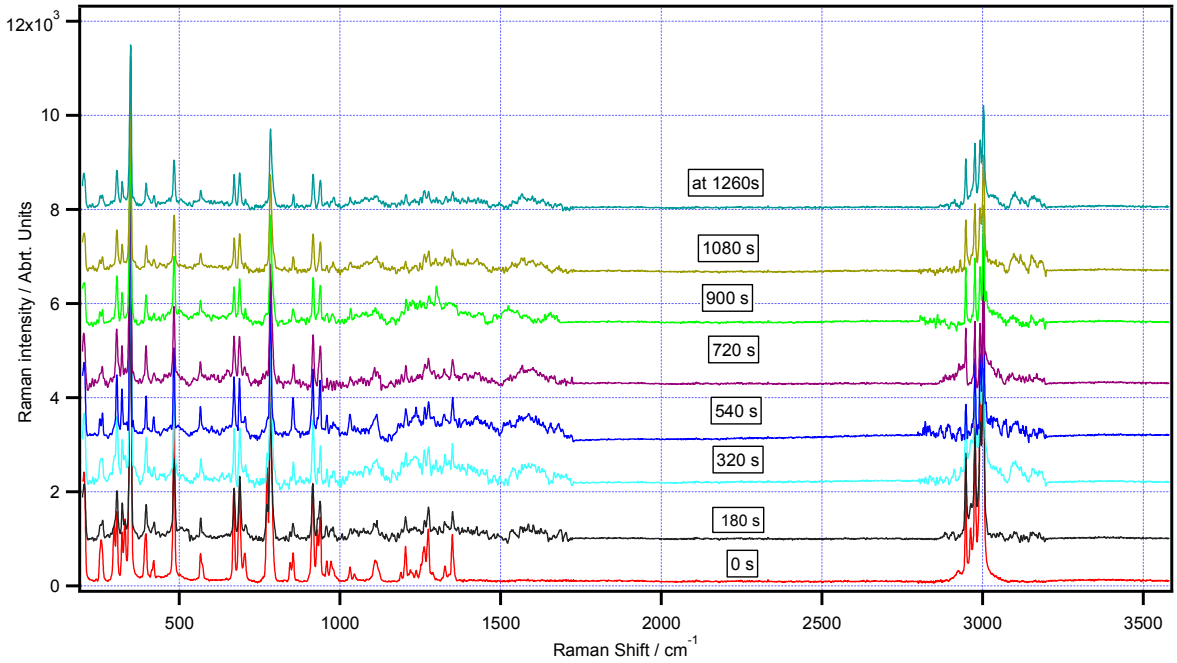

Figure 4.16: Raman spectra at regular time interval of lindane exposed to photo-oxidation by OH-radicals for different times

Table 4.5 summarizes the assignment of the main Raman bands of lindane. The band assignment is based on the results obtained from the theoretical calculation of the normal modes of lindane. It is worth to mention that the stretching vibrations of the abundant CCl bonds in the lindane molecule correspond to the mode observed at about 745 cm^{-1} in the Raman spectrum. In the spectral region 2925-2850 cm^{-1}, the CH stretching is observed.

Table 4.5: Assignment of Raman bands observed during indirect photolysis of lindane

Bands (cm-1)	Assignment	Bands (cm-1)	Assignment
200	CCl str.	1072	COH str.
349	CCl str.	1220	CH rock.
683	twi. Ring	1250.8	H-CH wag.
843	ring str.	1304	CH_2 twist.
924	ring str.	1700/1750	C=O str.
1041	ring str.	2948/3100	C-H str.
		3220/3250	OH str.

4.3.2 Kinetic Analysis

As in the case of simazine, the Raman spectra of lindane recorded at regular time intervals were analyzed as a function of reaction time in order to extract kinetic parameters for the photo-degradation. The following mono-exponential function $f(t) = A_0 \exp(-\lambda \bullet t)$ given in equation (46) has been used to model the time-dependent change in the Raman bands of lindane. The fitting rate constant λ in this case is determined from the kinetic analysis of the experimental Raman spectra of lindane. Knowing the ambient OH-radical concentration from the analysis of the reference molecule (TBA), the OH reaction rate constant of lindane $k_{OH} = k_{OH}$ (lindane) was derived from the fitted rate constant as follows (equation 53):

$$\lambda = k_{OH} . C_{OH} \rightarrow k_{OH} = \lambda / C_{[OH]} \quad (53)$$

- **Reaction time constants derived from the analysis of areas**

Table 4.6 gives the areas of the observed Raman bands for lindane at different times during indirect photo-degradation; these band areas were calculated using the Igor Pro software as in the case of the simazine. The following Figure 4.17 shows the corresponding plots of the areas as function of the reaction time and the fitted rate constants (the L values) extracted from the mono-exponential fitting of these plots.

Table 4.6: Areas of the Raman bands observed during lindane degradation by OH-radicals at different reaction times

Band (cm^{-1})	**202.201**	**256.668**	**396.783**	**482.836**	**669.1**	**687.129**	**784.028**	**914.988**	**2947.85**
Area (Arb. Units) / Time (s)									
0	35269.3	10983.4	11565.6	32108.3	15164.2	20639.2	51170.4	21499.4	14492.9
180	16955	5373.6	6916.54	19500.9	11604.2	13465.8	34482.7	12559.6	13711.1
320	20391.1	8262.02	8405.53	18134.9	7993.85	10289.7	33001.9	12188.1	7706.41
540	22485.2	4388.97	6233.23	14930.3	11656.3	8914.92	26971.8	12172.7	7127.72
720	12856.7	4029.82	6985.87	16549	8976.15	9906.51	30875.5	12180	6609.33
900	12438.8	2435.17	4768.08	15164.4	6740.64	8305.67	25904.6	8183.78	5990.59
1080	11960.7	4921.32	4194.65	11906.1	5436.11	7735.94	25475.8	7759.54	4491.52
1260	9666.07	4401.45	4661.83	10010.9	4793.82	6930.38	20340.8	6119.42	2861.37

Band (cm^{-1})	**2976.37**	**2992.8**
Area(Arb. Units) / Time(s)		
0	25167.6	36716.7
180	18896.5	24868.3
320	11801.8	10106.8
540	9969.28	9204.99
720	8888.86	5632.17
900	5866.21	6446.79
1080	4491.52	5870.56
1260	2861.37	2804.41

Figure 4.17 summarizes the variation of the areas as function of the experimental duration. It can be seen that the areas decrease exponentially with reaction time.

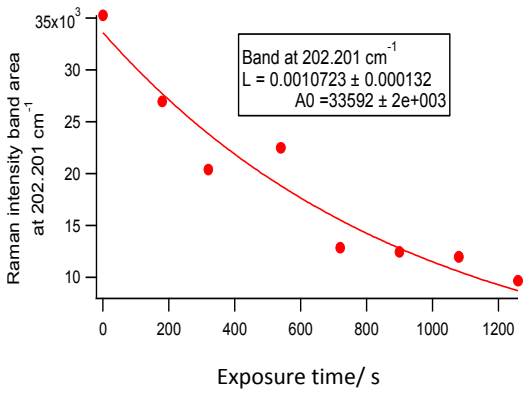
Band at 202.201 cm-1
L = 0.0010723 ± 0.000132
A0 =33592 ± 2e+003
Raman intensity band area at 202.201 cm-1
35x10^3
Exposure time/ s

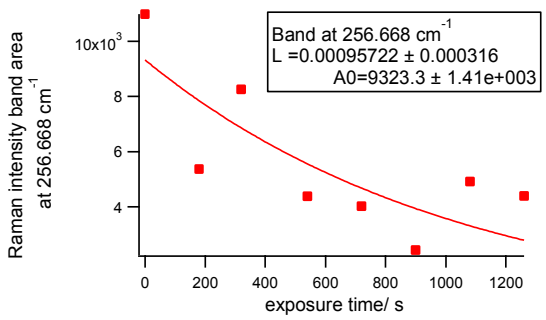
Band at 256.668 cm-1
L =0.00095722 ± 0.000316
A0=9323.3 ± 1.41e+003
Raman intensity band area at 256.668 cm-1
10x10^3
exposure time/ s

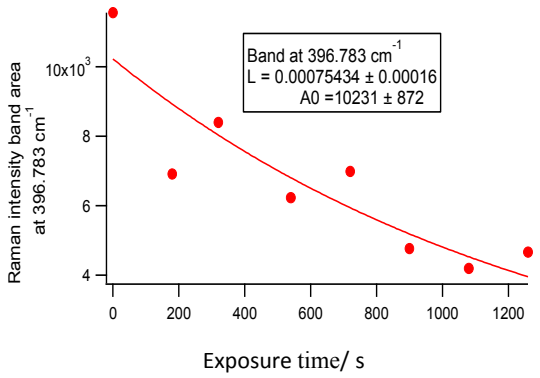
Band at 396.783 cm-1
L = 0.00075434 ± 0.00016
A0 =10231 ± 872
Raman intensity band area at 396.783 cm-1
10x10^3
Exposure time/ s

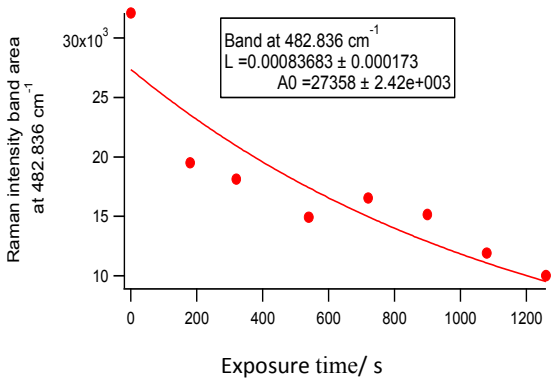
Band at 482.836 cm-1
L =0.00083683 ± 0.000173
A0 =27358 ± 2.42e+003
Raman intensity band area at 482.836 cm-1
30x10^3
Exposure time/ s

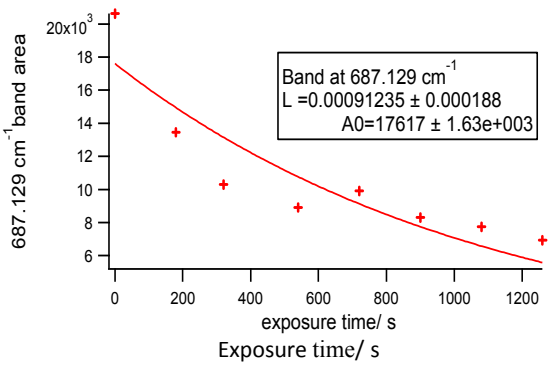
Band at 687.129 cm-1
L =0.00091235 ± 0.000188
A0=17617 ± 1.63e+003
687.129 cm-1 band area
20x10^3
exposure time/ s
Exposure time/ s

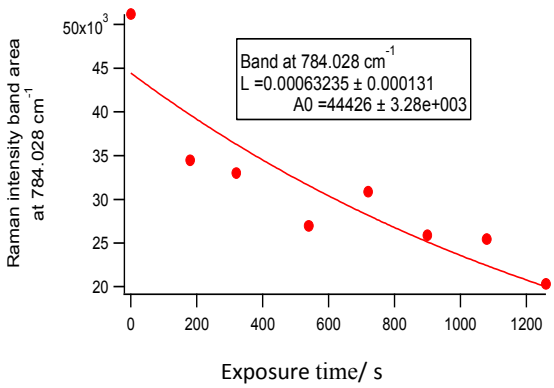
Band at 784.028 cm-1
L =0.00063235 ± 0.000131
A0 =44426 ± 3.28e+003
Raman intensity band area at 784.028 cm-1
50x10^3
Exposure time/ s

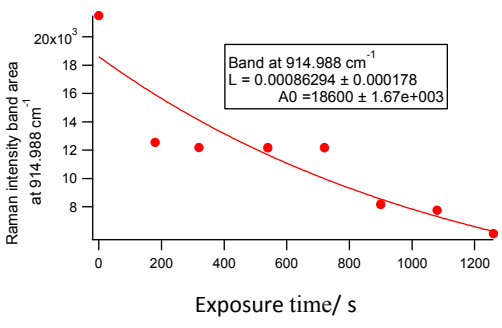
Band at 914.988 cm-1
L = 0.00086294 ± 0.000178
A0 =18600 ± 1.67e+003
Raman intensity band area at 914.988 cm-1
20x10^3
Exposure time/ s

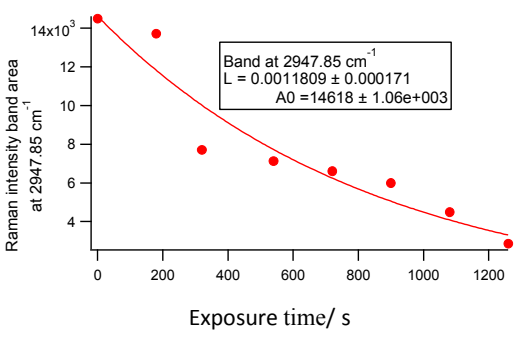
Band at 2947.85 cm-1
L = 0.0011809 ± 0.000171
A0 =14618 ± 1.06e+003
Raman intensity band area at 2947.85 cm-1
14x10^3
Exposure time/ s

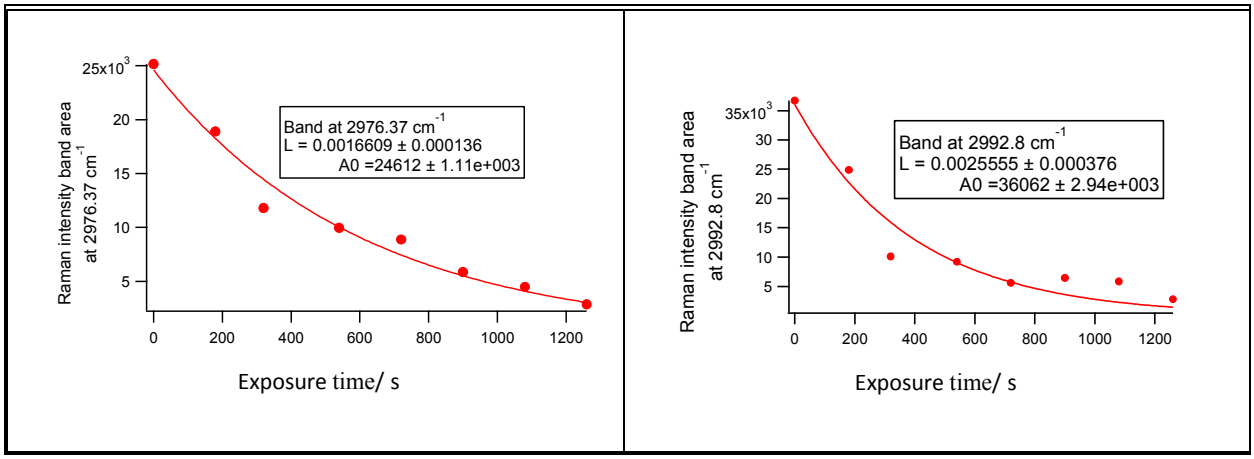

Figure 4.17: Plots of specific Raman band areas as function of time during lindane photolysis (symbols) and corresponding mono-exponential fits.

Figure 4.17 shows that the fitted rate constants obtained from the kinetic analysis of the Raman band areas of lindane are spread from (6.3235 ± 0.1310) x 10^{-4} to (2.555 ± 0.0376) x 10^{-3} s^{-1}. This means that the different bands considered behave differently during the degradation process.

- **OH rate constant of lindane photo-degradation**

Note again that the spectral changes which describe the overall temporal diminution of the original lindane molecules are those ones with the highest fitted rate constant values. As it can be seen in Figure 4.17, the higher rate constant value of the reaction is (2.555 ± 0.0376) x 10^{-3} s^{-1} and was obtained from the analysis of the areas of the Raman band of lindane at 2992.8 cm^{-1}. Furthermore, the Raman bands in the region around 2992.8 cm^{-1} are assigned to the stretching of CH bonds [187, 188]. The OH rate constant of the lindane photo-oxidation can be obtained from the fitted rate constant for the 2992.8 cm^{-1} area as follows:

$k_{OH} = \lambda / C_{OH}$ = (2.55 ± 0.04) x 10^{-3}/ **(163± 31)·10^{6}** = (156.44± 12.13)·10^{-13} $cm^3 \cdot s^{-1}$.

4.3.3 Characterization of lindane degradation products by NMR and mass spectrometry

NMR and MS data from the lindane subjected to photo-oxidation by OH-radicals have also been investigated. The ^{1}H NMR spectrum after photolysis of lindane is given in Figure 4.18, which contains some indications of the products formed during the reaction.

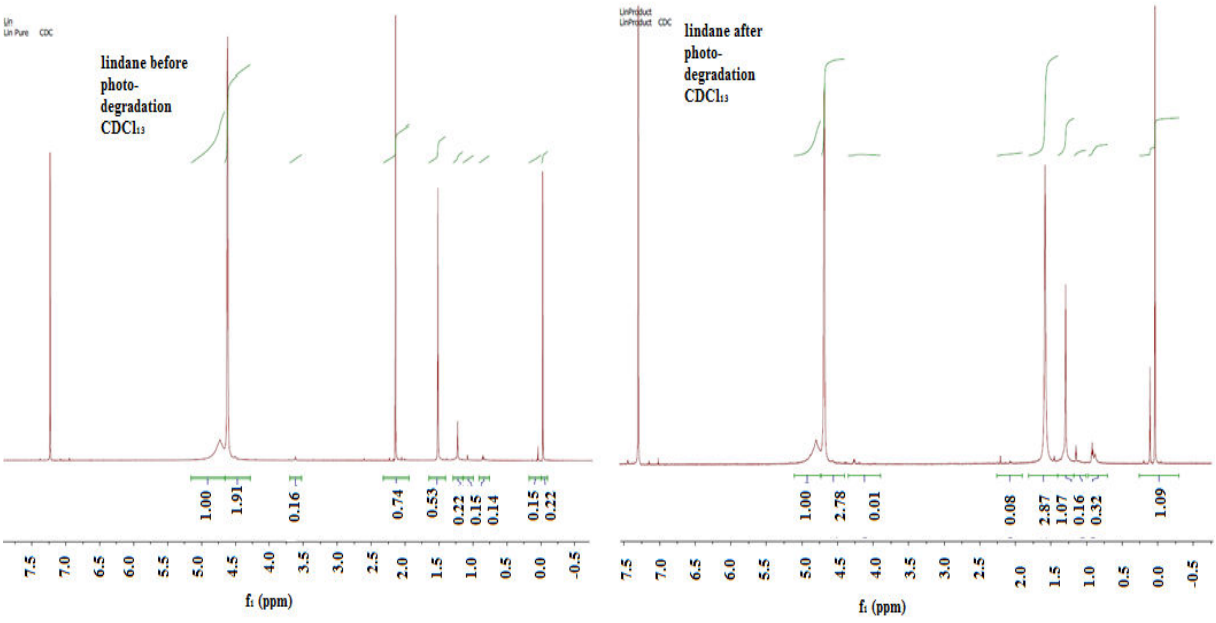

Figure 4.18: ^{1}H NMR spectrum of lindane after indirect photolysis by OH-radicals. (The lindane sample was prepared from 21.2 mg and 33.1 mg Aerosil R972 in 2.5 mL acetone and 1.5 mL chloroform.)**.**

The spectrum displays an OH signal at δ 7.3 ppm. The H-CCl protons give rise to the signal at δ 2.72 ppm. The ^{1}H resonance in OH (meta-position of s-triazine) is usually observed at δ 0.21 ppm. Moreover, the NMR spectrum indicates the disappearance of the CH radicals during photolysis of the lindane sample. This result suggests that there is a bond breaking reaction that takes place during the indirect photolysis. The exploitation of the MS data will give additional complementary information about the products formed during the reaction.

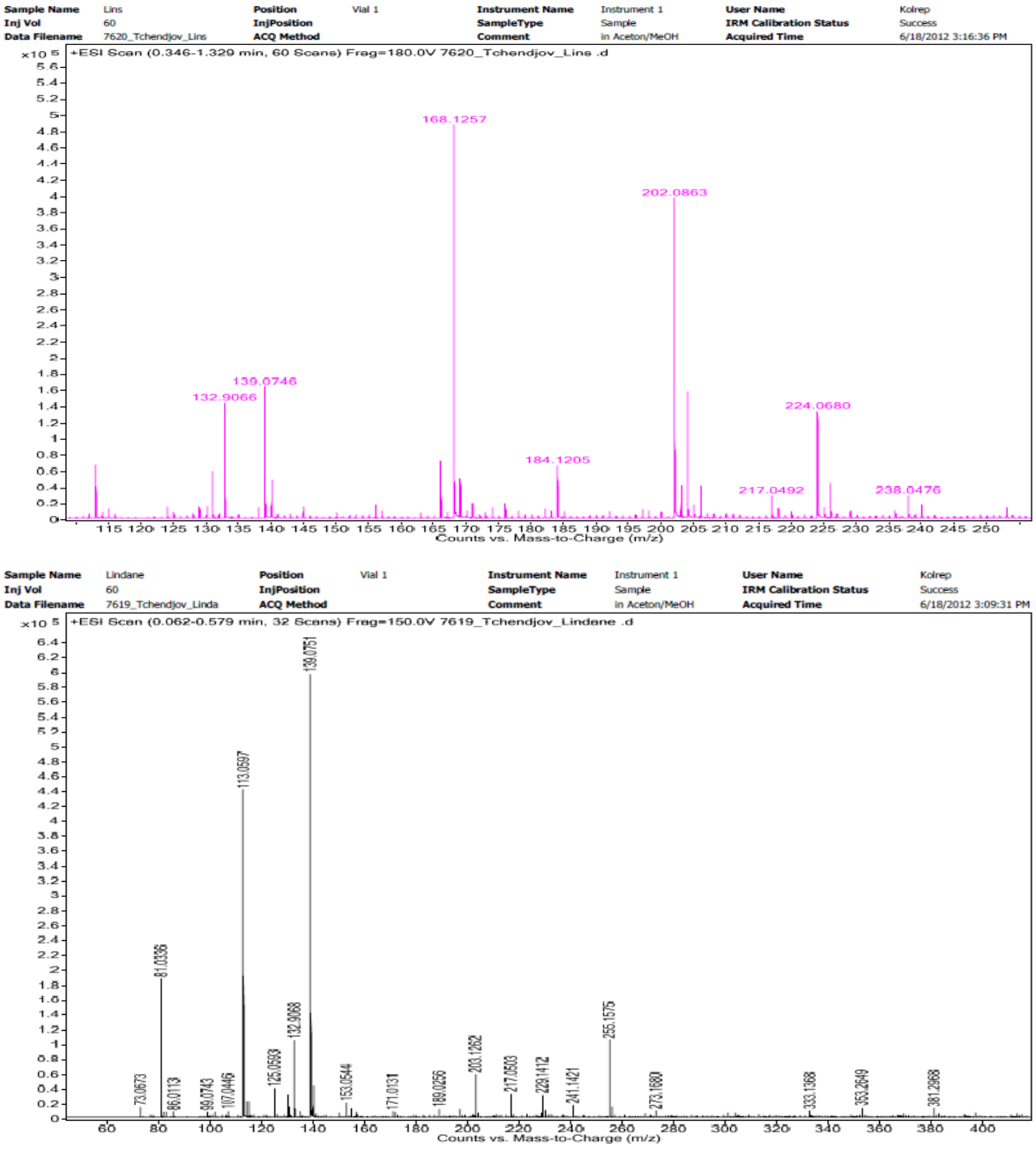

Figure 4.19: MS pattern after photolysis degradation of lindane recorded using an ESI source.

The analysis of the MS spectrum of the photo-oxidized lindane in Figure 4.19 reveals ion fragments with the m/z series 81.09, 113.09, and 139.07. The MS spectrum also shows a reduction of the CH radicals. According to both methods, the NMR and MS, they have been used for monitoring the degradation of semi-volatile organic compounds. The products obtained are 1,4-dihydroxybenzoquinone with ion m/z 139 and chlorobenzene with ion m/z 113 (see Appendix A4, Scheme A2.4.3.4).

4.4 Theoretical Model for calculations

The present Chapter provides details on the theoretical simulations performed in the framework of this dissertation in order to make correct assignments of the vibrations observed in the experimental Raman spectra of studied compounds and to verify the proposed mechanisms. The experimental reactants were taken for terbutylazine (TBA), simazine, and lindane, serving as reactants in the reaction of indirect photolysis, as well as on products of this reaction. In order to complement the full normal mode analysis, we have taken the IR absorption spectra of the same substances, since several vibrations (see Table 4.7 and Table 4.8) [189] cannot be reached in Raman spectra due to the consideration of symmetry.

Our choice for use of Quantum Chemistry Package "Turbomole" [190-192], widely used in academia and industry [193], was motivated in first order by the following consideration. It is well known that "Turbomole" is particularly suitable for the Cl-based compounds because of the appropriate treatment of the large quadrupole moment of the Cl atom and electron charge donation to the aromatic ring [194]. To provide an adequate description of the electronic structure of the molecules under study, we used the conventional methods of Hartree-Fock (HF) and density functional theory (DFT).

At the first step the geometry optimization of the molecular structure was performed. In the second stage the vibrational analysis in the harmonic approximation was conducted delivering the frequencies and intensities of Raman and IR spectra.

4.4.1 Model calculations and sample characterization with Raman and infrared (IR) spectroscopy

In the current work the so-called RI-J approximation of DFT was utilized. The efficient RI (Resolution of the Identity) guarantees a sufficient resolution for Coulomb interaction of energy and gradient calculations in the ground state and/or excited state [195, 196]. The use of this approach was justified by the fact that Hartree–Fock exchange does not suffer from the mentioned error [197], and RI-J method speeds up tenfold the non-hybrid DFT, allowing for DFT calculations in large molecular systems. The level of DFT theory used in the current work was B-P86. Motivated by the presence of chlorine, we have chosen the double zeta, split valence basis set SV (split valence) for all our calculations.

By calculating the vibrational spectrum in harmonic approximation we have introduced the internal normal coordinates. The fact, that energy optimization has converged was confirmed by the absence of negative frequencies in the harmonic vibrational spectrum obtained. Since the information on vibrational spectra, given by the harmonic approximation of ab-initio programs is not sufficient for the reconstruction of spectral changes and kinetic curves, several empirical assumptions should be made here. The knowledge of the anharmonicity term required for the force matrix correction is missing for these polyatomic molecules. No information on the mode-mode coupling is present either. A possible solution would consider the inversion of the problem by modeling the experimental Raman (IR) spectrum as a sum of the Lorentzian shapes given by all single harmonic modes from frequency (ω_{0i}) and intensity A_i delivered by the ab-initio calculation [198, 199] (see Equation (54)):

$$I(\omega) = \sum_{i=1}^{N} \left(\frac{A_i}{(\omega - \omega_{oi})^2 + \gamma_i^2} \right) \tag{54}$$

Here A_i stands for the intensity and ω_{0i} for the i-th individual vibrational frequency (ω_{0i}), taken from the normal mode analysis delivered by the program Turbomole. The only fitting parameter in this case is the set of the line-broadening factors (γ_i) defining the linewidth ($\Delta\omega_{0i}$) of each i-th harmonic ($\gamma_i = \frac{\Delta\omega_{0i}}{2}$), see also Appendix A0 for the results.

At the point ω= ω_{0i} peak amplitudes $I(\omega_{0i})$ are reproducing the intensities of the harmonic approximation, scaled down by the square of the linewidth γ_i. In this way the spectral intensity A_i given by the harmonic approximation is proportional to the area under the Lorentzian curve. A perfect demonstration of this approach is given by the Raman spectra of lindane, where practically all lines were fitted with the same FWHM and the peak amplitudes were equivalent to the harmonic intensities from ab-intio calculations. Unfortunately due to the increased effects of mode coupling as due to differences in anharmonicity constants for different modes the FWHM parameter γ_i in TBA and simazine needed to be fitted for each mode separately.

Peaks corresponding to the modes with intensities below 1% were neglected. By using this empirically fitted spectrum (equation 46) as a starting approximation to fit the real density of states dN/dE, a correct interaction potential can be reconstructed by solving this inverse problem. In any case, the fitted Raman and infrared spectra using equation (46), when compared with experimental spectra, are giving a hint to the determination of the realistic reaction paths [200]. The theoretical spectrum, simulating the spectral pattern evolving from the indirect photolysis reaction of each investigated pesticide sample, was taken as a linear combination of spectra calculated for all reaction products, in order to fit the experimental spectrum recorded at the end of the reaction.

After calculation of the vibrational spectra by Tubomole, the visualization of these vibrations in space was possible by using the program TmoleX. The output log file of the Turbomole code contains details not only results on structural optimization, but details the computed normal modes of vibration the mode IR and Raman activity test and the IR and Raman cross section respectively intensities, which are essential to simulate IR and Raman spectra. For more information, note that for the theoretical frequency calculations carried out, the following basics and principles apply in the Turbomole output log file (see Appendix A0): (i) imaginary (i.e. negative) wavenumbers indicate a negative curvature of the energy surface; (ii) zero frequency modes have no physical meaning except being generators of translations and rotations; (iii) each vibrational normal mode is given in terms of Cartesian displacement vectors of all atoms and has been normalized to unity (to use the reciprocal square root of the scalar product. In fact, when the scalar product is zero, the mode will disappear at the time where the transformation from mass weighted to internal coordinates is done.) [201]; (iv) band intensities or cross sections refer to independent non-degenerate normal modes; (v) dDIP/dQ is the normal mode derivative of the dipole moment.

Furthermore, the differential Raman cross sections that we have used refer to a scattering angle of 90 degree and to a negative frequency shift (Stokes lines). For the radiation polarization states (incident, scattered), note the following abbreviations: par, ort, and unpol for the parallel, orthogonal and unpolarized states, respectively. For example, (par, par) indicates that the incident radiation has its electric polarized parallel (par,) to the scattering plane and that the scattered wave is also polarized parallel (, par) to the scattering plane. The program Turbomole outputted the Raman cross sections for the different polarization states, including (par, par), (ort, unpol), or (unpol, par), since the Raman cross sections of the types

(par, ort), (ort, par) or (par, unpol) are all equal to (par, par), we have extracted the cross sections of the type (ort, unpol) for spectral simulations described above. All cross sections are given in percentage (%) relative to the most intense single mode of the same polarization type. We note that Raman cross sections depend on the sample temperature (here T = 298.15 K) and on the wavenumber of the exciting radiation (here: 18796.99 cm^{-1}).

4.4.2 Terbuthylazine (TBA): theoretical and experimental Raman analysis

In order to illustrate the application of the theoretical calculation principles described in this Chapter, we have first considered the simulated Raman spectrum of neat molecular terbuthylazine (TBA) presented together with the experimental spectrum in Figure 4.20. Some band assignment is also given in Table 4.7. The linewidth of the C-H stretching band in the region of 2840 – 3000 cm^{-1} in case of TBA turned out to be not much different from the FWHM of the low frequency components so that no special fit of line-broadening factor for methyl group vibrations was necessary. Since the wavenumbers stemming from the harmonic approximation are generally overestimated by the force constants in ab-initio programs, a slight red spectral shift correction of about 200 cm^{-1} was undertaken for the C-H vibrations in this range.

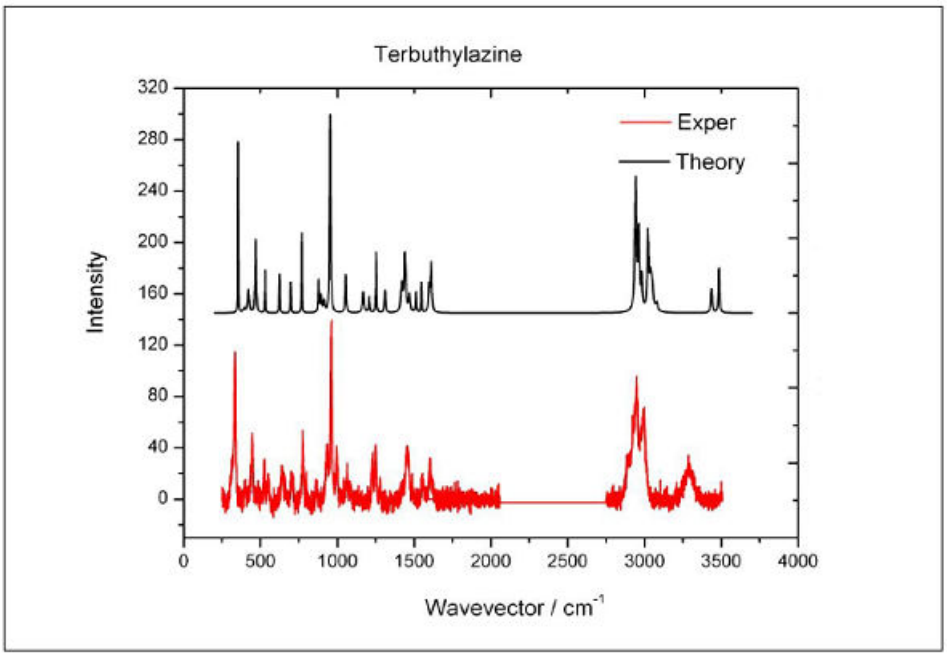

Figure 4.20: Comparison of the theoretical and experimental Raman spectra of TBA

Table 4.7 : Vibrational assignments of Raman active TBA modes displayed in Figure 4.20 (wavenumbers are given in cm^{-1}).

Experiment	Theory	Symmetry
334	353 *s*	*r* CH_3, *sc* C-C-N, sc C-C-C, ω ring
396	420 *w*	*v* C-Cl , *v* ring, asym *v* C-C-N, asym *v* C-C-N
445	452 *m*	*r* NH, *r* CH_2
519	531 *m*	asym *v* ring, *r* C-C-N-CH_3 backbone, *r* NH
641	625 *w*	*t* NH
696	698 *w*	asym *v* ring, *sc* C-N-C, ω CH_3
776	770 *m*	*v* CH_3-C-CH_3, *v* C-N-C
867	879 *w*	ω CH_3, *v* C-N-C, asym *v* ring
959	982 *s*	*v* ring, *v* CH_3-CH_2, ω CH_3
1064	1055 *w*	*sc* NH, *v* CH_3-CH_2, ω CH_3
1137	1163 *w*	*r* NH, *v* NH-CH_2, ω CH_3
1253	1253 *m*	*t* CH_2
1284	1310 *w*	ω CH_2, *r* NH, asym *v* ring
1455	1470 *m*	*r* NH, *sc* CH_3, *sc* CH_2
1553	1547 *w*	*sc* NH, *v* ring
1608	1611 *m*	ω NH, asym *v* N-C-N, *sc* (C-N-C) ring
2949	2936 *s*	*v* C-H_3
2998	3022 *s*	asym *v* C-H_3
3286 br. Band	3438 *m*	*op v* ω N-H (amino-terbuthyl)
3286 br. Band	3488 *m*	*op v* ω N-H (amino-ethyl)

The abbreviations used are: *s* – strong, *m* –medium,, *w*-weak, br – broad, *ip* – in-plane, *op* – out-of-plane, *v* stretching, *sc* – scissoring, *r*- rocking, τ- torsional, ω – wagging [202].

The mode assignment of the theoretical TBA spectrum in Figure 4.20 is presented in Table 4.7. We are focusing our attention on the selective discussion of the modes, which are changing their intensity in the course of the photolysis. The strong line observed at 353 cm^{-1} involves simultaneously the rocking motion of CH_3 residues belonging to the terbuthyl group, scissoring motion of the ethyamino C-C-N and terbuthylamino C-C-C chains, being coupled with the s-triazine ring wagging.

The next weak line at 420 cm^{-1} is responsible for a strong C-Cl stretching symmetrically synchronized with the s-triazine ring stretch. This mode is complemented by a bending (torsoinal) deformation of the backbone of the amino-terbuthyl and amino-ethyl side chains. The terbuthyl group is in this case moving with relatively larger amplitude than the ethyl group and is therefore more strongly coupled with the CCl and s-triazine ring stretching.

The vibration at 524 cm^{-1} involves the asymmetric ring deformation coupled to a symmetric rocking motion of the amino-terbuthyl group on one side and to the asymmetric rocking deformations within the amino-ethyl group on the other side. It also includes the rocking motion of NH groups. In contrast to the previous case no stretch of C-Cl bond is detected here. The next, moderately strong mode at 770 cm^{-1} is predominantly localized on the amino-terbuthyl group and is given by the symmetric stretch of nitrogen and methyl residues against the central carbon atom.

Other main features were provided by the change in the intensity of the vibrational mode responsible for the scissoring vibration of the NH, CH_2, and CH_3 residues of the amino-ethyl group (around 1470 cm^{-1}), as well as for the N-H wagging vibration coupled with a slight ring deformation (around 1611 cm^{-1}) (see Figure 4.21). The vibrational mode at 3022 cm^{-1} is matched with the asymmetric C-H stretching in the methyl groups, whereas the modes at 3438 cm^{-1} 3488 cm^{-1} belong to the wagging motions of NH residues in the amino-terbuthyl and amino-ethyl groups, respectively [203].

As a rule the vibrational spectra calculated with the harmonic and anharmonic approximation tend to overestimate the force constants (see Figure 4.21), what causes a strong blue shift of the calculated spectra for the high energy vibrations, such as OH and CH NH, etc..[204].

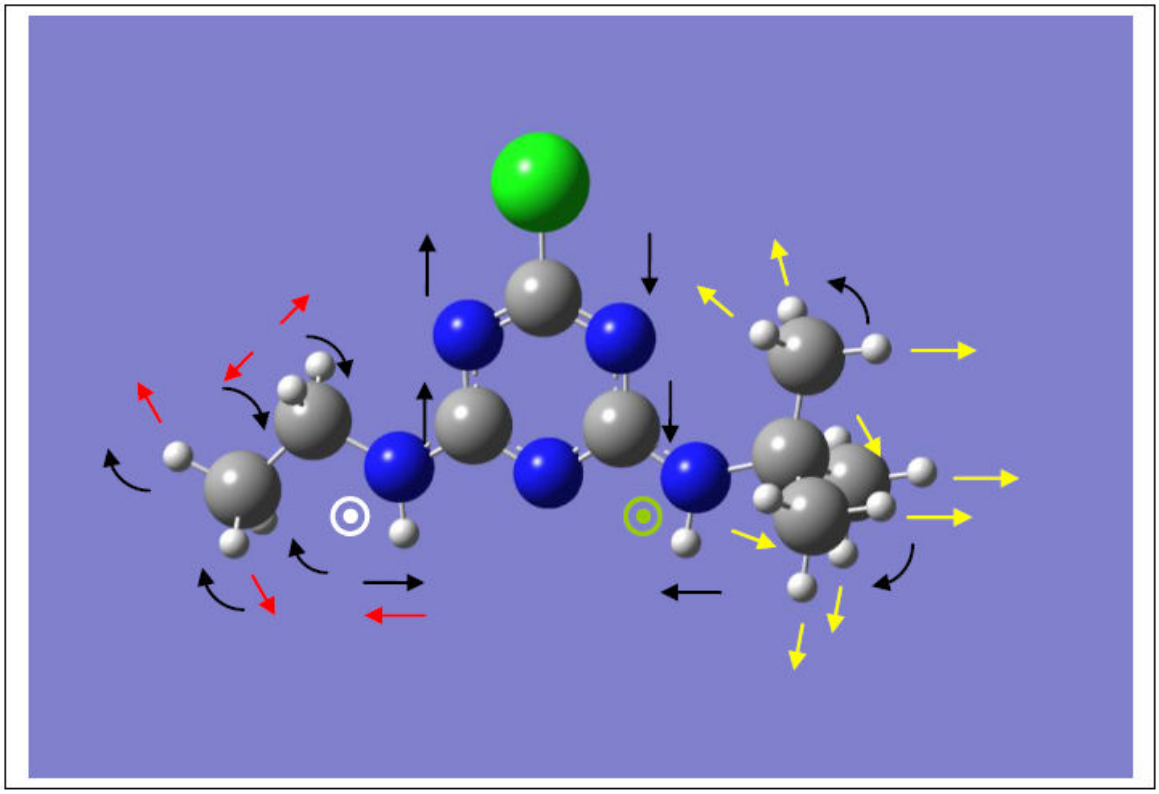

Figure 4.21 Selected vibrational modes of TBA, mode at 531 cm^{-1} given by the rocking vibration of of amino-terbuthyl and amino-ethyl groups, complemented by the asymmetric ring deformation and rocking motion of NH residues – black arrows.
Mode at 1470 cm^{-1} is represented by the scissoring motion of CH_2 and CH_3, and rocking of the NH residue in the amino-ethyl group – red arrows.
Mode at 3022 cm^{-1} corresponding to the asymmetric C-H stretch in methyl groups – yellow arrows.
Mode at 3438 cm^{-1} responsible for the out-of-plane NH wagging in the amino- terbuthyl group – green circles.
Mode at 3488 cm^{-1} responsible for the out-of-plane NH wagging in the amino- ethyl group – white circles.

The available literature data [199] and the observations from mass spectra of TBA before and after its indirect photolysis suggest the coexistence of the following three initial products, namely 4-ethylamino-6-tertiobuthylamino-1,3,5 triazine (I) 4-acetaldehydamino-6-ethylamino-1,3,5 triazine (II) and 2-hydroxy-6-amino- 4-ethylamino-s-triazine (III), shown in the Figure 4.22.

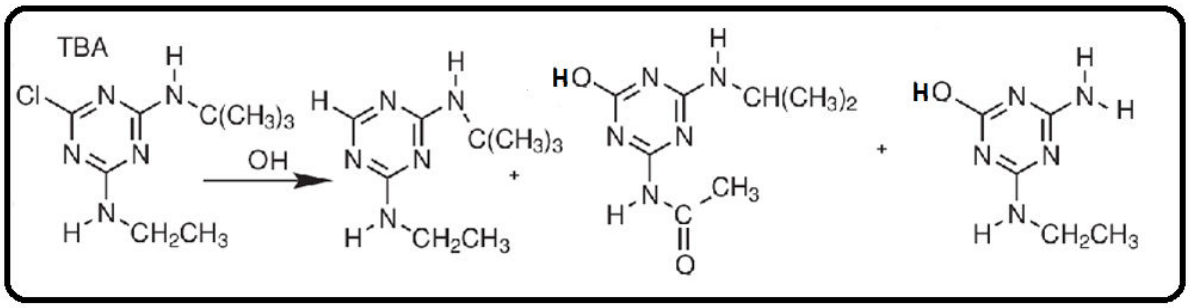

Figure 4.22: Tentative reaction pathway for three initial products of the indirect photolysis of TBA with OH-radicals. Source: Authors' own compilation and research using data from the following reference [205]

In order to simulate the spectra of the reaction mixture after indirect photolysis of TBA and compare this with the experimental spectrum recorded from the sample at the end of the reaction, i.e. in conditions in which the maximum of product is observed, the corresponding theoretical spectrum was formed by the linear combination of the calculated spectra of the individual initial main reaction products weighted by the relative proportions of these products. In comparison to the reactant TBA, product I results from the cleavage of the C-Cl and the formation of a C-H bond presented in Figure 4.23 (a) product II (N-tert-buthyl-N'-ethoxy-1-hydroxy-1,3,5-triazine-2,4-diamine) depicted in Figure 4.23 (b) shows the presence of the COH atom which is engaged in the C-0-H vibrational motion coupled to the strong ring deformation described by the mode around 1750 cm^{-1}. The mode at 1349 cm^{-1} exhibits slight C-N stretching vibration in the ring coupled to rocking motion of the neighboring NH residue of amino-ethyl and rocking of CH residue in amino-isopropyl. The main feature though is the appearance of the typical ketone bond with C-O vibration at ν = 1800 cm^{-1}.

For the third initial product III in Figure 4.23 (c) shows the motion described by a vibrational mode around 1617 cm^{-1}. This vibration involves the rocking motion of the O-H bond and stretching deformation of the newly formed carbon-hydroxyl group. In addition a stretch of C=N bond in the s-triazine ring, coupled to the C=N stretch between the ring and NH as well as NH_2 groups is observed. The latter vibration is complemented by the rocking vibration of NH residue.

Moreover the occurrence of product III (N-amine-N'-tert-buthyl-1-hydroxy-1,3,5-triazine-2,4-diamine) can be rationalized in terms of cleavage and then substitution of the Cl atom by a hydroxyl radical. The calculated vibrational mode at around 3460 - 3500 cm^{-1} might contain the O-H stretch. We recall that in the case of products as well as for the reactant TBA, no

energy scale correction of the calculated spectra caused by unreliable harmonic force constants was necessary. We took into account the results of TBA after indirect photolysis results obtained by mass spectroscopy (see Appendix Table A2.4.2.3), and considered only the products N-tert-butyl-N'-ethyl-1,3,5-triazine-2,4-diamine, N-tert-buthyl-N'-ethoxy-1-hydroxy-1,3,5-triazine-2,4-diamine, N-amine-N'-tert-buthyl-1-hydroxy-1,3,5-triazine-2,4-diamine presented in the following Figure 4.23 (a, b, c).

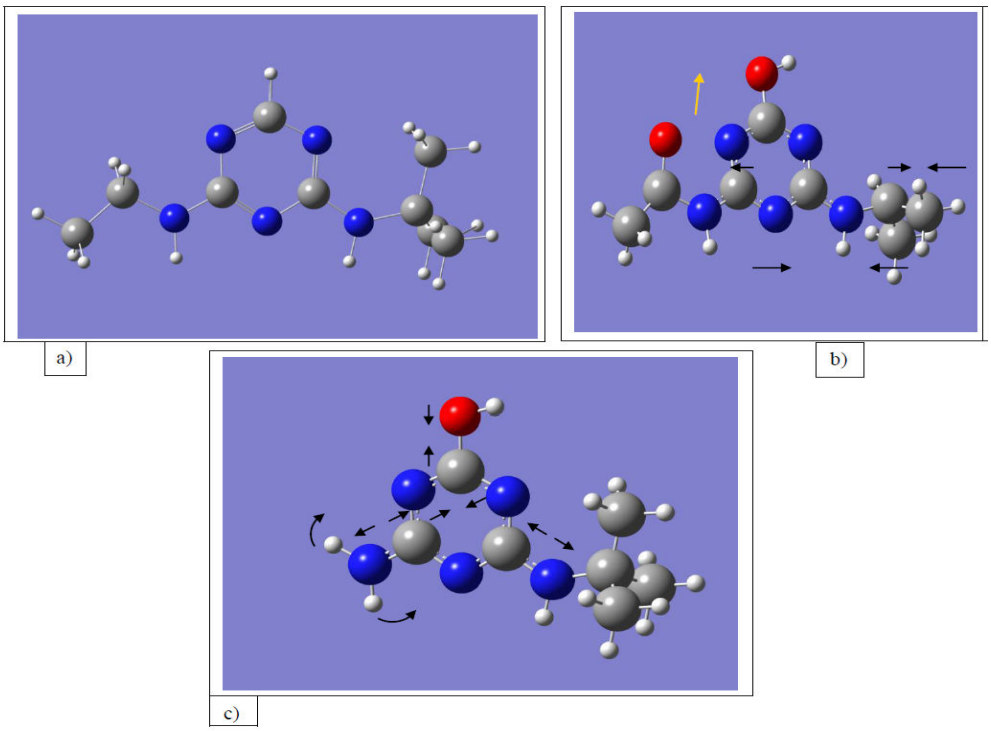

Figure 4.23: a) minority product I (N-tert-butyl-N'-ethyl-1,3,5-triazine-2,4-diamine), b) product II (N-tert-buthyl-N'-ethoxy-1-hydroxy-1,3,5-triazine-2,4-diamine) with the symmetries of the mode at 1349 cm^{-1} - black arrows, ketone bond C=O at 1800 cm^{-1} – yellow arrow c) product III (N-amine-N'-tert-buthyl-1-hydroxy-1,3,5-triazine-2,4-diamine) with the indicated vibrations at 1617 cm^{-1}

The substitution of the Cl atom by the hydroxyl group, as induced by OH-radicals, is also manifested by a relative change of the vibrational mode intensity in the band around 1600 cm^{-1} (as marked by the arrows in Figure 4.23) and by the formation of ketone bond C=O at 1800 cm^{-1}. Another important observation is the significant relative increase in the intensity of the C-H vibrational band, at 2900-3300 cm^{-1}, as shown in Figure 4.24 [206].

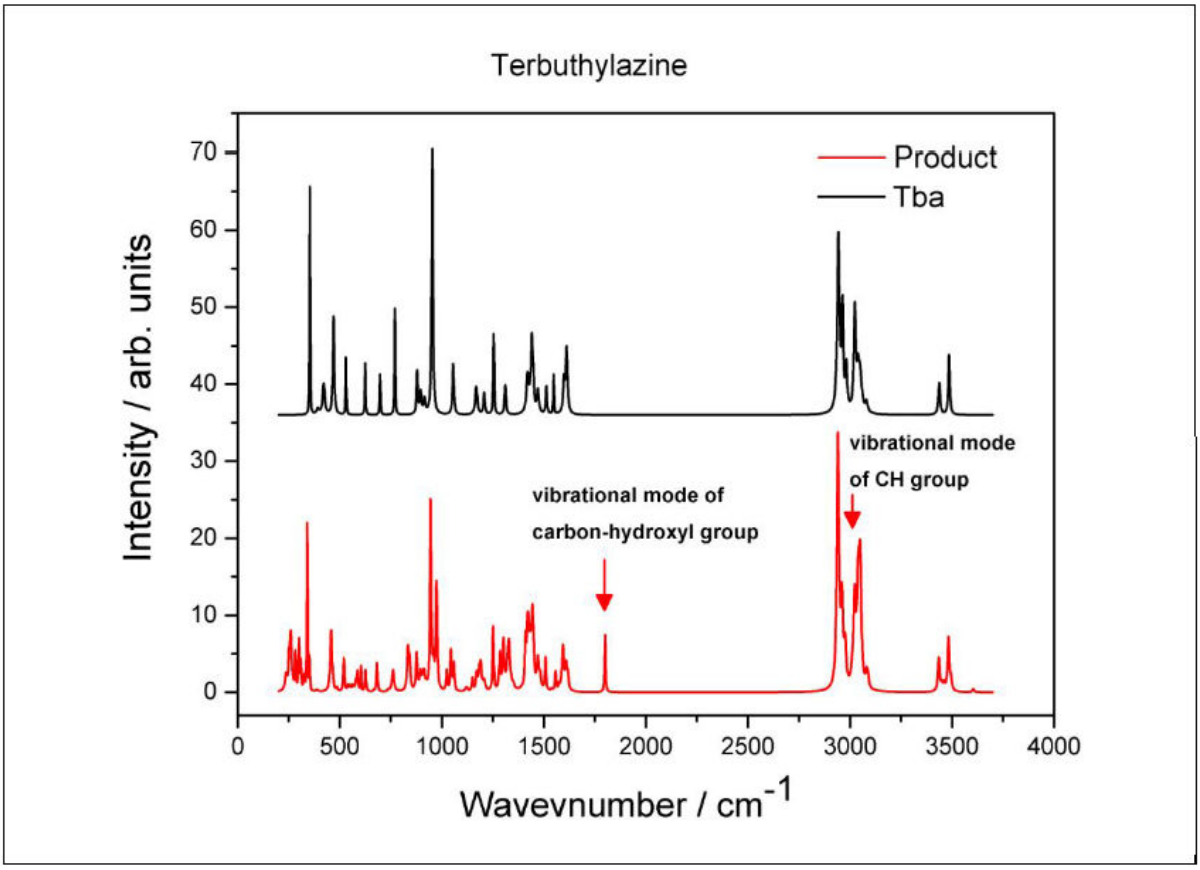

Figure 4.24: Comparison of the theoretical Raman spectra of the calculated TBA and its products (see Fig. 4.23).

Let us recall that the theoretical spectrum of the reaction mixture was considered as the linear combination of the spectra of the main initial reaction product mentioned above. The main spectral regions of interest for the final product $C_3N_3(OH)_3$ (see Fig.4.25) are outlined in the Table 4.8.

Table 4.8: Some vibrations of $C_3N_3(OH)_3$ shown in Figures 4.25 (a and b)

Functional group/vibration	C-OH stretch	C=N stretch in aromatic ring	O-H stretch
Wavenumber region (cm^{-1})	1018	1630	3500

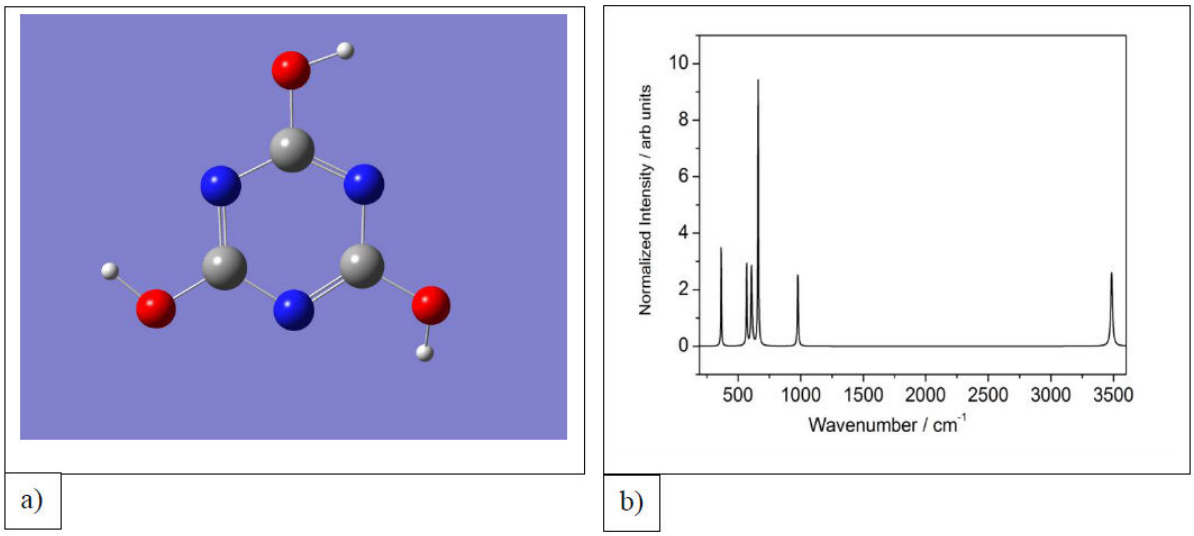

Figure 4.25: a.) Molecular structure of $C_3N_3(OH)_3$; b.) Calculated Raman spectrum of $C_3N_3(OH)_3$. In table 4.8, it is limited to characterize the molecule vibrations directly related to the links presented by the molecule of cyanide acid, considering the simulation spectrum in Figure 4.25 b.

A look at Table A 2.4.2.3 allows us to observe the mass spectrum of TBA after indirect photolysis. The mass m / z = 130.769 of the acid cyanuric is present but in small quantities, that is to say, it does not influence the major products. In addition, if we look at the literature, we can say that the photo-degradation of TBA gives as last product cyanuric acid [47].

4.5.2.1 Characterization of the results of TBA photolysis by infrared spectroscopy (IR)

The calculation of the infrared (IR) spectra was performed in the harmonic approximation with the Raman spectra by using the same program code Turbomole. Figure 4.26 shows the resulting theoretical spectra for terbuthylazine (TBA). The fitted full-widths at half maximum

(FWHM) values for the simulated vibrational modes presented in Figure 4.26 are summarized in Figure A1_2 and Figure A1_3 of the Appendix Section A0.

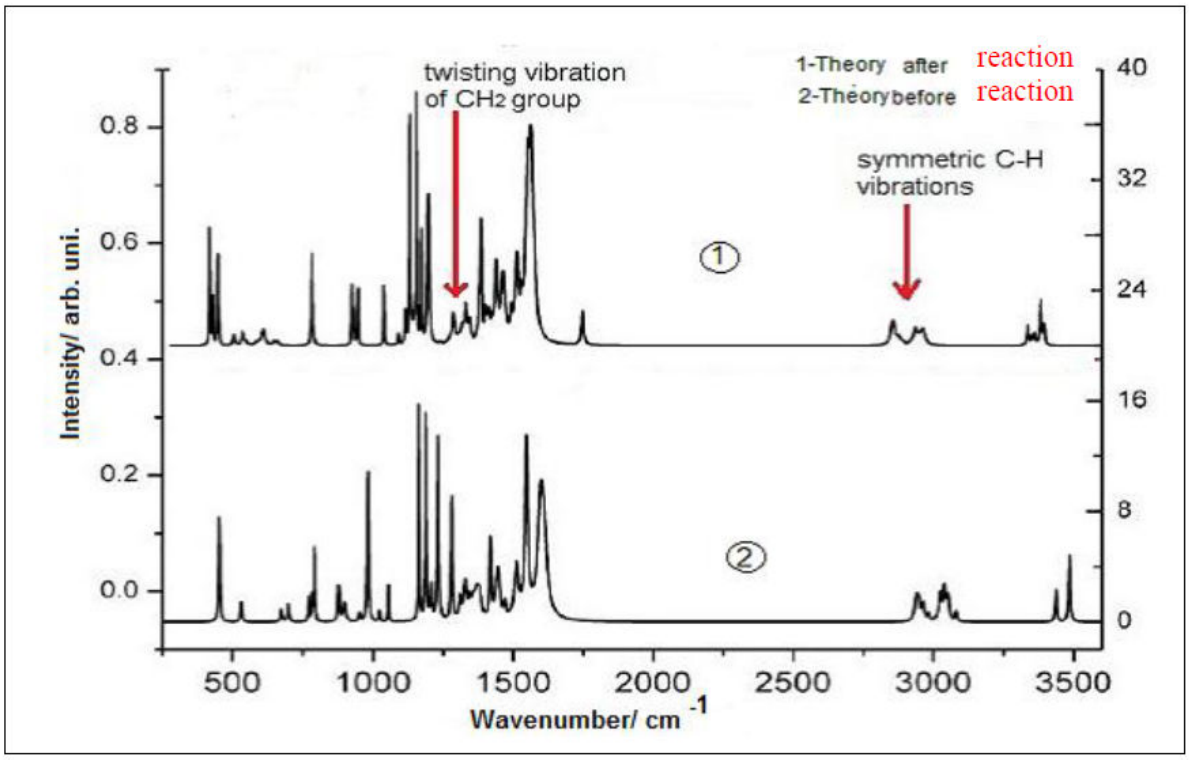

Figure 4.26: Product IR spectrum of TBA showing a strong reduction in the vibrational mode intensities around 1230 cm^{-1} corresponding to the wagging of the CH_2 and rocking motion of the methyl groups of TBA coupled with ring deformation (see also Figure 4.22).

The most important mode for the reaction analysis is located around 1230 cm^{-1} and is composed out of the wagging motion of the CH_2 residue accompanied by the rocking motion of the methyl groups and the asymmetric deformation of the s-triazine ring.

In addition, the vibrational modes at 1750-1800 cm^{-1} correspond to the C=O vibration the ketone group (see Figure 4.26 and Figure 4.27). The detection of the carbonyl signature in the IR product spectrum proves that the reaction of indirect photolysis can lead to the substitution of the Cl atom by the ketone group (see Figure 4.27). Furthermore, a drastic reduction of the band intensity between 2900-3400 cm^{-1}, responsible for the symmetric C-H stretch vibrations in two methyl groups and asymmetric in the third one, points to CH_3 elimination. Motivated by these observations we can assume the formation of three products as displayed in Figure 4.23 (product I, product II and product III). It should be also noted that the vibrational modes

at 800 cm^{-1} and the band between 950 and 1100 cm^{-1} remain practically unchanged. These vibrations mostly involve the deformation of the C-N band in the s-triazine ring, which is evidently left unchanged in the course of the reaction.

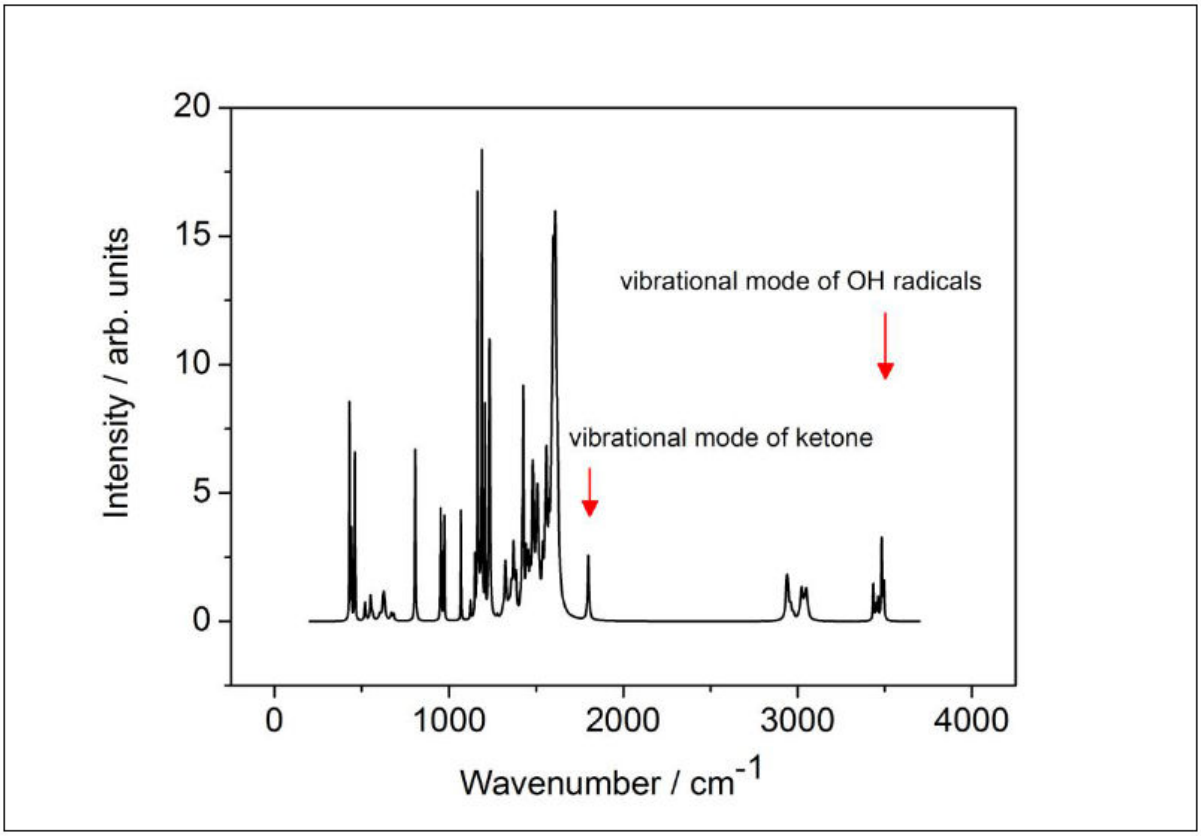

Figure 4.27: Product IR spectrum of TBA. Note the strong reduction in the vibrational mode intensity around 1230 cm^{-1} corresponding to the twist of the CH_2 and the rocking motion of methyl groups of TBA, (see also Figure 3.3). A strong decrease in the 2900-3400 cm^{-1} band intensity of the C-H-vibration in the methyl groups is clearly evident. The appearance of the vibrational mode in the region of 1800 cm^{-1} not being present in the TBA spectrum which gives evidence for the formation of a carbonyl group in the product. Source: compiled by the authors based on the following publication in the reference [207].

In summary, we can state from the IR spectra in Figure 4.27 that interactions of TBA with OH-radicals, as well as in the case of Raman, are pointing at three main products. These three products display the following reaction-sensitive characteristic modes: C-H stretching at 2900 cm^{-1}, C=O stretching at 1800 cm^{-1} and OH-stretching at 3400 cm^{-1}, respectively. Herewith, we have accomplished the spectral analysis and discussion of the results of photolysis for TBA, and we will subsequently proceed with the development of theoretical models for simazine.

4.5.3 Simazine (6-chloro-*N*,*N*′-diethyl-1,3,5-triazine-2,4-diamine)

Figure 4.28 and Table 4.9 show theoretical Raman spectra of simazine. The values of the observed Raman linewidth are presented in Figure A1-1 of the Appendix Section A1.3.1.2.

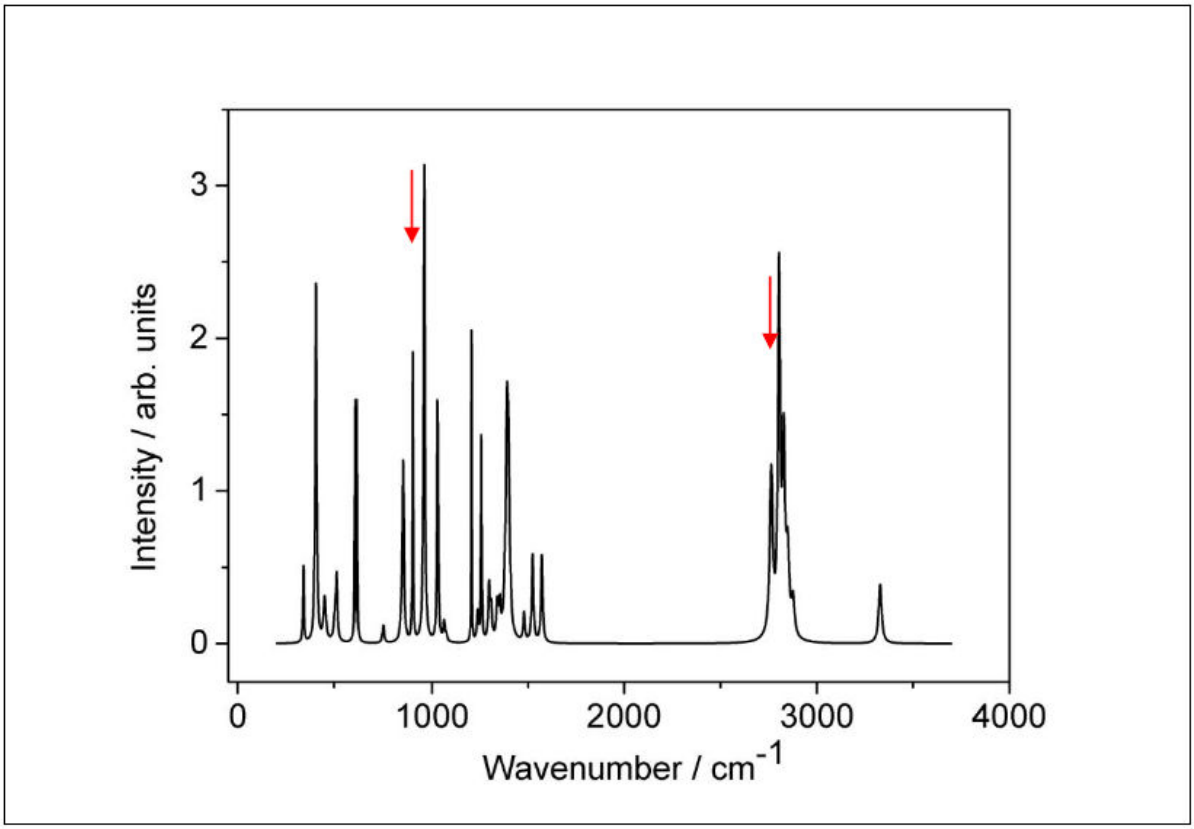

Figure 4.28: Theoretical Raman spectra of simazine. Two vibrational modes with ν = 927 cm^{-1} and ν = 2955 cm^{-1} are shown with red arrows.

Table 4.9: Vibrational assignments of Raman active modes of simazine displayed in Figure 4.28 (frequencies are given in cm^{-1}) [208].

Experiment	Theory	Symmetry
253	256 *w*	*t* CH_3, *r* NH
362	407 *s*	*v* C-Cl, *v* ring, *ω* CH_3, *r* CH_2, *r* NH
622	633 *m*	*v* ring, *r* CH_2, *r* NH
853	888 *m*	*v* C-Cl, *ω* CH_3, *r* CH_2
935	927 *m*	*v* ring(C-Cl), *ω* CH_3, *t* CH_2
983	968 *s*	trigonal *v* ring, *ω* CH_3, *r* CH_2
1072	1065 *m*	*ω* CH_3, *r* NH
1256	1286 *m*	*t* CH_2
1304	1317 *m*	*t* CH_2
1454	1414 *m*	*sc* CH_2
1624	1613 *w*	*v* C_{ring}-NH, *r* NH
2887	2944 *m*	*v* CH_3
2955	2962 *s*	*v* CH_2
3282 br. Band	3477 *w*	*v* NH

All abbreviations as in Table 4.7. Source: compiled by the authors based on the following publication in the reference [208]

The symmetry of vibrations was also decoded by viewing the animation of the individual modes with the TmoleX software. Figure 4.29 is illustrating the spatial representation of several vibrational modes in simazine.

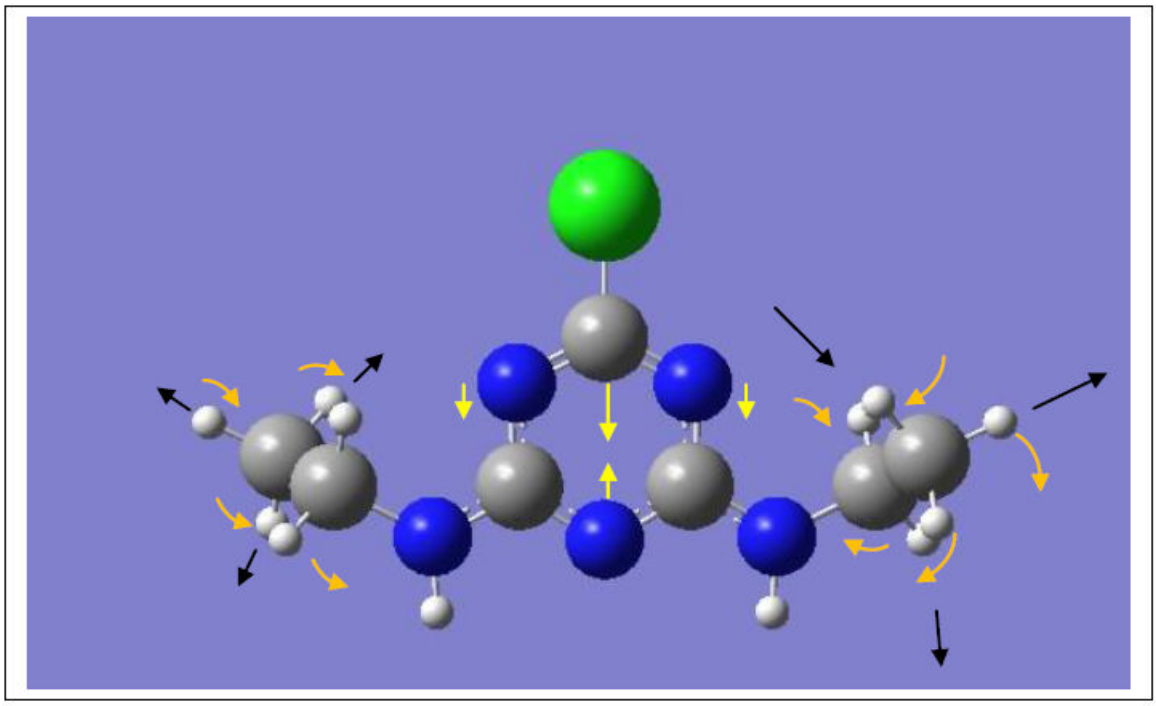

Figure 4.29: The reaction sensitive modes of simazine: the mode at ν = 927 cm^{-1} involving the symmetric ring deformation with C-Cl stretching, assisted by wagging of CH_3 and CH_2 groups – yellow arrows. The symmetric stretching mode with ν = 2945 cm^{-1}, corresponding to the C-H-stretch in the methyl group. The vectors of the C-H-stretch are marked with black arrows.

One of the important reaction-sensitive modes at ν = 927 cm^{-1} includes the strong stretching of the ring carbon connected to Cl, leading to the overall symmetric s-triazine ring deformation. This motion is accomplished by the wagging vibration of the methyl residues and twisting of the CH_2 groups (see yellow arrows in Figure 4.29).

The black arrows in Figure 4.29 show the typical patterns of symmetric C-H-stretching in the methyl group corresponding to the wavenumber 2945 cm^{-1}. This vibration mode under C_{2v} is degenerated, that mean three bands stem from the triply degenerate asymmetric stretching and one band from the active symmetric stretching [47, 209, 210].

At the next step the experimental Raman spectra were fitted to the weighted sum of two assumed reaction products (s-triazine, 6-hydroxy-1,3,5-triazine) in the same fashion as it was done in the case of TBA (see Figure 4.31). The calculated Raman spectra are presented in Figure 4.30, and the main spectral regions of interest being affected by the reaction of photolysis are reflected in the Table 4.10:

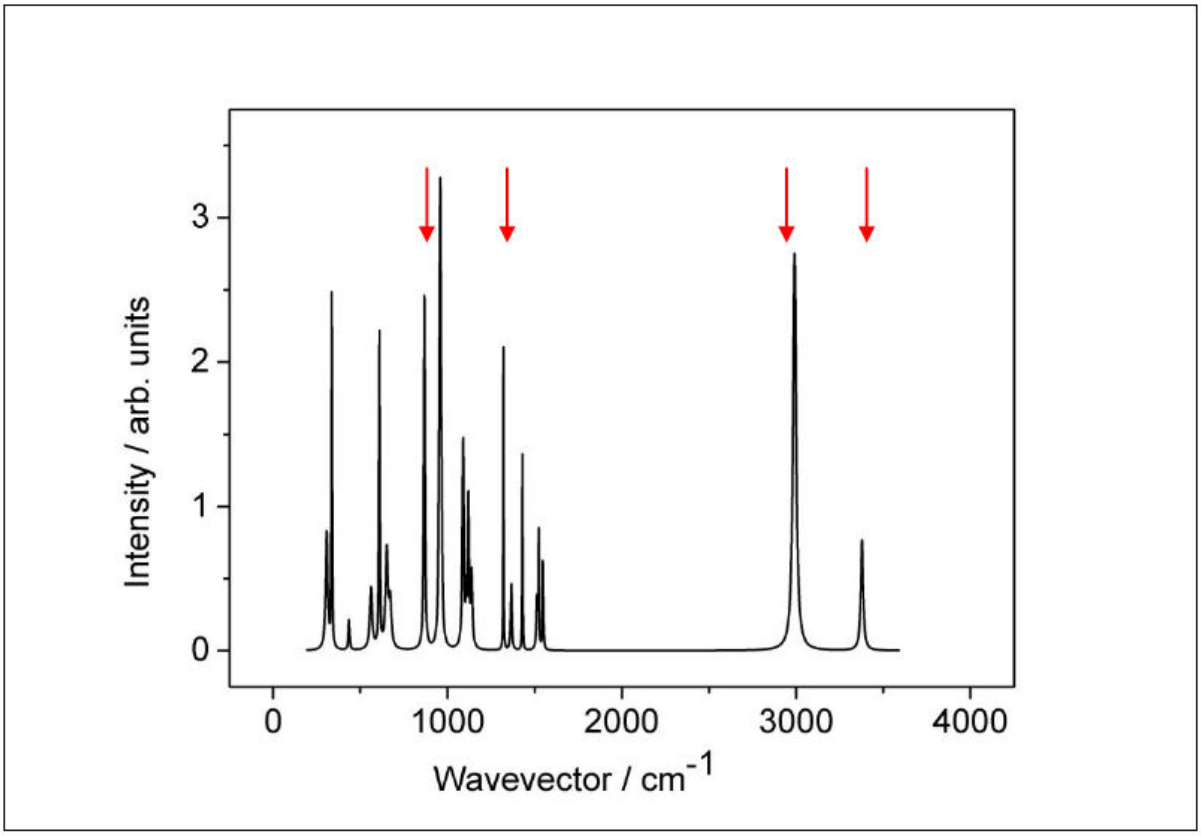

Figure 4.30: Calculated Raman spectra of the reaction product evolved in the course of the simazine reaction, resulting from the weighted summation of theoretical spectra for two suggested sub-products. The four reaction-affected regions, $\nu = 958$ cm^{-1}, $\nu = 1349$ cm^{-1}, $\nu = 2940$ cm^{-1}, and $\nu = 3300$ cm^{-1} are marked with red arrows (see Figure 4.29).

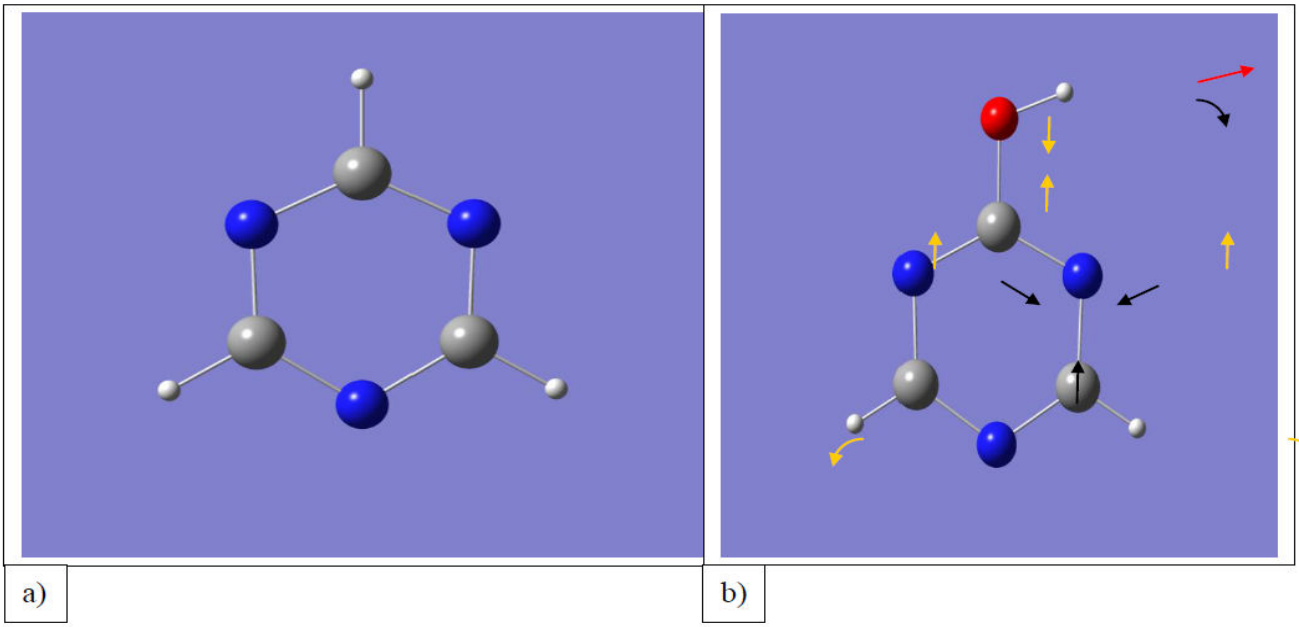

Figure 4.31: The reaction sensitive modes of products obtained by photolysis of simazine:
a) Minority product I;
b) Majority product II the mode at ν = 927 cm^{-1} involving the symmetric ring deformation with C-Cl stretching, assisted by wagging of CH_3 and CH_2 groups – yellow arrows;
The symmetric stretching mode with ν = 2944 cm^{-1}, corresponding to the C-H-stretch in the methyl group. The vectors of the C-H-stretch are marked with black arrows.
The O-H stretching vibration at ν = 3478 cm^{-1} – red arrow.

Table 4.10: Important regions of Raman frequencies, characteristic for the functional groups present in Figure 4.31 being affected by the reaction of photolysis of simazine.

Functional Group/vibration	trigonal N_{ring} stretch, OH rocking	C=N aromatic OH, NH rocking	C-H stretch	O-H stretch
Wavenumber region (cm^{-1})	900-1000	1350-1400	2900-3200	3400-3500

The main novel features of the total product spectra in Figure 4.30, dominated by sub-product II, are resulting from the Cl substitution by the hydroxyl group. The strong mode of simazine reactant at 927 cm^{-1} typical for C_{ring}-Cl deformation disappears and instead of that a new vibration belonging to carboxyl group with the OH-rocking motion appears at 982 cm^{-1}, marked yellow in Figure 4.31(b). The strong trigonal deformation of s-triazine ring is given by the symmetric deformation of nitrogen atoms

The second new mode at 1361 cm^{-1}, marked with red arrows in Figure 4.30(b) is given by the rocking motions of both C-H groups of the ring accomplished by the C_{ring} - CO stretching.

Due to the overall substitution the intensity of CH_3 symmetric stretch vibration in the product at 2945 cm^{-1} is strongly reduced, and at the same time is greatly enhanced around 3400 - 3500 cm^{-1} due to appearance of the OH stretching vibration fingerprinting the formed product (red arrow in Figure 4.31(b)).

4.4.4 Lindane (gamma-hexachlorocyclohexane, (γ-HCH))

In this paragraph we are turning to the analysis of the Raman spectra of lindane and products being formed in the course of the indirect photolysis of lindane. Lindane is a very persistent substance and spreads more rapidly in tropical climates than in temperate climates, probably due to its biodegradation. It is movable through the sandy soil and is also retained more strongly in the presence of a significant thickness of humus layers. Moreover, it presents a potential danger for water surface contamination and soid [211].

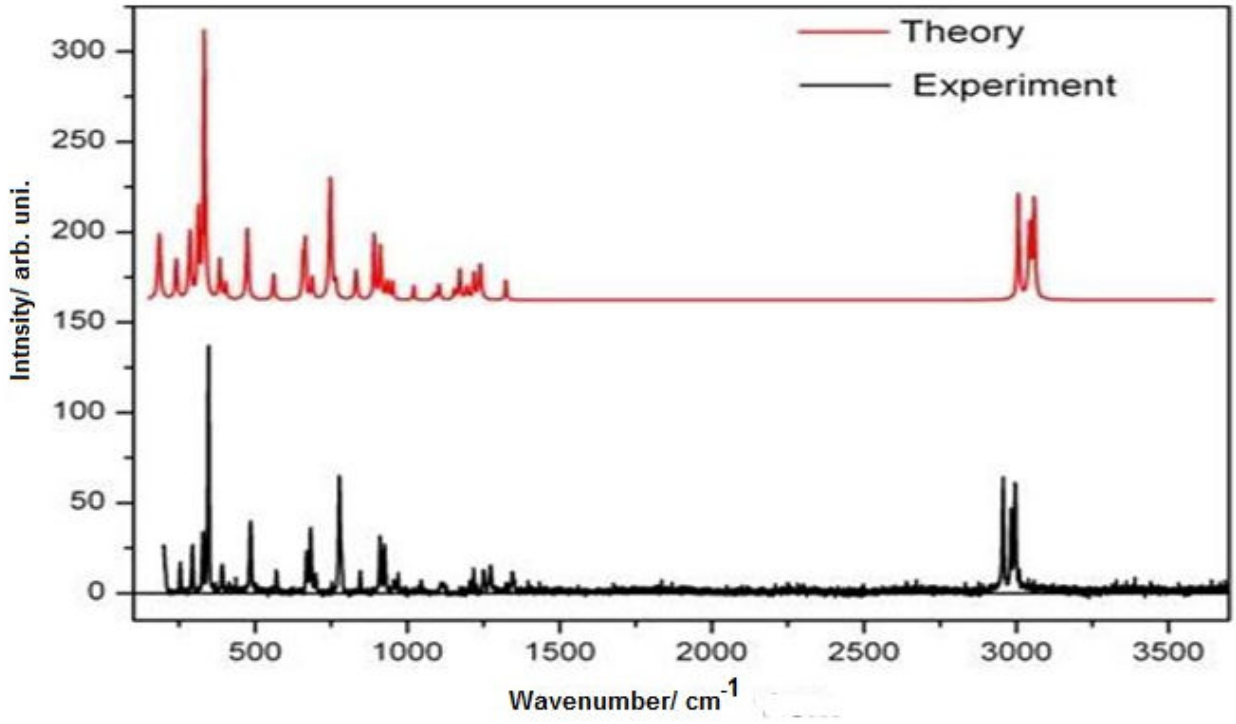

Figure 4.32: Comparison of Raman theoretical spectra and Raman experiment spectra of lindane.

The comparison of theoretical and experimental Raman spectra of lindane is presented in Figure 4.32, whereas the detailed analysis of vibrational symmetries is given in the Table

4.11. It should be emphasized that no special fit of FWHM, as in the case of TBA and simazine, was needed here. The calculated Raman harmonic line intensities almost perfectly reproduce the peak amplitudes of the experimental spectra and the Raman spectra can be expressed simply by the sum of all Lorentzian line-shapes with the equal half-width.

The one of the most intense lines in this spectrum (around 333 cm^{-1}) belongs to a “breathing" mode of the cyclohexane ring, containing the scissoring vibrations of C-H groups complemented by slow stretching of the C-Cl bond, (see Figure 4.33). The second important intense mode, possibly sensitive to loss of Cl, is the asymmetric vibration of hydrogen atoms in the C-H bond.

Table 4.11: Vibrational assignments of Raman active modes of lindane displayed in Figure 4.33 (wavenumbers are given in cm^{-1}) [200].

Experiment	Theory	Symmetry
200	186 *m*	*v* ring, *ip sc* CH, *ip v* C-Cl
250	241 *w*	*v* ring, *op r* C-Cl
293	286 *w*	*op v* ring, *sc* CH
349	333 *s*	*op v* ring, *ip v* C-Cl, *op sc* CH
392	384 *w*	*t* ring, *op r* C-Cl
485	474 *m*	*op v* ring
572	561 *w*	*op v* ring, *op r* CH
683	665 *m*	*op t* ring
776	747 *m*	asym *op v* ring
843	831 *w*	*v* ring
912	891 *m*	*v* ring, *ip sc* CH
924	912 *m*	*v* ring
1041	1020 *w*	*v* ring
1115	1104 *w*	*t* ring
1220	1171 *w*	*op r* plane CH
1252	1239 *w*	*op r* CH
1345	1323 *w*	*op r* CH
2960	3007 *m*	*op v* C-H
2995	3059 *m*	asym *ip v* C-H

All abbreviations as in Table 4.7 [200]

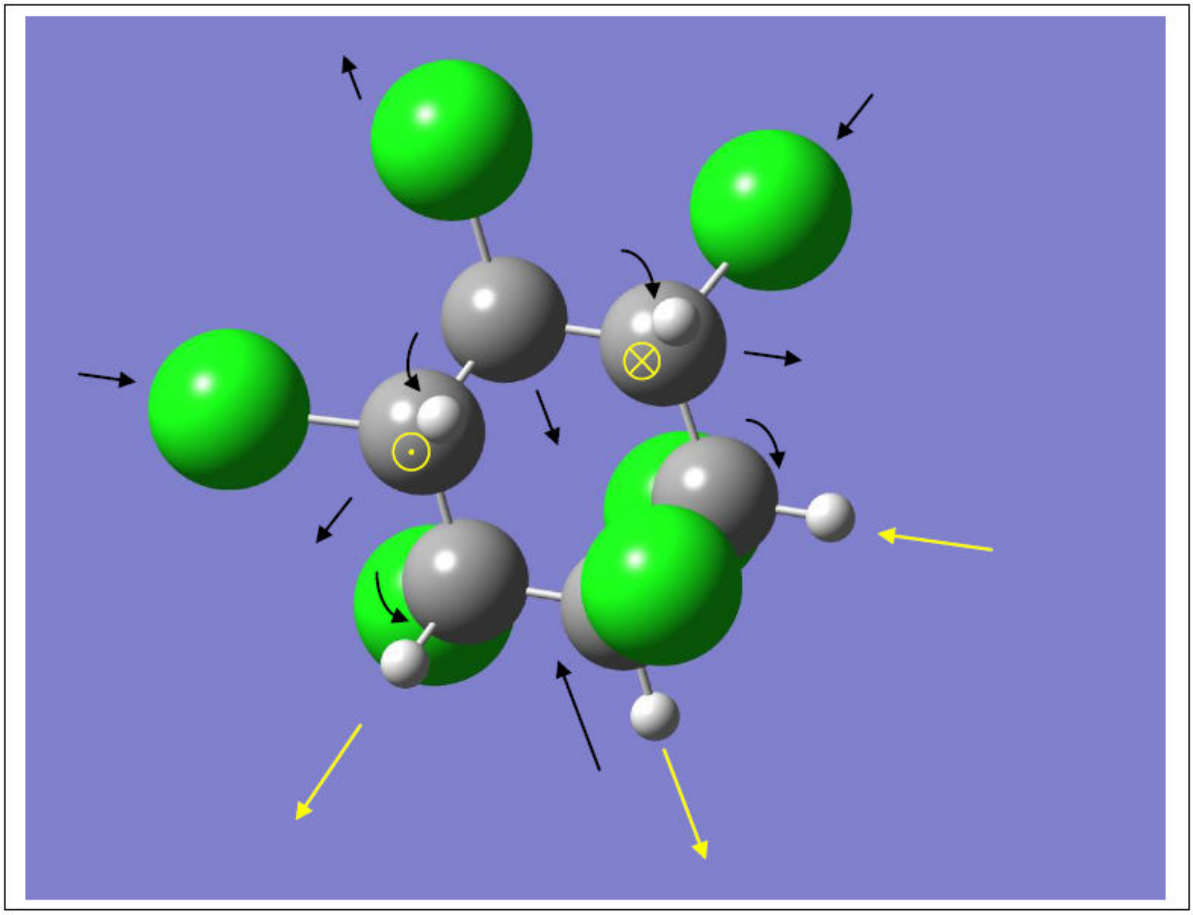

Figure 4.33: The breathing mode of the lindane ring at $\nu \approx 333$ cm^{-1} involving the stretching motion of Cl atoms accompanied by scissoring oscillation of hydrogen atoms - black arrows, and the asymmetric vibrations of hydrogen atoms with $\nu = 3059$ cm^{-1}, corresponding to the C-H stretch, marked with yellow arrows.

The almost equal fitted half-width values of the Raman lines for lindane are shown in the Figure A1-0 of the Appendix A0. According to the taken mass spectra, the indirect photolysis of lindane results in two major products have been confirmed in the following research work using other previous experiment [212]. Nevertheless, it is important to say that generally, when the indirect photolysis is complete, we are facing only one feasible reaction occurring in the following path, as other studies have shown [213, 214].

$$C_6H_6Cl_6 + 18\ OH_g + h\nu \rightarrow 6\ CO_2 + 6\ H_2O + 6Cl^- + 12H_g \qquad (55)$$

Both of the dominant products, m/z = 139 (1,4-dihydroxybenzoquinone) and m/z = 113 (2-chlorobenzene) (see section Appendix A2.4.3.5b), evolving from the lindane reaction are displayed in Figure 4.34 (a) and (b). Oxygen atoms are displayed in the red color, white color

is reserved for the hydrogen atoms, carbon atoms are marked grey and green color is used for chlorine atoms.

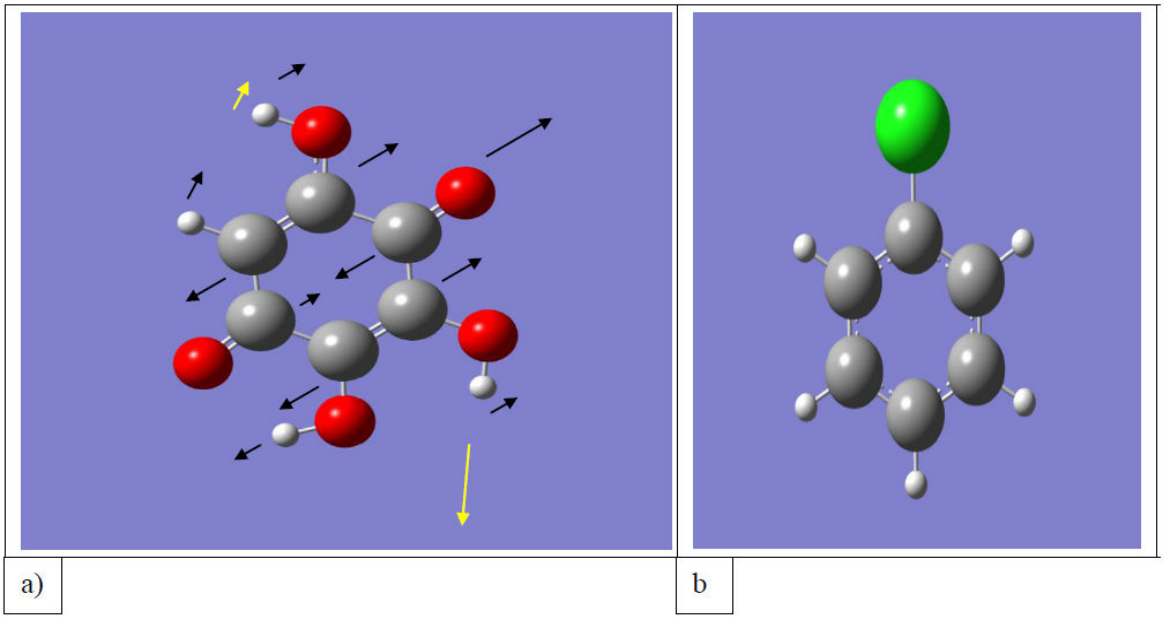

Figure 4.34: a.) Product I (1,4-dihydroxybenzoquinone); the breathing mode of the ring around $\lambda_{exp} \approx 1714$ cm^{-1} involving the C=O stretching in ketone group, as well as scissoring vibration of H in the hydroxyl groups (black arrows), and high energy vibrations of hydrogen atoms with $\lambda_{exp} = 3250$ cm^{-1}, corresponding to the OH stretch, (yellow arrows); b.) Product II (chlorobenzene) (see section appendix A4).

As can be seen from Figure 4.34 (a), two main new modes corresponding to the important functional vibration features appear in the spectra of the products. These vibrational modes are not present in the spectra of the reactant lindane. It can be seen in Figure 4.35 and Table 4.12 that some new bands are formed after indirect photolysis.

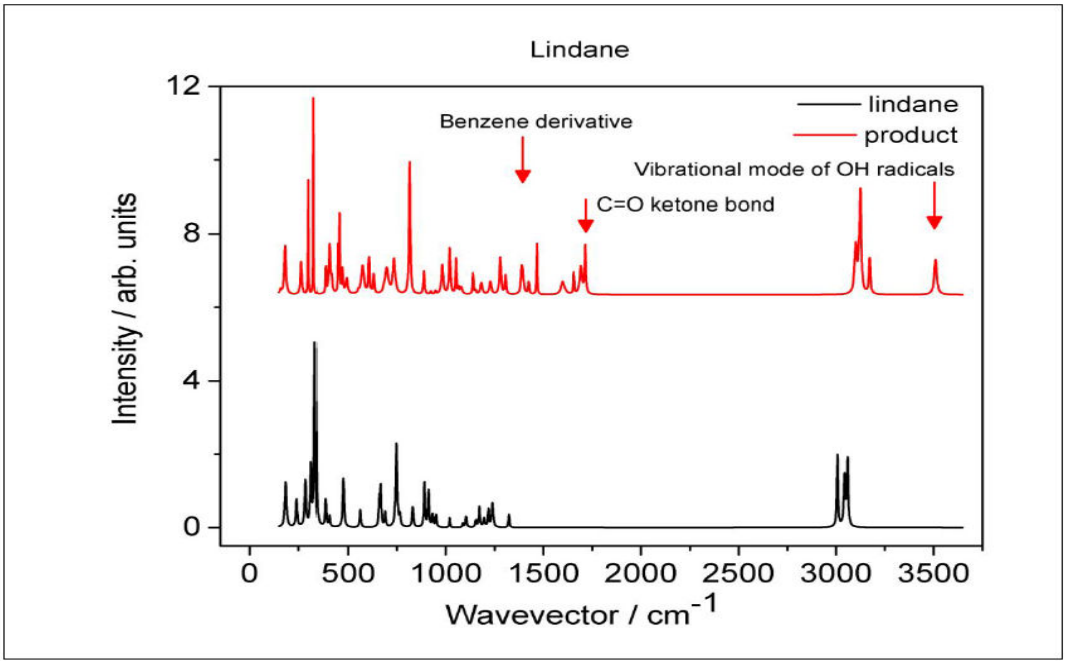

Figure 4.35: Theoretical comparison of Raman spectra of lindane and the new bands corresponding to the formation of the lindane product (see Fig. 4.34)

Table 4.12: The frequencies of most important Raman bands present in Figure 4.35 in the case of lindane product

Functional Group/vibration	C-H stretch	C=O stretch	Cl-C-C-Cl twisting	O-H stretch
Wavenumber region (cm^{-1})	2950-3100	1700-1750	350-374	3500-3550

The first one of these vibrational features is located in the vibrational spectrum between ν_{exp}=1700 -1750 cm^{-2} and it is typical for the vibrations in a ketone. This mode involves the breathing vibration of the carbon cyclohexane as well as C=O stretching in ketones and scissoring vibrations of H-atom in hydroxyl groups. It involves also C-OH stretching of the carbon-hydroxyl group bond at around 1600 cm^{-1}. The other feature is the high frequency stretching OH mode at ν = 3510 cm^{-1} being absent in lindane. The split C-H-mode vibrational mode structure of lindane near 3059 cm^{-1} is replaced by a broadened single vibrational mode. There are no distinct new features contributed by the product chlorobenzene and 1,4-dihydroxybenzoquinone, since most structural changes are given by the loss of Cl atoms, which mostly affects the low frequency part of the spectra.

The calculation methodology used here helped us to explain the object of our project and to achieve the results we will further exploit in the next chapter. There, we will also present the different devices that we have used.

We cannot conclude this chapter without investigating the effects of POPs on the environment and the possibility of application Raman microscopy to solve this problem.

4.5 Environmental Aspects and the possibility of the application of Raman microscopy

The impact of the persistent organic pollutants (POPs) on the environment depends on their atmospheric concentration, as a result of their dispersion, and their toxicity. Although the hazards of POPs are known since the Green Revolution of the 1970, they are permanently applied in the rural areas of the high industrialized and developing countries:

(a) To prevent disease by controlling mosquito populations,
(b) To disinfect and sterilize dental and surgical instruments ,
(c) To protect agriculture, industrial product, insect pests and fungus.

According to the World Health Organization (WHO), 40% of all deaths registered each year worldwide from infectious foodborne illness are caused by environmental toxins such as viruses, pesticides, herbicides and bacteria such as Listeria monocytogenes, Salmonella typhimurium and Escherichia coli 0157H7 [215]. For years there is always fierce resistance against the excessive application not only of the pesticides, but also of chemicals because of their impact on the environment, the public health and the water quality. Some environmental activists are often calling of the total prohibiting of chemical pesticides, especially of persistent organic pollutants. By the signing of the convention of Stockholm on Persistent Organic Pollutants in 2001 and (ratified 2004 by 150 countries), 12 chemical substances were identified, which should be completely banished from the world and later, in 2009, 10 substances have been added. Since then scientist from all over the world are working closely together:

- To identify other types of POPs
- To develop new methods to measure the risks exposure to the pesticides

- To understand how the POPs dissipate through the environment, and to evaluate their toxicity and concentration.

What is indisputable is that the pesticides have a destructive effect on health. In the present study, it is shown that their mixing with OH-radicals can contribute to diminish the environmental pollution. From which we draw consequences for sustainable application of the Raman spectroscopy as an effective technique for the analysis of chemical or photochemical reactions that cause the degradation of pesticides. Chemically and physically, this spectroscopy can serve to establish a system for sensitive, reliable and simple identifying of toxic elements content in the pesticides and probably to eliminate their negative effects on the environment in a sustainable way [216].

4.6 Summary

Numerous vibrational bands in the spectra for the pesticides particularly TBA, simazine and lindane have been collected prior, during, and after photo-degradation reactions and compared with the spectra obtained from theoretical calculations. The spectra were performed after structure optimization and frequency calculation with the help of the Quantum Chemistry code Turbomole or Gaussian 03. The quantum chemical calculation method helped to aasign the frequencies or wavenumbers of the vibrational modes for the investigated herbicides as well as for their photo-degradation products. For a reliable comparison of the calculated spectra with the experimental ones, a good correlation between the number of bands and their positions is necessary. Therefore, the spectra of the theoretically relevant reaction products effectively detected in MS were calculated separately, and then a linear combination was formed with different weights (in the case of TBA, lindane and simazine) corresponding to the respective intensities of the MS patterns of the different products. The present study confirms the results of previous investigations (using NMR, IR and MS as complementary methods) reporting cyanuric acid as the final degradation product for many herbicides, particularly for those containing s-triazine [217, 218]. The achieved results could be rationalized by a Retro-Diels-Alder ring cleavage as an important and complementary step of herbicide degradation[219].The Raman spectroscopy was used in the present work to demosntrate how technique can be helpful for environmental remediation and regulation in accordance with the Stockholm convention on persistent organic pollutants (POPs).

5. Conclusion

The purpose of this work was to demonstrate the suitability of Raman spectroscopy for (i) the determination of the concentration of OH-radicals and (ii) the characterization of the reaction of these OH-radicals after indirect photolysis with the semivolative compounds. Investigated substances were terbuthylazine (TBA), simazine, lindane, which are well-documented worldwide as environmental pollutants. The results clearly demonstrated the suitability of Raman spectroscopy as a powerful tool to investigate the kinetics (rate constants) of biocides degradation under environmental conditions. Furthermore, the approach of confocal Raman microscopy and the characteristic method IR spectroscopy were combined (i) to investigate indirect photolysis of selected seivolatile compoundsand (ii) to analyze the process of their photo-degradation. Selected pesticides included lindane and simazine, the achieved experimental results, were validated by comparison with theoretical predictions using the Turbomole method.

The reaction of OH-radicals with TBA, simazine and lindane was determined by changes in Raman mode intensities of TBA between the region 1000 cm^{-1} and 1600 cm^{-1}. In this region, we also observed the appearance of Raman signals of the oxidation product. Specifically, the C-C-stretch vibration of the heterocyclic ring could be assigned to the wavenumbers 950 - 1055 cm^{-1}. Other vibrations were 770-785 cm^{-1} (rocking) and 435-570 cm^{-1}. The C-Cl-stretching vibration occurred in the 505-760 cm^{-1} regime, and the C-Cl deformation vibration was found between 250 cm^{-1} and 450 cm^{-1}.

According to the Figure A1_0 and Figure A1_1 in Appendix A1, we can also see the values of fitted FWHM are bigger in Figure A1_1 and Figure A1_0 in Appendix A1, which means that coupling, is more intense in the case of simazine than with TBA and lindane. It should be pointed out that we obtained a coupling mode, and the fitted values increased with the vibrational mode from the basis of these results we could affirm that the non-aromatic cycle of lindane changes to 1,4-dihydroxybenzoquinone and chlorobenzene, whereas TBA's aromatic ring remains the same.

Three main products of the indirect photolysis of terbuthylazine with OH-radicals were identified: (i) 4,6-diethylamino-1,3,5-triazine (I), (ii) 4-acetaldehydamino-6-ethylamino-1,3,5-

triazine (II) and (iii) 2-hydroxy-6-amino-4-acetamino-1,3,5-triazine (III). Additionally, he stretching of CO appeared at 1600 cm^{-1} and 1500 cm^{-1} respectively. II was characterized by the CH twisting vibrational mode, which appeared in the region 2900 – 3300 cm^{-1}. In the early steps of our photolysis studies on semivolatile compounds, it was first necessary to be able to monitor the amount of reacting OH-radicals, which is required for the indirect degradation with time of biocide. First, we focused on TBA as a reference sample, for which data for its degradation reaction kinetics are available in the literature. The photolysis of TBA was studied and analyses were made before and after photo-degradation.

By using the software Tmolex, it was practical to visualize the vibration of terbuthylazine and to attribute at each wavenumber a moving of the molecule. This principle was the same for the theoretical calculation of the obtained productsBesides NMR investigations, the MS method was also used investigate the photo-degradation of simazine. Through the energy optimization, our study has successfully identified the symmetric stretching mode at ν = 2955 cm^{-1} in simazine, which allowed us to see precisely that there is a C-H stretch in the methyl group of simazine. The combination of the methyl group and the CH_2 group of simazine, due to asymmetric C-H stretching, involved the mutual rocking mode of CH_2-CH_3. In the case of simazine, this appeared at ν =3314 cm^{-1}.

Meanwhile, Lindane molecular calculations were also estimated. We remarked that the reaction of lindane with OH-radicals could result two major products, namely (i) 1,4-dihydroxybenzoquinone and (ii) chlorobezene. By the analysis of the vibrations, we observed rocking, torsion, stretching and twisting of molecules.The theoretical calculation indicated a breathing mode of the ring (ν =1820 cm^{-1}), and this involved the presence of a ketone vibrational mode. The second product showed a twisting Cl-C-C-Cl mode at 350-374 cm^{-1}.

The used theoretical approach allowed us not only to characterize the exact quantum mechanical descriptions of electronic structures, but also to demonstrate the discrepancy between the harmonic frequencies and their relevant experimental values [220]. For the experimental results, the first challenge was to make reproducible samples for the experiment by preparing them in such a way that many parameters do not vary: for example, maintaining a warm temperature (e.g. ≈ 60 °C or 333 K) (see section 3.1.2) and ensuring that different points of the sample surface are dried at the same time. In addition, the proper preparation of the sample was a crucial step. Here, one of the most important factors was to guarantee the

formation of a monolayer of the sample material covering the carrying substrate [221, 222] For our investigations, we were restricted to deal with at leastthin layers, after many attempts. The reaction kinetics then depends on the size of the sample surface area and thickness, which degrades with time as photo-decomposition, took place until the end of reaction [221].

Mass spectrometry was used in order to determine the different products obtained from the indirect photolysis of each pesticide. In the case of simazine, it has been shown that at the end of the reaction we also obtained cyanuric acidas was the case in most previous research [223], and when comparing the test results with NMR and MS. Many other parameters under control could also have varied [224]. The mass spectra and NMR obtained have led us to precise the interpretation of the results and better understanding of the mechanism yielding to photo-degradation of biocides. These results have also been found by many research groups [225, 226]. Previous studies focused on mechanisms relating to atrazine and TBA, with particular attention being given to the identification of the products of degradation [226]. These investigations were carried out using particulate TiO_2 as a photocatalyst under simulated solar light, and showed that the important factor is the speed of degradation of herbicides [227].

The achieved results showed the three different sources used for the production of OH-radicals. The first source was the ozone, which was supposed to produce OH-radicals for the photochemical reaction. The second source utilized was water (including NO_2), but the percentage of OH-radicals obtained by water photolysis was not enough to follow the degradation of the triazines studied. Instead of using an equation of a first-order reaction, a zero-order reaction was obtained after analyze of data. This explains why we obtained a linear form of curve, which brings us to the conclusion that the obtaining Raman spectra are non-exponentials. A zero-order reaction is one in which the rate is completely independent of the concentration of the reaction [226]. The third source ewas hydrogen peroxide, which successfully led to the formation of OH-radicals.

Profound analysis of experimental data clearly (i) showed the identification of several products and (ii) proposed degradation mechanisms. The objective was to investigate the reactive degradation of semi-volatile organic compounds in the laboratory under realistic conditions, which resemble the conditions in the atmospheric environment, and to determine reactive processes leading to the indirect oxidation of the substances under study.We could not only identify the products that are formed upon these reactive processes, but also follow

our results clearly by the observation of the indirect photolysis on samples. With the help of Raman spectroscopy, the degradation pathways and mechanisms could be further clarified, and with a better understanding of the degradation processes, a proper evaluation of the extent of contamination by the pesticides could be expected.

The experiments with the UV-lamp off were made under the same conditions as the one with UV-lamp on. The error limits have also been calculated. But not last, we could observe that the OH-radicals have a short lifetime.This observation is in tune with literature reports [228]

The temporal decay curves in Figure 4.5 (Chapter 4) show the intensity of characteristic Raman spectral features during the degradation of TBA with OH-radicals. These decay curves depict an exponential decay behavior of the selected Raman band intensity and were exploited to calculate the OH-concentration. According to literature reports, the degradation of TBA should be a first or pseudo-first order reaction [221, 229], because it is varying depending on the initial concentration of OH-radicals. Using the available kinetics data about TBA, the concentration of reacting radicals, including OH-radicals [230], was determined. For example, the OH-concentration was found (163± 31) $x10^6 \leq C_{[OH]}$ (molecules.cm^{-3}) ≤ (184 ± 9) $x10^6$. The value is fairly close to the results from Palm et al. [138] on Aerosil 200 *(*OH-radical concentrations ($10^5 < c_{OH}$ (cm^{-3}) $< 10^7$*)*.

For our study, we did not need to have a photocatalyst and are referring to the research results of Palm et al. [138] who conducted the photo-chemical reaction of TBA and found three main products mentioned above [231]. They did not obtain with the gas chromatography method the product 2-hydroxy-4-tert-butylamino-6-ethylamino-s-triazine, which is the main product of the photo-degradation of TBA [222]. In this case the OH-radicals have been replaced by a chlorine atom. Hence, an assumed electron transfer reaction involving OH-radicals was used to explain the formation of desalkyl in atrazine [232].

In the case of the IR spectra of TBA, a strong degradation was observed in the 2900-3400 cm^{-1} band, showing the intensity of the hydrogen vibration in methyl groups. This observation can be attributed to the loss of the methyl group and the creation of new products [233]. All of these results were consistent and comparable in theoretical model calculations. Furthermore, the comparisons of the theoretical simulations and experimental results have been performed for the herbicides, which are of complementary character. the spectra obtained with the

calculation process fits for reproducing the frequencies and intensities of the Raman experimental spectra measurements.

Concerning the TBA, we could observe a deviation between the experimental spectra and the calculation of the presence of C-H and O-H bonds. For lindane, practically no adjustment of the average linewidth was needed (Appendix A1), since the frequencies of the spectra calculated coincided to the measured Raman lines. This approach allowed the prediction of the product distribution for indirect photolysis processes, which are applied for different purposes (photo-decomposition, photolysis, etc.). There is a dramatic lack of detailed mechanistic studies of the different pathways leading to such photoproducts. However, the difficulties, which are mainly due to the very short lifetimes expected for most potential intermediates, can be easily overcome by the use of ultrafast kinetic techniques, such as laser flash photolysis or pulse radiolysis in the nano- or picosecond regime. It will be difficult to model the environmental fate of agrochemicals unless detailed mechanistic studies become available, and these should be taken as a major task and encouraged for the near future.

During the experimental measurements, it was important to consider every parameter that can variably (significantly) influence the results, including for example humidity, temperature and pressure [234]. Some recent studies demonstrate that the rate of degradation of TBA in aqueous solution depends on the nature of the triazine, and that the kinetics is given by a first-order reaction [235].

These studies have been carried out to verify the photo-degradation of triazine, particularly in aqueous solutions and natural water [236]. Investigations on photocatalyst associated with photo-degradation have reported that the rate of TBA photo-degradation in aqueous solutions is enhanced by the addition of ferric perchlorate or ferric sulfate. This report implies that some dissolved constituents of natural waters have a retarding effect on photo-degradation, possibly due to the competition with OH-radicals [237]. Cyanuric acid was view in several studies and even in this work as one of the final products of TBA photo-degradation, which was not further decomposed [237, 238].

On that basis, we can conclude that the results were good, and it was possible to repeat the experiment several times to ensure the reproducibility of these results, as shown in several case studies about photo-degradation rate constants of many pesticides, such as TBA [239,

239]. Moreover, the good reproducibility of our measurements was reflected in the expected exponential decay behavior in the Raman intensity of characteristic bands during photolysis.

List of figures

Lists of schemes

List of tables

References

[1] Guardans, R. and Castro-Jiménez, J. (2013). How enhancing atmospheric monitoring and modeling can be effective for the Stockholm Convention on POPs. *Atmosphere*, **4**, 445 – 471.

[2] Castro-Jiménez, J.; Berrojalbiz, N.; Mejanelle, L.; Dachs, J. (2013). Sources, transport and deposition of atmopsheric organic pollutants in the Mediterranean Sea**.** *ACS Symposium Series,* **1149**, Chapter 11, 231 – 260; Castro-Jiménez ,J.; Rotllant, G.; Ábalos, M.; Parera, J.; Dachs, J.; Company, J. B.; Calafat, A.; Abad, E. (2013). Accumulation of dioxins in deep-sea crustaceans, fish and sediments from a submarine canyon (NW Mediterranean)**.** *Progress in Oceanography,* **118**, 260 – 272.

[3] Bidleman, T. F.; Harner, T. (2000). Sorption to Aerosols. *handbook of Property Estimation Methods for Chemicals: Environmental and Health Sciences*, Boethling R. S., Mackay, D. eds., Lewis Publishers, Boca Raton FL., 233 – 260.

[4] Sheffield, P. E. and Landrigan, P. J. (2011). Global climate change and children's Health: Threats and strategies for prevention. *Environment Health Perspectives*, **119**, No. 3, 291 – 298; Schiedek, D.; Sundelin, B.; Readman, J. W.; Macdonal, R. W. (2007). Interaction between climate change and contaminants. *Marine pollution Bulletin*, **54**, 1845 – 1856; Huynen, M. M. T. E.; Martens, P.; Akin, S. (2013). Climate change: and amplifier of existing health risks in developing countries. *Environ Dev. Sustain*, Springer science and Business Media Dordrecht, **15**, 1425 – 1442.

[5] Nakaya, A. C. (2005). Is air pollution a serious threat to health? *Greenhaven press,* an imprint of Thomson Gale, a part of Thomson Corporation, 1 – 94; Pickrell, J. (2012). Ten of the most polluted places on the planet, *ABC environment*, 1 – 4; Schafer, K. S.; Kegley, S. E. (2002). Persistent toxic chemicals in the US food supp. *J. Epidemiol Community Health*, **56**, 813 – 817.

[6] Klöppel, W. and Kördel, B. S., (1997). Herbicide transport by surface runoff and herbicide retention in a filter strip-Rainfall and runoff simulation studies. *Chemosphere experimental and theoretical approaches in environment chemistry*, **35**, Iss. 1 – 2, 129 – 141; Cherif, S. and

Wortham, H. (1997). A new laboratory protocol to monitor the volatilization of pesticides from soils. *Intern. J. Environ. Anal. Chem.*, **68**, No 2, 199 – 212; Glotfelty, D. E.; Leech, M. M.; Jersey, J. and Taylor, A. W. (1989). Volization and wind erosion of soil surface applied atrazine, simazine, alachlor, and toxaphene. *J. Agric. Food Chem.,* **37**, 546 – 551; Nash, R. G. and Gish, T. J. (1989). Halogenated pesticide volatilization and dissipation from soil under controlled conditions. *Chemosphere*, **18**, 2353 – 2362.

[7] Fiedler, H. (2004). Stoffflussbilanz: Stockholm convention on Persistent Organic Pollutants (POPs). *Umweltbeobachterkonferenz, UNEP Chemicals 11-13, chemin des Anémones CH-1219 Chatelaine (GE), Switzerland,* 1 – 10; Secretariat of the Stockholm Convention on Persistent Organic Pollutants United Nations Environment Programme (2008). Guidelines on best available Techniques and Provisional Guidance on best Environmental Practices relevant to Article 5 and Annex C of the Stockholm Convention on Persistent Organic Pollutants, Geneva (Crematoria) 1 – 22.

[8] Li, Q. Q.; Loganath, A.; Chong, Y. S.; Tan, J. and Obbard J. P. (2006). Persistent organic pollutants and adverse health effects in humans. *J. of Toxicology and Environmental Health*, Part A 69, **21**, 1987 – 2005.

[9] Atkinson, R. (1996). Atmospheric Chemistry of PCBs, PCDDs and PCDFs. *Chlorinated organic micropollutants*, *Environ. Chem., Royal Society of Chemistry, Cambridge*, Hester, R. E., Harrison, R. M. (Eds.), **6**, 53 – 72.

[10] Denier van der Gon, H.; Bolscher, M.; Visschedijk, A.; Zandveld, P. (2007). Emissions of persistent organic pollutants and eight candidate POPs from UNECE–Europe in 2000, 2010 and 2020 and the emission reduction resulting from the implementation of the UNECE POP protocol. *Atmospheric Environment*, **41**, 9245 – 9261; Kallenborn, R.; Reiersen, L. O. and Daae-Olseng, C. (2012). Long-term atmospheric monitoring of persistent organic pollutants (POPs) in the Arctic: a versatile tool for regulators and environmental science studies. *Atmos. Poll. Res.***, 3**, 589 – 493; Rodan, B. D.; Pennington, D. W.; Eckley, N. and Boething R. S. (1999). Screening of persistent organic pollutants: Techniques to provide the scientific basis for POPs criteria in international negotiations. *Environ. Sci. Technol.*, **33**, 3482 – 3488.

[11] Pignatello, J. J.; Ferrandino F. J. and Huang L. Q. (1993). Elution of aged and freshly added herbicides from a soil. *Environ. Sci. Technol*., **27**, 1563 – 1571.

[12] Cornelissen, G.; Van Noort, P. C. M. and Govers, H. A. J. (1997). Desorption kinetics of chlorobenzenes, polycyclic aromatic hydrocarbons, and polychlorinated biphenyls: sediment extraction with Tenax and effects of contact time and solute hydrophobicity. *Environ. Toxicol. Chem*, **16**, 1351 – 1357.

[13] Zhang, Wei-xian (2003). Nanoscale Iron Particles for Environmental Remediation: An Overview. *Journal of Nanoparticle Research***, 5**, 323 – 332; O'Sullivan, G.; Sandau, C.; Li, L.Y., Iwayemi, A.; Li, F.; Komives, T. and Chakrabarti, T. (2010). Environmental Forensics for Persistent Organic Pollutants. *United Nations Industrial Development Organization*, 1 – 340.

[14] Khan, F. I.; Husain, T.; Hejazi R. (2004). An overview and analysis of site remediation technologies. *J. of Environmental Management*, **71**, 95 – 122.

[15] Koemives, T. and Gullner, G. (2000). Phytoremediation in Plant-Environment Interactions. 2nd ed., Marcel Dekker, Inc. Rights Reserved, New York, 437 – 452; Bittsánszky, A.; Gullner, G.; Guylai, G. and Komives, T., (2011). Part II case Studies: A case Study Uptake and Accumulation of Persistent Organic Pollutants in Cucurbitaceae Species. *Book of Organic Xenobiotics and Plants: From Mode of Action to Ecophysiology. Springer Science and Business Media B. V.*, **8**, 300 – 311; Sureshvarr, K.; Bharathiraja, B.; Jayakumar, M.; Jayamuthunagai, J. and Balaji, L. (2010). Removal of azo dye compounds from paper industries wastes using phytoremediation methodology. *Int. J. Chem. Sci.*, **8**, 687 – 700.

[16] Baldwin, C. J. (2015). The 10 principles of food industry sustainability. *John Wiley &Sons. Ltd, USA,* 22 – 50; Adelaide SA 5001 (2005). Responsible pesticide use. *Environment Protection Authority*, 1– 87.

[17] Wania, F.A.; Mackay, D. (1999). The evolution of mass balance models of persistant organic pollutant fate in the environment. *Environ. Pollut.*, **100**, 223 – 240,.

[18] Baker, J. I.; Hites, R. A. (1999). Evidence for the presence of PCDD/Fs in the environment prior to 1900 and further studies on their temporal trends. *Environ. Sci. Technol.*, **32**, 1580 – 1587.

[19] Seija, S.; Paasivirta, J. (2000). Degradation half-life times of PCDDs, PCDFs and PCBs for environmental fate modeling. *Chemosphere*, **40,** 943 – 949.

[20] Alcock, R. E.; Jones, K. .; McLachlan, M.S.; Johnston, A.E. (1999). Evidence for the presence of PCDD/Fs in the environment prior to 1900 and further studies on their temporal trends. *Environ. Sci. Technol.*, **33**, 206 – 207.

[21] Ritter, L.; Solomon, K. R.; Forget, J.; Stemeroff , M. and O´Leary, C. (1995). Persistent Organics Pollutants. *International Programme on Chemical Safety (IPCS) within the framework of the Inter-Organization Programme for the Sound Management of Chemicals (IOMC)*, 30 – 149.

[22] DiBenedetto, S. A.; Facchetti, A.; Ratner, M. A.; Marks T. J. (2009). Molecular Self-Assembled Monolayers and Multilayers for Organic and Unconventional Inorganic Thin-Film Transistor Applications. *Adv. Mater. (Advanced Materials)*, **21**, 1407–1433; Peercy, P. S. (2000). The Drive to Miniaturization. *Nature,* **406**, 1023 – 1026; Lu, W.; Lieber, C. M. (2006). Semiconductor Nanowires. *Phys. D*. **39**, 387 – 406 ; Love, J. Ch.; Estroff, L. A.; Kriebel, J. K.; Nuzzo, R. G.; Whitesides, G. M. (2005). Self-Assembled Monolayers of Thiolates on Metals as a Form of Nanotechnology. *Chem. Rev.,* **105**, 1103 − 1169.

[23] Schnoor, J. L. (1992). Fate of Pesticides and Chemicals in the Environment. *A Wiley-Interscience Publication, John Wiley & sons, INC.*, 26 – 400; Gozzi, F.; Oliveira, SC.; Dantas R. F.; Silva, V.O.; Quina, F.H.; Machulek, A. J. (2015). Kinetic studies of the reaction between pesticides and hydroxyl radical generated by laser flash photolysis. *J Sci Food Agric.*, 1 – 5.

[24] Atkinson, R.; Guicherit, R.; Hites, R. A.; Palm, W.; Seiber, J. N.; Pim de Voogt (1999). Transformations of Pesticides in the Atmosphere: A State of the Art. *Water, Air & Soil Pollution*, DOI: 10.1023/A:1005286313693 , 115, 219 – 243.

[25] Klöpffer, W., Wagner, B. O. (2007). Signification of photo-degradation in environmental risk assessment. Book of Atmospheric Degradation of Organic Substances. wiley, VCH, Weinheim, Germany, 1 – 20.

[26] Silvio, Can.; Tratnyek, P. G. (2003). Quatitative structure activity relationships for oxidation reaction of organic chemicals in water. *Environmental Toxicology and Chemistry*, **22**, No. 8, 1743 – 1754.

[27] Ren, X.; Sun, Y.; Wu, Z.; Meng, F.; Cui, Z. (2012). The OH-induced degradation mechanism of 4-chloro-2-methylphenoxyacetic acid (MCPA) with two forms in the water: A DFT comparison. *Chemosphere*, **88**, 39 – 48; Halmann, M. M. (1995). Photodegradation of Water Pollutants. *Lybrary of Congress Cataloging-in-Publication Data, CRV Press, INC., Israel* 18 – 200; Tsipi, D.; Botitsi,H.; Economou, A. (2015). Mass Spectrometry for the Analysis of Pesticide Residues and their Metabolites. *Wiley & Sons. Hoboken, New Jersey,* 1 – 263.

[28] Öber, T (2005). A QSAR for the hydroxyl radical reaction rate constant: validation, domain of application, and prediction. *Atm. Environ.*, **39**, 2189 – 2200; Güsten, H.; Medven, Z.; Sekusak, S.; Sabljić, A. (1995). Predicting tropospheric degradation of chemicals: from estimation to computation. *SAR QSAR Environ Res.*, 4, 197 – 209.

[29] Behnke, W.; Zetzsch, C. (1989). Über die Reaktivität von Linda gegenüber OH Radikalen. *Forschungesvorhaben 93 3110/6 (OH- Reactivity of Lindane), Umweltbundesamt*: Berlin.

[30] Zetzsch, C. (1991). Photochemischer Abbau in Aerosolen. *UWSF -Z. Umweltchem. Ökotox*., **3**, 59 – 64.

[31] Palm, W; Millet, M; Zetzsch, C. (1998). OH-radical reactivity of pesticides adsorbed on aerosol materials: first results of experiments with filter samples. *Ecotoxicology and Environmental Safety*, **41**, No. 1, 36 – 43.

[32] El-Shahawi, M. S.; Hamza, A.; Bashammakhb, A. S.; Al-Saggaf, W. T. (2010). An overview on the accumulation, distribution, transformations, toxicity and analytical methods for the monitoring of persistent organic pollutants. *Talanta*, **80**, 1587 – 1597; Solomon, K. R; Dohmen, P. ; Fairbrother, A ; Marchand, M; McCarty, L. (2009). Use of (eco)toxicity data as screening criteria for the identification and classification of PBT/POP compounds**.** *Integr Environ Assess Manag*, **5**, 680 – 696.

[33] Guardans, R. and Castro-Jiménez, J. (2013). How enhancing atmospheric monitoring and modeling can be effective for the Stockholm Convention on POPs. *Atmosphere*, **4**, 445 – 471.

[34] Vizcaino P. and Pistocchi A. (2014). Use of a Simple GIS-Based Model in Mapping the Atmospheric Concentration of γ-HCH in Europe, Atmosphere 5(4), 720 – 736.

[35] Aktar, Md. W.; Dwaipayan, S. and Ashim, Ch. (2009). Impact of pesticides use in agriculture: their benefits and hazards . *Interdiscip Toxicol.,* **2**, No. 1, 1 – 12.

[36] Berner, J.; Furgal, Chris. (2010). Potential impacts of indirect mechanisms of climate change on human health in the Arctic. *The Encyclopedia of Earth*, *Sidney Draggan, Food, Human Health and Environmental Health*, Ed. 9, section 15.3 of the Arctic Climate Impact Assessment, 10 – 30.

[37] Farrington, J. W.; Loehr, R.; Anderson, E.; Bohlen, W. F.; Cohen, Y.; Farley, K.; Giesy, J.; Henshel, D.; Lester, S.; Liegel, K.; McCarty, P.; O'Donaghue, J.; Opaluch, J.; Reible, D. (2001). A Risk Management Strategy for PCB-Contaminated Sediment. *National Academy Press, Washington*, D. C., 1 – 19.

[38] http://iir-de.wikidot.com/ persistent-organic-pollutants (updated on the 16/10/2014 at 16 h 57).

[39] Foglesong, R. E.; Green, S. M.; Lucht, R. P. and Dutton, J. Craig (1998). Dual-Pump Coherent Anti-Stokes Raman Scattering for Simultaneous Pressure/Temperature Measurement. *AIAA J.*, **36**, No. 2; Cheng, J.; Jia, Y. K.; Zheng, G and Xie, X. S. (2002). Laser-Scanning Coherent Anti-Stokes Raman Scattering Microscopy and Applications to Cell Biology, *Biophysical Journal*, **83**, No. 1, 502 – 509.

[40] Abramczyk, H. and Brozek-Pluska, B. (2003). Raman Imaging in Biochemical and Biomedical Applications. Diagnosis and Treatment of Breast Cancer. *Chem. Rev.*, **113**, 5766 – 5781.

[41] Edwards, H. G. M.; Villar, S. E. J.; David, A. R. and Faria, D. L. A. (2004). Nondestructive analysis of ancient Egyptian funerary relics by Raman spectroscopic techniques. *Analytica Chimica Acta*, **503**, 223 – 233; Williams, A. C. (2001). Some Pharmaceutical Applications of Raman Spectroscopy. *Handbook of Raman Spectroscopy. From the Research Laboratory to the Process Line*, edited by Lewis I R, Edwards HGM (eds.), Marcel Dekker, New York, 575 – 592; Edwards, H.G.M. (2001). Raman Spectroscopy in the Characterization of Archaeological Materials, Some Pharmaceutical Applications of Raman Spectroscopy.*Handbook of Raman Spectroscopy*, 575 – 592.

[42] Sur, U. K. and Chowdhury, J.(2013). Surface-enhanced Raman scattering:overview of a versatile technique used in electrochemistry and nanoscience. *Current Science*, **105**, No. 7, 923 – 939; Lyon, L. A.; Keating, Ch. D.; Fox, A. P.; Baker, B. E.; He, L.; Nicewarner, Sh. R.; Shawn, P. M. and Natan, M. J. (1998).Raman Spectroscopy. *Anal. Chem.***, 70**, 341R – 361R.

[43] Zoladek, A. (2011). Confocal Raman imaging of live cells. *Thesis submitted to the University of Nottingham*, 1– 14 ; Fussel A. L. (2014). Coherent Anti-Stokes Raman Scattering Microscopy for Pharmaceutics A shift in the right direction. *Dissertation submitted at the University of Twente, New Zealand*, 1 – 132.

[44] Kneipp, K. (2007). Surface-enhanced Raman scattering. *American Institute of Physics*, *Kneipp K, Kneipp H., and Kneipp J.,Surface-Enhanced Raman Scattering in Local Optical Fields of Silver and Gold Nanoaggregates-From Single-Molecule Raman Spectroscopy to Ultrasensitive Probing in Live Cell*, Acc. Chem. Res., **39,** 443 – 450.

[45] Dresselhaus, M. S.; Dresselhaus,G.; Saito, R.; Jorio, A. (2005). Raman spectroscopy of carbon nanotubes. *Physic Reports*, **409**, No. 2, 47 – 99; Colthup, N. B.; Daly, L. H.; Wiberley, S. E. (1990). Introduction to Infrared and Raman Spectroscopy. Academic Press limited, Inc 3ed., 500 – 543.

[46] David, W. H. (2007). Raman scattering theory. *Department of Mechanical and Aerospace Engineering, university of Florida*, 1 – 13.

[47] McCreery, R. L. (2000). Raman spectroscopy for chemical analysis. *The Ohio State university Columbus, John Wiley & Sons, interscience*, **157**, 200 – 415.

[48] Long, D. A. (2001). The Raman effect: a unified treatment of the theory of Raman scattering by Molecules,*Chichester, New York*, 579 – 584.

[49] Catalin, C. N.; Dreyer, Je.; Behr, N. and Raschk, Mar. B. (2006).Scanning-probe Raman spectroscopy with single-molecule sensitivity.*Physical Review B*, **73**, 193406 – 4.

[50] Schrader, B. and Moore, D. S. (1997). Laser-Based Molecular spectroscopy for chemical analysis-Raman scattering processes. *Pure & Appli. Chem.*, *IUPAC Recommendations,* **69**, No. 7, 1451 – 1468.

[51] Peeran, M. and Srinivasamurthy, G. K. (2005). Comparison of Raman and IR Spectroscopy. *Chem Vista*., p.3; Housecroft, C. E. and Sharpe, A. G. (2005). Chapter 3: An introduction to molecular symmetry in Inorganic Chemistry, 2nd ed, 80 – 95.

[52] Standard, J. M. (2013). Note on Raman Spectroscopy. *Spring, Chemistry*, **362**, 1 - 5; Atkins P. W.; Overtom T. L.; Rourke, J. P; Weller, M. T. and Armstrong, E. A. (2010). Inorganic Chemistry,*Great Britain by Oxford University Press,* 5th ed, Shriver and Atkins, Macmillan Publishing Solutions, 188 – 198.

[53] Mayo, D. W. (2003). Chapter 12: Survey of Infrared and Raman group frequencies. *Course Notes on the Interpretation of Infrared and Raman Spectra*, Mayo D. W., Miller F. A.; Hannah, R. W., *John Wiley & Sons - Interscience, John Willey and Sons Publication*, 355 – 372; Byrne, H. J.; Sockalingum, G. D. and Stone, N. (2011). Chapter 4: Raman Micoscopy: complement or Competitor. *Royal Sociaty of Chemistry Analytical Spectroscopy Series*, 105 – 143.

[54] Schwoerer, M.; Volf, H. C. (2007). Chapter 5: Molecular and lattice dynamic in organic molecular crystals. *Organic Molecular Solids*, *John Wiley & Sons -VCH Verlag GmbH and Co. KG and A, Weinhem*, 100 – 124; Furukawa, Y.(2002).Chapter 5: Near-infrared Ft-Raman spectroscopy. *Near-Infrared spectroscopy: Principles, Instruments, Applications, Siesler H. W., Ozaki Y., Kawata S., Heise H. M., John Wiley & Sons -VCH Velag GmbH, Weiheim (Germany)*, 1st ed., 86 – 108.

[55] Ferraro, J. R.; Nakamoto, K. and Brown, C. W. (2003). Chapter 1: Basic theory. *Introductory Raman Spectroscopy, 2nd Ed., Elsevier Science (USA)*, 1 – 94.

[56] Bouchard, M.; Smith, D. C. (2003) Catalogue of 45 reference Raman spectra of minerals concerning research in art history or archaeology, especially on corroded metals and coloured glass. *Spectrochimica Acta Part A,* **59,** 2247 – 2266.

[57] Smith, E. and Dent, G. (2005). Modern Raman Spectroscopy – A Practical Approach files. *John Wiley and Sons*, 100 – 200.

[58] Grant, R. F. (1975). Introduction to modern optics. *Dover Publications, Inc.,* second edition, New York, 200 – 328.

[59] Wolverson, D. (1995). Raman Spectroscopy. *An Introduction of Laser Spectroscopy*, pp. 91 – 114; Sharna, A. and Schulman, S. G. (2000). An Introduction to Fluorescence Spectroscopy. *Techniques in Analytical Chemistry*, 1 – 36.

[60] Jimenez-Sandoval, S. (2000). Micro-Raman spectroscopy: a powerful technique for materials research. *Microelectronics J.*, **31**, 419 – 427; Lewis, I. R.; Edwards,H. G. M.

(2001). Handbook of Raman Spectroscopy: From the Research Laboratory to the Process Line, 387 – 421.

[61] Karu, T. I. (2003). Low-Power Laser therapy. *CRC Press LLC*; Yadav, A. and Kapruwan, P. (2014). Raman vs. Infrared spectroscopy and advantages of Raman over Infrared spectroscopy, *Ranbaxy laboratories*, 1 – 14.

[62] Gonzalez-Lima, F. and Rojas, J. C. (2011). Low-level light therapy of the eye and brain. *Dove Press J.*, Open access to scientific and medical research; Simpson, E. (2012). The basic principles of laser technology, uses and safery measures in anaethesia. *World federation of societies of Anaesthesia*, 1 – 9.

[63] Wells, O. C. (1993). Materials Characterization. *consise encyclopedia, Pergamon press*, oxford, 300 – 423.

[64] Ferraro, R. L. and Nakamoto, Ka. (1994). Introductory Raman Spectroscopy. *academic press USA*, 662 – 676.

[65] Hassing, S.; Jernshoej, K. D. and Christensen, L. S. (2012). *Raman* spectroscopy is an example of a fast, non-destructive and on-site tool for control of food Quality. *Tech. Raman-spectroscopy*, 1 – 27.

[66] Fahrbach, F. O.; Rohrbach, A. (2012). Propagation stabilita of self-reconstructing Bessel beams enables contrast-enhanced imaging in thick media. *Nature Communication*, 1 – 8; Nemitz, N. (2004). Setup of stable hight-resolution laser system.*Diploma thesis, University of Stuttgart*, 1– 105.

[67] Nelist, P. D.; Cosgriff, E. C.; Behan, G.; Kirkland, A. I. (2008). Imaging modes for scanning confocal electron microscopy in a doudle Aberration.Corrected transmission electron microscope. *Micrisc. Microaanal*, **14**, 82 – 88.

[68] Geerd, St.W., Diercksen, H. F. (2013). Methods in Computational Molecular Physics. *Nato Science Series C*, New York, Springer, **4,** 1 – 20; Dai, H.-L.; Field, R. W. (1995). Molecular Dynamics and Spectroscopy by Stimulated Emission Pumping. *Advanced Series in*

Physical Chemistry, world Scientific Publishing, Singapore, New Jersey, London, Hond Kong, **4**, 10 – 73.

[69] Boeker, E. ; van Grondelle, R. (2011). Environmental Physics: Sustainable Energy and Climate Change. Chap. 8, *Wiley & Sons*, 337 – 369; March, N. H., Mucci, J. F. (1993). Chemical Physics of Free Molecules. *Springer*, New York , 123 – 153.

[70] Coupy, C. and Brissaud, D. (1996). Application in Art, Jewelry and Forensic Science. *Raman microscopy: Developments and Applications* (eds. Turrell G., Corset J.), 1– 240.

[71] Godoi, R.H.M.; Potgieter-Vermaak , S.; De Hoog, J.; Kaegi, R.; Van Grieken, R. (2006). Substrate selection for optimum qualitative and quantitative single atmospheric particles analysis using nano-manipulation sequential thin-window electron probe X-ray microanalysis and micro- Raman spectrometry. *Spectrochimica Acta Part B*, **61**, 375 – 388.

[72] Cifuentes, A. (2012). Food Analsis: Present, future, and foodmics. *ISRN Analytical Chem.,* **2012**, 1 – 16; Lu X.; Rasco, B. A.; Jabal,J. M. F.; Aston,D. E. ; Lin,M. and Konkel, M. E. (2011). Investigating Antibacterial Effects of Garlic (Allium sativum) Concentrate and Garlic-Derived Organosulfur Compounds on Campylobacter jejuni by Using Fourier Transform Infrared Spectroscopy, Raman Spectroscopy, and Electron Microscopy. *Appl. Environ. Microbiol.*, **77**, No. 15, 5257 – 5269.

[73] Williams, T. L. and Collette, T. W. (2001**).** Environmental Applications of Raman Spectroscopy to Aqueous Systems, in: Handbook of Raman Spectroscopy. 683 – 732; Lednev I. K. (2012). Application of Raman spectroscopy for an Easy-to-Use, on-Field, Rapid, Aondestructive, confirmatory identification of body fluids. *Departement of chemistry, University at Albany Suny 1400 Washington Ave*, 1 - 80; Costa, J. C. S. ; Ando, R. A. ; Sant'Ana,A. C. and Corio, P. (2012). Surface-Enhanced Raman Spectroscopy Studies of Organophosphorous Model Molecules and Pesticides. *Phys. Chem. Chem. Phys.***,** 14**,** No. 45, 15645 – 15651.

[74] Zhang, D.; Wang, P.; Slipchenko, M. N.; Cheng, J. X. (2014). Fast vibrational imaging of single cells and tissues by stimulated Raman scattering microscopy. *Acc. Chem. Res.*, **47**,

2282 – 90; Patel, I. I.; Steuwe, C.; Reichelt, S. and Mahajan, S. (2013). Coherent anti-Stokes Raman scattering for label-free biomedical imaging. *J. Opt.*, **15**, 1 – 18.

[75] Thomas, G. J. (1999). Raman spectroscopy of protein and nucleic acid assemblies. *Annu. Rev. Biophys. Biomol. Struct.*, **28**, 1 – 27.

[76] Tague, T. (2009). Infrared and Raman Microscopy. *Pushing the Limits of Spatial Resolution in Microscopy and Microanalysis*, **15**, 562 - 563; Dar, F.; Mamedov, S.; Whitely, A. (2005). Limits of Spatial Resolution of a Raman Microscope. *Microscopy and Microanalysis*, **11**, 728 – 129.

[77] McQueenie, R.; Stevenson, R.; Benson, R; MacRitchie, N.; McInnes, I.; Maffia, P.; Faulds, K.; Graham, D.; Brewer, J.; Garside, P. (2012). Detection of inflammation in vivo by surface-enhanced Raman scattering provides higher sensitivity than conventional fluorescence imaging. *Anal Chem.* **84**, No. 14, 5968 – 75.

[78] Potter, T. L.; Mohamed, M. A.; Ali H. (2007). Solid-phase extraction combined with high-per-formance liquid chromatography atmospheric pressure chemical ionization mass spectrometry analysis of pesticides in water: Method performance and application in a reconnaissance survey of residues in drinking water in Greater Cairo, Egypt. J. Ag-ric. Food Chem., **55**, 204 – 210. Portoles, T.; Pitarch E.; Lopez, F. J.; Hernandez, F. (2011). Development and validation of a rapid and wide-scope qualitative screening method for detection and identification of organic pollutants in natural water and wastewater by gas chromatography time-offlight mass spectrometry. *J. Chromatogr. A*, **1218,** 303–315.

[79] Mehrsheikh, A.; Bleeke M.; Brosillon, S.; Laplanche, A.; Roche, P. (2006). Investigation of the mechanism of chlorination of glyphosate and glycine in water. *Water Research*, 40, 3003 – 3014.

[80] Koo, I.; Ali, D.; Yang, K.; Park, Y.; Yong, AE.; Vanloon, GW. et al. 2009. 31P NMR and ESI-MS studies of metal ion-phosphorus pesticide residue complexes. *Can J Chem*, 87, 433 – 9; Tamura, H.; Yoshikawa, H.; Gaido, KW.; Ross SM.; De-Lisle RK.; Welsh WJ. et al. (2003). Interaction of organophosphate pesticides and related compounds with the androgen receptor. *Environ Health Perspect*, **111**, 545 - 552.

[81] Klotzkin, D. J. (2014). Chapter 2: The basic of Lasers. *Introduction to semiconductor lasers for optical communications, Springer Scince and Busness Media*, New York, 11– 29; Reichegger, A. and Evers, J. Temporal dynamics of stimulated emission with applications in nuclear quantum optics. *Quantum Physics*, 1 –16.

[82] Kneipp, J.; Kneipp, H.; and Kneipp, K. (2008). SERS-a single-molecule and nanoscale tool for bioanalytics. *Chem. Soc Rev.*, Vol. **37,** 1052 – 1060; Wang, Y. and Wang, L. V. (2012). Forster resonance energy transfer photoacoustic microscopy. *J. Of Biomedical Optics*, **17**, No.8, 086007 – (1 – 6).

[83] Koo, T. (1996). Measurement of Glucose in Human blood serum using near-infrared Raman Spectroscopy. *Master inMassachusetts Institute of Technology All rights reserved*; Zaidi, S. F. H. (2013). Advanced Dynamic Interrogation Techniques for Hybrid Distributed/Discrete Optical Fiber Sensors. *Scuola Superiore Sant'Anna*., 1 – 141.

[84] Pilling, and Seakins, P. W. (1995). Reaction kinetics. *Oxford science publications*, 1 – 178.

[85] Akhter, M. (2007). Chemical kinetics. *Dept. of chemistry faculty of science Jamia Hamdard, Hamdard Nagar*, New Delhi- 110062, 1 – 36.

[86] Diem, M. (1993). Introduction to Modern Vibrational Spectroscopy. John Wiley & Sons, New York **;** Lewis, I.R.; Edwards, G.M. (2001). Handbook of Raman Spectroscopy, *CRC Press, New York*; Shane, P.; Min, K.; Cakmak, M. (2003). Kinetic studies of polyurethane polymerization with Raman spectroscopy.*Colloid and Polymer Science*, **44**, No. 18, 5137 – 5144; Poggendorf, S.; Mba, G. A.; Engel, D.; Sadowski, G. (2011). Diffusion of poly(ethylene glycol) and ectoine in NIPAAm hydrogels with confocal Raman spectroscopy.*Colloid and Polymer Science*, **289,** 545 **–** 559**.**

[87] Stöckel, St.; Kirchhoff, J.; Neugebauer, U.; Rösch, P.; Popp, J. (2016). The application of Raman spectroscopy for the detection and identification of microorganisms. *Journal of Raman Spectroscopy*, **47**, 89 – 109.

[88] McCreery, R. L. (2000). Raman Spectroscopy for Chemical Analysis. *Wiley-Interscience*, Chichester, West Sussex, UK, **157**, 10 – 452.

[89] Kenneth, A. C. (1990). Chemical kinetics, the study of reaction rates in solution. *John John Wiley & Sons -VCH and Sons*, 1 – 463.

[90] Petrucci, R. H.; William, S. H.; Greoffrey, H. and Jeffry, D. M. (2007). General Chemistry: Principles & Modern Applications. *Upper Saddle River*, N.J.: Pearson Education, 9th ed., 1000 – 1168.

[91] Kenneth, A. Con. (1991). Chemical Kinetics, the study of reaction rates in solution. *John Wiley and Sons,* Inc, 1 – 1160.

[92] Fawl, S. (1985). Chapter11: Rate laws, Kinetics, Mechanisms and activation energies. General Chemistry, 22 – 52.

[93] Atkinson, R.; Baulch, D. L.; Cox, R. A.; Crowley, J. N.; Hampson, R. F.; Hynes, R. G.; Jenkin, M. E.; Rossi, M. J; Troe, J. (2004). Evaluated kinetic and photochemical data for atmospheric chemistry (IUPAC): gas phase reactions of Ox, HOx, NOx and SOx species. *Atmos. Chem. Phys.*, **4**, 1461 – 1738.

[94] Edward, D. and Jose-Luis, J. (2004). Kinetics and atmospheric chemistry. *Atm. Chem.*, 1 – 36.

[95] McNaught, A. D. and Wilkinson, A. (1997). Elementary reaction. Blackwell Scientific Publications, Oxford, **68**, 1 – 148.

[96] Cook, G. B.; Gray, P.; Knapp, D. G. and Scott, S. K. (1989). Bimolecular routes to cubic autocatalysis. *Journal of Physical Chemistry*, **93,** 2749 – 2755.

[97] Harris, C. M. (2012). The SFC comeback. *Anal. Chem.,* **74**, 87 – 91; Maurer, H. H.; Pfleger, K.; Weber, A. A. (2007). Mass Spectral and GC Data of Drugs, Poisons, Pesticides, Pollutants and their Metabolites. *Wiley-VCH, Weinheim,* 100 – 1000

[98] Zhou, Y.; Zhuang, X (2007). Kinetic Analysis of sequential Multi-step Reactions. *J. Phys Chem B.,* **111**(48), 13600 – 13610.

[99] Keeler, J. (2011). Understanding NMR Spectroscopy. *Wiley & Sons, Hoboken*; Bakhmutov, V. I. (2012). Solid-State NMR in Materials Science: Principles and Applications. *Taylor & Francis, Boca Raton, London New york*, 2 – 163.

[100] Klotzkin, D. J. (2014). Chapter 2: The basic of Lasers. *Introduction to semiconductor lasers for optical communications, Springer Scince and Busness Media*, New York, 11– 29; Reichegger, A. and Evers, J. Temporal dynamics of stimulated emission with applications in nuclear quantum optics. *Quantum Physics*, 1 –16.

[101] Kneipp, J.; Kneipp, H.; and Kneipp, K. (2008). SERS-a single-molecule and nanoscale tool for bioanalytics. *Chem. Soc Rev.*, Vol. **37,** 1052 – 1060; Wang, Y. and Wang, L. V. (2012). Forster resonance energy transfer photoacoustic microscopy. *J. Of Biomedical Optics*, **17**, No.8, 086007 – (1 – 6).

[102] Koo, T. (1996). Measurement of Glucose in Human blood serum using near-infrared Raman Spectroscopy. *Master inMassachusetts Institute of Technology All rights reserved*; Zaidi, S. F. H. (2013). Advanced Dynamic Interrogation Techniques for Hybrid Distributed/Discrete Optical Fiber Sensors. *Scuola Superiore Sant'Anna*, 1 – 141.

[103] Pilling, and Seakins, P. W. (1995). Reaction kinetics. *Oxford science publications*.

[104] Diem, M. (1993). Introduction to Modern Vibrational Spectroscopy. John Wiley & Sons, New York ; Lewis, I.R.; Edwards, G.M. (2001). Handbook of Raman Spectroscopy, *CRC Press, New York*; Shane, P.; Min, K.; Cakmak, M. (2003). Kinetic studies of polyurethane polymerization with Raman spectroscopy. *Colloid and Polymer Science*, 44, No. 18, 5137 – 5144; Poggendorf, S.; Mba, G. A.; Engel, D.; Sadowski, G. (2011). Diffusion of poly(ethylene glycol) and ectoine in NIPAAm hydrogels with confocal Raman spectroscopy.*Colloid and Polymer Science*, 289, 545 – 559.

[105] Efremov, E. ; Ariese, F.; Gooijer, C. (2008). Achievements in resonance Raman spectroscopy: A Review of a technique with a distinct analytical chemistry potential. *Analytica Chimica Acta*, **606**, 119 – 134; Salzer, R. and Siesler, H.W. (2014). Infraredand Raman Spectroscopic Imaging, John Wiley & Sons -VCH, Weinheim, 2nd Ed., 1 – 656.

[106] McNaught, A. D. and Wilkinson, A. (1997). Elementary reaction. Blackwell Scientific Publications, Oxford, **68**, 1 – 148.

[107] Cook, G. B.; Gray, P.; Knapp, D. G. and Scott, S. K. (1989). Bimolecular routes to cubic autocatalysis. *Journal of Physical Chemistry*, **93,** 2749 – 2755.

[108] Kenneth, A. C. (1990). Chemical kinetics, the study of reaction rates in solution. *John John Wiley & Sons -VCH and Sons*, 1 – 463.

[109] Petrucci, R. H.; William, S. H.; Greoffrey, H. and Jeffry, D. M. (2007). General Chemistry: Principles & Modern Applications. *Upper Saddle River*, N.J.: Pearson Education, 9th ed., 1000 – 1168.

[110] Kenneth, A. Con. (1991). Chemical Kinetics, the study of reaction rates in solution. *John Wiley and Sons,* Inc, 1 – 1160.

[111] Fawl, S. (1985). Chapter11: Rate laws, Kinetics, Mechanisms and activation energies. General Chemistry, 22 – 52.

[112] Edward, 5D. and Jose-Luis, J. (2004). Kinetics and atmospheric chemistry. *Atm. Chem.*, 1 – 36

[113] Kwamena, N. A; Thornton, J. A. And Abbatt, J. P. D. (2004). Kinetics of surface-bound Benzo[a]pyrene and ozone on solide organic and salt aerosols. *J. Phys. Chem.*, 108, 11626 – 11634; Zhang, R.; Krzyszowska-Waitkus, A. J.; Vance, G. F.; Qi, J. (2000). Pesticide transport in field soils. *Advance in Environmental Research*, 4, 59 – 68; Atkinson (2003). Kinetics of the gas-phase reactions of OH-radicals with alkanes and cycloalkanes. *Atmos. Chem. Phys.*, 3, 2233 –2307.

[114] Pflieger, M.; Goriaux, M.; Temime-Roussel, B.; Gligorovski, S.; Monod, A. and Wortham, H. (2009). Validation of an experimental setup to study atmospheric heterogeneous ozonolysis of semi-volatile organic compounds. *Atmospheric Chemistry and Physics*, **9**, 2215 – 2225.

[115] Vandenabeele, P. (2012). Practical Raman Spectroscopy: An Introduction Analytical techniques in the sciences. *Wiley & Sons: Hoboken, NJ (Google eBook)*; Hummel, D. O. (2002). Atlas of Plastics Additives : Analysis by Spectrometric Methods. *Springer : Berlin-*

Heildelberg-New York, Chapter 3 and 4; Kerker, M.; Wang, D.-S.; Chew, H.; Siiman, O.; Bumm, L.A. (1982). Surface Enhanced Raman Scattering. *in : Chang R.K., Furtak, T.E. (eds.), Plenum Press: New York*, 109 – 128; Morris, M.D. (1992). Applied Laser Spectroscopy. *in :Andrews, D.L. (ed.), VCH Publishers Inc.: New York*; Guilbault, G.G. (1990). Practical Fluorescence. *Second Edition, Marcel Dekker, Inc. : New York*; Lakowicz, J.R. (1983). Principles of Fluorescence Spectroscopy. *Plenum Press : New York* ; Berlman, LB . (1971). Handbook of fluorescence spectra in aromatic molecules. *Academic Press : New York, Chapter 5*, **2**, 26 – 300.

[116] Werner, R. Haag; David, Y.C. C. (1992). Rate constants for reaction of hydroxyl radicals with several drinking water contaminants. *Environ. Sci. Technol.,* **26**, 1005 – 1013.

[117] Acero, Ju. L.; Stemmler, K. and Guten, U. V. (2000). Degradation Kinetics of Atrazine and Its Degradation Products with Ozone and OH Radicals: A Predictive Tool for Drinking Water Treatment. *Environ. Sci. Technol.*, **34**, 591 – 597; Lacorte, S.; Lartiges, S. B.; Garrigues, P.; Barcelo, D. (1995). Degradation of organosphorus pesticides and their transformation products in Estuarine waters. *Environ. Sci. Technol.*, **29**, 431 – 438.

[118] Atkinson, R. (1985). Kinetics and mechanisms of the gas-phase reactions of the hydroxyl radical with organic compound under atmospheric concitions. *Chem. Rev.*, **85**, 69 – 201.

[119] Linsenbuhler, M.; Werth, J. H.; Dammer, S. M.; Knudsen, H. A.; Hinrichsen, H.; Wirth, K. E. and Wolf, D. E. (2006). Cluster size distribution of charged nanopowerders in suspensions. *Powder Techn.*, **167**, 124 – 133.

[120] Behnke, W.; Hollaender, W.; Koch, W.; Nolting, F.; Zetzsch ,C. (1988). A smog chamber for study of the photochemical degradation of chemicals in the presence of aerosols. *J. Aerosol Sci.*, **22**, 1113 – 1120.

[121] Wagner, E. and Brunner, H. (1960). Aerosil, Herstellung, Eigenschaften und Verhalten in organischen Flüssigkeiten. *Angew. Chem.*, **72**, 744 – 750.

[122] Toprasri, P. (2003). Factors affecting physical properties and drug release from hydrophilic and hydrophobic colloidal silicon dioxide gels. *Thesis of Master of pharmacy, Silpakorn University*, 1 – 121.

[123] Gerhard, Menzel GmbH, Saarbrückener Straße 248, 38116 Braunschweig (Germany); Schulz, C.; Ruesten-Lange, M. von; Krueger, A.; Lendlein, A.; Jung, F. (2012). Viability and function of primary human endothelial cells on smooth poly(ether imide) films. *Clinical hemorheeology and Microcirculation IOS Press,* 1 – 22.

[124] Allen, F. H.; Kennard, O. and Wastson, D. G. (1987). Table of bond lengths determined by X-Ray and Neutron Diffraction. Part1. Bond Lengths in Organic compounds. *J. Chem. Soc. Perkin Trans. II,* 1 – 19.

[125] Zsolnay, A. (1994). The lack of effect of the dissolved organic material in soil on the water solubility of the herbicide, terbuthylazine. *The Science of the Total En.*, **152**, 101 – 104

[126] Pedrosa, V. A.; Caetano, J.; Machado, S. A. S.; Freire, R. S.; Bertotti, M. (2007). Acetylcholinesterase Immobilization on 3-mercaptopropionic Acid Self Assembled Monolayer for Determination of Pesticides. *Electroanalysis*, **19**, 1415 – 1420.

[127] Brubaker, W. W.; Hites, A. R. (1997). Polychlorinated dibenzo-p-dioxins and dibenzofurans: Gas-phase hydroxyl radical reactions and related atmospheric removal. *Environ. Sci. Technol.*, **31**, 1805 – 1810.

[128] Hein, R.; Crutzen, Pa. J. and Heimann, M. (1997). An inverse modeling approach to investigate the global atmospheric methane cycle. *Glo. Biogeochem. Cyc.*, **11**, No. 1, 43 – 76.

[129] Gligorovski, S.; Strekowski, R.; Barbati, S. And Vione, D. (2015). Environmental implications of hydroxyl Radicals ($^{\cdot}$OH). *Chem. Rev.*, **115**, 13051 – 13092.

[130] Baxendale, J. H. and Wilson, J. A. (1957). The photolysis of hydrogen peroxide at high light intensities. *Trans. Faraday Soc.*, **53**, 344 – 356.

[131] Jianzhong, M.; Jie, T.; Xiuji, Z. and Xiaoshan, Z. (2002). Estimates of the Chemical Budget for Ozone at Waliguan Observatory. *J. of Atm. Chem.*, Kluwer Academic Publishers. Printed in the Netherlands, **41,** 21 – 48.

[132] Tezcanli-Güyer, G.; Ince, N. H. (2004). individual and combined effects of ultrasound, ozone and UV irradiation: a case study with textile dyes. *Institute of Environmental Sciences*, Bogacizici University 34342 Bekek, Istanbul, Turkey, science direct, Utrasonics, **42**, 603 – 609.

[133] Joseph, J. M.; Destaillats, H.; Hung, H. M.; Hoffmann, M. R. (2000). The sonochemical degradation of azobenzene and related azo dyes: rate enhancement via Fenton´s reactions. *J. Phys. Chem.*, **104(A)**, 301 – 307.

[134] Ince, N. H.; Tezcanli, G.; Belen, R.; Apikyan, I. G. (2000). Ultrasound as a catalyzer of aqueous reaction systems: the state of the art and environment applications. *Appl. Catal. B. Environ.*, **29**, 167 – 176.

[135] Helmenstine, A. M. (2013). Hydrogen peroxide shelf life. *Chem. 101*, p.2; Clark, D. E. (2000) Peroxides and peroxide-forming compounds. *Ph. D. Texas A &M University*, 1 – 16.

[136] Schumb, W. C.; Satterfield, C. N. and Wentworth, R. L. (1977). Part four: Hydrogen peroxide. *A Monograph prepared with support from the office of Naval research contract No. N5 ori-07819 NR-092-008,* 200 – 204; Crowell, R. A.; Lian, R; Sauer, M. C.; Oulianov, D. A. and Shkrob, I. A. (2004). Geminate recombination of hydroxyl radicals generated in 200 nm photodissociation of aqueous hydrogen peroxide. Chem. Phys. Lett. **383** (5), 481 – 485.

[137] Moeller, T. (1957). Inorganic syntheses. *McGraw-Hill Book company, Inc*, **5**, 20 – 271; Carter, D. (2013). Chapter 14: Titration of hydrogen peroxide. *Pre-lab assignments*, 1 – 10.

[138] Palm, W. -U.; Elend, M.; Krueger, H-U. and Zetzsch, C. (1997). OH-radical reactivity of airborne terbutylazine adsorbed on inert aerosol. *Environ. Sc. & Techn.*, **31**, No. 12, 3389 – 3396.

[139] Aerosil Fumed Silica-search by Industry/ Effect (16. 07. 09).

[140] Schurath, U. and Naumann, K.-H. (1998). Heterogeneous processes involving atmospheric particulate matter. *Pure & Appl. Chem.,* **70**, 1353 – 1361.

[141] Gupta, R.K.; Ghosh, K.; Kahol, P. K.; Yoon, J.; Guh, S. (2008). Pulsed laser thin film growth of di-octyl substituted polyfluorene and its co-polymers. *Appl. Surf. Sc.*, **254**, 7069 – 7073.

[142] Cao, L. (2014). Numerical investigation of tropospheric halogen release and ozone depletion in the Polar spring. *Dissertation, Ruprecht-Karls-Universität Heidelberg,* 1 – 145.

[143] Schiffman, A.; Nelson, D. D. and Nesbitt, D. J. (1993). Quantum yields for OH production from 193 and 248 nm photolysis of HNO_3 and H_2O_2. *J. Chem. Phys.*, **98**, 6935 – 6946.

[144] Garbin, J. R.; Milori, D. M. B. P.; Simoes, M. L.; Silva, W. T. L.; Neto, L. M. (2007). Influence of humic substances on the photolysis of aqueous pesticide residues. *Chemosphere*, **66**, 1692 – 1698.

[145] Smith, C. A.; Molina, L. T.; Lamb, J. J. and Molina, M. J. (1984). Kinetics of the reaction of OH with pernitric and nitric acids. *Int. J. of Chem. Kinet.*, **16**, 41 – 55.

[146] Klöpffer, W.; Wagner, B. O. (2007). Atmospheric degradation of organic substance. *Wiley-VCH Verla GmbH & Co. KGaA*, 51 – 126.

[147] Sinkkonen, S.; Paasivirta, J. (2000). Degradation half life time of PCDDs, PCDF and PCBs for environment fate modeling. *Chemosphere*, **40**, Issues 9-11, 943 – 949.

[148] Sun, F.; Zhu, T.; Shang, Han L. (2005). Gas-phase reaction of dichlorvos, carbaryl, chlordimeform, and 2, 4,-D buttyl Ester with OH Radicals. *International Journal of Chemical kinetics*, **37**, 755 – 762; Cheeseman, KH; Slater, TF.(1993). An introduction to free radicals chemistry. *Br Med Bull.*, **49**, 48 – 493; McCord, JM. (2000). The evolution of free radicals and oxidative stress. *Am J Med.*, **108**, 652 – 659; Johnson, F; Giulivi, C. (2005). Superoxide

dismutases and their impact upon human health. *Mol Aspects Med.*, **26**, 340 – 352; Meister, A. (1988). Glutathione metabolism and its selective modification. *J Biol Chem.*, **263**, 17205 – 8; Kahl, R. and Hildebrandt, A.G. (1986). Methodology for studying antioxidant activity and mechanisms of action of antioxidants. *Food and Chemical Toxicology*, **24**, 1007 – 1014; Gaetani, G; Ferraris, A; Rolfo, M; Mangerini, R; Arena, S; Kirkman, H. (1996). Predominant role of catalyse in the disposal of hydrogen peroxide within human erythrocytes. *Blood*, **87**, No.4 , 1595 – 1599

[149] Schumb, W. C.; Satterfield, C. N.; Wentworth, R. L. (1955). Hydrogen Peroxide, *ACS Monograph series*, **565,** Reinhold, New York; Chramosta, N. ; DeLaat, J. ; Dore, M. ; Pouillot, M. (1993). Determination des constantes cinetiques de reaction des radicaux hydroxyles sur quelques s-triazines. *environ. Techno.,* **14**, 215 – 226.

[150] Norman, V. Klas.; Marchington, Dav. and McGowant, H. C. E. (1994). H_20_2 Determination by the I_3^- Method and by $KMn0_4$ titration. *Analytlcal Chemistry*, **66**, No.18, 2921 – 2925; Lide, D. R. Ed. CRC.(1998 - 1999). Handbook of Chemistry and Physics. *CRC Press, 79th ed., Boca Raton, FL*.

[151] Rühl E. (2004). Messung von Reaktionsgeschwindigkeitskonstanten zum Abbau von Langlebigen, partikelgebundenen Substanzen durch indirekte Photooxidation. *(Umweltforschungsplan des Bundesministeriums für Umwelt, Naturschutz und Reaktorsicherheit), Free University Berlin, Institut für Physikalische Chemie, UBA-FB*; 00,79, 1 – 59; Behki, Ram M. and Khan, S. U., (1994). Degradation of atrazine, propazine, and simazine by Rhodococcus strain B-30. *J. Agric. Food Chem.*, **42**, 1337 – 1241.

[152] Pavia, D. L.; Lampman, G. M. and Kriz, G. S. (1979). *Introduction to spectroscopy: A guide for students of organic chemistry*. Philadelphia: W.B. Saunders Co., 1 – 530

[153] Zhi-Min, Z.; Shan, C. Yi-Zeng, L; Zhao-Xia, L.; Qi-Ming, Z; Li-Xia, D.; Fei Y., and Hua, Z. (2009). An intelligent background-correction algorithm for highly fluorescent samples in Raman spectroscopy.*J. Raman Spectrosc*., 1 – 11

[154] Sadezky, A.; Muckenhuber, H.; Grothe, H.; Niessner, R.; Poesch, U. (2005). Raman microspectroscopy of soot and related carbonaceous materials: Spectral analysis and structural information. *Carbon*, **43**, 1731 – 1742.

[155] Wang, Y.; Bian, S.; Lui, X; Wang, F. and Meng, Q. (2013). Fabrication of Poly(triazine dithiol) Functional nanofilm by Galvanostatic polymerization on Aluminum. *Int. J. Electrochem. Sci.,* **8**, 10818 – 10826.

[156] Balachandran, V.; Lakshmi, A. and Janaki, A. (2011). Vibration spectroscopic study and NBO analysis on 2-chloro-4,6-diamino.1,3,5-triazine using DFT method. *Recent Research in Science and Technology,***3**(1), 114 – 123.

[157] Pal, B.; Li, Z.; Takenaka, S; Tsuyama, S. and Kitagawa, T. (2005). Resonance Raman investigation of YV-I and GTP on structure of CO-bound heme of soluble guenylate cyclase. *BMC Pharmacology*.

[115] Vandenabeele, P. (2012), Practical Raman Spectroscopy: An IntroductionAnalytical techniques in the sciences. *Wiley & Sons: Hoboken, NJ (Google eBook)*; Smith, E; Dent, G. (2005). Modern Raman Spectroscopy: A Practical Approach. *Wiley& Sons : Hoboken, NJ* ; Hummel, D.O. (2002). Atlas of Plastics Additives : Analysis by Spectrometric Methods. *Springer : Berlin-Heildelberg-New York, Chapter 3 and 4*; Kerker, M.; Wang, D.-S.; Chew, H.; Siiman, O.; Bumm, L.A. (1982). Surface Enhanced Raman Scattering. *in : Chang R.K., Furtak, T.E. (eds.), Plenum Press: New York*, 109-128; Morris, M.D. (1992). Applied Laser Spectroscopy. *in :Andrews, D.L. (ed.), VCH Publishers Inc.: New York*; Guilbault, G.G. (1990). Practical Fluorescence. *Second Edition, Marcel Dekker, Inc. : New York*; Lakowicz, J.R. (1983). Principles of Fluorescence Spectroscopy. *Plenum Press : New York* ; Berlman, LB . (1971). Handbook of fluorescence spectra in aromatic molecules. *Academic Press : New York,* **2**, Chapter 5.

[117] Acero, Ju. L.; Stemmler, K. and Guten, U. V. (2000). Degradation Kinetics of Atrazine and Its Degradation Products with Ozone and OH Radicals: A Predictive Tool for Drinking Water Treatment. *Environ. Sci. Technol.*, **34**, 591 – 597; Lacorte, S.; Lartiges, S. B.;

Garrigues, P.; Barcelo, D. (1995). Degradation of organosphorus pesticides and their transformation products in Estuarine waters.*Environ. Sci. Technol.*, **29**, No2, 431 – 438.

[4.16158] Rai, A. K.; Das, I. M. L.; Uttam, K. N.(2010).Emerging Trends in Laser & Spectroscopy and Applications.*Allied Publishers*, 1 – 452.

[159] Da Silva, J. P.; Ferreira, L. F. V.; Osipov, I.; Machado, I. F., (2010). Surface photochemistry of pesticides containing 4-chlorophenoxyl chromophore.*J. of Hazardous Materials*, **179**, 187 – 191.

[160] Gunasekara, A. S. (2004). Environmental fate of Simazine. *Department of pesticide regulation, 1001 I Street Sacramento, CA 95812*, 36; Wolf, D. C and Jackson, R. L., (1982). atrazine degradation, sorption and bioconcentration in water systems. *GRA and I, Govemment Report Announcement Index, (NTISPBB83-150151)*.

[161] Getenga, Z., Dörfler, U.; Iwobi, A; Schmid, M.; Schroll, R. (2009). Atrazine and terbuthylazine mineralization by an Arthrobacter sp. Isolated from a sugarcane-cultivated soil in Kenya. *Chemosphere*, **77**, 534 – 539.

[162] Toribara, T. Y.; Coleman, J. R.; Dahneke, B. E.; and Feldman, I. (2012). Environmental pollutants. *Plenum press, New* York, 1 – 444.

[163] Nagabalasubramanian P. B.; Karabacak, M., Periandy, S. (2012). Vibrational frequencies, structural confirmation stability and HOMO–LUMO analysis of nicotinic acid ethyl ester with experimental (FT-IR and FT-Raman) techniques and quantum mechanical calculations. *J. of Molecular Structure,* **1017**, 1–13; Karabacak, M.; Cinar, M.; Ermeca S. and Kurtb, M. (2010). Experimental vibrational spectra (Raman, infrared) and DFT calculations on monomeric and dimeric structures of 2- and 6-bromonicotinic acid. *J. Raman Spectrosc.,* 41, 98 – 105.

[164] Diels O., Alder K. (1928): *Synthesen in der hydroaromatischen Reihe*. In: Justus Liebigs Annalen der Chemie. **460**, 1, S. 98–122.; Diels, O.; Alder, K. (1929). Synthesen in der hydroaromatischen Reihe, IV. *Berichte der deutschen chemischen Gesellschaft,* **62**, 2081–2087; Holmes H. L.: *The Diels-Alder Reaction Ethylenic and Acetylenic Dienophiles.* In: *Organic Reactions.* **4**, 2, 2004, S. 1007–1019.

[165] Da-Wen, S. (2009). Infrared Spectroscopy for Food Quality Analysis and Control.*Park Avenue South, New York, USA,* 10010 - 1710.

[166] Budzikiewicz, H. und Schäfer, M. (2005). Massenspektrometrie –Eine Einführung, *Wiles-VCH: Weinheim*; Gross, J. H. (2011). Mass spectrometry–A Textbook. *2nd ed. Springer-Verlag : Heidelberg and Berlin*;Hoffmann, E. d. and Stroobant, V. (2001). Mass spectrometry : Principles and applications. *2nd ed. Wiley: Chichester and New York*; Finehout, E. J. and Lee, K. H. (2004). An introduction to mass spectrometry applications in biological research.*Biochem Mol Biol Educ*., **32**, 93 – 100; Hesse, M. M.; Meier, H.; Zeeh, B. (2011).Spektroskopische Methoden in der organischen Chemie, *8. Aufl., Georg Thieme Verlag: Stuttgart*; Smith, R.M.; Busch, K. L. (2004). Understanding Mass Spectra: A Basic Approach. *John Wiley & Sons: Chichester*; DeHoffmann, E.; Stroobant E. (2007). Mass Spectrometry: Principles and Applications. *3rd ed., John Wiley & Sons: Chichester*; Throck, Watson J, Sparkman, O.D. (2007). Introduction to Mass Spectrometry.*4th ed., John Wiley & Sons: Chichester*.

[167] Krishnan, V. V and Murali, N. (2013). Radiation damping in modern NMR experiments: Progress and challenges. *Progress in NMR.Spectroscopy*, **68**, 41 – 57; Keeler J. (2010).Understanding NMR Spectroscopy.*2nd. Ed. Wiley :Chichester*; Levitt, M.H. (2008). Spin Dynamics: Basics of Nuclear Magnetic Resonance. *Wiley :Chichester*; John, M; Chalmers, J. M.; Howell, G. M. E.; Michael, Hargreaves D. M. D. (Eds.) (2012). Infrared and Raman Spectroscopy in Forensic Science. *Wiley: Chichester*; Yang, L. (2009). Materials Characterization: Introduction to Microscopic and Spectroscopic Methods. *Wiley: Chichester*;Meiler, W. and Meusinger, R. R. (1991).NMR of Coals and Coal Products.*Annual reports on NMR Spectroscopy,* **23**, 375 – 409.

[168] Bain, A. D. (2003). Chemical exchange in NMR.*Elsevier B.V. All rights reserved*, **43**, 63 – 103

[169] Lachenmeier, D. W. Eberhard Hu., Fang Fa., Schütz Bi., Dvortsak Pe., Sproll Co. and Spraul Ma., (2009). NMR-Spectroscopy for Nontargeted Screening and Simultaneous Quantification of Health-Relevant Compounds in Foods: The Example of Melamine. *J. Agric. Food Chem*., **57**, No.16, 7194 – 7199

[170] Welhouse, G. J. and Wolliam, F. B. (1992). NMR spectroscopic investication of hydrogen bonding in Atrazine.*sci. environ.*, **26**, 959 – 964

[171] Semencic, M. C., Dropucic M., Barisic L., and Rapic V., Synthesis of the First Heteroannularly Substituted Ferrocene Amino Acid and Isomeric Carbamic Acid Derivatives Containing Chiral Centres, CCACAA **79** (4) 599 - 612 (2006)**;** Rausch A. (2005). Diastereoselektive synthese von 1,3,2-Oxazaborolidinen aus chiralen 1,3,2-Diazaborolen, Dissertation zur Erlangung des Grades eines Doktors der Naturwissenschaften der Universität Bielefeld; Yang X., Lu R., Xu T., Xue P., Liu X. and Zhao Y. (2007) Supporting Information for: Novel Carbazole-based Organogels Modulated by *Tert*-butyl Moieties, The Royal Society of Chemistry

[172] Hatfield, S. E. (2007). Applications of triazine chemistry: Education, remediation, and drug delivery. Texas A&M University

[173] Welhouse, G. J. and Bleam, W. F. (1993). Atrazine Hydrogen-Bonding Potentials. Department of Soil Science, University ofWisconsin-Madison, Madison, Wisconsin 53706, *Environ. Sci. Technol.* W93, **27***,* No.3, 494 – 500; Roberts J.D., (1959). Nuclear Magnetic Resonance: Applications to Organic Chemistry. *McGraw-Hill Book Company, New York*

[174] Burrows, H. D.; Canle, M. L., Santaballa, J. A; Steenken, S. (2002). Reaction pathways and mechanisms of photodegradation of pesticides. *J. of Photo. And Photo. B: Biology,* **67**, 71 – 108.

[175] Welhouse, G. J. and Bleam, W. F**.,** (1993b). Cooperative Hydrogen Bonding of Atrazine. Department of Soil Science, University of Wlsconsln-Madison, Madison, Wisconsin 53706**,** *Environ. Sci. Technol.*, **27**, No.3**,** 500 – 505.

[176] Lucas A. D., Bekheit H. K. M., Goodrow M. H., Jones A. D., Kullman Seth, Matsumura F.; Woodrow James E., Seiber J. N., and Hammock B. D. (1993). Development of Antibodies against Hydroxyatrazine and Hydroxysimazine: Application to Environmental Samples; *J. Agric. Food Chem.*, **41***,* 1523 – 1529.

[177] Ross A. G.; Townsend, S. D.; Danishefsky S. J. (2013).Applications to Generating Useful Structural Patterns. *J. Org. Chem.*, **78**, 204 **–** 210;Domigo, L. R.; Aurell, M. J.; Pérez, P.; Contreras, R. (2002). Quantitative characterization of the global electrophilicity power of commondiene/dienophile pairs in Diels–Alder reactions.*Tetrahedron*, **58**, Iss.22, 4417 - 4423**;** Nicolaou, K. C.; Snyder, S. A.; Montagnon, T.; Vassilikogiannakis, G. (2002). The

Diels-Alder Reaction in Total Synthesis.*Angew. Chem. Int. Ed*., **41**, 1668 – 1698; Atherton, J. C. C.; Jones, S. (2003). Diels-Alder Reactions of Anthracene, 9-Substituted Anthracenes and 9, 10-Disubstituted Anthracenes. *Tetrahedron* , **59**, 9039 – 57.

[178] Müller, J.-F.; Peeters, J.; Stavrakou, T. (2014). Fast Photolysis of Carbonyl Nitrates from Isoprene. Atmos. *Chem. Phys.*, **14**, 2497–2508; Schwarzenbach, R.P.; Gschwend, P.M.; Imboden, D.M (2002). Environmental Organic Chemistry, 2.ed., Wiley & Sons, Hoboken, 649 – 689; Diaz-de-Mera, Y; Arada, A.; Notario, A.; Rodriguez, D.; Rodriguez, Bravo, I. (2015). Photolysis study of fluorinated ketones under natural sunlight conditions. *Phys. Chem.***, 17,** 22991 – 22998.

[179] Huthmacher, K.; Most, D. (2002). Cyanuric Acid and Cyanuric Chloride in: *Ullmann's Encyclopedia of Industrial Chemistry, Wiley-VCH:Weinheim*.

[180] Kaufman, D. D.; Kearney, P. C.; Sheet, T. J. (1963). Simazine: Degradation by Soil Microorganism. *Science*, **142**, 405 – 406.

[181] Konstantinou, I. K and Albanis, T. A. (2002). Potocatalytic transformation of pesticides in aqueous titanium dioxide suspensions using artificial and solar light: intermediates and degradation pathways. *Applied Catalysis B:Environment*, **1310**, 1 – 17.

[182] Reynaldo, D. B.; Phillip, V. B. and Chris, C., (2000). Photocatalytic destruction of ethyl T-butyl ether(ETBE)and T-amyl methyl ether (TAME). *Chemistry section., Purdue university North Central, 1401S. US 42 1, Westville, IN 46391*,

[183] Banoub, J.; Gentil, E.; Kiceniuk, J. (1995). Analysis of Organophosphorus Pesticide Residues by Low Energy Tandem Mass Spectrometry Using Electrospray Ionization. *Int. J. Environ. Anal. Chem.*, **61**, 143 – 167.

[184] Meyer, A. (2010). Pathway dependent isotope fractionation in triazine degradation. *Thesis for Technische Universität München*, 1 – 127.

[185] Balci, B. Oturan, N.; Cherrier R., Oturan, M. A. (2009). Degradation of atrazine in aqueous medium by electrocatalytically generated hydroxyl radicals. A kinetic and mechanistic study.*Water Research*, **43**, 1924 – 1934.

[186] Fodjo, E. K.; Riaz S.; Li D.; Qu L.; Marius N. P; Albert T. and Long Y. (2012). Cu@Ag/β-$AgVO_3$ as a SERS substrate for the trace level detection of carbamate pesticides. *Anal. Methods*, **4**, 3785 – 3791.

[187] Jakubowska, J. (2007). Effect of irrigation water type on soil organic matter (SOM) fractions and their interactions with hydrophobic compounds. *PhD Dissertation*, *Centre for Environmental Research-UFZ*, 1 – 125.

[188] Izquierdo-Lorenzo, I.; Sanchez-Cortes, S. and Garcia-Ramos, J. V. (2010). Adsorption of Beta-Adrenergic Agonists Used in Sport Doping on Metal Nanoparticles: A Detection Study Based on Surface-Enhanced Raman Scattering. *American Chem. Society, Langmuir*, 26, 14663 – 14670.

[189] Schrader, B. (ed.) (1995). Infrared and Raman Spectroscopy: Methods and Applications. VCH Verlgasgesellschaft, Weinheim ; Myers Kelley, A. (2010). Hyper-Raman Scattering by Molecular Vibrations. Annual Review of Physical Chemistry. **61**, 41 – 61.

[190] Ahlrichs, R.; Weigend, F. (2011). Quantum Chemical Traeatments of Metal Clusters 2. *Phil. Trans. R. Soc. A*, **368**, 1245 – 1263; Schäfer, A.; Klamt, A.; Sattel, D.; Lohrenz, J. C. W.; Eckert, F. (2000). COSMO Implementation in Turbomole: Extension of an efficient quantum chemical code toward liquid systems. *Phys. Chem. Chem. Phys.*, **2**, 2187 – 2193.

[191] Ahlrichs, R., Bär M, Häser M., Horn H., Kölmel C. (1989). Electronic Structure Calculations on Workstation Computers: the Program System turbomole. *Chem.Phys. Lett.*, **162**, 163 – 169; Furche, F. and Rappoport, D. (2005). Density functional methods for excited states: equilibrium structure and electronic spectra. Chapter III of Computational Photochemistry, ed. by M. Olivucci, Theoretical and Computational Chemistry, *Elsevier, Amsterdam*, **16**, 93 – 128; Rappoport, D. and Furche, F. (2005). Analytical time-dependent density functional derivative methods within the RI-*J* approximation, an approach to excited states of large molecules. *J. Chem. Phys*., **122**, 1 – 9; Furche, F. and Ahlrichs, R. (2004). Erratum: Time-dependent density functional methods for excited state properties. J. Chem. Phys., **121**, 12772 – 12773.

[192] Reimers, Jef. R.; Zheng-Li, C.; Ante, Bi. and Noel, S. H. (2003). The Appropriateness of Density-Functional Theory for the Calculation of Molecular Electronics Properties. *Ann. N.Y. Acad. Sci.1006*, 235 – 251.

[193] Tian, W.; Datta, S.; Hong, S. et al. (1998). Conductance spectra of molecular wires. *J.Chem. Phys.,* **109**, 2874 – 2882.

[194] Samanta, M. P.; Tian, W.; Datta S.; Henderson J. I. and Kubiak C. P. (1996). Electronic conduction through organic molecule. *Phys. Rev. B,* **53**, R7626 – 7629.

[195] Gough, K. M. and Murphy, W. F. (1986). Intensity parameters for the Raman trace scattering of ethane. *J. Chem. Phys*., **85**, 4000 – 4290.

[196] Gough, K. M.; Lupinetti, C. and Dawes, R. (2004). Computation and interpretation of Raman scattering intensities. *J. of computational Methods in sciences and engineering*, IOS Press, **4**, 597 – 609; Rappoport, D. and Furche, F. Photoinduced Intramolecular Charge Transfer in 4-(Dimethyl)aminobenzonitrile − A Theoretical Perspective. *J. Am. Chem. Soc.,* **126**, 1277 – 1284; Rappoport, D. and Furche, F. (2007). Lagrangian approach to molecular vibrational Raman intensities using time-dependent hybrid density functional theory. *J. Chem. Phys.*, **126**, 201104 (1 – 6).

[197] Pacheca, A. B. (2011). Electronic structure calculation in quantum chemistry. *LSU Center for computation and technology*, 1 – 51; Long, W.; Weile, J.; Xuebin, Ch; Yue, W.; Weiguo, G.; Lin-Wang, W. (2011). Large scale plane wave pseudopotential density functional theory calculations on GPU clusters. *SC11, Washington- USA, J. Phys. Scien. Eng*., 12 – 18.

[198] Kohn, W.; Sham, L. J. (1965). Self-Consistent Equations Including Exchange and Correlation Effects. *Physical Review*, **140** (4 A), A1133 – A1138.

[199] Sanlaville, Y.; Guittonneau, S.; Mansour, M.; Feicht, E. A.; Meallier, P. and Kettrup, A. (1996). Photosensitized degradation of terbuthylazine in water. *Elsevier science, Chemosphere*, **33**, 353 – 362.

[200] Diels, O.; Alder, K. (1928). Synthesen in der hydroaromatischen Reihe. *Justus Liebig's Annalen der Chemie***, 460**, 98 – 122.

[201] Ochterski, J. W. (1999). Vibrational Analysis in Gaussian. Technical Support Information, Gaussian Inc., 1 – 10.

[202] Jean C. S.; Costa, J. C. S.; Ando, A. R.; Camargo, P. H. C. and Corio, P. (2011). Understanding the Effect of Adsorption Geometry over Substrate Selectivity in the Surface-Enhanced Raman Scattering Spectra of Simazine and Atrazine. *J. Phys. Chem. C.,* 4184 – 4190; Nguyen, T. T (1986). Infrared spectroscopic study of the formamide-Na-Montmorillonite complex. Conversion of s-triazine to formamide. *Clay and Minerals*, **34**, 521 – 528.

[203] Sundaraganesan, N.; Joshua, B. D.; Megenathan, C. and Sebatian, S. (2008). Vibration spectroscopic studies supported by HF/DFT calculations of 2, 4, 6- triminopyrimidine. *Indian Journal of Chemistry,* **47A**, 821 – 829; Wojciechowski, P. M.; Zierkiewicz, W. and Michalskaa, D. (2003). Electronic structures, vibrational spectra, and revised assignment of aniline and its radical cation: Theoretical study. *J. of chemical physics*, **118,** 10900 – 10911.

[204] Bower, D. I.; Maddams, W. F. (1989). The vibration spectroscopy of polymers. *Cambridge solid state science serie*, 1 – 337.

[205] Fenner, K.; Canonica , S.; Wackett , L.; Elsner, M. (2013). Evaluating Pesticide Degradation in the Environment: Blind Spots and Emerging Opportunities. *Science,* **341**, 752–758; Bouya ,H.; M. Errami, M.; Chakir, A; Roth, E (2015). Kinetics of the heterogeneous photo oxidation of the pesticide bupirimate by OH-radicals and ozone under atmospheric conditions. *Chemosphere* **134**, 301–306.

[206] Bell, R. J.; Dean, P. and Hibbins-butler, D. C. (1970). Localization of normal modes in vitreous silica Germania and beryllium fluoride. *J. Phy. C: Solid St. Phy.* **3,** 2111 – 2118.

[207] Chefetz, B.; Bilkisb, Y. I.; Polubesova, T. (2004). Sorption–desorption behavior of triazine and phenylurea herbicides in Kishon river sediments. *Water Research*, **38**, 4383 – 4394.

[208] Lim; E. C. (1979). Excited States. *Academic Press, Inc., New York 10003*, **4**, 17 – 40.

[209] Bauernschmitt, R.; Ahlrichs, R. (1996). Treatment of electronic excitations within the adiabatic approximation of time dependent density functional theory. *Chem. Phy. Lett.*, **256**, 454 – 464.

[210] Do, H. and Besley N. (2015). Calculation of the vibrational frequencies of carbon clusters and fullerenes with empirical potentials. *Phys. Chem. Phys.*, **17**, 3898 – 3908.

[211] Chaudhry, Q.; Schröder P.; Werck-Reichhart D.; Grajek W.; Marecik R. (2002) Prospects and Limitations of Phytoremediation for the Removal of Persistent Pesticides in the Environment. Environmental Science and Pollution Research, **9**(1), 4 – 17.

[212] Tu, C. M. (1976). Utilization and degradation of lindane by soil microorganisms. *Arch. Microbiol.*, **108**, 259 – 263.

[213] Quintero, J. C.; Moreira, M. T.; Feijoo, G.; Lema, J. M. (2005). Anaerobic degradation of hexachlorocyclohexane isomers in liquid and soil slurry systems. *Chemosphere*, **61**, 528 – 536.

[214] Nienow, A. M.; Bezares-Cruz, J. C.; Poyer, I. C.; Hua, I.; Jafvert, C. T. (2008). Hydrogen peroxide-assisted UV photodegradation of lindane. *Chemosphere*, **72**, 1700 – 1705.

[215] Handy, R. D.; Kammer, F. V. D.; Lead, J. R.; Hassellöv, M.; Owen, R. and Crane, M. (2008). The Ecotoxicology and Chemistry of Manufactured Nanoparticles. *Ecotoxicology*, **17**, 287 – 314; Gregory R. Siragusa and James S. Dickson (1993). Inhibition of Listeria Monocytogenes, Salmonella Typhimuriumand and Escherichia Coli 0157:H7 on Beef Muscle Tissue by Lactif or Acetic Acid Contained in Calcium Alginate Gels: Journal of Food Safety, **13**, 147–158.

[216] Williams, T. L.; Martin, R. B.; Colette, T. W. (2013). Determination of Perchlorate Contamination in some fertilizers by Raman Stectroscopy. *IET Sci. Meas. Technol.*, 1 – 7; Thibeau, R. J.; Van Haverbeke, R. J.; Brown, C. W. (1978). Detection of Water Pollutants by Laser Excited Resonance Raman Spectroscopy; *Pesticides and Fungicides, Appl. Spec.*, **32**,

98 – 100; Mesnage, R.; Bernay, B. and Seralini, G. E. (2013). Ethoxylated adjuvants of glyphosate-based herbicides are active principles of human celltoxicity. *Toxicology*, **313**, 122 – 128.

[217] LeBaron, H. M; McFarland, J. E.; and Burnside, O. B. (2008). The triazine herbicides 50 years revolutionizing agriculture: Chapter 23, Nonbiological degradation of triazine herbicides:photolysis and hydrolysis. *Elsevier BV. All rights reserved*, 329 – 354.

[218] Pelizzetti, E. (1990). Photocatalytic degradation of atrazine and other s-triazine herbicides. *Environ. Sci. Technol,* **24**, 1559 – 1565.

[219] Maier, M. E. (2015). esign and synthesis of analogues of natural products. *Org. Biomol. Chem*, **13**, 5302 – 5343; Fagnoni, M.; Dondi, D.; Ravelli, D. and Albini, A. (2007). Photocalysis for the formation of the C-C bonds. *Chem. Rev.,* **107**, 2725 – 2756.

[220] Buczek, A.; Kupka, T.; Broda, M. A. (2011). Estimation of formamide harmonic and anharmonic modes in the Kohn-Sham limit using the polarization consistent.*J. Mol Model*, **17**, 2265 – 2274.

[221] Burbano, A. A.; Dionysiou, D.D.; Richardson, T. L. and Suidan, M. T. (2002) Degradation of MTBE Intermediates using Fenton's Reagent.*J. of environmental engineering*, 799 – 805; Subramanian, B.; Yang, Q.; Yang, Qi.; Khodadoust, A. P.; Zhou, S. and Ray, A. K. (2003). Kinetic studies for photocatalytic degradation of Eosin B on a Thin film of Titanium Dioxide. *Ind. Eng. Chem. Res.*, **42**, 6020 – 6033; Dionysiou, D. D. (2007). Photodegradation of pentachlorophenol in room temperature ionic liquids. *J. of photochemistry and photobiology A: Chemistry*, **192**, 114 – 121.

[222] Tomoaki, N.; Naoto, O.; Hideo, O.; Hirofum, H. (2004). Degradation of the antifouling compound Irgarol 1051 by manganese peroxidase from the white rot fungus Phanerochaetechrysosporium.*Chemosphere*, **55**, No. 3, 487 – 491; Pape, B. E.; Zabik, M. J. (1970). Photochemistry of bioactive compounds. Photochiestry of selected 2-chloro and 2-methylthio-4',6'-.di(alkylamino)-s-triazine herbicides. *J. Agric. Food Chem*., **18**, 202 – 207.

[229] Berkemeier, T; Huisman, A. J.; Ammann, M.; Shiraiwa, M.; Koop, T and Poeschl, U. (2013). Kinetic regimes and limiting cases of gas uptake and heterogeneous reactions in atmospheric aerosols and clouds: a general classification scheme. *Atmos. Chem. Phys.*, **13**, 6663 – 6686; Gross, S. and Bertram, A. K. (2009). Products and kinetics of the reactions of an alkane monolayer and a terminal alkene monolayer with NO_3 radicals. *J. of geophysical research: Atmopheres*, **114**, Iss. D2, D02307 (1 – 14).

[223] Pelizzetti, E.; Minero, C.; Carlin, V.; Vincent, M; Pramauro, E. (1992). Identification of photocatalytic degradation parthway of 2-Cl-sTriazine Herbicides.*Chemosphere*, **24**, Iss. 7, 891 – 910.

[224] Carlsen, S. C. K.; Spliid, N. H.; Svensmark, B. (2006). Drift of 10 herbicides after tractor spray application.1. Secondary drift (evaporation).*Chemosphere*, **64,** No. 5, 787 – 794; Tarr, M. A. (2003). Chemical degradation Methods for wastes and pollutants, environmental and industrial applications. Book of Marcel Dekker, all Rights Reserved, Switzerland, 70 – 479; Maldonado, M. I.; Malato, S.; Prez-Estada, L. A; Gernjak, W.; Oller, I.; Domenech, X. Peral, J. (2006). Partial degradation of five pesticides and an industrial pollutant by ozonation in pilot-plant scale reactor. *J. of Hazardous Materials,* **B138**, 363 – 369.

[225] Stefan, M.I.;Mack, J. andBolton, J. R.,(2000). Degradation Pathways during the Treatment of Methyl tert-Butyl Ether by the UV/H_2O_2 Process.*Environ. Sci. Technol.*, **34**, No. 4, 650 – 658.

[226] Cavalier, T. C.; Lavy, T. L.; Mattice, J. D. (1991). Persistence of Selected Pesticides in Ground-Water Samples**.***Ground water*, **29**, Iss. 2, 225 – 231.

[227] Lazar, M. A.; Varghese, S. and Santhosh, S. N. (2012). Photocatalytic water treatment by titanium dioxide: recent updates. *Catalysts,* **2**, 572 – 601; Khataee, A. R.; Kasiri, M. B.; Alidokht, L. (2011). Application of response surface methodology in the optimization of photocatalytic removal of environmental pollutants using nanocatalysts.*Environmental technology*, **32**, Iss. 15, 1669 – 1684.

[228] Heard, D. (2005). Free-Radicals in the troposphere. Their Measurement, Interpretation of Fiel-Data and Future Directions. *Transport and transformation of pollutantants (T and TP)*,

1 – 120; Lelieveld, J.; Dentener, F. J.; Peters, W. and Krol, M. C (2004).On the role of hydroxyl radicals in the self-cleansing capacity of the troposphere. *Atmos. Chem.. Phys.*, **4**, 2337 – 2344.

[230] France, J. L.; Reay, H. J.; King, M. D.; Voisin, D.; Jacobi, H. W.; Domine, F.; Beine, H; Anastasio, C.; MacArthur, A and Lee-Taylor, J. (2012). Hydroxyl radical and NOx production rates, black carbon concentrations and light-absorbing impurities in snow from field measurements of light penetration and nadir reflectivity of onshore and offshore coastal Alaskan snow. *J. of Geophys. Res.*, **117**, D00R12 (1 – 21); Michoud, V.; Colomb, A.; Borbon, A.; Miet, K.; Beekmann, M.; Camredon, M.; Aumont, B.; Perrier, S.; Zapf, P.; Siour, G.; Ait-Helal, W.; Afif, C.; Kukui, A.; Furger, M.; Dupont, J. C.; Haeffelin, M. and Doussin, J. F. (2014). Study of the unknown HONO daytime source at a European suburban site during the Megapoli summer and winter field campaigns.*Atmos. Chem. Phys.,* **14**, 2805 – 2822.

[231] Marionlack, L. and Reinhard, N. (2002).Photocatalytic Atrazine Degradation by Synthetic Minerals, Atmospheric Aerosols, and Soil Particles. *Environ. Sci. Technol*., **36**, 5342 – 5347.

[232] Chan, G. Y. S.; Hudson, M. J.; Isaacs, N. S. (1992). Degradation of atrazine by hydrolysis and by hydroxyl radicals. *J. Phys. Org. Chem*., **5**, Iss. 9, 600 – 608.

[233] Nick, K.; Schöler, H. F.; Mark, G.; Söylemez, T.; Akhlaq, M. S.; Schuchmann, H.-P.; von Sonntag, C. (1992). Degradation of some triazine herbicides by UV radiation such as used in the UV disinfection of drinking water.*J. Water Supply Res. Tech. – Aqua*, **41**, No. 2, 82 – 87.

[234] Alzoubi, M.; Than, A. M.; Stojcevski, A. (2014). The influence of instruments uncertainty on the forest fire danger indices (FFDI).*Intern.J. of Adv. Res.In Elec., Electronic and instrumentation engineering*, **3**, 2320 – 3765; Monsalve, F.; Tomás, C.; Fraile, R. (2013). Influence of Meteorological parameters and air pollutants onto the morbidity due to respiratory diseases in Castilla-La Mancha, Spain. *Aerosol and Air Quality Research*, **13**, 1297 – 1312.

[235] Lam, S.; Sin, J.; Abdullay, A. and Mohamed, A. R. (2012). Degradation of wasterwater containing organic dyes photocatalysed by zinc oxide: a review. *Desalination and water treatment*. **41**, Iss. 1 – 3, 131 – 169; Thullner, M.; Centler, F.; Richnow, H.; Fischer, A. (2012). Quantification of organic pollutant degradation in contaminated aquifers using compound specific stable isotope analysis-Review of recent developments.*Organic geochemistry*, **42**, 1440 – 1460.

[236] Evgenidou, E. and Fytianos, K. (2002).Photodegradation of triazine herbicides in aqueous solutions and natural waters. *J. Agric. Food Chem.*, **50**, 6423 – 6427; Dbira, S.; Bedoui, A.; Bensalah, N. (2014) Investigations on the degradation of triazine herbicides in water by photo-feton process. *Ame. J. of Ana.Chem.*, **5**, 500 – 517.

[237] Ravelli, D.; Dondi, D.; Fagnoni, M. and Albini A. (2009). Photocatalysis.A multi-faceted concept for green chemistry.*Chem. Soc. Res.*, **38**, 1999 – 2011;Ma C.; Hong, G.; Chen, H.; Hang, N. and Shen, Y. (2011). Photooxidation contribution study on the decomposition of Azo Dyes in Aqueous solutions by VUV-Bases AOPs.*International J. of photoenergy*, **2011**, 4 – 8.

[238] Priya, S. P. D. (2006). Semiconductor oxides mediated photocatalytic removal of chemical and bacterial pollutants from wastewater. *Thesis of school of environmental studies cochin university of science and technology, India*, 40 – 152; Mamián M.; Torres W.; Larmat F. E. (2009). Electrochemical degradation of atrazine in aqueous solution at a platinum electrode. *Portugaliae electrochimicaActa*, **27**, No. 3, 371 – 379.

[239] Li-hong, Z.; Pei-jun, L.; Zong-qing, G.; Oni, A. A. (2006). Photochemical behavior of benzo[a]pyrene on soil surfaces under Uv light irradiation. *J. of environmental Sciences*, **18**, No. 6, 1226 – 1232; Derbalah, A. S. H.; Wakatsuki, H.; Yamazaki, T. and Sakugawa, H. (2004). Photodegradation kinetics of fenitrothion in various aqueous media and its effect on steroid hormones biosynthesis. *Geochem. J.,* **38**, 201 – 213.

APPENDIX A

(Supporting Information of Chapter 2- Introduction)

Table A0.1 below presents statistics of the reduction of some POPs over the years, and especially according to the convention Stockholm concerning the effect of several POPs in the atmosphere.

Table A0.1: Summary of POP emissions in the atmosphere between 1990 and 2012

	Pollutant				
Years	**Benzo (b,j,k) fluaranthen (kg)**	**HCH (kg)**	**PCB (kg)**	**Dioxine (kg)**	**HCB (kg)**
1990	**2004**	**60.2**	**1672.1**	**0.7474**	**5.3**
1991	**1413**	**63.7**	**1696.5**	**0.6224**	**5.2**
1992	**968**	**36.9**	**1678.1**	**0.493**	**5.1**
1993	**505**	**23.5**	**1670.6**	**0.3639**	**5.1**
1994	**194**	**18.5**	**1670.6**	**0.2438**	**4.8**
1995	**187**	**13.1**	**1536.6**	**0.2295**	**4.5**
1996	**172**	**18.5**	**1304.2**	**0.2063**	**4.4**
1997	**164**	**14.5**	**1345.1**	**0.197**	**4.6**
1998	**150**	**0**	**1280**	**0.1842**	**4.6**
1999	**123**	**0**	**1165**	**0.1656**	**4.6**
2000	**122**	**0**	**1071.5**	**0.1517**	**4.5**
2001	**98**	**0**	**883.8**	**0.1313**	**4.2**
2002	**92**	**0**	**711.8**	**0.1099**	**3.8**
2003	**89**	**0**	**544.6**	**0.0925**	**3.4**
2004	**87**	**0**	**187.9**	**0.0692**	**3**
2005	**85**	**0**	**194**	**0.0689**	**3**

2006	**86**	**0**	**210**	**0.0708**	**3.1**
2007	**87**	**0**	**211.4**	**0.0709**	**3.1**
2008	**85**	**0**	**219.4**	**0.0718**	**3.2**
2009	**76**	**0**	**198**	**0.062**	**3.3**
2010	**65**	**0**	**233**	**0.0701**	**3.7**
2011	**84**	**0**	**233.6**	**0.0642**	**3.5**
2012	**84**	**0**	**236.1**	**0.0666**	**3.6**

Section appendix A3: the output log file

(Supporting Information of Chapter 3- Theoretical Model for calculations)

```
          NORMAL MODES and VIBRATIONAL FREQUENCIES (cm**(-1))
          ---------------------------------------------------

 imaginary wave numbers indicate a negative curvature of the energy
surface.
 zero frequency modes have no physical meaning except being generators of
 translations and rotations. each vibrational normal mode - given in terms
of
 cartesian displacement vectors of all atoms - has been normalized to
unity.
 to obtain mass-weigthed normal coordinates in a.u. divide the tabulated
 modes by sqrt(reduced mass * 1822.88853).
 band intensities or cross sections refer to independent non-degenerate
normal
 modes, that is, the intensities of degenerate modes have yet to be added.
 dDIP/dQ is the normal mode derivative of the dipole moment.
 differential RAMAN cross sections refer to a scattering angle of 90 deg
 and to a negative frequency shift (stokes lines). (par,par) indicates that
 the scattered wave has its electric field polarized in parallel (   ,par)
 to the scattering plane and that the incident radiation also is polarized
 parallel (par,   ) to the scattering plane. (ort,   ) indicates
polarization
 orthogonal to the scattering plane while (unpol,   ) refers to cross
 sections with respect to unpolarized radiation. RAMAN cross sections of
 the types (par,ort), (ort,par) or (par,unpol) are all equal to (par,par).
 all cross sections are given in % relative to the most active single mode
 of the same polarization type.
 RAMAN cross sections depend on the sample temperature (here T= 298.15K)
 and on the wave number of the exciting radiation (here 18796.99cm**(-1)).
 complementary information is output to the control file (cf. $raman
spectrum).
```

WARNING: values of Raman intensities are questionable for saddle point structures

mode		1	2	3	4	5	6
frequency		i59.96	i44.32	0.00	0.00	0.00	0.00
symmetry		a	a				
IR		YES	YES	-	-	-	-
|dDIP/dQ| (a.u.)		0.0000	0.0000	0.0000	0.0000	0.0000	0.0000
intensity (km/mol)		0.00	0.00	0.00	0.00	0.00	0.00
intensity (%)		0.00	0.00	0.00	0.00	0.00	0.00
RAMAN		YES	YES	-	-	-	-
(par,par)		0.00	0.00	0.00	0.00	0.00	0.00
(ort,ort)		0.00	0.00	0.00	0.00	0.00	0.00
(ort,unpol)		0.00	0.00	0.00	0.00	0.00	0.00
depol. ratio		0.00	0.00	0.00	0.00	0.00	0.00
1	cl	x	0.00000	0.00000	-0.04811	0.04899	0.19916	0.08405
		y	0.00000	0.00000	0.02167	0.01303	0.01034	0.09753
		z	0.02898	0.08096	0.13876	0.32412	-0.02892	-0.00303
2	c	x	0.00000	0.00000	-0.00495	0.00978	0.13768	0.09388
		y	0.00000	0.00000	0.02451	0.01045	0.00629	0.09817
		z	0.01279	0.03699	0.11174	0.19826	-0.00300	-0.01844
3	n	x	0.00000	0.00000	0.00710	-0.00117	0.12051	0.09663
		y	0.00000	0.00000	0.05472	-0.01699	-0.03674	0.10506
		z	0.01288	0.01460	0.13312	0.12466	0.03250	-0.05042
4	c	x	0.00000	0.00000	0.04047	-0.03149	0.07296	0.10423
		y	0.00000	0.00000	0.05581	-0.01798	-0.03830	0.10530
		z	-0.00641	-0.04735	0.11115	0.02878	0.05148	-0.06130
5	n	x	0.00000	0.00000	0.05651	-0.04606	0.05012	0.10788
		y	0.00000	0.00000	0.08516	-0.04464	-0.08010	0.11199
		z	-0.00702	-0.13170	0.12892	-0.05498	0.08829	-0.09365
6	c	x	0.00000	0.00000	0.04615	-0.03665	0.06488	0.10552
		y	0.00000	0.00000	0.12004	-0.07633	-0.12979	0.11994
		z	0.00416	-0.02725	0.17038	-0.07130	0.11624	-0.12341
7	c	x	0.00000	0.00000	0.00871	-0.00264	0.11821	0.09699
		y	0.00000	0.00000	0.12492	-0.08076	-0.13674	0.12105
		z	0.00582	-0.20989	0.20103	0.02825	0.10081	-0.11695

8	h	x	0.00342	0.03274	0.01851	-0.02062	0.15593	0.07373
		y	0.00025	-0.11623	0.12895	-0.00877	-0.13272	0.12498
		z	0.00412	-0.29056	0.19823	0.07592	0.08387	-0.10306
9	h	x	0.00000	0.00000	0.00377	0.00186	0.12526	0.09587
		y	0.00000	0.00000	0.15178	-0.10517	-0.17500	0.12717
		z	0.00974	-0.20101	0.23085	0.00712	0.12396	-0.14076
10	h	x	-0.00342	-0.03273	-0.02453	0.03664	0.11388	0.11491
		y	-0.00025	0.11623	0.09873	-0.13262	-0.10920	0.11206
		z	0.00412	-0.29056	0.19823	0.07592	0.08387	-0.10306
11	c	x	-0.00802	-0.11221	0.03044	-0.00948	0.01388	0.13814
		y	-0.00105	0.15630	0.11462	-0.17884	-0.13595	0.11442
		z	0.00776	0.10599	0.17590	-0.13427	0.13963	-0.14289
12	h	x	-0.01431	-0.20395	-0.00208	0.02941	0.00698	0.15699
		y	-0.00221	0.26030	0.08770	-0.23229	-0.10766	0.10518
		z	0.00511	0.01211	0.17188	-0.09012	0.12315	-0.12914
13	h	x	-0.00824	-0.11632	0.02446	-0.00381	0.02102	0.13746
		y	-0.00066	0.17038	0.14097	-0.20480	-0.17375	0.12034
		z	0.01531	0.18616	0.20594	-0.15398	0.16243	-0.16646
14	h	x	-0.00801	-0.10575	0.05693	-0.03327	-0.02547	0.14497
		y	-0.00107	0.15884	0.11115	-0.17804	-0.13131	0.11353
		z	0.00576	0.22490	0.15419	-0.20722	0.15134	-0.14808
15	c	x	0.00802	0.11221	0.09154	-0.09078	0.07359	0.07967
		y	0.00105	-0.15630	0.15754	-0.00298	-0.16935	0.13276
		z	0.00776	0.10600	0.17590	-0.13428	0.13963	-0.14289
16	h	x	0.00801	0.10574	0.11937	-0.11635	0.03555	0.08521
		y	0.00107	-0.15883	0.15501	0.00167	-0.16544	0.13228
		z	0.00576	0.22491	0.15419	-0.20722	0.15134	-0.14808
17	h	x	0.00824	0.11631	0.08671	-0.08664	0.08186	0.07788
		y	0.00066	-0.17039	0.18470	-0.02563	-0.20777	0.13903
		z	0.01531	0.18616	0.20594	-0.15398	0.16243	-0.16646
18	h	x	0.01431	0.20395	0.10335	-0.11086	0.11000	0.05610
		y	0.00221	-0.26030	0.16175	0.07112	-0.16527	0.13683
		z	0.00511	0.01211	0.17188	-0.09012	0.12315	-0.12914
19	n	x	0.00000	0.00000	0.01102	-0.00473	0.11493	0.09752
		y	0.00000	0.00000	-0.00384	0.03622	0.04669	0.09171
		z	-0.00641	0.02525	0.07283	0.19017	-0.02166	0.00353
20	c	x	0.00000	0.00000	0.04426	-0.03493	0.06757	0.10509
		y	0.00000	0.00000	0.00008	0.03265	0.04110	0.09261
		z	-0.02791	-0.01565	0.05373	0.09097	-0.00003	-0.00998
21	n	x	0.00000	0.00000	0.06276	-0.05174	0.04122	0.10931
		y	0.00000	0.00000	-0.02767	0.05786	0.08063	0.08629
		z	-0.04561	-0.01606	0.01367	0.07493	-0.01675	0.01067

22	c	x	0.00000	0.00000	0.04941	-0.03961	0.06023	0.10626
		y	0.00000	0.00000	-0.06089	0.08805	0.12796	0.07872
		z	-0.18758	0.02368	-0.00978	0.15616	-0.05585	0.04587
23	h	x	0.04647	0.00952	0.01183	0.00357	0.06229	0.12310
		y	0.26412	-0.03751	-0.07929	0.02939	0.14443	0.07152
		z	-0.38127	0.05310	-0.00191	0.20621	-0.06773	0.05378
24	h	x	-0.04648	-0.00952	0.05470	-0.05346	0.10418	0.08207
		y	-0.26413	0.03751	-0.04917	0.15277	0.12100	0.08439
		z	-0.38127	0.05310	-0.00191	0.20621	-0.06773	0.05378
25	c	x	0.00000	0.00000	0.07702	-0.06469	0.02091	0.11255
		y	0.00000	0.00000	-0.08629	0.11112	0.16414	0.07293
		z	0.19100	-0.01249	-0.05381	0.11127	-0.06541	0.06161
26	h	x	-0.04374	-0.00849	0.11461	-0.10802	0.01962	0.09534
		y	-0.27183	0.03759	-0.06856	0.17152	0.14876	0.08002
		z	0.37907	-0.04024	-0.06234	0.06328	-0.05456	0.05464
27	h	x	0.00000	0.00000	0.06664	-0.05526	0.03569	0.11019
		y	0.00000	0.00000	-0.11149	0.13401	0.20004	0.06719
		z	0.10244	0.01524	-0.07143	0.17360	-0.09520	0.08839
28	h	x	0.04374	0.00849	0.07108	-0.05012	-0.02291	0.13698
		y	0.27183	-0.03759	-0.09913	0.04627	0.17255	0.06696
		z	0.37907	-0.04024	-0.06234	0.06328	-0.05456	0.05464
29	n	x	0.00000	0.00000	0.06018	-0.04940	0.04489	0.10872
		y	0.00000	0.00000	0.02906	0.00633	-0.00018	0.09921
		z	-0.03030	-0.05608	0.07122	0.00801	0.03636	-0.04194
30	h	x	0.00000	0.00000	0.08145	-0.06872	0.01459	0.11356
		y	0.00000	0.00000	0.08181	-0.04160	-0.07533	0.11123
		z	-0.02121	-0.15121	0.10840	-0.12118	0.09848	-0.09786
31	h	x	0.00000	0.00000	0.08760	-0.07431	0.00583	0.11496
		y	0.00000	0.00000	-0.02413	0.05464	0.07558	0.08709
		z	-0.19235	-0.04686	0.00000	0.00000	0.00000	0.00000

reduced mass(g/mol)	1.882	3.120	5.600	8.005	6.050	6.189

mode	7	8	9	10	11	12
frequency	0.00	0.00	33.11	80.01	90.14	121.94
symmetry			a	a	a	a
IR	-	-	YES	YES	YES	YES
|dDIP/dQ| (a.u.)	0.0000	0.0000	0.0010	0.0011	0.0007	0.0005

intensity (km/mol)			0.00	0.00	1.63	2.08	0.86	0.48
intensity (%)			0.00	0.00	0.13	0.17	0.07	0.04
RAMAN			-	-	YES	YES	YES	YES
(par,par)			0.00	0.00	100.00	21.93	15.57	19.52
(ort,ort)			0.00	0.00	100.00	21.93	18.35	19.86
(ort,unpol)			0.00	0.00	100.00	21.93	17.16	19.72
depol. ratio			0.00	0.00	0.75	0.75	0.64	0.74
1	cl	x	0.02859	0.00425	0.00000	0.00000	-0.00730	0.29254
		y	-0.13710	-0.02038	0.00000	0.00000	0.09319	0.00022
		z	0.06497	-0.08834	0.02742	-0.03530	0.00000	0.00000
2	c	x	0.06106	0.00907	0.00000	0.00000	-0.00734	0.04743
		y	-0.13497	-0.02006	0.00000	0.00000	0.09040	-0.01547
		z	0.02028	0.00996	0.04721	0.03267	0.00000	0.00000
3	n	x	0.07012	0.01042	0.00000	0.00000	-0.00136	0.00408
		y	-0.11224	-0.01668	0.00000	0.00000	0.09174	-0.09573
		z	-0.00216	0.00562	0.09030	-0.06264	0.00000	0.00000
4	c	x	0.09523	0.01415	0.00000	0.00000	-0.00749	-0.05926
		y	-0.11142	-0.01656	0.00000	0.00000	0.08997	-0.08927
		z	-0.03634	0.08282	0.11151	-0.01208	0.00000	0.00000
5	n	x	0.10730	0.01595	0.00000	0.00000	-0.03391	-0.05574
		y	-0.08934	-0.01328	0.00000	0.00000	0.04122	-0.07293
		z	-0.06253	0.08877	0.16549	-0.15732	0.00000	0.00001
6	c	x	0.09951	0.01479	0.00000	0.00000	-0.00771	-0.09151
		y	-0.06310	-0.00938	0.00000	0.00000	-0.06888	0.06182
		z	-0.06384	0.02674	-0.02556	-0.04882	0.00000	0.00000
7	c	x	0.07134	0.01060	0.00000	0.00000	0.08820	-0.20089
		y	-0.05943	-0.00883	0.00000	0.00000	-0.08407	0.08114
		z	-0.02756	-0.06645	-0.16945	0.01221	0.00001	0.00000
8	h	x	0.05511	-0.01436	-0.08499	0.04037	0.11307	-0.22502
		y	-0.04559	-0.06147	-0.07210	0.02886	-0.05957	0.05684
		z	-0.01193	-0.08201	-0.16526	0.00728	-0.00058	0.00163
9	h	x	0.06762	0.01005	0.00000	0.00000	0.09848	-0.21045
		y	-0.03922	-0.00583	0.00000	0.00000	-0.14273	0.13869
		z	-0.03163	-0.10709	-0.29232	0.07053	0.00001	-0.00001
10	h	x	0.06993	0.03294	0.08500	-0.04037	0.11307	-0.22501
		y	-0.08994	0.04132	0.07209	-0.02885	-0.05958	0.05684
		z	-0.01193	-0.08201	-0.16526	0.00728	0.00059	-0.00163
11	c	x	0.12119	0.05003	0.14303	-0.08839	-0.05628	-0.03815
		y	-0.08251	0.06539	0.10135	-0.04245	-0.12540	0.13716
		z	-0.08430	0.04426	-0.05199	-0.02265	-0.00109	0.00562

12	h	x	0.12103	0.07322	0.25189	-0.16190	-0.02193	-0.09247
		y	-0.11390	0.11706	0.18021	-0.08256	-0.09123	0.09534
		z	-0.06996	0.03222	-0.03354	-0.04106	0.00049	-0.00248
13	h	x	0.11732	0.05006	0.14681	-0.09196	-0.03769	-0.06265
		y	-0.06298	0.06976	0.09827	-0.03431	-0.21746	0.25731
		z	-0.08788	0.00266	-0.19946	0.07122	0.00014	0.01499
14	h	x	0.14185	0.05380	0.13998	-0.08036	-0.14951	0.08262
		y	-0.08546	0.06665	0.10449	-0.04479	-0.11522	0.12392
		z	-0.11081	0.11130	0.05473	-0.07545	-0.00609	0.01409
15	c	x	0.10015	-0.01713	-0.14302	0.08839	-0.05627	-0.03815
		y	-0.01954	-0.08056	-0.10136	0.04246	-0.12539	0.13716
		z	-0.08430	0.04426	-0.05199	-0.02265	0.00110	-0.00562
16	h	x	0.12036	-0.01483	-0.13999	0.08036	-0.14951	0.08262
		y	-0.02111	-0.08249	-0.10449	0.04479	-0.11521	0.12391
		z	-0.11081	0.11130	0.05473	-0.07545	0.00608	-0.01409
17	h	x	0.09589	-0.01837	-0.14680	0.09195	-0.03769	-0.06266
		y	0.00118	-0.07895	-0.09829	0.03432	-0.21745	0.25730
		z	-0.08788	0.00266	-0.19946	0.07121	-0.00014	-0.01500
18	h	x	0.08473	-0.04264	-0.25189	0.16190	-0.02192	-0.09248
		y	-0.00525	-0.13476	-0.18022	0.08256	-0.09122	0.09534
		z	-0.06997	0.03222	-0.03354	-0.04106	-0.00049	0.00248
19	n	x	0.07307	0.01086	0.00000	0.00000	-0.01368	-0.00061
		y	-0.15630	-0.02323	0.00000	0.00000	0.09206	0.05735
		z	0.01369	0.07811	0.01738	0.14985	0.00000	-0.00001
20	c	x	0.09808	0.01458	0.00000	0.00000	-0.01081	-0.06494
		y	-0.15335	-0.02279	0.00000	0.00000	0.09331	0.04488
		z	-0.02132	0.15193	0.04517	0.17614	0.00000	0.00000
21	n	x	0.11200	0.01665	0.00000	0.00000	0.02579	-0.06676
		y	-0.17423	-0.02589	0.00000	0.00000	0.03957	0.04580
		z	-0.03067	0.22537	0.00559	0.25239	0.00000	-0.00001
22	c	x	0.10196	0.01515	0.00000	0.00000	-0.03092	-0.10983
		y	-0.19922	-0.02961	0.00000	0.00000	-0.11513	-0.07096
		z	-0.00590	0.22992	-0.14393	-0.13653	0.00001	0.00000
23	h	x	0.09719	0.03691	-0.06646	-0.17440	-0.12044	-0.18324
		y	-0.22382	0.02122	0.06358	0.16167	-0.13702	-0.09028
		z	0.01159	0.19561	-0.20241	-0.28683	0.00334	0.00403
24	h	x	0.08243	-0.01021	0.06646	0.17439	-0.12044	-0.18324
		y	-0.17964	-0.08118	-0.06359	-0.16167	-0.13701	-0.09027
		z	0.01159	0.19561	-0.20241	-0.28683	-0.00332	-0.00402
25	c	x	0.12273	0.01824	0.00000	0.00000	0.13121	0.02424
		y	-0.21833	-0.03245	-0.00001	0.00000	-0.26901	-0.20181
		z	-0.02527	0.32220	-0.14346	-0.14276	0.00000	0.00000

26	h	x	0.12715	-0.00391	0.06911	0.19439	0.23556	0.11410
		y	-0.19407	-0.08415	-0.06448	-0.17352	-0.25271	-0.18780
		z	-0.04214	0.35674	-0.09002	0.00172	0.00000	0.00005
27	h	x	0.11492	0.01708	0.00000	0.00000	0.06478	-0.03266
		y	-0.23729	-0.03527	-0.00001	-0.00001	-0.43107	-0.34069
		z	-0.00623	0.32506	-0.25460	-0.45293	0.00001	0.00000
28	h	x	0.14213	0.04393	-0.06910	-0.19438	0.23556	0.11410
		y	-0.23892	0.01980	0.06447	0.17351	-0.25272	-0.18780
		z	-0.04214	0.35674	-0.09002	0.00172	0.00001	-0.00005
29	n	x	0.11006	0.01636	0.00000	0.00000	-0.01042	-0.09527
		y	-0.13155	-0.01955	0.00000	0.00000	0.10014	-0.02776
		z	-0.04726	0.15802	0.09891	0.12491	0.00000	0.00000
30	h	x	0.12607	0.01874	-0.00001	0.00000	-0.09970	0.00906
		y	-0.09186	-0.01365	0.00000	0.00000	0.04977	-0.08070
		z	-0.08666	0.15097	0.18233	-0.11356	-0.00001	0.00001
31	h	x	0.13069	0.01942	0.00000	0.00000	0.11430	-0.01580
		y	-0.17156	-0.02550	0.00000	0.00000	0.05158	0.05204
		z	-0.05704	0.27988	-0.01822	0.07510	0.00000	0.00000

reduced mass(g/mol)	6.655	4.853	3.324	3.781	3.780	6.403

mode	13	14	15	16	17	18
frequency	146.55	153.06	190.33	238.68	253.46	259.29
symmetry	a	a	a	a	a	a
IR	YES	YES	YES	YES	YES	YES
|dDIP/dQ| (a.u.)	0.0009	0.0008	0.0004	0.0000	0.0005	0.0005
intensity (km/mol)	1.33	1.12	0.29	0.00	0.43	0.40
intensity (%)	0.11	0.09	0.02	0.00	0.04	0.03
RAMAN	YES	YES	YES	YES	YES	YES
(par,par)	0.88	0.66	0.37	0.05	8.89	8.21
(ort,ort)	0.88	0.66	0.37	0.05	12.76	27.32
(ort,unpol)	0.88	0.66	0.37	0.05	11.10	19.13
depol. ratio	0.75	0.75	0.75	0.75	0.52	0.23

1	cl	x	0.00000	0.00000	0.00000	0.00000	0.07774	0.03044
		y	0.00000	0.00000	0.00000	0.00000	-0.01275	-0.02259
		z	0.22288	0.05408	-0.03406	0.00250	0.00000	0.00000

2	c	x	0.00000	0.00000	0.00000	0.00000	-0.04645	0.01141
		y	0.00000	0.00000	0.00000	0.00000	-0.01473	-0.01306
		z	-0.30317	-0.09251	0.05040	-0.00629	0.00000	0.00000
3	n	x	0.00000	0.00000	0.00000	0.00000	-0.03667	0.01691
		y	0.00000	0.00000	0.00000	0.00000	0.01080	0.01270
		z	-0.57429	0.26444	-0.09931	-0.01321	0.00000	0.00000
4	c	x	0.00000	0.00000	0.00000	0.00000	-0.01916	0.00858
		y	0.00000	0.00000	0.00000	0.00000	0.02320	0.01968
		z	-0.14129	0.16133	0.09952	-0.00439	0.00000	0.00000
5	n	x	0.00000	0.00000	0.00000	0.00000	0.01733	-0.03039
		y	0.00000	0.00000	0.00000	0.00000	0.09026	0.03024
		z	0.11825	-0.15371	-0.07483	0.01779	0.00000	0.00000
6	c	x	0.00000	0.00000	0.00000	0.00000	0.04541	-0.07995
		y	0.00000	0.00000	0.00000	0.00000	0.06471	0.03973
		z	0.03800	-0.05981	-0.03841	0.00501	0.00000	0.00000
7	c	x	0.00000	0.00000	0.00000	-0.00001	0.21449	-0.02114
		y	0.00000	0.00000	0.00000	0.00000	0.04794	0.03510
		z	0.02215	-0.02951	-0.02674	-0.01238	0.00000	0.00000
8	h	x	0.05877	-0.01120	0.01544	-0.20666	0.27588	0.00517
		y	-0.00900	0.01186	0.00221	0.01720	0.10233	0.05746
		z	-0.01002	-0.01909	-0.03285	0.10437	-0.00450	-0.00083
9	h	x	0.00000	0.00000	0.00000	-0.00001	0.23948	-0.00949
		y	0.00000	0.00000	0.00000	0.00001	-0.08702	-0.02395
		z	0.10003	-0.04524	-0.00296	-0.25637	-0.00001	-0.00001
10	h	x	-0.05877	0.01120	-0.01544	0.20663	0.27591	0.00519
		y	0.00900	-0.01186	-0.00221	-0.01721	0.10233	0.05746
		z	-0.01002	-0.01909	-0.03285	0.10437	0.00452	0.00084
11	c	x	0.03859	-0.07406	-0.04999	0.01142	-0.00732	-0.22157
		y	0.03486	-0.03797	-0.01614	0.00996	0.01654	0.02045
		z	0.03575	-0.04049	-0.02122	0.00479	0.00514	0.05526
12	h	x	0.10088	-0.16371	-0.11297	-0.23745	0.15921	-0.24648
		y	0.09251	-0.10042	-0.05392	-0.25268	0.20821	0.14725
		z	0.04081	-0.05683	-0.03536	-0.00057	0.00121	-0.01522
13	h	x	0.04620	-0.08270	-0.05630	-0.05782	0.04880	-0.18882
		y	0.00143	-0.00440	0.00799	0.33321	-0.25186	-0.15031
		z	-0.03389	0.06387	0.05010	0.18301	-0.08919	0.14430
14	h	x	0.01028	-0.04184	-0.02504	0.33903	-0.28058	-0.40786
		y	0.03887	-0.04319	-0.02013	-0.03108	0.04972	0.04244
		z	0.09546	-0.10834	-0.06002	-0.16701	0.11284	0.11660
15	c	x	-0.03858	0.07406	0.04999	-0.01141	-0.00732	-0.22158
		y	-0.03486	0.03797	0.01613	-0.00996	0.01653	0.02044
		z	0.03575	-0.04049	-0.02122	0.00479	-0.00514	-0.05526

16	h	x	-0.01026	0.04184	0.02504	-0.33901	-0.28066	-0.40788
		y	-0.03887	0.04319	0.02013	0.03107	0.04973	0.04244
		z	0.09545	-0.10834	-0.06002	-0.16700	-0.11288	-0.11660
17	h	x	-0.04619	0.08270	0.05629	0.05782	0.04881	-0.18882
		y	-0.00142	0.00439	-0.00799	-0.33320	-0.25194	-0.15032
		z	-0.03388	0.06387	0.05010	0.18302	0.08923	-0.14430
18	h	x	-0.10087	0.16371	0.11297	0.23745	0.15926	-0.24649
		y	-0.09250	0.10041	0.05392	0.25266	0.20826	0.14725
		z	0.04081	-0.05683	-0.03536	-0.00057	-0.00121	0.01522
19	n	x	0.00000	0.00000	0.00000	0.00000	-0.04678	0.03189
		y	0.00000	0.00000	0.00000	0.00000	-0.02693	-0.04404
		z	-0.16541	-0.49950	0.15407	0.00321	0.00000	0.00000
20	c	x	0.00000	0.00000	0.00000	0.00000	-0.04054	0.06582
		y	0.00000	0.00000	0.00000	0.00000	-0.03585	-0.04314
		z	-0.00272	-0.05754	0.09611	-0.00235	0.00000	0.00000
21	n	x	0.00000	0.00000	0.00000	0.00000	-0.04342	0.09911
		y	0.00000	0.00000	0.00000	0.00000	-0.06359	-0.06474
		z	0.06958	0.05326	-0.34111	0.00343	0.00000	0.00000
22	c	x	0.00000	0.00000	0.00000	0.00000	-0.06740	0.14534
		y	0.00000	0.00000	0.00000	0.00000	-0.08219	0.00147
		z	-0.00479	0.01206	-0.05385	0.00136	0.00000	0.00000
23	h	x	-0.04380	-0.04178	0.16138	-0.00137	-0.05446	0.18438
		y	0.04535	0.03821	-0.08849	0.00005	-0.07570	0.01195
		z	-0.04288	-0.01722	0.03776	0.00106	-0.00311	-0.00184
24	h	x	0.04380	0.04179	-0.16138	0.00138	-0.05446	0.18438
		y	-0.04535	-0.03821	0.08849	-0.00004	-0.07570	0.01195
		z	-0.04288	-0.01722	0.03776	0.00106	0.00311	0.00184
25	c	x	0.00000	0.00000	0.00000	0.00001	-0.15749	0.10395
		y	0.00000	0.00000	0.00000	0.00000	-0.01174	0.05733
		z	-0.00268	0.01796	0.02658	-0.00045	0.00000	0.00000
26	h	x	0.06006	0.04540	-0.29814	0.00682	-0.23433	0.07888
		y	-0.05430	-0.04230	0.19421	-0.00433	-0.02204	0.05273
		z	0.04322	0.05441	-0.14415	0.00336	-0.00092	0.00030
27	h	x	0.00000	0.00000	0.00000	0.00000	-0.11106	0.12115
		y	0.00000	0.00000	0.00000	0.00000	0.10367	0.09798
		z	-0.09314	-0.04460	0.46443	-0.01054	0.00001	0.00000
28	h	x	-0.06006	-0.04540	0.29814	-0.00680	-0.23432	0.07888
		y	0.05430	0.04230	-0.19422	0.00433	-0.02205	0.05272
		z	0.04322	0.05441	-0.14415	0.00336	0.00092	-0.00030
29	n	x	0.00000	0.00000	0.00000	0.00000	-0.01318	0.05459
		y	0.00000	0.00000	0.00000	0.00000	-0.00360	-0.02144
		z	0.19671	0.30153	0.35783	-0.00989	0.00000	0.00000

30	h	x	-0.00001	0.00000	0.00000	0.00000	0.05855	-0.02376
		y	0.00000	0.00000	0.00000	0.00000	0.08429	0.03039
		z	0.43671	-0.18913	0.03226	0.03296	-0.00001	-0.00001
31	h	x	0.00000	0.00000	0.00000	0.00000	-0.02285	0.09141
		y	0.00000	0.00000	0.00000	0.00000	-0.06112	-0.06472
		z	0.31601	0.55300	-0.20491	-0.00297	0.00000	0.00000

reduced mass(g/mol)		9.450	7.446	5.107	1.024	2.543	3.080

mode		19	20	21	22	23	24
frequency		272.77	290.32	304.24	314.73	338.82	353.24
symmetry		a	a	a	a	a	a
IR		YES	YES	YES	YES	YES	YES
|dDIP/dQ|	(a.u.)	0.0009	0.0004	0.0009	0.0001	0.0001	0.0015
intensity	(km/mol)	1.57	0.33	1.59	0.02	0.02	4.06
intensity	(%)	0.13	0.03	0.13	0.00	0.00	0.33
RAMAN		YES	YES	YES	YES	YES	YES
(par,par)		0.36	1.84	1.33	1.23	1.48	1.14
(ort,ort)		0.36	2.64	2.91	1.23	1.48	7.35
(ort,unpol)		0.36	2.30	2.23	1.23	1.48	4.69
depol. ratio		0.75	0.52	0.34	0.75	0.75	0.12

1	cl	x	0.00000	-0.02852	0.04699	0.00000	0.00000	-0.07187
		y	0.00000	-0.02241	0.08262	0.00001	0.00000	0.06210
		z	-0.00396	0.00000	0.00000	-0.00024	0.00363	0.00000
2	c	x	0.00000	0.02164	-0.05486	0.00000	0.00000	0.16371
		y	0.00000	-0.00935	0.03398	0.00000	0.00000	0.02809
		z	0.01106	0.00000	0.00000	0.00259	-0.01101	0.00000
3	n	x	0.00000	0.01274	-0.04507	0.00000	0.00000	0.15771
		y	0.00000	-0.02731	0.05434	0.00000	0.00000	-0.00347
		z	-0.00669	0.00000	0.00000	0.00871	-0.00573	0.00000
4	c	x	0.00000	-0.00411	0.00961	0.00000	0.00000	0.06843
		y	0.00000	-0.03030	0.05685	0.00000	0.00000	-0.03340
		z	0.00934	0.00000	0.00000	0.00752	0.02535	0.00000
5	n	x	0.00000	-0.00281	-0.01161	0.00000	0.00000	0.02554
		y	0.00000	-0.03119	0.00984	0.00000	0.00000	-0.11078
		z	-0.00274	0.00000	0.00000	0.02294	0.15944	0.00000

6	c	x	0.00000	-0.00638	-0.02089	0.00000	0.00000	0.00505
		y	0.00000	-0.00733	-0.03381	0.00000	0.00000	-0.08068
		z	-0.00212	0.00000	0.00000	-0.00351	0.03774	0.00000
7	c	x	0.00000	-0.04371	-0.20545	-0.00002	0.00001	-0.02820
		y	0.00000	-0.00370	-0.02066	0.00000	0.00000	-0.08364
		z	-0.00314	0.00000	0.00000	-0.00950	-0.19211	0.00000
8	h	x	0.00597	-0.05470	-0.29073	0.44925	-0.03569	-0.02226
		y	-0.00214	-0.01540	-0.09398	-0.07242	-0.21508	-0.08193
		z	-0.00734	0.00016	0.00535	-0.28160	-0.29110	0.00047
9	h	x	0.00000	-0.04757	-0.23883	-0.00002	0.00001	-0.02684
		y	0.00000	0.02218	0.16068	0.00001	0.00000	-0.08805
		z	0.00382	-0.00002	-0.00012	0.50874	-0.30618	0.00000
10	h	x	-0.00597	-0.05466	-0.29054	-0.44930	0.03570	-0.02225
		y	0.00214	-0.01542	-0.09401	0.07240	0.21507	-0.08194
		z	-0.00734	-0.00013	-0.00523	-0.28160	-0.29111	-0.00045
11	c	x	-0.00334	0.02739	0.05247	0.01785	-0.08325	-0.03906
		y	-0.00206	0.01966	-0.05016	0.00352	-0.14059	0.07456
		z	-0.00161	-0.00383	-0.04326	-0.00974	0.01239	0.09978
12	h	x	-0.00464	0.30351	0.24718	-0.08563	-0.11325	-0.10047
		y	-0.00213	0.30258	0.04325	-0.11804	-0.21753	0.25521
		z	-0.00220	0.00583	0.01210	-0.00592	0.03253	-0.01369
13	h	x	-0.00278	0.09309	0.08579	-0.01365	-0.05904	-0.04067
		y	-0.00505	-0.28413	-0.19870	0.14973	-0.27143	0.07987
		z	0.00155	-0.22720	-0.21605	0.05921	0.11728	0.13845
14	h	x	-0.00637	-0.28109	-0.09039	0.16636	-0.20806	-0.05575
		y	-0.00177	0.05921	-0.03300	-0.01492	-0.13165	0.08156
		z	-0.00326	0.20674	0.01297	-0.08869	-0.13904	0.30705
15	c	x	0.00334	0.02739	0.05249	-0.01784	0.08324	-0.03905
		y	0.00206	0.01966	-0.05015	-0.00353	0.14059	0.07456
		z	-0.00161	0.00383	0.04326	-0.00974	0.01237	-0.09978
16	h	x	0.00636	-0.28107	-0.09028	-0.16639	0.20804	-0.05576
		y	0.00178	0.05920	-0.03300	0.01492	0.13166	0.08155
		z	-0.00326	-0.20673	-0.01292	-0.08872	-0.13907	-0.30704
17	h	x	0.00278	0.09308	0.08579	0.01367	0.05904	-0.04066
		y	0.00505	-0.28411	-0.19860	-0.14978	0.27143	0.07985
		z	0.00155	0.22720	0.21602	0.05927	0.11726	-0.13845
18	h	x	0.00464	0.30350	0.24714	0.08570	0.11324	-0.10047
		y	0.00213	0.30257	0.04319	0.11807	0.21755	0.25521
		z	-0.00220	-0.00584	-0.01210	-0.00592	0.03252	0.01368
19	n	x	0.00000	0.01527	-0.03754	0.00000	0.00000	0.15106
		y	0.00000	0.01021	-0.01038	0.00000	0.00000	0.04069
		z	0.02054	0.00000	0.00000	-0.00053	0.00573	0.00000

20	c	x	0.00000	-0.00267	0.02254	0.00000	0.00000	0.03603
		y	0.00000	0.01608	-0.02300	0.00000	0.00000	0.03870
		z	-0.01173	0.00000	0.00000	-0.00143	-0.00699	0.00000
21	n	x	0.00000	-0.02069	0.08259	0.00001	0.00000	0.01184
		y	0.00000	0.05641	-0.12122	-0.00001	0.00000	0.01444
		z	-0.10319	0.00000	0.00000	0.00253	0.00930	0.00000
22	c	x	0.00000	-0.01385	0.08803	0.00001	0.00000	-0.07633
		y	0.00000	0.06356	-0.11940	-0.00001	0.00000	-0.12443
		z	0.06923	0.00000	0.00000	0.00016	0.00067	0.00000
23	h	x	0.04661	-0.03240	0.13556	-0.00105	-0.00353	-0.10583
		y	-0.08697	0.05532	-0.09979	0.00082	0.00222	-0.12412
		z	0.14301	0.00338	-0.00740	-0.00065	-0.00171	-0.00437
24	h	x	-0.04661	-0.03240	0.13556	0.00107	0.00353	-0.10583
		y	0.08697	0.05532	-0.09979	-0.00083	-0.00222	-0.12412
		z	0.14301	-0.00338	0.00740	-0.00064	-0.00171	0.00437
25	c	x	0.00000	0.06912	-0.07931	0.00000	0.00000	-0.20311
		y	0.00000	-0.00909	0.03705	0.00000	0.00000	-0.04960
		z	0.00609	0.00000	0.00000	0.00011	-0.00048	0.00000
26	h	x	0.39346	0.14024	-0.22236	-0.00140	-0.00233	-0.33378
		y	-0.27424	0.00067	0.01719	0.00114	0.00266	-0.06530
		z	0.24418	0.00077	-0.00146	-0.00085	-0.00266	-0.00264
27	h	x	0.00000	0.02558	0.00901	0.00000	0.00000	-0.12651
		y	0.00000	-0.11665	0.25439	0.00002	0.00000	0.14279
		z	-0.58552	0.00000	0.00000	0.00230	0.00344	0.00000
28	h	x	-0.39346	0.14025	-0.22236	0.00137	0.00233	-0.33378
		y	0.27424	0.00066	0.01720	-0.00113	-0.00266	-0.06530
		z	0.24418	-0.00078	0.00146	-0.00085	-0.00266	0.00264
29	n	x	0.00000	-0.01613	0.03958	0.00000	0.00000	0.03183
		y	0.00000	-0.01380	0.03282	0.00000	0.00000	0.01663
		z	0.02446	0.00000	0.00000	-0.00511	-0.02725	0.00000
30	h	x	0.00000	0.00707	-0.07733	-0.00001	0.00000	-0.00432
		y	0.00000	-0.03237	0.01857	0.00000	0.00000	-0.10616
		z	-0.00050	0.00000	0.00000	0.01775	0.24133	0.00001
31	h	x	0.00000	-0.04918	0.14849	0.00001	0.00000	0.09156
		y	0.00000	0.05234	-0.11135	-0.00001	0.00000	0.02400
		z	0.00947	0.00000	0.00001	0.00036	-0.00812	0.00001

reduced mass(g/mol)	1.218	1.302	2.785	1.027	2.372	3.796

mode	25	26	27	28	29	30

frequency		392.61	421.04	439.81	452.05	469.24	530.46
symmetry		a	a	a	a	a	a
IR		YES	YES	YES	YES	YES	YES
|dDIP/dQ| (a.u.)		0.0013	0.0017	0.0005	0.0055	0.0004	0.0029
intensity (km/mol)		2.83	4.94	0.36	52.97	0.34	14.94
intensity (%)		0.23	0.40	0.03	4.34	0.03	1.22
RAMAN		YES	YES	YES	YES	YES	YES
(par,par)		2.90	4.37	0.13	2.45	5.50	1.16
(ort,ort)		3.38	16.05	0.13	2.45	19.11	2.34
(ort,unpol)		3.17	11.04	0.13	2.45	13.28	1.84
depol. ratio		0.64	0.20	0.75	0.75	0.22	0.37
1	cl	x	0.01946	0.04362	0.00000	0.00000	-0.02186	0.02967
		y	0.11616	-0.29256	-0.00001	0.00000	-0.03047	0.00924
		z	0.00000	0.00000	-0.00188	-0.00164	0.00000	0.00000
2	c	x	-0.11821	-0.07861	-0.00001	0.00000	0.06513	0.00674
		y	0.00470	0.01140	0.00000	0.00000	0.01845	-0.00290
		z	0.00000	0.00000	0.00612	0.01289	0.00000	0.00000
3	n	x	-0.12992	-0.00375	-0.00001	0.00000	0.04394	0.08859
		y	-0.04073	0.15979	0.00001	0.00000	-0.03191	0.17060
		z	0.00000	0.00001	-0.01877	-0.00031	0.00000	0.00000
4	c	x	-0.05018	0.04216	0.00000	0.00000	-0.06982	0.00865
		y	-0.04392	0.19855	0.00001	0.00000	-0.04053	0.17124
		z	0.00000	0.00000	-0.03202	-0.00318	0.00000	0.00000
5	n	x	-0.03015	-0.01635	0.00000	0.00000	-0.12150	-0.09618
		y	-0.07001	0.05002	0.00000	0.00000	-0.08469	0.07044
		z	0.00000	0.00002	-0.18499	0.00756	0.00000	-0.00001
6	c	x	0.01259	0.02700	0.00000	0.00000	-0.17568	-0.16158
		y	-0.12503	-0.13789	-0.00001	0.00000	0.01590	-0.05912
		z	-0.00001	-0.00002	0.15986	-0.00468	0.00000	0.00000
7	c	x	0.09568	-0.05406	0.00000	0.00000	0.08864	-0.01034
		y	-0.15808	-0.16528	-0.00002	0.00000	-0.00742	-0.12491
		z	0.00001	0.00002	-0.07565	0.00183	0.00000	0.00000
8	h	x	0.14146	-0.09944	-0.02720	0.00010	0.25258	0.08463
		y	-0.11841	-0.20110	-0.23633	0.00670	0.12615	-0.04817
		z	-0.00353	0.00440	-0.18916	0.00544	-0.01202	-0.00606
9	h	x	0.11051	-0.07446	0.00000	0.00000	0.15006	0.02225
		y	-0.24748	-0.06589	-0.00001	0.00000	-0.33984	-0.31353
		z	-0.00001	0.00003	-0.18023	0.00426	-0.00001	-0.00001

10	h	x	0.14150	-0.09944	0.02719	-0.00009	0.25260	0.08465
		y	-0.11844	-0.20118	0.23629	-0.00670	0.12616	-0.04817
		z	0.00358	-0.00433	-0.18917	0.00544	0.01202	0.00606
11	c	x	0.04483	0.03928	0.13052	-0.00395	-0.00163	-0.00867
		y	0.09071	0.04776	-0.08211	0.00227	0.04835	0.04731
		z	0.10101	0.10425	0.10489	-0.00300	-0.11597	-0.06671
12	h	x	-0.01410	-0.03310	0.28833	-0.00944	0.16237	0.11130
		y	0.26007	0.20085	-0.17933	0.00517	-0.01191	0.06034
		z	-0.00612	-0.00216	0.23068	-0.00712	-0.00558	-0.01214
13	h	x	0.01716	0.01495	0.12854	-0.00385	-0.01659	-0.03728
		y	0.23130	0.17118	-0.05188	0.00124	0.13738	0.20318
		z	0.07863	0.10794	-0.06924	0.00318	-0.34016	-0.28139
14	h	x	0.16645	0.14108	0.17883	-0.00607	0.11009	0.15508
		y	0.08390	0.04225	-0.08876	0.00258	0.03588	0.03174
		z	0.35758	0.33004	0.01514	-0.00075	-0.12679	0.02425
15	c	x	0.04484	0.03931	-0.13051	0.00395	-0.00163	-0.00867
		y	0.09069	0.04773	0.08213	-0.00227	0.04836	0.04731
		z	-0.10102	-0.10428	0.10486	-0.00300	0.11598	0.06671
16	h	x	0.16647	0.14113	-0.17880	0.00607	0.11009	0.15508
		y	0.08388	0.04222	0.08877	-0.00258	0.03589	0.03174
		z	-0.35758	-0.33004	0.01507	-0.00074	0.12679	-0.02425
17	h	x	0.01718	0.01499	-0.12853	0.00385	-0.01660	-0.03728
		y	0.23129	0.17116	0.05191	-0.00124	0.13739	0.20318
		z	-0.07863	-0.10792	-0.06926	0.00319	0.34015	0.28139
18	h	x	-0.01408	-0.03301	-0.28833	0.00944	0.16236	0.11129
		y	0.26005	0.20079	0.17938	-0.00517	-0.01190	0.06035
		z	0.00609	0.00209	0.23068	-0.00712	0.00559	0.01215
19	n	x	-0.10872	-0.13908	-0.00001	0.00000	0.01715	0.13045
		y	-0.02134	0.10203	0.00001	0.00000	0.07937	-0.18030
		z	0.00000	0.00000	0.00082	0.04847	0.00000	0.00000
20	c	x	-0.02917	-0.03405	0.00000	0.00000	-0.02142	0.04236
		y	-0.03821	0.13789	0.00001	0.00000	0.08568	-0.18697
		z	0.00000	0.00000	0.00248	-0.00535	0.00000	0.00000
21	n	x	0.01477	0.05000	0.00000	0.00000	0.08364	-0.09779
		y	-0.06512	0.02359	0.00000	0.00000	-0.02735	-0.04652
		z	0.00000	0.00000	-0.00514	-0.05452	0.00000	0.00000
22	c	x	0.08156	0.03199	0.00000	0.00000	0.10929	-0.10201
		y	0.02400	-0.03580	0.00000	0.00000	-0.08425	0.09101
		z	0.00000	0.00000	-0.00237	-0.02434	0.00000	0.00000
23	h	x	0.12171	0.02624	-0.00224	-0.04034	0.12385	-0.08821
		y	0.03238	-0.03034	0.00443	0.05478	-0.07060	0.07790
		z	-0.00016	-0.00434	-0.00545	-0.06385	-0.00621	0.00945

24	h	x	0.12171	0.02624	0.00225	0.04034	0.12384	-0.08821
		y	0.03238	-0.03034	-0.00443	-0.05478	-0.07059	0.07789
		z	0.00016	0.00434	-0.00545	-0.06385	0.00621	-0.00946
25	c	x	0.09908	-0.01751	0.00000	0.00000	0.01340	-0.00524
		y	0.04041	0.01360	0.00000	0.00000	0.02407	-0.01639
		z	0.00000	0.00000	-0.00015	-0.00052	0.00000	0.00000
26	h	x	0.12692	-0.07530	-0.00213	-0.02300	-0.09256	0.13035
		y	0.04283	0.00617	-0.00032	-0.00688	0.01045	-0.00056
		z	0.00105	-0.00088	0.00004	0.00477	-0.00183	0.00324
27	h	x	0.08499	0.01761	0.00000	0.00000	0.07982	-0.08861
		y	0.00277	0.10074	0.00001	0.00000	0.18655	-0.22151
		z	0.00000	0.00000	0.00378	0.04750	0.00000	0.00000
28	h	x	0.12692	-0.07530	0.00213	0.02300	-0.09257	0.13035
		y	0.04283	0.00617	0.00032	0.00688	0.01045	-0.00056
		z	-0.00105	0.00088	0.00004	0.00477	0.00183	-0.00324
29	n	x	-0.03997	0.01440	0.00000	0.00000	-0.07602	0.09798
		y	-0.04788	0.26616	0.00001	0.00000	0.03364	-0.01825
		z	0.00000	0.00000	0.02345	-0.03647	0.00000	0.00000
30	h	x	-0.06985	-0.20080	0.00000	0.00000	-0.09886	-0.25228
		y	-0.06589	0.07427	0.00000	0.00000	-0.08659	0.09176
		z	0.00004	0.00008	-0.41898	-0.02272	0.00001	0.00002
31	h	x	-0.00091	0.14492	0.00001	0.00000	0.21700	-0.30127
		y	-0.06617	0.03817	0.00000	0.00000	-0.00735	-0.07647
		z	-0.00001	0.00001	0.06947	0.98508	-0.00004	0.00002

reduced mass(g/mol)	3.504	7.389	2.586	1.105	2.859	4.216

mode	31	32	33	34	35	36
frequency	624.72	654.39	673.11	697.65	708.99	769.95
symmetry	a	a	a	a	a	a
IR	YES	YES	YES	YES	YES	YES
|dDIP/dQ| (a.u.)	0.0060	0.0011	0.0024	0.0029	0.0010	0.0020
intensity (km/mol)	65.02	2.07	10.30	15.41	1.79	7.00
intensity (%)	5.32	0.17	0.84	1.26	0.15	0.57
RAMAN	YES	YES	YES	YES	YES	YES
(par,par)	2.10	0.05	0.53	1.05	0.20	0.67
(ort,ort)	2.10	0.05	3.72	2.12	0.20	6.03

	(ort,unpol)		2.10	0.05	2.35	1.67	0.20	3.73
	depol. ratio		0.75	0.75	0.11	0.37	0.75	0.08
1	cl	x	0.00000	0.00000	0.00636	-0.00457	0.00000	-0.00820
		y	0.00000	0.00000	-0.02694	-0.04375	0.00000	0.01085
		z	-0.00387	-0.04999	0.00000	0.00000	-0.00108	0.00000
2	c	x	0.00000	0.00000	-0.14028	0.12030	0.00000	0.07032
		y	0.00000	0.00000	0.05627	0.12328	0.00000	-0.03688
		z	0.04329	0.73559	0.00000	0.00000	0.02585	0.00000
3	n	x	0.00000	0.00000	-0.22515	-0.02178	0.00000	0.03835
		y	0.00000	0.00000	-0.07618	-0.00602	0.00000	-0.06652
		z	0.03669	-0.18939	0.00000	0.00000	-0.16591	0.00000
4	c	x	0.00000	0.00000	0.05906	-0.28969	0.00000	0.01044
		y	0.00000	0.00000	-0.02401	0.00471	0.00000	-0.04943
		z	-0.07372	-0.28219	0.00000	-0.00001	0.55122	0.00000
5	n	x	0.00000	0.00000	0.06399	-0.14626	0.00000	0.12465
		y	0.00000	0.00000	0.06758	0.34273	0.00000	0.15915
		z	-0.08665	0.12632	0.00000	0.00000	-0.16343	0.00000
6	c	x	0.00000	0.00000	-0.07278	0.03373	0.00000	0.11175
		y	0.00000	0.00000	-0.01825	-0.00498	0.00000	0.02361
		z	0.01124	-0.00454	0.00000	0.00000	0.00261	0.00000
7	c	x	0.00000	0.00000	-0.00552	-0.00669	0.00000	-0.00174
		y	0.00001	0.00000	-0.13641	-0.04461	0.00000	-0.25242
		z	0.00218	-0.00362	0.00000	0.00000	0.00093	0.00000
8	h	x	0.00466	-0.00281	0.03432	-0.15088	-0.00371	-0.15288
		y	-0.01976	0.01112	-0.10795	-0.14783	-0.00281	-0.38429
		z	-0.01113	0.00380	-0.00553	0.01744	0.00346	0.01114
9	h	x	0.00000	0.00000	0.00842	-0.05733	0.00000	-0.05553
		y	0.00001	0.00000	-0.23038	0.21768	0.00001	0.00673
		z	-0.01007	-0.00062	0.00000	0.00000	0.00719	0.00000
10	h	x	-0.00466	0.00281	0.03433	-0.15089	0.00370	-0.15288
		y	0.01977	-0.01112	-0.10796	-0.14783	0.00282	-0.38429
		z	-0.01113	0.00380	0.00553	-0.01744	0.00346	-0.01113
11	c	x	0.00474	-0.00381	-0.05158	0.06543	-0.00353	-0.05760
		y	-0.00468	0.00205	0.04196	-0.04865	0.00325	0.07949
		z	0.00922	-0.00366	-0.08722	0.11350	-0.00673	-0.15706
12	h	x	0.05630	-0.03793	-0.00619	0.08088	0.02640	-0.15776
		y	-0.01349	0.00385	0.04887	-0.00839	0.00088	0.10627
		z	0.04048	-0.02300	-0.06856	0.10398	0.01153	-0.22441
13	h	x	0.00257	-0.00331	-0.06409	0.05015	-0.00281	-0.05404
		y	0.00553	-0.00384	0.10290	0.04332	0.00150	0.03535
		z	-0.04487	0.02671	-0.18042	0.07196	-0.02173	-0.05235

14	h	x	0.04721	-0.02393	0.00779	0.15736	0.01347	-0.13411
		y	-0.01201	0.00517	0.03651	-0.05708	-0.00003	0.08952
		z	0.00499	-0.00363	-0.06233	0.19348	-0.00878	-0.19215
15	c	x	-0.00474	0.00380	-0.05158	0.06543	0.00353	-0.05760
		y	0.00467	-0.00205	0.04196	-0.04865	-0.00326	0.07949
		z	0.00921	-0.00366	0.08722	-0.11349	-0.00674	0.15706
16	h	x	-0.04722	0.02393	0.00779	0.15736	-0.01347	-0.13411
		y	0.01200	-0.00517	0.03651	-0.05708	0.00003	0.08953
		z	0.00500	-0.00363	0.06233	-0.19348	-0.00879	0.19214
17	h	x	-0.00256	0.00330	-0.06409	0.05015	0.00281	-0.05404
		y	-0.00555	0.00384	0.10290	0.04332	-0.00150	0.03535
		z	-0.04489	0.02672	0.18041	-0.07195	-0.02174	0.05234
18	h	x	-0.05631	0.03793	-0.00619	0.08088	-0.02640	-0.15777
		y	0.01348	-0.00385	0.04887	-0.00840	-0.00088	0.10627
		z	0.04048	-0.02299	0.06856	-0.10398	0.01152	0.22441
19	n	x	0.00000	0.00000	-0.03902	0.22327	0.00000	-0.01232
		y	0.00000	0.00000	0.01551	0.01452	0.00000	0.04776
		z	-0.01663	-0.17865	0.00000	0.00000	0.14873	0.00000
20	c	x	0.00000	0.00000	0.26595	-0.01484	0.00000	-0.09040
		y	0.00000	0.00000	0.05390	0.02378	0.00000	0.02495
		z	0.01703	-0.29915	0.00000	0.00001	-0.53315	0.00000
21	n	x	0.00000	0.00000	0.15573	0.02700	0.00000	-0.04493
		y	0.00000	0.00000	0.30639	0.04563	0.00000	-0.08005
		z	-0.00898	0.08550	0.00000	0.00000	0.13003	0.00000
22	c	x	0.00000	0.00000	-0.03573	0.07881	0.00000	0.00517
		y	0.00000	0.00000	-0.00026	-0.07133	0.00000	-0.01038
		z	-0.00117	0.01909	0.00000	0.00000	0.02881	0.00000
23	h	x	0.00095	-0.02132	-0.19920	0.04574	-0.02720	0.05643
		y	0.00006	0.08355	-0.02591	-0.06760	0.10162	-0.00075
		z	-0.00070	-0.04422	-0.00697	-0.00479	-0.05079	0.00113
24	h	x	-0.00095	0.02131	-0.19921	0.04574	0.02719	0.05644
		y	-0.00006	-0.08355	-0.02591	-0.06759	-0.10162	-0.00075
		z	-0.00070	-0.04422	0.00697	0.00479	-0.05079	-0.00113
25	c	x	0.00000	0.00000	-0.09684	0.02908	0.00000	0.02156
		y	0.00000	0.00000	-0.08028	0.00250	0.00000	0.02583
		z	-0.00006	-0.00107	0.00000	0.00000	0.00271	0.00000
26	h	x	-0.00044	0.02716	-0.25904	-0.09524	0.04187	0.07123
		y	-0.00061	0.03839	-0.09289	-0.00835	0.05406	0.02926
		z	0.00048	-0.02532	-0.00810	-0.00569	-0.03150	0.00297
27	h	x	0.00000	0.00000	-0.01620	0.10592	0.00000	-0.00133
		y	0.00000	0.00000	0.12936	0.19026	0.00000	-0.03419
		z	0.00094	-0.01599	0.00000	0.00000	-0.02503	0.00000

28	h	x	0.00044	-0.02716	-0.25904	-0.09524	-0.04188	0.07123
		y	0.00061	-0.03839	-0.09289	-0.00835	-0.05406	0.02926
		z	0.00048	-0.02532	0.00810	0.00569	-0.03150	-0.00297
29	n	x	0.00000	0.00000	0.19502	-0.15999	0.00000	-0.05664
		y	0.00000	0.00000	-0.20325	-0.25375	-0.00001	0.02652
		z	-0.00011	0.17717	0.00000	0.00000	-0.02440	0.00000
30	h	x	-0.00002	0.00001	0.06126	-0.09134	-0.00001	0.26596
		y	0.00000	0.00000	0.06853	0.33432	0.00000	0.14168
		z	0.98065	-0.35090	0.00005	-0.00002	0.52324	0.00005
31	h	x	0.00000	0.00000	0.14402	0.13616	0.00000	-0.00262
		y	0.00000	0.00000	0.30350	0.06191	0.00000	-0.07435
		z	0.03244	0.09775	-0.00001	0.00000	-0.01027	0.00000

reduced mass(g/mol)	1.216	10.505	6.297	6.601	8.717	3.622
mode	37	38	39	40	41	42
frequency	782.71	792.11	878.09	894.96	897.59	914.34
symmetry	a	a	a	a	a	a
IR	YES	YES	YES	YES	YES	YES
|dDIP/dQ| (a.u.)	0.0021	0.0035	0.0034	0.0006	0.0044	0.0026
intensity (km/mol)	7.48	21.35	20.68	0.63	34.25	12.39
intensity (%)	0.61	1.75	1.69	0.05	2.80	1.01
RAMAN	YES	YES	YES	YES	YES	YES
(par,par)	0.83	0.05	2.55	5.50	1.72	2.35
(ort,ort)	0.83	0.05	5.53	5.50	3.20	4.68
(ort,unpol)	0.83	0.05	4.25	5.50	2.57	3.68
depol. ratio	0.75	0.75	0.35	0.75	0.40	0.38

1	cl	x	0.00000	0.00000	0.00872	0.00000	0.00112	0.00262
		y	0.00000	0.00000	-0.02205	0.00000	0.02719	-0.01230
		z	-0.00109	0.00433	0.00000	0.00003	0.00000	0.00000
2	c	x	0.00000	0.00000	-0.05853	0.00000	-0.01204	-0.01701
		y	0.00000	0.00000	0.11419	0.00000	-0.15095	0.07307
		z	0.03915	-0.24103	0.00000	0.00021	0.00000	0.00000
3	n	x	0.00000	0.00000	-0.01900	0.00000	0.04420	-0.00678
		y	0.00000	0.00000	0.13646	0.00000	-0.01293	0.05569
		z	-0.03232	0.21800	0.00000	-0.00202	0.00000	0.00000
4	c	x	0.00000	0.00000	-0.06050	0.00000	0.01677	-0.01404

		y	0.00000	0.00000	0.04049	0.00000	0.00850	0.00712
		z	0.04806	-0.33876	0.00000	0.00160	0.00000	0.00000
5	n	x	0.00000	0.00000	-0.08489	0.00000	0.00941	0.00883
		y	0.00000	0.00000	-0.17495	0.00000	0.03622	-0.04900
		z	-0.00882	0.05826	0.00000	0.01552	0.00000	0.00000
6	c	x	0.00000	0.00000	0.17157	0.00000	-0.01707	-0.00398
		y	0.00000	0.00000	-0.05371	0.00000	0.01443	0.09667
		z	-0.00008	0.00114	0.00000	0.13211	0.00000	0.00000
7	c	x	0.00000	0.00000	0.07792	0.00000	-0.01298	-0.07707
		y	0.00000	0.00000	0.04115	0.00001	-0.01653	-0.10353
		z	-0.00023	0.00128	0.00000	0.06474	0.00000	0.00000
8	h	x	-0.00061	0.00407	-0.13177	-0.02682	0.01460	0.15108
		y	0.00034	-0.00348	-0.10485	-0.28551	0.00066	0.02541
		z	0.00047	-0.00413	0.02828	-0.07442	-0.00438	-0.04343
9	h	x	0.00000	0.00000	0.00987	0.00000	-0.00524	-0.00440
		y	0.00000	0.00000	0.41882	0.00003	-0.06189	-0.48867
		z	0.00056	-0.00546	0.00000	-0.10730	0.00000	0.00000
10	h	x	0.00061	-0.00407	-0.13178	0.02680	0.01460	0.15109
		y	-0.00034	0.00349	-0.10486	0.28550	0.00065	0.02541
		z	0.00047	-0.00413	-0.02828	-0.07443	0.00439	0.04344
11	c	x	0.00000	-0.00061	0.00521	-0.11688	-0.00025	0.05169
		y	0.00018	-0.00050	0.03336	0.06047	-0.00138	0.05767
		z	-0.00021	0.00069	-0.11902	-0.05222	0.01673	0.04468
12	h	x	0.00091	-0.00505	-0.22532	0.19301	0.03201	-0.01372
		y	0.00010	-0.00011	0.14560	-0.08735	-0.02568	-0.18913
		z	0.00043	-0.00267	-0.29063	0.16989	0.04455	0.12636
13	h	x	0.00009	-0.00127	0.01374	-0.12647	0.00028	0.10883
		y	-0.00020	0.00219	-0.04324	0.14571	-0.00018	-0.24386
		z	0.00016	-0.00382	0.15964	-0.45908	-0.01795	0.22941
14	h	x	0.00026	-0.00105	-0.13969	0.06636	0.01240	-0.21015
		y	0.00010	-0.00020	0.05326	0.03816	-0.00357	0.07656
		z	-0.00035	0.00134	-0.04591	-0.21386	-0.00893	-0.31045
15	c	x	0.00000	0.00061	0.00520	0.11687	-0.00026	0.05170
		y	-0.00018	0.00050	0.03336	-0.06048	-0.00137	0.05766
		z	-0.00021	0.00068	0.11902	-0.05222	-0.01673	-0.04468
16	h	x	-0.00026	0.00105	-0.13969	-0.06634	0.01240	-0.21016
		y	-0.00010	0.00020	0.05327	-0.03817	-0.00357	0.07656
		z	-0.00035	0.00134	0.04593	-0.21389	0.00894	0.31041
17	h	x	-0.00009	0.00127	0.01373	0.12646	0.00028	0.10884
		y	0.00020	-0.00219	-0.04323	-0.14570	-0.00017	-0.24387
		z	0.00016	-0.00382	-0.15962	-0.45906	0.01797	-0.22944
18	h	x	-0.00091	0.00505	-0.22531	-0.19301	0.03202	-0.01374

		y	-0.00010	0.00011	0.14559	0.08737	-0.02568	-0.18911
		z	0.00043	-0.00267	0.29061	0.16990	-0.04456	-0.12633
19	n	x	0.00000	0.00000	0.06334	0.00000	-0.01754	0.01561
		y	0.00000	0.00000	-0.04993	0.00000	-0.09779	0.00637
		z	-0.02799	0.24028	0.00000	-0.00074	0.00000	0.00000
20	c	x	0.00000	0.00000	0.00256	0.00000	-0.03836	-0.00852
		y	0.00000	0.00000	-0.02767	0.00000	-0.02160	-0.00623
		z	0.03364	-0.39842	0.00000	0.00195	0.00000	0.00000
21	n	x	0.00000	0.00000	-0.02345	0.00000	-0.06541	-0.01830
		y	0.00000	0.00000	0.05026	0.00000	0.12868	-0.00595
		z	0.01912	0.08673	0.00000	-0.00019	0.00000	0.00000
22	c	x	0.00000	0.00000	0.02354	0.00000	0.02680	0.00113
		y	0.00000	0.00000	-0.03666	0.00000	-0.08392	-0.01333
		z	-0.07219	-0.04289	0.00000	0.00001	0.00000	0.00000
23	h	x	-0.15434	-0.15760	-0.06168	0.00021	-0.21368	-0.01072
		y	-0.42767	-0.27193	-0.05006	0.00000	-0.12981	-0.01527
		z	0.22798	0.13952	-0.00088	0.00002	0.00142	0.00016
24	h	x	0.15434	0.15760	-0.06167	-0.00022	-0.21368	-0.01072
		y	0.42767	0.27193	-0.05006	-0.00001	-0.12981	-0.01527
		z	0.22798	0.13952	0.00088	0.00002	-0.00142	-0.00016
25	c	x	0.00000	0.00000	0.04973	0.00000	0.14638	0.01698
		y	0.00000	0.00000	-0.00426	0.00000	-0.00550	0.00583
		z	-0.04151	-0.03314	0.00000	0.00007	0.00000	0.00000
26	h	x	-0.25105	-0.18323	-0.10881	0.00006	-0.28834	-0.01049
		y	-0.34677	-0.25285	-0.00649	0.00015	-0.00375	0.00680
		z	0.18104	0.12918	-0.01497	-0.00004	-0.04562	-0.00344
27	h	x	0.00000	0.00000	0.14398	0.00001	0.40548	0.03556
		y	0.00000	0.00000	0.22677	0.00001	0.62905	0.05038
		z	0.18476	0.14103	0.00000	-0.00006	0.00000	0.00000
28	h	x	0.25105	0.18323	-0.10881	-0.00007	-0.28835	-0.01049
		y	0.34677	0.25285	-0.00648	-0.00015	-0.00375	0.00680
		z	0.18104	0.12918	0.01497	-0.00003	0.04562	0.00344
29	n	x	0.00000	0.00000	-0.04336	0.00000	-0.02394	-0.01148
		y	0.00000	0.00000	-0.06355	0.00000	0.06963	-0.04134
		z	-0.02852	0.24287	0.00000	0.00043	0.00000	0.00000
30	h	x	0.00000	0.00000	-0.19450	0.00000	0.02238	0.03067
		y	0.00000	0.00000	-0.16507	0.00000	0.03542	-0.05187
		z	0.01460	-0.06914	-0.00001	-0.06580	0.00000	-0.00001
31	h	x	0.00000	0.00000	-0.04934	0.00000	-0.13489	-0.02556
		y	0.00000	0.00000	0.04841	0.00000	0.12364	-0.00699
		z	0.03387	0.02205	0.00000	-0.00050	0.00000	0.00000

reduced mass(g/mol)		1.179	6.966	3.041	1.690	2.164	1.653
mode		43	44	45	46	47	48
frequency		935.40	952.49	981.76	1016.93	1023.27	1055.05
symmetry		a	a	a	a	a	a
IR		YES	YES	YES	YES	YES	YES
|dDIP/dQ| (a.u.)		0.0000	0.0017	0.0061	0.0009	0.0013	0.0017
intensity (km/mol)		0.00	4.92	65.63	1.55	3.07	5.38
intensity (%)		0.00	0.40	5.37	0.13	0.25	0.44
RAMAN		YES	YES	YES	YES	YES	YES
(par,par)		0.09	10.46	1.10	1.65	1.46	2.89
(ort,ort)		0.09	48.69	1.93	1.65	1.78	12.00
(ort,unpol)		0.09	32.31	1.57	1.65	1.64	8.10
depol. ratio		0.75	0.16	0.43	0.75	0.62	0.18
1 cl	x	0.00000	0.00105	-0.00087	0.00000	-0.00099	0.00318
	y	0.00000	0.02178	-0.03981	0.00000	0.00473	-0.01018
	z	-0.00008	0.00000	0.00000	0.00006	0.00000	0.00000
2 c	x	0.00000	-0.00753	0.00849	0.00000	0.01320	-0.02312
	y	0.00000	-0.14435	0.27794	0.00000	-0.03846	0.08956
	z	0.00025	0.00000	0.00000	-0.00013	0.00000	0.00000
3 n	x	0.00000	-0.17614	-0.28191	0.00000	0.01189	-0.02167
	y	0.00000	-0.17497	-0.13878	0.00000	-0.01578	0.05734
	z	-0.00111	0.00000	0.00000	-0.00041	0.00000	0.00000
4 c	x	0.00000	-0.09701	0.07223	0.00000	-0.01053	0.01330
	y	0.00000	0.02455	0.00263	0.00000	0.01309	-0.03536
	z	0.00080	0.00000	0.00000	0.00688	0.00000	0.00000
5 n	x	0.00000	-0.13048	0.14169	0.00000	0.00989	0.11412
	y	0.00000	-0.00208	-0.01532	0.00000	0.05458	-0.01794
	z	-0.00124	0.00000	0.00000	0.02574	0.00000	0.00000
6 c	x	0.00000	0.05773	-0.05169	0.00000	0.00525	-0.00901
	y	0.00000	0.03769	-0.04466	0.00000	-0.05143	0.00516
	z	0.01388	0.00000	0.00000	-0.06544	0.00000	0.00000
7 c	x	0.00000	0.02219	-0.03297	0.00000	-0.10526	-0.02064
	y	0.00000	-0.04892	0.05009	0.00000	0.05280	0.00381
	z	0.08265	0.00000	0.00000	-0.08237	0.00000	0.00000
8 h	x	-0.02147	-0.03138	0.10010	0.01871	0.22399	0.03544

		y	-0.38990	-0.09162	0.14486	0.30659	0.24835	0.03596
		z	-0.11747	0.00327	-0.02002	0.07415	-0.06304	-0.01055
9	h	x	0.00000	0.00292	0.01128	0.00000	-0.00836	-0.00161
		y	-0.00001	0.05171	-0.17816	-0.00002	-0.43682	-0.09621
		z	-0.17965	0.00000	0.00000	0.12010	0.00000	0.00000
10	h	x	0.02148	-0.03138	0.10010	-0.01870	0.22400	0.03544
		y	0.38990	-0.09161	0.14485	-0.30656	0.24839	0.03595
		z	-0.11747	-0.00327	0.02002	0.07416	0.06303	0.01055
11	c	x	0.00470	0.04428	-0.02513	-0.06245	0.05299	-0.03089
		y	-0.06234	0.04086	-0.03217	-0.08376	-0.03695	-0.01871
		z	-0.04263	-0.00365	-0.01069	0.04083	-0.06567	0.00559
12	h	x	-0.12044	-0.07353	0.00730	0.16989	-0.22121	0.05331
		y	0.24634	-0.05889	0.06369	0.07841	0.17533	0.01952
		z	-0.24708	-0.01746	-0.03776	0.08375	-0.30028	0.03019
13	h	x	-0.04214	0.07811	-0.04880	-0.11187	0.03559	-0.04552
		y	0.15935	-0.14708	0.09478	0.22150	0.00689	0.07061
		z	0.03807	0.20211	-0.10264	-0.30349	0.22683	-0.12095
14	h	x	0.10433	-0.14755	0.08213	0.28360	-0.05438	0.07655
		y	-0.06191	0.05808	-0.04037	-0.11431	-0.01677	-0.02910
		z	0.35881	-0.16963	0.13854	0.29102	0.18901	0.06159
15	c	x	-0.00470	0.04428	-0.02513	0.06245	0.05299	-0.03089
		y	0.06234	0.04086	-0.03216	0.08376	-0.03696	-0.01871
		z	-0.04263	0.00365	0.01069	0.04083	0.06567	-0.00559
16	h	x	-0.10434	-0.14755	0.08213	-0.28361	-0.05436	0.07655
		y	0.06191	0.05808	-0.04037	0.11431	-0.01679	-0.02910
		z	0.35882	0.16962	-0.13854	0.29100	-0.18903	-0.06159
17	h	x	0.04214	0.07811	-0.04880	0.11187	0.03558	-0.04552
		y	-0.15935	-0.14709	0.09479	-0.22151	0.00690	0.07061
		z	0.03807	-0.20213	0.10265	-0.30351	-0.22680	0.12095
18	h	x	0.12045	-0.07354	0.00730	-0.16991	-0.22120	0.05331
		y	-0.24635	-0.05888	0.06369	-0.07839	0.17534	0.01952
		z	-0.24708	0.01747	0.03775	0.08378	0.30027	-0.03019
19	n	x	0.00000	0.21866	0.25711	0.00000	-0.01089	0.04405
		y	0.00000	-0.22373	0.01981	0.00000	0.00438	-0.03651
		z	-0.00005	0.00000	0.00000	0.00023	0.00000	0.00000
20	c	x	0.00000	0.04687	-0.01965	0.00000	-0.00998	-0.06707
		y	0.00000	0.02810	0.00196	0.00000	0.00361	-0.01437
		z	0.00008	0.00000	0.00000	-0.00183	0.00000	0.00000
21	n	x	0.00000	0.11728	-0.13536	0.00000	0.00479	-0.06567
		y	0.00000	0.06722	-0.12198	0.00000	0.00914	0.02428
		z	0.00000	0.00000	0.00000	0.00046	0.00000	0.00000
22	c	x	0.00000	0.04879	-0.10391	0.00000	0.01410	0.20137

		y	0.00000	0.08157	-0.10731	0.00000	0.00668	0.14329
		z	0.00000	0.00000	0.00000	0.00000	0.00000	0.00000
23	h	x	0.00002	0.13293	-0.22501	0.00049	0.02994	0.29575
		y	0.00000	0.10626	-0.15013	-0.00021	0.01236	0.19834
		z	0.00000	-0.00541	0.01379	0.00023	-0.00152	-0.01427
24	h	x	-0.00002	0.13293	-0.22501	-0.00049	0.02994	0.29575
		y	0.00000	0.10626	-0.15013	0.00021	0.01236	0.19834
		z	0.00000	0.00541	-0.01379	0.00023	0.00152	0.01427
25	c	x	0.00000	-0.12267	0.13904	0.00000	-0.01057	-0.05928
		y	0.00000	-0.05563	0.09982	0.00000	-0.00864	-0.18441
		z	0.00001	0.00000	0.00000	0.00014	0.00000	0.00000
26	h	x	0.00001	0.03670	0.05406	0.00020	-0.00544	-0.34780
		y	0.00000	-0.07277	0.12737	0.00023	-0.01158	-0.21966
		z	0.00001	0.02698	-0.02523	-0.00001	0.00231	-0.01196
27	h	x	0.00000	-0.23662	0.22744	0.00000	-0.01654	0.02965
		y	0.00000	-0.32730	0.30582	0.00000	-0.02277	0.04959
		z	0.00000	0.00000	0.00000	-0.00011	0.00000	0.00000
28	h	x	-0.00001	0.03670	0.05406	-0.00020	-0.00544	-0.34780
		y	0.00000	-0.07277	0.12736	-0.00023	-0.01158	-0.21965
		z	0.00001	-0.02697	0.02523	-0.00001	-0.00231	0.01197
29	n	x	0.00000	-0.04662	0.04447	0.00000	-0.01009	-0.06854
		y	0.00000	0.31700	0.13850	0.00000	-0.01386	0.01913
		z	-0.00013	0.00000	0.00000	-0.00091	0.00000	0.00000
30	h	x	0.00000	-0.21793	0.14503	-0.00001	-0.07957	0.29279
		y	0.00000	0.00992	-0.01401	0.00000	0.06524	-0.03965
		z	0.00510	-0.00001	0.00001	-0.03372	0.00000	0.00001
31	h	x	0.00000	0.22473	-0.19248	0.00000	0.01868	-0.28712
		y	0.00000	0.08535	-0.13281	0.00000	0.01148	0.00373
		z	0.00003	0.00000	0.00000	-0.00062	0.00000	0.00000

reduced mass(g/mol)	1.211	5.727	5.792	1.416	1.457	2.688

mode	49	50	51	52	53	54
frequency	1075.82	1131.72	1163.56	1188.10	1206.89	1232.12
symmetry	a	a	a	a	a	a
IR	YES	YES	YES	YES	YES	YES
|dDIP/dQ| (a.u.)	0.0005	0.0007	0.0049	0.0065	0.0033	0.0077
intensity (km/mol)	0.41	0.83	41.86	74.83	19.61	106.73

intensity (%)			0.03	0.07	3.43	6.12	1.61	8.74
RAMAN			YES	YES	YES	YES	YES	YES
(par,par)			0.48	0.30	0.77	3.44	3.45	1.59
(ort,ort)			0.63	0.30	0.98	15.08	3.45	1.59
(ort,unpol)			0.57	0.30	0.89	10.09	3.45	1.59
depol. ratio			0.57	0.75	0.58	0.17	0.75	0.75
1	cl	x	-0.00794	0.00000	-0.00245	0.00028	0.00000	-0.00057
		y	-0.00156	0.00000	0.00237	-0.00138	0.00000	-0.00288
		z	0.00000	-0.00004	0.00000	0.00000	-0.00001	0.00000
2	c	x	0.07360	0.00000	0.00970	-0.00617	0.00000	-0.00438
		y	0.01679	0.00000	-0.03991	0.04206	0.00000	0.05414
		z	0.00000	0.00059	0.00000	0.00000	-0.00019	0.00000
3	n	x	-0.00452	0.00000	-0.02776	0.01616	0.00000	0.03566
		y	-0.15332	0.00000	-0.06097	-0.00118	0.00000	-0.02512
		z	0.00000	0.00071	0.00000	0.00000	0.00135	0.00000
4	c	x	0.01123	0.00000	0.08203	-0.00283	0.00000	-0.05434
		y	0.06406	0.00000	0.08591	-0.02867	0.00000	-0.02616
		z	0.00000	-0.00250	0.00000	0.00000	-0.00754	0.00000
5	n	x	-0.12497	0.00000	-0.01043	0.00737	-0.00001	-0.10922
		y	0.02561	0.00000	0.00835	-0.00734	0.00000	-0.04186
		z	0.00000	0.00023	0.00000	0.00000	-0.02634	0.00000
6	c	x	-0.00301	0.00000	0.04453	-0.25043	0.00001	0.16974
		y	-0.01516	0.00000	-0.08204	0.11410	0.00000	0.25373
		z	0.00000	-0.00037	0.00000	0.00000	0.34331	-0.00001
7	c	x	0.03178	0.00000	-0.00608	0.09372	0.00000	-0.06115
		y	-0.00086	0.00000	0.02503	-0.04077	0.00000	-0.05646
		z	0.00000	0.00026	0.00000	0.00000	-0.13693	0.00000
8	h	x	-0.05465	0.00003	0.04013	-0.24134	-0.06913	0.09549
		y	-0.04626	-0.00084	0.04972	-0.15530	0.38327	-0.10459
		z	0.01822	-0.00023	-0.01139	0.10494	0.11877	-0.09493
9	h	x	0.00448	0.00000	-0.00199	0.02380	0.00000	-0.01195
		y	0.14192	0.00000	0.01881	0.25658	-0.00001	-0.29752
		z	0.00000	-0.00049	0.00000	0.00000	0.35410	-0.00001
10	h	x	-0.05465	-0.00003	0.04012	-0.24134	0.06914	0.09549
		y	-0.04625	0.00084	0.04973	-0.15531	-0.38326	-0.10457
		z	-0.01822	-0.00023	0.01139	-0.10494	0.11878	0.09493
11	c	x	0.03325	0.00007	-0.01661	0.08701	0.01063	-0.04202
		y	0.02509	0.00007	0.03402	-0.03581	-0.01820	-0.07928
		z	-0.00286	0.00014	0.01025	-0.02383	-0.09740	-0.00586
12	h	x	-0.05193	0.00008	0.02738	-0.14401	-0.18202	0.14766

		y	-0.03674	-0.00029	-0.06092	0.02840	0.17321	0.18430
		z	-0.01695	0.00031	0.07173	-0.15584	-0.27887	-0.02960
13	h	x	0.05142	0.00016	0.00009	0.07201	-0.03789	-0.08612
		y	-0.08287	-0.00038	-0.04280	-0.01927	0.15508	0.19129
		z	0.12540	0.00015	-0.07458	0.32510	0.03916	-0.04436
14	h	x	-0.08972	-0.00006	-0.02065	-0.11540	-0.14262	0.19422
		y	0.03628	0.00006	0.03038	-0.01104	0.01337	-0.08839
		z	-0.08309	-0.00038	-0.14103	0.22257	0.06500	0.20632
15	c	x	0.03325	-0.00007	-0.01661	0.08701	-0.01064	-0.04202
		y	0.02509	-0.00007	0.03401	-0.03581	0.01820	-0.07928
		z	0.00286	0.00014	-0.01024	0.02383	-0.09741	0.00587
16	h	x	-0.08972	0.00006	-0.02066	-0.11539	0.14264	0.19422
		y	0.03628	-0.00006	0.03038	-0.01105	-0.01337	-0.08840
		z	0.08308	-0.00038	0.14103	-0.22257	0.06500	-0.20632
17	h	x	0.05142	-0.00016	0.00009	0.07201	0.03789	-0.08612
		y	-0.08286	0.00038	-0.04280	-0.01928	-0.15508	0.19130
		z	-0.12540	0.00015	0.07458	-0.32510	0.03917	0.04436
18	h	x	-0.05193	-0.00008	0.02737	-0.14401	0.18203	0.14766
		y	-0.03673	0.00029	-0.06091	0.02840	-0.17321	0.18431
		z	0.01696	0.00031	-0.07172	0.15583	-0.27888	0.02960
19	n	x	-0.05087	0.00000	0.01619	-0.02008	0.00000	-0.04085
		y	0.16211	0.00000	0.05625	-0.01259	0.00000	0.01306
		z	0.00000	0.00287	0.00000	0.00000	-0.00065	0.00000
20	c	x	0.06540	0.00000	-0.02626	0.00354	0.00000	0.10556
		y	-0.07495	0.00000	-0.03010	-0.01136	0.00000	-0.05603
		z	0.00000	-0.00413	0.00000	0.00000	0.00284	0.00000
21	n	x	-0.03933	0.00000	-0.17143	-0.05354	0.00000	-0.00676
		y	-0.09141	0.00000	0.12648	0.04268	0.00000	0.02051
		z	0.00000	0.04890	0.00000	0.00000	-0.00044	0.00000
22	c	x	0.01314	0.00000	0.19113	0.05522	0.00000	0.05016
		y	0.11701	0.00000	-0.17893	-0.05926	0.00000	-0.04595
		z	0.00000	-0.17474	0.00000	0.00000	-0.00056	0.00000
23	h	x	-0.03928	0.28399	0.26534	0.06811	-0.00199	-0.12358
		y	0.09189	-0.39970	-0.09608	-0.03520	-0.00138	-0.08148
		z	0.01377	0.16056	-0.04404	-0.01468	0.00019	-0.00081
24	h	x	-0.03928	-0.28399	0.26534	0.06811	0.00198	-0.12357
		y	0.09189	0.39970	-0.09608	-0.03520	0.00137	-0.08148
		z	-0.01377	0.16056	0.04404	0.01468	0.00019	0.00081
25	c	x	0.03897	0.00000	-0.07919	-0.02246	0.00000	-0.02206
		y	-0.10748	0.00000	0.06449	0.02204	0.00000	0.03376
		z	0.00000	0.12331	0.00000	0.00000	0.00061	0.00000
26	h	x	-0.30763	0.20563	0.27231	0.08516	0.00076	0.08041

		y	-0.10001	0.34655	0.00457	0.00358	0.00153	-0.00054
		z	-0.04394	-0.11054	0.07380	0.02263	-0.00041	0.03118
27	h	x	0.17944	0.00000	-0.21186	-0.06084	0.00000	-0.07317
		y	0.25085	0.00000	-0.28471	-0.08025	0.00000	-0.09584
		z	0.00000	-0.24534	0.00000	0.00000	-0.00097	0.00000
28	h	x	-0.30763	-0.20563	0.27231	0.08516	-0.00075	0.08041
		y	-0.10001	-0.34655	0.00457	0.00358	-0.00153	-0.00054
		z	0.04394	-0.11054	-0.07380	-0.02263	-0.00041	-0.03118
29	n	x	0.10478	0.00000	0.02885	0.04394	0.00000	0.01933
		y	0.01642	0.00000	-0.03682	0.02621	0.00000	0.06341
		z	0.00000	-0.00018	0.00000	0.00000	0.00136	0.00000
30	h	x	-0.40276	0.00000	-0.38205	0.32505	0.00000	0.16514
		y	0.06005	0.00000	0.05145	-0.04179	0.00000	-0.06917
		z	-0.00001	0.00005	-0.00001	0.00001	0.02129	0.00000
31	h	x	-0.46797	0.00000	-0.37640	-0.19269	-0.00002	-0.44662
		y	-0.14982	0.00000	0.10779	0.02686	0.00000	-0.03590
		z	0.00000	0.10028	0.00000	0.00000	0.00137	0.00000

reduced mass(g/mol)	2.744	1.543	2.929	2.384	2.739	2.876

mode	55	56	57	58	59	60
frequency	1253.61	1280.77	1310.31	1329.24	1344.42	1353.34
symmetry	a	a	a	a	a	a
IR	YES	YES	YES	YES	YES	YES
|dDIP/dQ| (a.u.)	0.0001	0.0055	0.0037	0.0086	0.0024	0.0023
intensity (km/mol)	0.02	53.91	24.36	131.18	9.82	9.24
intensity (%)	0.00	4.41	1.99	10.74	0.80	0.76
RAMAN	YES	YES	YES	YES	YES	YES
(par,par)	4.97	0.99	4.73	2.36	1.08	0.13
(ort,ort)	4.97	3.99	4.86	2.38	1.08	0.22
(ort,unpol)	4.97	2.70	4.80	2.37	1.08	0.18
depol. ratio	0.75	0.19	0.73	0.74	0.75	0.44
1 cl x	0.00000	-0.00078	0.00101	-0.00165	0.00000	0.00026
y	0.00000	0.00383	-0.00230	-0.00407	0.00000	-0.00022
z	-0.00005	0.00000	0.00000	0.00000	-0.00001	0.00000
2 c x	0.00000	0.00282	0.10912	-0.14771	0.00000	0.01421

		y	0.00000	-0.17399	0.10352	0.17801	0.00000	0.03637
		z	-0.00111	0.00000	0.00000	0.00000	-0.00011	0.00000
3	n	x	0.00000	-0.11364	0.00239	0.16069	0.00000	0.00790
		y	0.00000	0.04488	0.00820	-0.18406	0.00000	-0.01269
		z	0.00115	0.00000	0.00000	0.00000	0.00034	0.00000
4	c	x	0.00000	0.11276	-0.08998	0.08066	0.00000	0.02606
		y	0.00000	0.10415	-0.12862	0.11694	0.00000	-0.01771
		z	-0.00127	0.00000	0.00000	0.00000	-0.00161	0.00000
5	n	x	0.00000	-0.02530	-0.06173	0.03195	0.00000	0.00043
		y	0.00000	-0.06486	0.02373	0.00935	0.00000	0.01300
		z	0.00006	0.00000	0.00000	0.00000	0.00088	0.00000
6	c	x	0.00000	0.00835	0.04811	-0.00798	0.00000	0.00459
		y	0.00000	0.18910	-0.02215	0.02267	0.00000	-0.01590
		z	0.00058	0.00000	0.00000	0.00000	0.02319	0.00000
7	c	x	0.00000	0.00979	-0.01742	0.00697	0.00000	0.01576
		y	0.00000	-0.03683	0.00510	0.01278	0.00000	0.09048
		z	-0.00023	0.00000	0.00000	0.00000	-0.00894	0.00000
8	h	x	-0.00038	-0.04233	0.05481	-0.07525	-0.02900	-0.13995
		y	0.00029	-0.12990	0.01969	-0.06356	0.00077	-0.30842
		z	0.00017	-0.02056	-0.02821	0.00462	0.00670	-0.12768
9	h	x	0.00000	0.01217	-0.00945	0.02728	0.00000	0.09111
		y	0.00000	-0.07856	-0.01394	-0.10694	0.00000	-0.36622
		z	0.00101	0.00000	0.00000	0.00000	0.05795	0.00001
10	h	x	0.00038	-0.04233	0.05481	-0.07524	0.02900	-0.13994
		y	-0.00029	-0.12990	0.01969	-0.06355	-0.00076	-0.30840
		z	0.00017	0.02056	0.02821	-0.00462	0.00670	0.12769
11	c	x	0.00005	-0.00564	-0.00666	-0.00248	-0.04132	-0.02946
		y	-0.00001	-0.05020	0.00527	-0.00613	0.03333	0.02915
		z	-0.00015	-0.01052	0.00347	-0.00206	-0.08761	-0.05304
12	h	x	-0.00030	0.09287	0.00282	0.02203	0.28992	0.17219
		y	0.00026	0.09006	0.00993	0.00739	-0.21727	-0.15494
		z	-0.00044	-0.01829	0.00323	0.00577	0.20514	0.13961
13	h	x	-0.00002	-0.03763	-0.00062	-0.00709	-0.00624	0.00566
		y	0.00021	0.12028	-0.01392	0.02168	-0.14929	-0.14720
		z	0.00017	0.08450	-0.03138	0.01469	0.38323	0.23275
14	h	x	-0.00032	0.05459	0.02283	0.00254	0.16722	0.14441
		y	0.00006	-0.04501	0.00137	-0.00507	0.01226	0.01158
		z	-0.00001	0.15671	-0.03744	0.02036	0.34044	0.21509
15	c	x	-0.00005	-0.00564	-0.00666	-0.00248	0.04132	-0.02945
		y	0.00000	-0.05020	0.00527	-0.00613	-0.03333	0.02915
		z	-0.00015	0.01052	-0.00347	0.00206	-0.08761	0.05304
16	h	x	0.00032	0.05460	0.02283	0.00254	-0.16722	0.14440

		y	-0.00006	-0.04502	0.00137	-0.00507	-0.01226	0.01157
		z	-0.00001	-0.15671	0.03744	-0.02036	0.34044	-0.21509
17	h	x	0.00002	-0.03763	-0.00062	-0.00709	0.00624	0.00566
		y	-0.00020	0.12027	-0.01392	0.02168	0.14929	-0.14720
		z	0.00017	-0.08450	0.03138	-0.01469	0.38323	-0.23274
18	h	x	0.00031	0.09287	0.00282	0.02203	-0.28992	0.17218
		y	-0.00026	0.09006	0.00993	0.00738	0.21728	-0.15493
		z	-0.00044	0.01829	-0.00323	-0.00578	0.20514	-0.13961
19	n	x	0.00000	0.10621	-0.09537	-0.02594	0.00000	-0.01960
		y	0.00000	0.09841	-0.10910	-0.00507	0.00000	-0.03926
		z	0.00065	0.00000	0.00000	0.00000	-0.00008	0.00000
20	c	x	0.00000	-0.09999	-0.05443	0.03977	0.00000	-0.03317
		y	0.00000	0.03529	0.04990	-0.20893	0.00000	0.02338
		z	-0.00043	0.00000	0.00000	0.00000	0.00032	0.00000
21	n	x	0.00000	-0.05605	-0.07193	0.02729	0.00000	-0.01131
		y	0.00000	-0.01523	0.04479	0.07532	0.00000	-0.00287
		z	0.03513	0.00000	0.00000	0.00000	-0.00003	0.00000
22	c	x	0.00000	-0.06892	-0.10269	-0.09235	0.00000	0.02323
		y	0.00000	0.01048	-0.05980	-0.02586	0.00000	0.01280
		z	0.01049	0.00000	0.00000	0.00000	-0.00005	0.00000
23	h	x	0.65652	0.35571	0.54057	0.33577	0.00002	-0.08516
		y	0.08600	0.13509	0.20466	0.13243	-0.00006	-0.02727
		z	0.03874	-0.02475	-0.09348	-0.05394	-0.00002	0.01379
24	h	x	-0.65651	0.35573	0.54058	0.33577	-0.00002	-0.08516
		y	-0.08599	0.13509	0.20466	0.13243	0.00006	-0.02727
		z	0.03874	0.02475	0.09347	0.05394	-0.00002	-0.01379
25	c	x	0.00000	0.02415	0.01387	-0.01531	0.00000	0.01897
		y	0.00000	-0.04565	-0.04681	-0.04890	0.00000	0.02696
		z	-0.07871	0.00000	0.00000	0.00000	0.00000	0.00000
26	h	x	-0.09787	-0.04410	0.06146	0.13634	-0.00005	-0.10483
		y	-0.19171	0.03470	0.10010	0.12103	0.00004	-0.08149
		z	0.04803	-0.05771	-0.09065	-0.09404	-0.00004	0.06013
27	h	x	0.00000	0.10737	0.13323	0.11731	0.00000	-0.05375
		y	0.00000	0.15637	0.23372	0.26639	0.00000	-0.14467
		z	0.10534	0.00000	0.00000	0.00000	-0.00015	0.00000
28	h	x	0.09787	-0.04410	0.06146	0.13634	0.00006	-0.10483
		y	0.19172	0.03470	0.10010	0.12103	-0.00004	-0.08149
		z	0.04803	0.05771	0.09065	0.09404	-0.00004	-0.06013
29	n	x	0.00000	0.02933	0.19682	-0.16424	0.00000	0.01588
		y	0.00000	-0.09410	0.04481	0.03056	0.00000	-0.00671
		z	-0.00081	0.00000	0.00000	0.00000	0.00031	0.00000
30	h	x	0.00000	-0.24913	-0.01036	-0.15702	0.00001	-0.19143

		y	0.00000	-0.03563	0.01686	0.03550	0.00000	0.03477
		z	-0.00003	0.00000	0.00000	0.00000	-0.01295	0.00000
31	h	x	0.00000	0.49097	0.17341	0.50747	0.00000	0.12564
		y	0.00000	0.05482	0.08029	0.13667	0.00000	0.01553
		z	0.06527	0.00000	0.00000	0.00000	-0.00002	0.00000

reduced mass(g/mol)	1.093	2.976	2.760	3.703	1.246	1.305

mode	61	62	63	64	65	66
frequency	1358.20	1370.46	1380.96	1408.83	1412.90	1419.08
symmetry	a	a	a	a	a	a
IR	YES	YES	YES	YES	YES	YES
|dDIP/dQ| (a.u.)	0.0076	0.0076	0.0065	0.0007	0.0001	0.0060
intensity (km/mol)	102.81	103.53	75.89	0.85	0.02	62.99
intensity (%)	8.41	8.47	6.21	0.07	0.00	5.16
RAMAN	YES	YES	YES	YES	YES	YES
(par,par)	1.00	0.59	1.12	3.09	0.22	8.29
(ort,ort)	1.04	0.75	1.43	3.17	0.22	8.88
(ort,unpol)	1.03	0.68	1.30	3.14	0.22	8.63
depol. ratio	0.72	0.59	0.59	0.73	0.75	0.70

1	cl	x	0.00025	0.00049	-0.00009	0.00035	0.00000	0.00094
		y	-0.00107	-0.00009	-0.00040	0.00003	0.00000	0.00011
		z	0.00000	0.00000	0.00000	0.00000	-0.00001	0.00000
2	c	x	0.01441	0.02125	0.01138	-0.01156	0.00000	-0.01956
		y	0.08050	0.03030	0.03451	-0.00453	0.00000	0.00824
		z	0.00000	0.00000	0.00000	0.00000	0.00004	0.00000
3	n	x	0.02266	-0.00331	0.00832	0.00028	0.00000	0.00636
		y	-0.03877	0.00222	-0.02313	0.01568	0.00000	0.02060
		z	0.00000	0.00000	0.00000	0.00000	-0.00075	0.00000
4	c	x	0.06342	0.04823	0.02333	0.02221	0.00001	0.06425
		y	-0.01580	-0.03451	0.01148	-0.03709	-0.00001	-0.05882
		z	0.00000	0.00000	0.00000	0.00000	0.00026	0.00000
5	n	x	-0.00899	0.00001	-0.00917	0.00542	0.00000	0.02546
		y	0.00627	0.00900	0.00084	0.01262	0.00000	0.01816
		z	0.00000	0.00000	0.00000	0.00000	0.00018	0.00000
6	c	x	-0.00158	-0.00576	0.00815	0.01089	0.00000	-0.01169

		y	0.05698	0.02657	0.01636	0.00023	0.00000	0.01119
		z	0.00000	0.00000	0.00000	0.00000	0.00517	0.00000
7	c	x	0.00450	0.01493	-0.02522	0.03745	0.00001	-0.01182
		y	-0.03213	0.02504	-0.10235	-0.02540	0.00000	-0.00977
		z	0.00000	0.00000	0.00000	-0.00001	0.03615	0.00000
8	h	x	-0.01447	-0.09926	0.20815	-0.33755	0.28104	0.14602
		y	0.06216	-0.10316	0.31707	0.27772	0.15856	-0.05847
		z	0.05889	-0.00949	0.10305	0.34484	-0.03045	-0.10233
9	h	x	-0.01046	0.04436	-0.11849	0.06929	0.00001	-0.04190
		y	0.05476	-0.15740	0.44948	-0.26833	-0.00005	0.18459
		z	0.00000	0.00001	-0.00003	0.00010	-0.47596	0.00000
10	h	x	-0.01447	-0.09924	0.20812	-0.33744	-0.28114	0.14602
		y	0.06215	-0.10315	0.31706	0.27778	-0.15850	-0.05848
		z	-0.05889	0.00950	-0.10306	-0.34484	-0.03054	0.10233
11	c	x	0.02214	0.01374	-0.02780	-0.02053	0.00982	0.01249
		y	-0.03440	-0.01734	0.01372	-0.00368	-0.02599	-0.00913
		z	0.03659	0.01929	-0.04800	-0.00414	-0.01462	-0.01964
12	h	x	-0.07687	-0.04171	0.20190	0.12476	0.20984	0.11184
		y	0.14344	0.07089	-0.09365	0.15796	0.00733	-0.12653
		z	-0.09666	-0.04914	0.12116	-0.00939	0.07854	0.09343
13	h	x	-0.01820	-0.00830	-0.01362	-0.00454	-0.06991	-0.04396
		y	0.17075	0.09452	-0.07164	-0.07187	0.34134	0.23723
		z	-0.12666	-0.06255	0.24065	0.13679	0.15420	0.08622
14	h	x	-0.12592	-0.07802	0.10918	0.15139	-0.28802	-0.24809
		y	-0.01422	-0.00498	0.00287	-0.02293	0.01386	0.02781
		z	-0.14622	-0.07889	0.17475	-0.11177	-0.03747	0.09980
15	c	x	0.02214	0.01374	-0.02780	-0.02053	-0.00982	0.01246
		y	-0.03441	-0.01734	0.01372	-0.00369	0.02599	-0.00915
		z	-0.03659	-0.01929	0.04800	0.00415	-0.01462	0.01964
16	h	x	-0.12592	-0.07802	0.10919	0.15129	0.28806	-0.24794
		y	-0.01422	-0.00498	0.00286	-0.02292	-0.01387	0.02777
		z	0.14623	0.07889	-0.17474	0.11177	-0.03744	-0.09952
17	h	x	-0.01820	-0.00830	-0.01362	-0.00456	0.06991	-0.04398
		y	0.17075	0.09452	-0.07166	-0.07177	-0.34136	0.23722
		z	0.12666	0.06254	-0.24064	-0.13682	0.15417	-0.08644
18	h	x	-0.07687	-0.04171	0.20190	0.12481	-0.20980	0.11206
		y	0.14344	0.07089	-0.09365	0.15794	-0.00728	-0.12620
		z	0.09666	0.04914	-0.12116	0.00936	0.07854	-0.09339
19	n	x	-0.03511	-0.01792	-0.01666	0.00553	0.00000	0.00165
		y	-0.06792	-0.04811	-0.02645	-0.00907	0.00000	-0.04169
		z	0.00000	0.00000	0.00000	0.00000	0.00012	0.00000
20	c	x	-0.06279	-0.03526	-0.03457	0.02257	0.00001	0.04844

		y	0.02140	0.05565	0.00446	0.03095	0.00001	0.08312
		z	0.00000	0.00000	0.00000	0.00000	-0.00001	0.00000
21	n	x	-0.02656	-0.01053	-0.01863	0.01787	0.00000	0.04432
		y	0.00277	-0.02528	-0.00356	-0.00590	0.00000	-0.01500
		z	0.00000	0.00000	0.00000	0.00000	0.00000	0.00000
22	c	x	0.03087	0.08136	0.04243	-0.02353	-0.00001	-0.04904
		y	0.01765	0.05528	0.02885	-0.01691	0.00000	-0.03840
		z	0.00000	0.00000	0.00000	0.00000	-0.00002	0.00000
23	h	x	-0.11158	-0.26357	-0.13049	0.06238	0.00030	0.11712
		y	-0.03467	-0.08196	-0.04465	0.03673	0.00002	0.10221
		z	0.01794	0.05291	0.02970	-0.02628	-0.00001	-0.07624
24	h	x	-0.11158	-0.26357	-0.13049	0.06238	-0.00027	0.11712
		y	-0.03467	-0.08196	-0.04465	0.03673	0.00000	0.10221
		z	-0.01794	-0.05291	-0.02970	0.02628	0.00001	0.07624
25	c	x	0.05624	-0.10102	-0.02545	0.00931	0.00000	0.02008
		y	0.06675	-0.07971	-0.01313	-0.00113	0.00000	-0.00657
		z	0.00000	0.00000	0.00000	0.00000	-0.00004	0.00000
26	h	x	-0.27602	0.37344	0.07620	-0.02403	0.00011	-0.05679
		y	-0.19432	0.15007	-0.00424	0.03886	-0.00004	0.11392
		z	0.14185	-0.10616	0.00508	-0.03164	0.00000	-0.09276
27	h	x	-0.12345	0.11468	0.01435	-0.00084	0.00000	-0.00486
		y	-0.35779	0.43320	0.08191	-0.02435	-0.00001	-0.06229
		z	0.00000	0.00000	0.00000	0.00000	0.00021	0.00000
28	h	x	-0.27602	0.37344	0.07620	-0.02403	-0.00012	-0.05679
		y	-0.19432	0.15007	-0.00424	0.03886	0.00006	0.11392
		z	-0.14185	0.10616	-0.00508	0.03164	0.00002	0.09276
29	n	x	0.02272	0.00953	0.01558	-0.02613	-0.00001	-0.07369
		y	-0.01269	-0.01534	-0.00922	0.00028	0.00000	-0.00804
		z	0.00000	0.00000	0.00000	0.00000	0.00006	0.00000
30	h	x	-0.38507	-0.32589	-0.06045	-0.17646	-0.00005	-0.42611
		y	0.04953	0.04478	0.00953	0.03264	0.00001	0.06701
		z	-0.00001	-0.00001	0.00000	0.00000	0.00521	0.00000
31	h	x	0.32815	0.08330	0.21294	-0.20348	-0.00005	-0.45172
		y	0.05022	-0.01477	0.02565	-0.03331	-0.00001	-0.07565
		z	0.00000	0.00000	0.00000	0.00000	0.00005	0.00000

reduced mass(g/mol)	1.510	1.484	1.310	1.111	1.044	1.406

mode	67	68	69	70	71	72
frequency	1419.67	1433.41	1439.52	1444.30	1446.10	1450.84

symmetry		a	a	a	a	a	a
IR		YES	YES	YES	YES	YES	YES
|dDIP/dQ| (a.u.)		0.0003	0.0024	0.0019	0.0009	0.0079	0.0033
intensity (km/mol)		0.13	9.94	6.28	1.58	111.10	19.37
intensity (%)		0.01	0.81	0.51	0.13	9.09	1.59
RAMAN		YES	YES	YES	YES	YES	YES
(par,par)		7.47	7.64	4.48	3.61	6.91	0.82
(ort,ort)		7.47	7.64	4.48	3.65	7.03	2.11
(ort,unpol)		7.47	7.64	4.48	3.64	6.98	1.56
depol. ratio		0.75	0.75	0.75	0.74	0.74	0.29
1	cl	x	0.00000	0.00000	0.00000	0.00015	-0.00042	0.00011
		y	0.00000	0.00000	0.00000	0.00000	-0.00015	0.00020
		z	0.00001	0.00003	0.00002	0.00000	0.00000	0.00000
2	c	x	-0.00001	0.00000	0.00000	-0.00767	0.01671	-0.00282
		y	0.00000	0.00000	0.00000	0.01161	-0.00564	0.00145
		z	-0.00003	0.00004	0.00013	0.00000	0.00000	0.00000
3	n	x	0.00000	0.00000	0.00000	0.00604	-0.00458	0.00254
		y	0.00001	0.00000	0.00000	-0.00751	-0.00433	-0.00119
		z	0.00003	-0.00002	0.00101	0.00000	0.00000	0.00000
4	c	x	0.00002	0.00000	0.00000	0.02814	-0.05662	0.00630
		y	-0.00002	0.00000	0.00000	-0.00269	0.02492	0.00306
		z	-0.00107	-0.00010	-0.00036	0.00000	0.00000	0.00000
5	n	x	0.00001	0.00000	0.00000	-0.00683	0.01044	0.01420
		y	0.00000	0.00000	0.00000	0.00155	-0.00811	0.00273
		z	0.00027	0.00001	0.00318	0.00000	0.00000	0.00000
6	c	x	0.00000	0.00000	0.00000	-0.01067	0.00998	-0.05480
		y	0.00000	0.00000	0.00000	0.03140	-0.04848	-0.01818
		z	0.00755	0.00004	-0.04924	0.00000	0.00000	0.00000
7	c	x	0.00000	0.00000	0.00000	-0.00521	0.00473	-0.01164
		y	0.00000	0.00000	0.00000	-0.01040	0.01920	0.01780
		z	-0.00332	0.00001	-0.03043	0.00000	0.00000	0.00000
8	h	x	-0.02505	-0.00003	-0.31537	0.05820	-0.05670	0.17698
		y	-0.01495	0.00000	-0.20638	-0.02342	0.00528	-0.16408
		z	0.00416	0.00002	0.02789	-0.03817	0.02253	-0.19094
9	h	x	-0.00001	0.00000	0.00000	-0.02076	0.02513	-0.03865
		y	0.00006	0.00000	0.00001	0.07748	-0.09092	0.18838
		z	0.04565	0.00008	0.51840	0.00002	-0.00001	0.00002
10	h	x	0.02515	0.00003	0.31538	0.05823	-0.05671	0.17701

		y	0.01490	0.00000	0.20640	-0.02341	0.00527	-0.16406
		z	0.00423	0.00002	0.02788	0.03818	-0.02253	0.19094
11	c	x	-0.03260	-0.00007	0.01402	-0.00306	-0.00034	-0.01788
		y	-0.02116	-0.00003	-0.02170	0.01092	-0.01856	-0.01592
		z	0.00863	0.00000	0.00180	0.01040	-0.01100	0.01341
12	h	x	0.25323	0.00035	0.16169	-0.15919	0.25357	0.17576
		y	0.41832	0.00066	-0.02571	0.00924	0.05839	0.36893
		z	-0.05441	-0.00012	0.08380	-0.07216	0.08724	-0.06889
13	h	x	-0.02115	0.00000	-0.05474	0.04873	-0.06939	-0.00270
		y	-0.05232	-0.00030	0.31022	-0.22766	0.30459	-0.07952
		z	0.26015	0.00042	0.08722	-0.10900	0.18472	0.22460
14	h	x	0.23751	0.00057	-0.27968	0.20029	-0.23946	0.20274
		y	-0.05037	-0.00009	0.01566	-0.01495	0.01150	-0.04428
		z	-0.35278	-0.00055	-0.03548	0.03967	-0.11909	-0.32328
15	c	x	0.03261	0.00007	-0.01402	-0.00306	-0.00034	-0.01788
		y	0.02116	0.00003	0.02170	0.01093	-0.01856	-0.01592
		z	0.00864	0.00000	0.00180	-0.01040	0.01100	-0.01341
16	h	x	-0.23765	-0.00057	0.27963	0.20031	-0.23946	0.20276
		y	0.05038	0.00009	-0.01565	-0.01496	0.01151	-0.04428
		z	-0.35284	-0.00055	-0.03551	-0.03967	0.11909	0.32328
17	h	x	0.02112	0.00000	0.05473	0.04873	-0.06939	-0.00270
		y	0.05246	0.00030	-0.31018	-0.22767	0.30459	-0.07955
		z	0.26010	0.00042	0.08723	0.10900	-0.18472	-0.22460
18	h	x	-0.25317	-0.00035	-0.16169	-0.15920	0.25357	0.17575
		y	-0.41839	-0.00066	0.02567	0.00924	0.05839	0.36894
		z	-0.05446	-0.00012	0.08378	0.07217	-0.08724	0.06889
19	n	x	0.00000	0.00000	0.00000	-0.00156	-0.00384	-0.00011
		y	-0.00001	0.00000	0.00000	-0.01637	0.02130	-0.00730
		z	-0.00003	-0.00005	-0.00011	0.00000	0.00000	0.00000
20	c	x	0.00001	0.00000	0.00000	-0.00713	-0.02301	0.00357
		y	0.00002	0.00000	0.00000	0.02153	-0.04887	0.01353
		z	0.00016	0.00068	-0.00028	0.00000	0.00000	0.00000
21	n	x	0.00001	0.00000	0.00000	-0.00349	-0.00820	0.00812
		y	0.00000	0.00000	0.00000	0.00321	0.01967	-0.00374
		z	0.00000	0.00175	0.00002	0.00000	0.00000	0.00000
22	c	x	-0.00001	0.00000	0.00000	0.01560	0.01963	-0.00540
		y	-0.00001	0.00000	0.00000	0.00970	0.02474	-0.00782
		z	0.00001	-0.02190	0.00001	0.00000	0.00000	0.00000
23	h	x	0.00003	-0.01997	-0.00042	0.02080	0.01130	-0.00348
		y	0.00009	-0.04001	-0.00003	-0.15108	-0.20835	0.05004
		z	-0.00007	0.00119	-0.00001	0.11151	0.15919	-0.04005
24	h	x	0.00004	0.01997	0.00042	0.02080	0.01130	-0.00348

		y	-0.00004	0.04002	0.00003	-0.15108	-0.20835	0.05004
		z	-0.00003	0.00119	-0.00001	-0.11151	-0.15919	0.04005
25	c	x	0.00001	0.00000	0.00000	0.02213	0.00906	-0.00067
		y	0.00000	0.00000	0.00000	-0.03319	-0.01854	0.00244
		z	0.00006	-0.04623	0.00001	0.00000	0.00000	0.00000
26	h	x	-0.00085	0.49730	0.00019	-0.16086	-0.09386	0.01245
		y	0.00010	-0.03008	0.00004	0.38533	0.23050	-0.02693
		z	-0.00015	0.04489	0.00000	-0.30990	-0.18305	0.02154
27	h	x	0.00000	0.00000	0.00000	-0.08566	-0.06119	0.00852
		y	-0.00002	0.00000	0.00000	-0.26993	-0.17295	0.02237
		z	-0.00123	0.70195	0.00017	0.00001	0.00000	0.00000
28	h	x	0.00082	-0.49729	-0.00018	-0.16087	-0.09387	0.01245
		y	-0.00003	0.03007	-0.00006	0.38534	0.23050	-0.02693
		z	-0.00010	0.04489	-0.00001	0.30990	0.18305	-0.02154
29	n	x	-0.00002	0.00000	0.00000	-0.00511	0.03345	-0.01162
		y	0.00000	0.00000	0.00000	-0.00733	0.00952	-0.00397
		z	0.00024	-0.00002	-0.00027	0.00000	0.00000	0.00000
30	h	x	-0.00012	0.00000	0.00001	-0.08080	0.18080	-0.01579
		y	0.00002	0.00000	0.00000	0.01099	-0.02809	0.00597
		z	-0.01106	-0.00018	0.01296	0.00000	0.00000	0.00000
31	h	x	-0.00013	0.00000	0.00001	-0.02835	0.12092	-0.05781
		y	-0.00002	0.00000	0.00000	0.00021	0.03484	-0.01178
		z	-0.00041	-0.01385	-0.00007	0.00000	0.00000	0.00000

reduced mass(g/mol)	1.044	1.037	1.060	1.071	1.173	1.077

mode	73	74	75	76	77	78
frequency	1469.97	1511.60	1547.33	1598.13	1611.09	2935.17
symmetry	a	a	a	a	a	a
IR	YES	YES	YES	YES	YES	YES
|dDIP/dQ| (a.u.)	0.0031	0.0117	0.0161	0.0262	0.0192	0.0031
intensity (km/mol)	16.89	243.24	458.70	1221.85	655.66	17.38
intensity (%)	1.38	19.91	37.54	100.00	53.66	1.42
RAMAN	YES	YES	YES	YES	YES	YES
(par,par)	5.10	2.84	0.19	2.85	6.85	0.42
(ort,ort)	9.11	3.71	2.34	12.07	23.13	0.42
(ort,unpol)	7.39	3.34	1.42	8.12	16.16	0.42

	depol. ratio		0.42	0.57	0.06	0.18	0.22	0.75
1	cl	x	-0.00029	0.00202	-0.00085	0.00119	-0.00134	0.00000
		y	0.00038	0.00053	0.00807	0.00309	0.00290	0.00000
		z	0.00000	0.00000	0.00000	0.00000	0.00000	0.00000
2	c	x	0.01540	-0.31388	0.01713	-0.27943	0.21048	0.00000
		y	-0.00262	-0.02499	0.03487	-0.05688	-0.04552	0.00000
		z	0.00000	0.00000	0.00000	0.00000	0.00000	-0.00001
3	n	x	-0.00517	0.12142	0.06318	0.16725	-0.07613	0.00000
		y	-0.00732	-0.01069	-0.18517	-0.06395	0.05182	0.00000
		z	0.00000	0.00000	0.00000	0.00000	0.00000	-0.00001
4	c	x	-0.01149	0.15796	-0.02975	-0.36226	-0.13299	0.00000
		y	0.02805	-0.16187	0.37498	-0.00053	0.07480	0.00000
		z	0.00000	0.00000	0.00000	0.00000	0.00000	0.00016
5	n	x	-0.00464	-0.22455	-0.00811	0.23103	0.14582	0.00000
		y	-0.00655	0.09450	-0.07159	-0.05400	-0.04686	0.00000
		z	0.00000	0.00000	0.00000	0.00000	0.00000	-0.00006
6	c	x	0.00549	0.03677	0.02326	-0.01870	-0.03105	0.00000
		y	-0.00805	-0.07984	-0.00068	0.05470	0.02215	0.00000
		z	0.00000	0.00000	0.00000	0.00000	0.00000	-0.00197
7	c	x	0.00199	-0.01364	0.00369	0.00171	0.01057	0.00000
		y	0.00345	0.01992	0.00646	-0.01409	-0.00423	0.00000
		z	0.00000	0.00000	0.00000	0.00000	0.00000	-0.00021
8	h	x	-0.02683	0.02285	-0.07826	0.01264	-0.02442	0.00056
		y	0.00983	0.00600	0.01812	-0.00580	-0.00646	-0.00194
		z	0.01721	-0.02290	0.04353	0.00139	0.01367	0.00172
9	h	x	0.00865	0.00348	0.02277	-0.01001	0.00020	0.00000
		y	-0.03688	-0.03757	-0.10950	0.04786	0.01174	0.00000
		z	0.00000	0.00000	0.00000	0.00000	0.00000	-0.00011
10	h	x	-0.02683	0.02285	-0.07826	0.01264	-0.02442	-0.00056
		y	0.00982	0.00601	0.01812	-0.00580	-0.00646	0.00194
		z	-0.01721	0.02290	-0.04353	-0.00139	-0.01367	0.00172
11	c	x	0.00066	0.01470	-0.00495	-0.01562	-0.00391	0.01420
		y	-0.00106	0.00788	-0.00548	-0.00689	-0.00263	-0.02184
		z	-0.00072	-0.00032	0.00262	-0.00166	-0.00136	0.02536
12	h	x	0.01599	0.04698	0.01324	-0.00561	-0.00493	0.14955
		y	-0.00549	0.00693	0.00172	-0.00978	0.00391	-0.13938
		z	0.00941	0.01431	0.00889	0.00723	-0.00356	-0.28436
13	h	x	-0.00657	-0.00136	-0.01289	-0.00777	-0.00248	-0.37379
		y	0.03331	0.06106	0.05378	-0.01202	-0.01416	-0.08108
		z	0.00529	0.06963	-0.03225	-0.04639	-0.00334	-0.00326
14	h	x	-0.03208	-0.09896	-0.03030	0.05221	0.02124	0.05719

		y	0.00250	0.01563	-0.00398	-0.00906	-0.00270	0.47592
		z	-0.00548	-0.08517	-0.00554	0.05775	0.01734	-0.00434
15	c	x	0.00066	0.01470	-0.00495	-0.01562	-0.00391	-0.01420
		y	-0.00106	0.00788	-0.00548	-0.00689	-0.00263	0.02184
		z	0.00072	0.00032	-0.00262	0.00166	0.00136	0.02535
16	h	x	-0.03208	-0.09896	-0.03030	0.05221	0.02124	-0.05718
		y	0.00250	0.01563	-0.00398	-0.00907	-0.00270	-0.47585
		z	0.00548	0.08517	0.00554	-0.05775	-0.01734	-0.00433
17	h	x	-0.00657	-0.00136	-0.01289	-0.00777	-0.00248	0.37373
		y	0.03331	0.06106	0.05378	-0.01202	-0.01416	0.08107
		z	-0.00529	-0.06963	0.03225	0.04639	0.00334	-0.00326
18	h	x	0.01599	0.04698	0.01324	-0.00560	-0.00493	-0.14953
		y	-0.00549	0.00693	0.00172	-0.00978	0.00391	0.13936
		z	-0.00941	-0.01431	-0.00889	-0.00723	0.00356	-0.28432
19	n	x	-0.00455	0.11503	-0.05301	0.11187	-0.13137	0.00000
		y	0.00394	0.02693	-0.18388	0.06968	-0.05134	0.00000
		z	0.00000	0.00000	0.00000	0.00000	0.00000	0.00001
20	c	x	-0.01049	0.17536	-0.02899	-0.01596	0.45684	0.00000
		y	-0.01271	0.19387	0.32787	0.09500	0.05485	0.00000
		z	0.00000	0.00000	0.00000	0.00000	0.00000	-0.00002
21	n	x	-0.00874	-0.22510	0.01264	-0.05080	-0.27066	0.00000
		y	-0.00919	-0.09969	-0.05850	-0.03615	-0.07086	0.00000
		z	0.00000	0.00000	0.00000	0.00000	0.00000	0.00000
22	c	x	0.05273	0.04484	-0.02893	0.02446	0.02779	0.00000
		y	-0.05894	0.02207	0.00803	0.00092	0.01412	0.00000
		z	0.00000	0.00000	0.00000	0.00000	0.00000	-0.00004
23	h	x	-0.26943	0.03203	0.10229	-0.04618	0.07159	-0.00004
		y	0.43046	0.00867	-0.01329	0.03697	-0.02203	0.00018
		z	-0.38756	0.02610	0.04163	-0.03437	0.05497	0.00025
24	h	x	-0.26943	0.03204	0.10229	-0.04618	0.07159	0.00004
		y	0.43046	0.00867	-0.01329	0.03697	-0.02203	-0.00018
		z	0.38756	-0.02610	-0.04163	0.03437	-0.05497	0.00025
25	c	x	0.00588	0.01407	0.00514	-0.00067	0.01569	0.00000
		y	-0.01512	-0.01519	-0.00445	-0.00197	-0.00939	0.00000
		z	0.00000	0.00000	0.00000	0.00000	0.00000	-0.00001
26	h	x	-0.06031	-0.05683	0.00388	-0.00088	-0.04939	-0.00001
		y	0.18081	-0.00031	-0.03440	-0.00550	-0.00182	0.00004
		z	-0.14446	-0.01723	0.01927	0.00318	-0.01039	0.00006
27	h	x	-0.04591	0.01700	0.03035	0.00091	0.01569	0.00000
		y	-0.13756	-0.00416	0.05796	-0.00341	-0.00315	0.00000
		z	0.00000	0.00000	0.00000	0.00000	0.00000	0.00000
28	h	x	-0.06031	-0.05683	0.00388	-0.00088	-0.04939	0.00001

		y	0.18081	-0.00031	-0.03440	-0.00550	-0.00182	-0.00004
		z	0.14446	0.01723	-0.01927	-0.00318	0.01039	0.00006
29	n	x	0.01121	0.02800	0.01121	0.17736	-0.16417	0.00000
		y	-0.00384	0.00385	-0.13473	0.01797	0.02563	0.00000
		z	0.00000	0.00000	0.00000	0.00000	0.00000	-0.00003
30	h	x	0.11337	0.60252	0.61067	-0.77311	-0.30264	0.00000
		y	-0.01951	0.00126	-0.13285	0.05895	-0.00172	0.00000
		z	0.00000	0.00001	0.00001	-0.00001	0.00000	0.00174
31	h	x	0.13283	0.43054	-0.41343	0.01208	0.66200	0.00000
		y	0.00776	-0.02043	-0.10711	-0.03358	0.04067	0.00000
		z	0.00000	0.00000	0.00000	0.00000	0.00000	0.00004

reduced mass(g/mol)	1.103	5.488	5.119	5.339	6.187	1.037

mode	79	80	81	82	83	84
frequency	2939.41	2942.64	2948.02	2962.13	2981.14	3017.25
symmetry	a	a	a	a	a	a
IR	YES	YES	YES	YES	YES	YES
|dDIP/dQ| (a.u.)	0.0040	0.0038	0.0038	0.0035	0.0022	0.0010
intensity (km/mol)	28.72	26.20	25.49	22.20	8.70	1.72
intensity (%)	2.35	2.14	2.09	1.82	0.71	0.14
RAMAN	YES	YES	YES	YES	YES	YES
(par,par)	0.80	0.44	1.53	4.11	10.66	1.29
(ort,ort)	45.75	58.05	8.85	41.02	10.66	1.29
(ort,unpol)	26.49	33.36	5.71	25.20	10.66	1.29
depol. ratio	0.01	0.01	0.13	0.08	0.75	0.75
1 cl	x	0.00000	0.00000	-0.00001	-0.00001	0.00000	0.00000
	y	0.00001	0.00002	0.00002	0.00001	0.00000	0.00000
	z	0.00000	0.00000	0.00000	0.00000	0.00000	0.00000
2 c	x	0.00018	-0.00019	-0.00008	0.00009	0.00000	0.00000
	y	-0.00008	-0.00012	0.00001	-0.00011	0.00000	0.00000
	z	0.00000	0.00000	0.00000	0.00000	-0.00011	-0.00002
3 n	x	-0.00016	0.00009	0.00001	0.00023	0.00000	0.00000
	y	0.00013	0.00004	0.00008	0.00022	0.00000	0.00000
	z	0.00000	0.00000	0.00000	0.00000	0.00005	-0.00002
4 c	x	0.00038	-0.00025	-0.00018	0.00022	0.00000	0.00000

		y	-0.00040	-0.00010	-0.00018	-0.00022	0.00000	0.00000
		z	0.00000	0.00000	0.00000	0.00000	-0.00006	0.00015
5	n	x	-0.00016	0.00011	0.00004	0.00040	0.00000	0.00000
		y	0.00016	0.00001	0.00002	-0.00003	0.00000	0.00000
		z	0.00000	0.00000	0.00000	0.00000	0.00001	0.00007
6	c	x	0.00143	-0.00002	-0.00002	-0.00049	0.00000	0.00000
		y	-0.00029	-0.00003	-0.00001	0.00141	0.00000	0.00000
		z	0.00000	0.00000	0.00000	0.00000	0.00000	0.00000
7	c	x	0.00407	0.00034	0.00016	-0.03543	0.00000	0.00000
		y	0.00464	0.00026	0.00014	-0.04262	0.00000	0.00000
		z	0.00000	0.00000	0.00000	0.00000	-0.00001	-0.00051
8	h	x	0.02351	0.00105	0.00052	-0.17941	0.00002	-0.00021
		y	-0.02013	-0.00103	-0.00057	0.17486	-0.00001	0.00027
		z	0.04312	0.00211	0.00109	-0.33845	0.00002	0.00101
9	h	x	-0.09716	-0.00611	-0.00299	0.77921	0.00000	0.00000
		y	-0.01669	-0.00108	-0.00053	0.13650	0.00000	0.00000
		z	0.00000	0.00000	0.00000	0.00000	-0.00002	0.00143
10	h	x	0.02351	0.00105	0.00052	-0.17941	-0.00002	0.00020
		y	-0.02013	-0.00103	-0.00057	0.17486	0.00001	-0.00027
		z	-0.04312	-0.00211	-0.00109	0.33845	0.00002	0.00101
11	c	x	-0.01413	-0.00029	0.00001	-0.00016	-0.00001	0.03250
		y	0.02146	0.00055	0.00008	0.00432	0.00002	0.05515
		z	-0.02585	-0.00066	-0.00007	-0.00362	0.00000	0.01493
12	h	x	-0.14888	-0.00385	-0.00040	-0.01879	0.00000	0.09996
		y	0.13831	0.00355	0.00035	0.01755	0.00002	-0.07618
		z	0.28739	0.00735	0.00072	0.03777	0.00001	-0.18111
13	h	x	0.36841	0.00876	0.00056	0.02728	0.00019	-0.43275
		y	0.07994	0.00188	0.00012	0.00549	0.00004	-0.08196
		z	0.00299	0.00011	0.00002	0.00095	0.00001	-0.00369
14	h	x	-0.05613	-0.00144	-0.00019	-0.00690	-0.00003	-0.05463
		y	-0.47050	-0.01188	-0.00139	-0.07269	-0.00027	-0.50003
		z	0.00616	0.00014	0.00002	0.00226	0.00000	0.00866
15	c	x	-0.01413	-0.00029	0.00001	-0.00016	0.00001	-0.03250
		y	0.02147	0.00055	0.00008	0.00432	-0.00002	-0.05515
		z	0.02586	0.00066	0.00007	0.00362	0.00000	0.01493
16	h	x	-0.05613	-0.00144	-0.00019	-0.00690	0.00003	0.05463
		y	-0.47057	-0.01188	-0.00139	-0.07269	0.00027	0.50001
		z	-0.00615	-0.00014	-0.00002	-0.00226	0.00000	0.00866
17	h	x	0.36847	0.00876	0.00056	0.02728	-0.00019	0.43274
		y	0.07995	0.00188	0.00012	0.00549	-0.00004	0.08195
		z	-0.00299	-0.00011	-0.00002	-0.00095	0.00001	-0.00369
18	h	x	-0.14890	-0.00385	-0.00040	-0.01879	0.00000	-0.09995

		y	0.13833	0.00355	0.00035	0.01755	-0.00002	0.07618
		z	-0.28743	-0.00735	-0.00072	-0.03777	0.00001	-0.18110
19	n	x	-0.00009	0.00006	-0.00006	-0.00005	0.00000	0.00000
		y	-0.00003	0.00033	0.00051	0.00004	0.00000	0.00000
		z	0.00000	0.00000	0.00000	0.00000	0.00020	0.00001
20	c	x	0.00021	-0.00080	-0.00139	0.00018	0.00000	0.00000
		y	0.00003	-0.00111	-0.00177	-0.00004	0.00000	0.00000
		z	0.00000	0.00000	0.00000	0.00000	0.00033	-0.00001
21	n	x	-0.00013	0.00112	0.00280	-0.00007	0.00000	0.00000
		y	-0.00003	0.00074	0.00114	0.00000	0.00000	0.00000
		z	0.00000	0.00000	0.00000	0.00000	0.00094	0.00000
22	c	x	-0.00009	0.00349	0.01093	0.00008	0.00000	0.00000
		y	0.00092	-0.02985	-0.06090	-0.00032	0.00000	0.00000
		z	0.00000	0.00000	0.00000	0.00000	-0.09117	0.00001
23	h	x	0.00098	-0.03315	-0.07373	-0.00043	-0.07571	0.00001
		y	-0.00533	0.17181	0.35986	0.00185	0.40330	-0.00005
		z	-0.00769	0.24573	0.51588	0.00259	0.53768	-0.00007
24	h	x	0.00098	-0.03315	-0.07373	-0.00043	0.07570	-0.00001
		y	-0.00533	0.17181	0.35986	0.00185	-0.40328	0.00005
		z	0.00769	-0.24573	-0.51589	-0.00259	0.53766	-0.00007
25	c	x	-0.00050	0.02092	-0.01471	0.00001	0.00000	0.00000
		y	-0.00105	0.04373	-0.01596	0.00015	0.00000	0.00000
		z	0.00000	0.00000	0.00000	0.00000	0.02612	0.00001
26	h	x	-0.00133	0.05587	-0.02474	0.00017	0.02182	0.00001
		y	0.00783	-0.32721	0.14923	-0.00090	-0.11231	-0.00004
		z	0.01138	-0.47423	0.21114	-0.00130	-0.15782	-0.00005
27	h	x	0.00827	-0.34904	0.22082	-0.00048	0.00000	0.00000
		y	-0.00354	0.14852	-0.09881	0.00016	0.00000	0.00000
		z	0.00000	0.00000	0.00000	0.00000	0.00594	0.00000
28	h	x	-0.00133	0.05587	-0.02474	0.00017	-0.02182	-0.00001
		y	0.00783	-0.32721	0.14923	-0.00090	0.11231	0.00004
		z	-0.01138	0.47423	-0.21114	0.00130	-0.15782	-0.00005
29	n	x	-0.00029	0.00042	0.00044	-0.00024	0.00000	0.00000
		y	-0.00002	0.00011	0.00018	0.00001	0.00000	0.00000
		z	0.00000	0.00000	0.00000	0.00000	-0.00015	0.00001
30	h	x	-0.00359	-0.00029	-0.00023	-0.00157	0.00000	0.00000
		y	0.00016	-0.00020	0.00014	0.00211	0.00000	0.00000
		z	0.00000	0.00000	0.00000	0.00000	-0.00007	-0.00335
31	h	x	0.00002	0.00292	-0.00342	0.00012	0.00000	0.00000
		y	-0.00016	-0.00470	-0.00770	-0.00026	0.00000	0.00000
		z	0.00000	0.00000	0.00000	0.00000	-0.00680	-0.00002

reduced mass(g/mol)		1.038	1.044	1.055	1.042	1.107	1.103
mode		85	86	87	88	89	90
frequency		3022.03	3025.09	3037.62	3039.24	3046.06	3051.75
symmetry		a	a	a	a	a	a
IR		YES	YES	YES	YES	YES	YES
|dDIP/dQ| (a.u.)		0.0049	0.0041	0.0023	0.0035	0.0029	0.0046
intensity (km/mol)		43.10	29.77	9.27	21.23	15.46	37.71
intensity (%)		3.53	2.44	0.76	1.74	1.27	3.09
RAMAN		YES	YES	YES	YES	YES	YES
(par,par)		17.68	6.30	3.70	13.99	13.10	14.02
(ort,ort)		22.25	6.30	3.70	17.00	16.60	14.07
(ort,unpol)		20.29	6.30	3.70	15.71	15.10	14.05
depol. ratio		0.60	0.75	0.75	0.62	0.59	0.75
1	cl	x	0.00000	0.00000	0.00000	0.00000	0.00000	0.00001
		y	0.00001	0.00000	0.00000	-0.00001	0.00001	-0.00004
		z	0.00000	0.00000	0.00000	0.00000	0.00000	0.00000
2	c	x	0.00000	0.00000	0.00000	0.00000	-0.00004	-0.00048
		y	-0.00007	0.00000	0.00000	0.00000	-0.00005	0.00043
		z	0.00000	-0.00005	0.00001	0.00000	0.00000	0.00000
3	n	x	-0.00003	0.00000	0.00000	-0.00012	0.00002	0.00095
		y	0.00023	0.00000	0.00000	-0.00015	0.00002	-0.00005
		z	0.00000	0.00002	-0.00001	0.00000	0.00000	0.00000
4	c	x	0.00057	0.00000	0.00000	-0.00057	-0.00007	0.00002
		y	-0.00038	0.00000	0.00000	0.00037	-0.00004	-0.00055
		z	0.00000	-0.00003	0.00000	0.00000	0.00000	0.00000
5	n	x	-0.00020	0.00000	0.00000	-0.00018	0.00002	-0.00066
		y	0.00055	0.00000	0.00000	-0.00012	0.00000	-0.00039
		z	0.00000	0.00001	-0.00046	0.00000	0.00000	0.00000
6	c	x	-0.00095	0.00000	0.00000	0.00172	-0.00001	0.00214
		y	-0.00251	0.00000	0.00000	-0.00060	0.00000	0.00050
		z	0.00000	0.00000	0.00158	0.00000	0.00000	0.00000
7	c	x	0.00174	0.00000	0.00000	-0.01788	0.00044	0.08272
		y	-0.00189	0.00000	0.00000	0.00783	-0.00019	-0.03118
		z	0.00000	0.00001	-0.00327	0.00000	0.00000	0.00000
8	h	x	-0.01243	-0.00001	0.01052	0.05099	-0.00128	-0.21840

		y	0.01373	0.00002	-0.00844	-0.05406	0.00135	0.23564
		z	-0.02357	-0.00003	0.01800	0.10755	-0.00259	-0.45292
9	h	x	0.00684	0.00000	-0.00003	0.11006	-0.00278	-0.56379
		y	0.00341	0.00000	0.00000	0.01827	-0.00050	-0.10229
		z	0.00000	0.00000	-0.00043	0.00000	0.00000	0.00000
10	h	x	-0.01243	0.00001	-0.01054	0.05098	-0.00128	-0.21839
		y	0.01373	-0.00002	0.00847	-0.05406	0.00135	0.23564
		z	0.02357	-0.00003	0.01805	-0.10753	0.00259	0.45289
11	c	x	-0.02764	-0.00008	-0.05089	0.05202	-0.00011	0.01194
		y	-0.05622	0.00004	0.01959	-0.01438	-0.00003	-0.00138
		z	-0.01854	0.00005	0.03786	-0.03552	0.00003	-0.00741
12	h	x	-0.12040	0.00034	0.23780	-0.22232	0.00020	-0.04470
		y	0.09765	-0.00030	-0.22120	0.20713	-0.00021	0.04202
		z	0.22446	-0.00066	-0.47192	0.44032	-0.00042	0.09107
13	h	x	0.39469	0.00062	0.38791	-0.41746	0.00116	-0.10417
		y	0.07327	0.00013	0.08428	-0.09004	0.00024	-0.02096
		z	0.00315	0.00002	0.00906	-0.01084	0.00002	-0.00345
14	h	x	0.05567	-0.00004	-0.01874	0.01476	0.00001	0.00043
		y	0.50592	-0.00032	-0.09539	0.05553	0.00040	-0.00323
		z	-0.01190	0.00000	0.00632	-0.00667	0.00000	-0.00043
15	c	x	-0.02765	0.00008	0.05086	0.05205	-0.00011	0.01194
		y	-0.05622	-0.00004	-0.01959	-0.01439	-0.00003	-0.00138
		z	0.01854	0.00005	0.03784	0.03554	-0.00003	0.00741
16	h	x	0.05567	0.00004	0.01873	0.01477	0.00001	0.00043
		y	0.50593	0.00032	0.09537	0.05558	0.00040	-0.00323
		z	0.01190	0.00000	0.00632	0.00668	0.00000	0.00043
17	h	x	0.39471	-0.00062	-0.38768	-0.41767	0.00116	-0.10418
		y	0.07327	-0.00013	-0.08423	-0.09008	0.00024	-0.02096
		z	-0.00315	0.00002	0.00905	0.01084	-0.00002	0.00345
18	h	x	-0.12040	-0.00034	-0.23768	-0.22245	0.00020	-0.04470
		y	0.09765	0.00030	0.22108	0.20724	-0.00021	0.04202
		z	-0.22446	-0.00066	-0.47169	-0.44058	0.00042	-0.09108
19	n	x	0.00000	0.00000	0.00000	0.00000	0.00005	0.00025
		y	0.00008	0.00000	0.00000	-0.00004	0.00014	0.00011
		z	0.00000	0.00007	-0.00001	0.00000	0.00000	0.00000
20	c	x	0.00015	0.00000	0.00000	-0.00015	-0.00035	-0.00012
		y	-0.00011	0.00000	0.00000	0.00006	-0.00020	-0.00022
		z	0.00000	0.00011	0.00002	0.00000	0.00000	0.00000
21	n	x	-0.00004	0.00000	0.00000	0.00005	-0.00033	0.00011
		y	0.00000	0.00000	0.00000	-0.00001	0.00032	0.00003
		z	0.00000	0.00062	-0.00001	0.00000	0.00000	0.00000
22	c	x	0.00003	0.00000	0.00000	-0.00002	0.00133	-0.00006

		y	-0.00005	0.00000	0.00000	0.00003	-0.00530	0.00009
		z	0.00000	-0.02692	0.00006	0.00000	0.00000	0.00000
23	h	x	-0.00011	-0.01930	0.00005	0.00008	-0.00485	0.00014
		y	0.00028	0.11509	-0.00025	-0.00015	0.02609	-0.00052
		z	0.00040	0.15512	-0.00033	-0.00020	0.03399	-0.00060
24	h	x	-0.00011	0.01930	-0.00005	0.00008	-0.00485	0.00014
		y	0.00028	-0.11508	0.00025	-0.00015	0.02609	-0.00052
		z	-0.00040	0.15512	-0.00033	0.00020	-0.03399	0.00060
25	c	x	-0.00009	0.00000	0.00000	0.00019	0.07311	-0.00036
		y	0.00009	0.00000	0.00000	-0.00017	-0.05657	0.00023
		z	0.00000	-0.09006	0.00013	0.00000	0.00000	0.00000
26	h	x	0.00006	-0.06477	0.00009	-0.00009	-0.02021	0.00004
		y	-0.00030	0.39452	-0.00057	0.00060	0.17093	-0.00052
		z	-0.00041	0.54586	-0.00078	0.00087	0.25467	-0.00083
27	h	x	0.00098	0.00000	0.00000	-0.00207	-0.82620	0.00426
		y	-0.00042	0.00000	0.00000	0.00087	0.34072	-0.00173
		z	0.00000	-0.01354	0.00002	0.00000	0.00000	0.00000
28	h	x	0.00006	0.06477	-0.00009	-0.00009	-0.02021	0.00004
		y	-0.00030	-0.39452	0.00057	0.00060	0.17093	-0.00052
		z	0.00042	0.54586	-0.00078	-0.00087	-0.25467	0.00083
29	n	x	-0.00021	0.00000	0.00000	0.00018	0.00010	0.00003
		y	0.00004	0.00000	0.00000	-0.00002	0.00003	0.00011
		z	0.00000	-0.00004	-0.00001	0.00000	0.00000	0.00000
30	h	x	0.00559	0.00000	0.00000	0.00061	-0.00007	-0.00060
		y	0.00121	0.00000	0.00000	0.00060	0.00003	0.00134
		z	0.00000	-0.00007	0.00169	0.00000	0.00000	0.00000
31	h	x	0.00012	0.00000	0.00000	-0.00011	-0.00299	-0.00005
		y	0.00001	0.00000	0.00000	0.00017	-0.00152	0.00052
		z	0.00000	-0.00449	0.00007	0.00000	0.00000	0.00000

reduced mass(g/mol)	1.102	1.105	1.105	1.104	1.102	1.098

mode	91	92	93
frequency	3080.08	3436.90	3485.12
symmetry	a	a	a
IR	YES	YES	YES
|dDIP/dQ| (a.u.)	0.0022	0.0036	0.0052
intensity (km/mol)	8.28	23.07	48.45

intensity (%)			0.68	1.89	3.96
RAMAN			YES	YES	YES
(par,par)			4.30	2.48	3.64
(ort,ort)			4.30	12.06	14.07
(ort,unpol)			4.30	7.95	9.60
depol. ratio			0.75	0.15	0.19
1	cl	x	0.00000	-0.00001	-0.00001
		y	0.00000	-0.00001	0.00001
		z	0.00000	0.00000	0.00000
2	c	x	0.00000	-0.00022	-0.00020
		y	0.00000	0.00012	-0.00018
		z	0.00006	0.00000	0.00000
3	n	x	0.00000	0.00032	0.00013
		y	0.00000	-0.00086	0.00007
		z	0.00044	0.00000	0.00000
4	c	x	0.00000	0.00055	-0.00045
		y	0.00000	0.00138	-0.00009
		z	-0.00010	0.00000	0.00000
5	n	x	0.00000	0.00741	0.00008
		y	0.00000	0.07112	-0.00061
		z	0.00018	0.00000	0.00000
6	c	x	0.00000	-0.00026	-0.00007
		y	0.00000	0.00047	-0.00002
		z	-0.00163	0.00000	0.00000
7	c	x	0.00000	-0.00025	-0.00002
		y	0.00000	-0.00066	0.00001
		z	-0.09347	0.00000	0.00000
8	h	x	0.29629	-0.00038	-0.00006
		y	-0.30382	0.00104	-0.00010
		z	0.56119	-0.00112	0.00019
9	h	x	-0.00001	0.00033	0.00040
		y	0.00000	-0.00020	0.00004
		z	-0.00929	0.00000	0.00000
10	h	x	-0.29630	-0.00038	-0.00006
		y	0.30385	0.00104	-0.00010
		z	0.56121	0.00112	-0.00019
11	c	x	0.00163	-0.00007	0.00000
		y	-0.00059	-0.00025	0.00002
		z	-0.00097	-0.00009	0.00000
12	h	x	-0.00802	-0.00012	-0.00002

		y	0.00609	0.00048	0.00000
		z	0.01768	0.00069	-0.00006
13	h	x	-0.01034	-0.00014	0.00027
		y	-0.00296	-0.00031	0.00001
		z	-0.00026	0.00016	0.00007
14	h	x	0.00002	0.00121	-0.00004
		y	0.00205	0.00041	-0.00016
		z	0.00056	0.00120	-0.00002
15	c	x	-0.00163	-0.00007	0.00000
		y	0.00059	-0.00025	0.00002
		z	-0.00097	0.00009	0.00000
16	h	x	-0.00002	0.00121	-0.00004
		y	-0.00205	0.00041	-0.00016
		z	0.00056	-0.00120	0.00002
17	h	x	0.01034	-0.00014	0.00027
		y	0.00296	-0.00031	0.00001
		z	-0.00026	-0.00016	-0.00007
18	h	x	0.00802	-0.00012	-0.00002
		y	-0.00609	0.00048	0.00000
		z	0.01767	-0.00069	0.00006
19	n	x	0.00000	0.00013	0.00018
		y	0.00000	-0.00002	0.00090
		z	-0.00006	0.00000	0.00000
20	c	x	0.00000	-0.00029	0.00121
		y	0.00000	-0.00004	-0.00061
		z	0.00000	0.00000	0.00000
21	n	x	0.00000	0.00016	0.00887
		y	0.00000	-0.00055	-0.07220
		z	0.00001	0.00000	0.00000
22	c	x	0.00000	-0.00004	-0.00104
		y	0.00000	0.00000	0.00015
		z	0.00000	0.00000	0.00000
23	h	x	-0.00002	0.00006	-0.00421
		y	-0.00001	0.00001	0.00354
		z	-0.00001	0.00005	0.00564
24	h	x	0.00002	0.00006	-0.00421
		y	0.00001	0.00001	0.00354
		z	-0.00001	-0.00005	-0.00564
25	c	x	0.00000	0.00000	0.00009
		y	0.00000	-0.00002	0.00015
		z	-0.00001	0.00000	0.00000
26	h	x	0.00000	-0.00001	0.00131

```
                 y   0.00005  0.00010  0.00072
                 z   0.00006  0.00011 -0.00115
 27   h          x   0.00000  0.00010 -0.00135
                 y   0.00000  0.00000  0.00064
                 z   0.00000  0.00000  0.00000
 28   h          x   0.00000 -0.00001  0.00131
                 y  -0.00005  0.00010  0.00072
                 z   0.00006 -0.00011  0.00115
 29   n          x   0.00000  0.00051  0.00047
                 y   0.00000  0.00018 -0.00015
                 z  -0.00001  0.00000  0.00000
 30   h          x   0.00000 -0.11140  0.00093
                 y   0.00000 -0.99116  0.00805
                 z  -0.00016  0.00000  0.00000
 31   h          x   0.00000 -0.00088 -0.12371
                 y   0.00000  0.00809  0.98955
                 z  -0.00002  0.00000  0.00000

reduced mass(g/mol)     1.104    1.074    1.077


 keyword $raman spectrum missing in file <control>


   ***  raman data written onto $raman spectrum
        file=<control>  ***


    ------------------------------------------------------------------------
-
         total  cpu-time :   0.19 seconds
         total wall-time :   0.24 seconds
    ------------------------------------------------------------------------
-


   ****  intense : all done  ****


    2012-02-09 17:41:05.389

 intense ended normally
```

Appendix Section A1.3.1.2.

The fitted full-widths at half maximum (FWHM) values

Freqeuncy (cm^{-1})	Intensity (rel. units)	Fitted FWHM (cm^{-1})
356	2.0	6
461	10	16
520	4.0	6
675	4.3	6
696	4.3	6
881	8.0	6
956	18.8	6
999	10.6	6
1057	25.2	6
1150	9.0	6
1233	6.6	6
1465	6.8	6
1475	10.8	6
1520	11.3	6
1525	19.0	6
1568	8.0	6
1626	4.5	10
1645	49.0	10
1663	41.2	10
1665	19.0	10
1675	29.0	10
1676	11.0	10
1712	27.0	10
1786	9.0	10
3203	202.0	22.6
3241	119.0	22.6
3242	154.0	22.6
3259	216.0	22.6
3285	94.0	22.6
3314	40.2	22.6

Figure A1_2. Parameters for the calculated Raman spectra of terbuthylazine (TBA).

Freqeuncy (cm^{-1})	Intensity (rel. units)	Fitted FWHM (cm^{-1})
452.0	52.97	5.3
530.5	14.94	6.3
673.1	10.3	6.9
697.6	15.41	6.9
770.0	7.0	4
782.7	7.48	4
792.1	21.35	4
878.1	20.68	5.7
897.6	34.25	9.8
952.5	4.92	5.7
981.8	65.63	4.9
1023.3	3.07	4
1055.1	5.38	2.8
1163.6	41.86	3.2
1188.1	74.83	4.5
1206.9	19.61	5.7
1232.1	106.7	5.7
1280.8	53.9	4.9
1310.3	24.36	8
1329.2	131.1	13.9
1344.4	9.82	6.3
1353.2	9.24	9.8
1358.2	102.81	19.6
1370.5	103.53	16
1381.0	76.89	13.9
1419.1	62.99	6.6
1433.4	9.94	8.9
1439.5	6.28	4.9
1446.1	111.1	12
1450.8	19.37	10
1470.0	16.89	8
1511.6	243.24	16
1547.4	458.7	12
1598.1	1221.85	24.9
1611.1	655.66	24.9
2935.2	17.38	12.6
2939.4	28.72	11.3
2942.6	26.2	12.6
2948.0	25.49	9.8
2962.1	22.2	8.5
2981.1	8.7	8
3022.0	43.1	13.9
3025.1	29.77	10
3036.6	9.27	5.7
3039.2	21.23	8
3040.1	15.46	12
3051.8	37.71	9.8
3080.1	8.29	6.9
3436.9	23.07	6.3
3485.1	48.45	6.3

Figure A1_3. Parameters for the calculated infrared spectra of terbuthylazine (TBA).

a.) Lindane (hexachlorocyclohexane, (ɣ-HCH)) and simazine

Freqeuncy (cm^{-1})	Intensity (rel. units)	Fitted FWHM (cm^{-1})
184.0	12.41	9.8
185.7	17.96	9.8
240.9	11.96	8
285.8	22.64	8.5
313.3	19.50	6.9
333.1	59.95	6.9
383.9	8.94	6.9
403.2	3.59	6.9
474.4	21.61	8
560.7	5.81	6.9
657.7	9.08	6.9
664.8	9.41	6
687.6	4.96	6.9
747.2	45.77	8.9
765.2	3.49	6.9
830.8	8.88	8
890.6	12.30	6.3
911.4	12.14	6.9
932.7	4.08	6.9
950.2	4.01	6.9
1020.2	1.45	4.7
1087.9	0.83	5.7
1103.6	4.49	7.7
1154.0	2.22	6.9
1171.2	6.67	6.9
1195.8	4.36	8.5
1218.9	5.85	6.9
1239.2	13.19	8.9
1323.4	2.94	5.7
3006.9	23.59	6.9
3042.9	5.03	9.8
3043.6	11.87	9.8
3044.6	16.85	9.8
3059.3	25.23	7.5

Figure A1_0. Parameters for the calculated Raman spectra of lindane.

Freqeuncy (cm^{-1})	Intensity (rel. units)	Fitted FWHM (cm^{-1})
353.2	4.69	2.8
393.6	3.17	15
421.0	11.04	12
469.2	13.28	7.3
530.5	1.84	3.5
625.7	2.1	4
697.6	1.67	4
770.0	3.73	5.5
878.1	4.25	6.3
895.0	5.5	10
914.3	3.68	10
952.5	32.31	6.9
1055.0	8.1	8
1168.1	10.09	12
1206.9	3.45	8
1253.6	4.97	4.9
1310.3	4.8	8
1419.1	8.63	16
1419.7	7.47	3.5
1433.4	7.64	14
1439.5	4.48	6
1444.3	3.84	10
1446.1	6.98	9.4
1470.0	7.39	11.3
1511.6	3.34	6.9
1547.3	1.42	3.7
1598.1	8.12	10
1611.1	16.16	10
2929.4	26.49	16
2942.6	33.36	10
2948.0	5.71	14
2962.1	25.2	10
2981.1	10.66	10
3022.0	20.29	10
3025.1	6.6	10
3037.6	3.7	10
3039.2	15.71	18
3046.1	15.1	18
3051.8	14.05	18
3080.1	4.3	13
3436.9	7.95	10
3485.1	9.6	8

Figure A1_1 Parameters for the calculated Raman spectra of simazine.

Section appendix A4: Results and discussion

(Supporting Information of Chapter 4- Results and Discussion)

A2.4 Characterization of the products of different pesticides by nuclear magnetic resonance and mass spectroscopy

The photodegradation pathway of TBA in the presence of hydrogen peroxide can be seen in Scheme A2.4.3.4

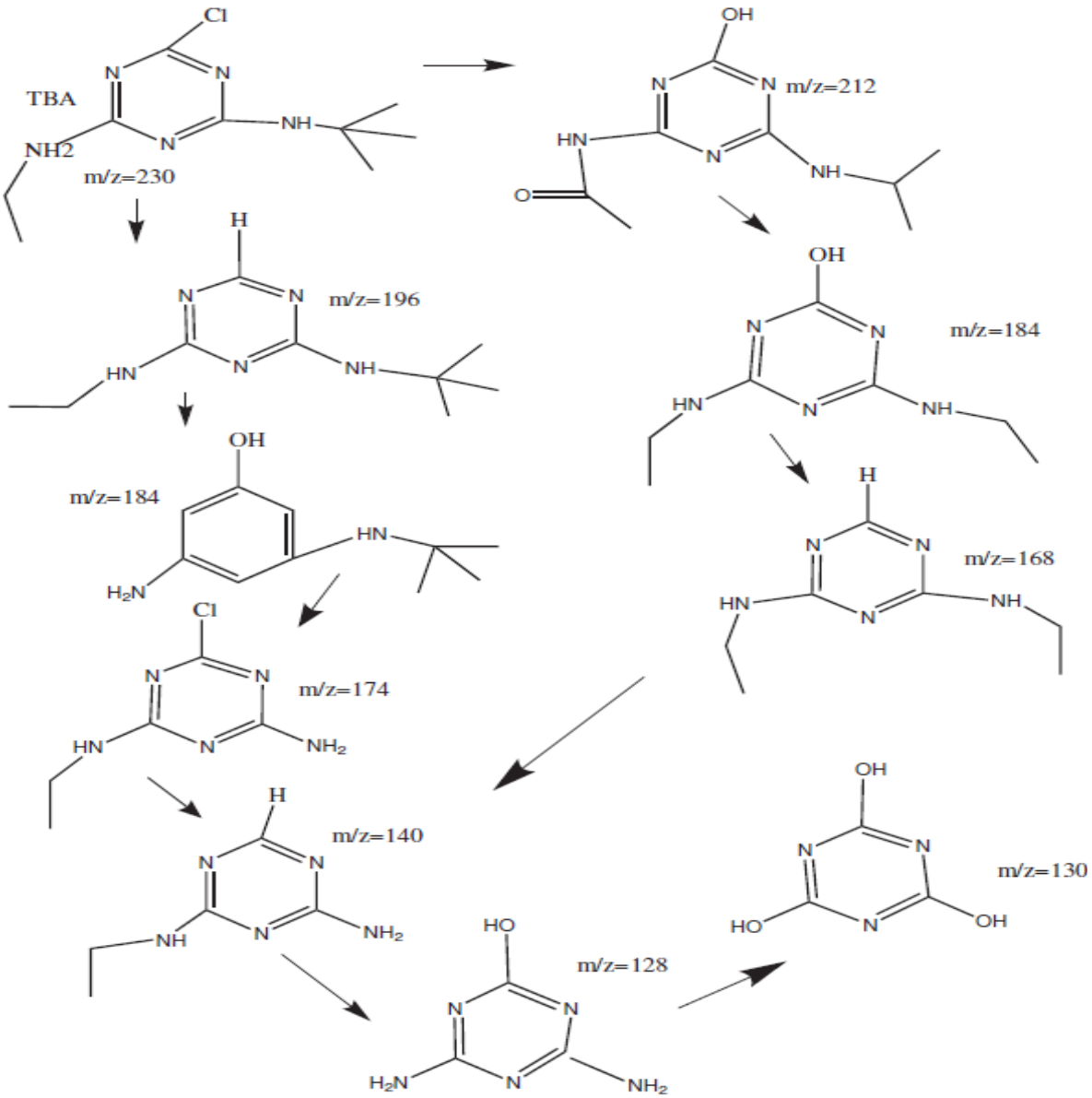

Scheme A2.4.3.4: The photodegradation pathway of TBA in the presence of OH-radicals

Table A2.4.2.3: Proposed interpretation of photo-degradation products of terbuthylazine according to MS spectra.

m/z	Chemical name	detected
230	2-ter-butylamino-4-chloro-6-ethylamino	yes
212	N-tert-buthyl-N'-ethoxy-1-hydroxy-1,3,5-triazine-2,4-diamine	yes
196	N-tert-butyl-N'-ethyl-1,3,5-triazine-2,4-diamine	yes
184	N-amine-N'-tert-buthyl-1-hydroxy-1,3,5-triazine-2,4-diamine	yes
174	2-chloro-deterisobutylterbuthylazine	yes
140	deterisobutylterbuthylazine	yes
128-h	ammeline	yes
130	Cyanuric acid	yes

a) Simazine

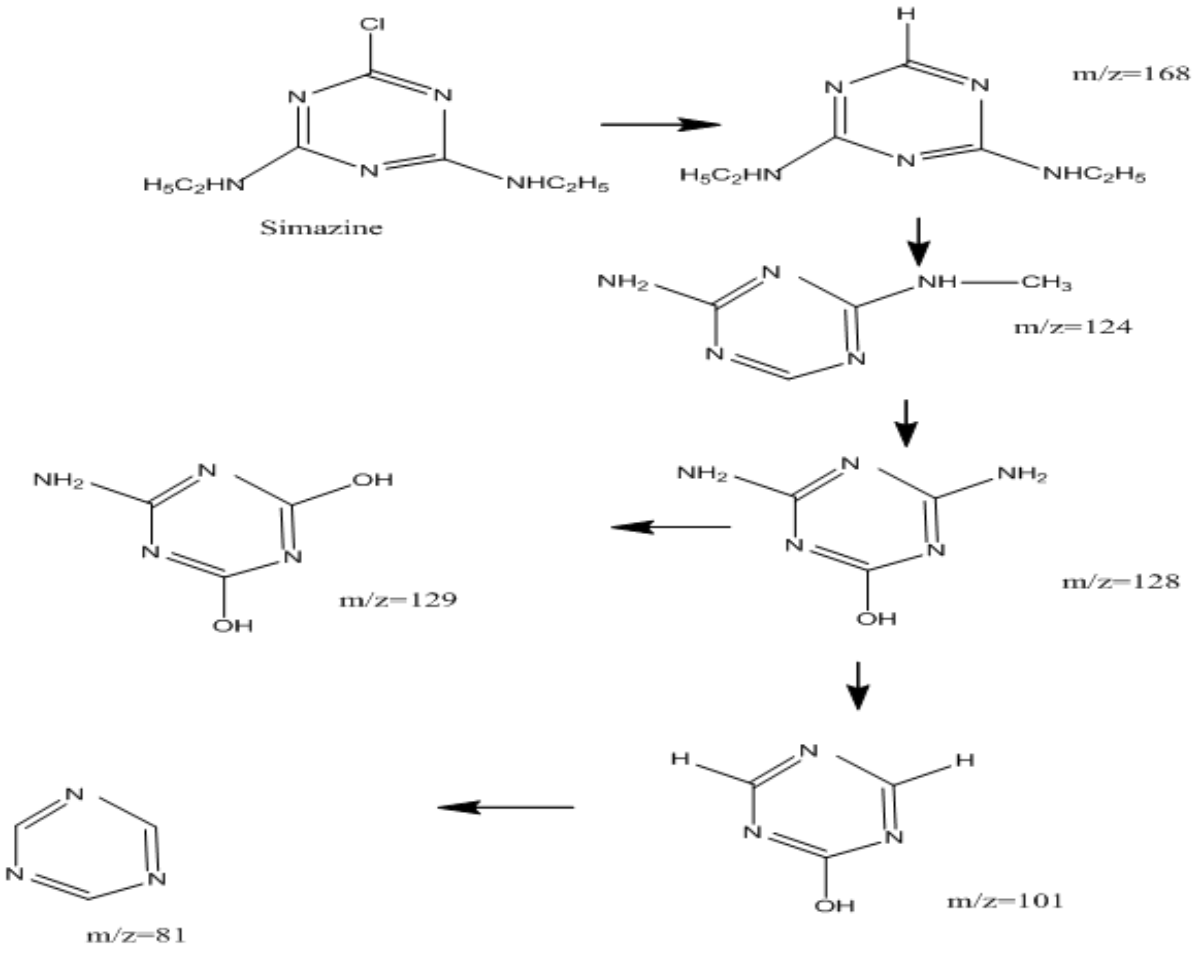

Scheme A2.4.3.5a: Reaction mechanism of simazine degradation

Table A2.4.2.4a: Proposed interpretation of photo-degradation products of simazine according to MS spectra

m/z	Chemical name	detected
202	6-chloro-N,N-diethyl-1,3,5-triazine-2,4-diamine	yes
168	3,5-diethyltriazine	yes
124	2-methyl-2,6-diaminotriazine	yes
68	s- triazine	yes
128	6-hydroxy-2,4-diamino-1,3,5-triazine	no
129	2,6-hydroxy-4-amino-1,3,5-triazine	yes
130	2,6-hydroxy-4-amino-1,3,5-triazine	no

b) Lindane

Proposed decomposition of lindane in the presence of OH-radicals.

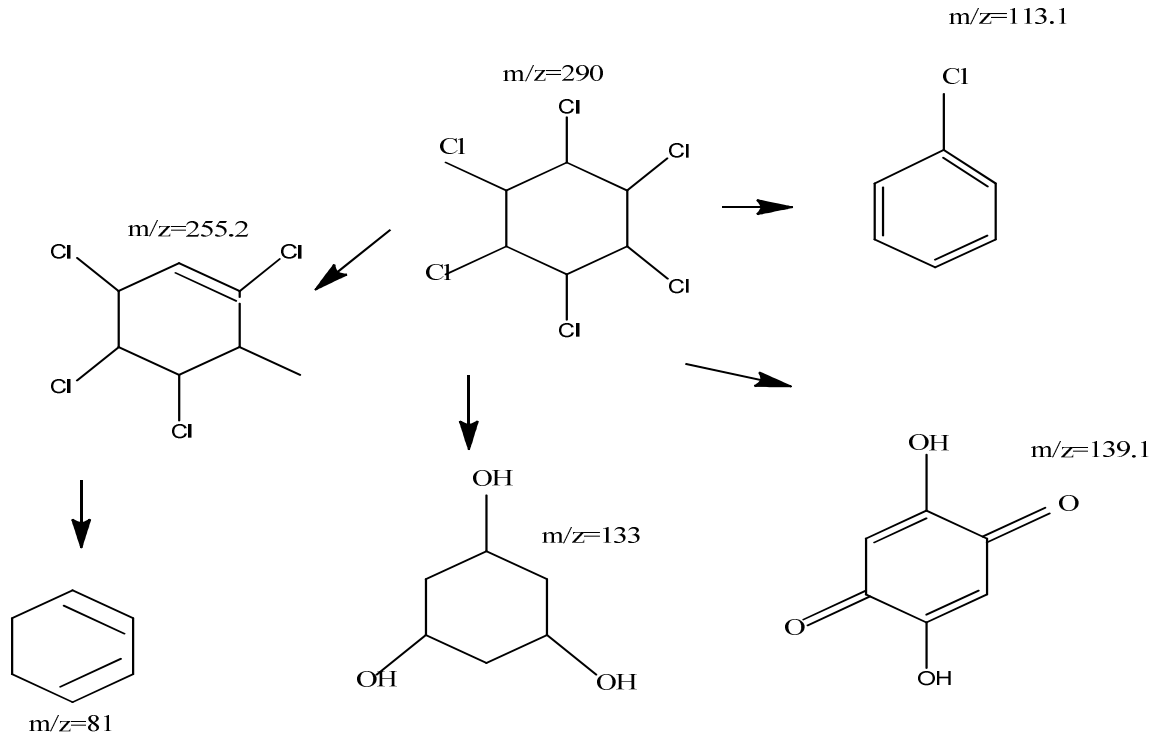

Scheme A2.4.3.5b: Proposed pathways for the photodecomposition of lindane in the presence of OH-radicals.

Table A2.4.2.4b: Proposed interpretation of photo-degradation products of lindane according to MS spectra

m/z	Chemical name	detected
290	hexachlorocyclohexane	yes
255,2	Pentachlorocyclohexene	yes
139,1	3,6-dihydroxycyclodihexanoe	yes
133	1,3,5-trihydroxycyclohexane	yes
113,1	chlorobezene	yes
81	1,3-cyclorodihexene	yes